Study of C. maltaromaticum CNCM I-3298 to improve performance of biological time-temperature integrators and gain more insight into lactic acid bacteria cryoresistance

Amélie Girardeau

Thèse de doctorat

NNT : 2021UPASB068

université PARIS-SACLAY

Étude de *C. maltaromaticum* CNCM I-3298 afin d'améliorer les performances d'intégrateurs temps-température biologiques et de mieux comprendre la cryorésistance des bactéries lactiques

Study of C. maltaromaticum *CNCM I-3298 to improve performance of biological time-temperature integrators and gain more insight into lactic acid bacteria cryoresistance*

Thèse de doctorat de l'université Paris-Saclay

École doctorale n° 581,
Agriculture, Alimentation, Biologie, Environnement et Santé (ABIES)
Spécialité de doctorat : Microbiologie
Unité de recherche : Université Paris-Saclay, INRAE, AgroParisTech, UMR SayFood, 91300, Massy, France
Référent : AgroParisTech

Thèse présentée et soutenue à Paris-Saclay, le 02/12/2021, par

Amélie GIRARDEAU

Composition du Jury

Nathalie DESMASURES Professeure, Université de Caen	Présidente
Muriel MERCIER-BONIN Directrice de recherche, INRAE centre Occitanie-Toulouse	Rapporteur & Examinatrice
Laurent BENEY Professeur, AgroSup Dijon	Rapporteur & Examinateur

Direction de la thèse

Ioan-Cristian TRELEA Professeur, AgroParisTech	Directeur de thèse
Fernanda FONSECA Directrice de recherche, INRAE centre IdF-Versailles-Grignon	Co-Directrice de thèse
Stéphanie PASSOT Professeure, AgroParisTech	Co-Encadrante & Invitée

à mon Père

"We live on an island surrounded by a sea of ignorance.
As our island of knowledge grows, so does the shore of our ignorance."

- John Archibald Wheeler

Publications & communications

Articles in peer-reviewed journals

Girardeau A, Puentes C, Keravec S, Peteuil P, Trelea IC, Fonseca F (2019). Influence of culture conditions on the technological properties of *Carnobacterium maltaromaticum* CNCM I-3298 starters. *Journal of Applied Microbiology*, 126(5):1468-1479.
https://doi.org/10.1111/jam.14223

Puentes C, **Girardeau A**, Passot S, Fonseca F, Trelea I-C (2021). Dynamic modeling of *Carnobacterium maltaromaticum* CNCM I-3298 growth and metabolite production, and model-based process optimization. *Foods*, 10(8):1922.
https://doi.org/10.3390/foods10081922

Girardeau A, Passot S, Meneghel, Cenard S, Lieben P, Trelea I-C, Fonseca F (submitted in September 2021). Insights into lactic acid bacteria cryoresistance using FTIR micro-spectroscopy and other analytical approaches. *Analytical and Bioanalytical Chemistry journal*.

Book chapters

Girardeau A, Biscola V, Keravec S, Corrieu G, Fonseca F (2020). Application of Lactic Acid Bacteria in Time-Temperature Integrators: A Tool to Monitor Quality and Safety of Perishable Foods. In: Albuquerque M, de Moreno A, LeBlanc JG, Bedani R (eds) Lactic Acid Bacteria, a Functional Approach. CRC Press Taylor & Francis UK, London, pp 241-260
https://doi.org/10.1201/9780429422591-14

Fonseca F, **Girardeau A,** Passot S (2021). Freeze-Drying of Lactic Acid Bacteria: A Stepwise Approach for Developing a Freeze-Drying Protocol Based on Physical Properties. In: Wolkers WF, Oldenhof H (eds) Cryopreservation and Freeze-Drying Protocols. Springer US, New York, NY, pp 703–719
https://doi.org/10.1007/978-1-0716-0783-1_38

Oral communications in peer-reviewed international conferences

Girardeau A, Meneghel J, Trelea I-C, Passot S, Fonseca F. Complementary analytical approaches improving knowledge on lactic acid bacteria cryoresistance. 56th annual meeting of the Society for Cryobiology. July 22 to 25, 2019 in San Diego, California, USA. Awarded a "***Student Travel Award***" and selected to be among four finalists to

present at a special "***Crystal Awards***" session, based on the submitted extended abstract.

Girardeau A, Passot S, Cenard S, Lieben P, Trelea I-C, Fonseca F. Effects of pH stress during growth on the physiological, biophysical and biochemical properties of *Carnobacterium maltaromaticum* cells. Microbial Stress (virtual) conference organized by the European Federation of Biotechnology. November 16 to 18, 2020.

Poster presentation in a peer-reviewed international conference

Girardeau A, Puentes C, Keravec S, Peteuil P, Trelea IC, Fonseca. Mapping the physiological states of *Carnobacterium maltaromaticum* obtained by applying stressful fermentation conditions. Microbial Stress conference organized by the European Federation of Biotechnology. April 23 to 25 in Kinsale, Cork, Ireland. Selected for a **flash poster presentation** on stage during the conference. Won the **best poster award** at ABIES doctoral day.

Scientific vulgarization

Presenter at the AgroParisTech stand at the 2020 *Salon de l'Agriculture* in Paris.

General Table of Contents

List of Figures **7**

List of Tables **17**

Abbreviations & Nomenclature **21**

Foreword **23**

Part I Literature review **27**

I.1. Time-Temperature Integrators 29
I.1.1. Time-Temperature Integrators (TTI) 31
I.1.2. Production and performance evaluation of LAB-based TTI 37
I.1.3. Parametrization strategies 45
I.1.4. Concluding remarks 49

I.2. *Carnobacterium maltaromaticum* 51
I.2.1. General characteristics 53
I.2.2. Modulating the technological properties of LAB for industrial applications 62
I.2.3. Other useful technological properties of *C. maltaromaticum* 69
I.2.4. Concluding remarks 71

I.3. Cryopreservation of lactic acid bacteria 73
I.3.1. Physical events taking place during the cryopreservation of LAB 75
I.3.2. Stresses and damages induced by cryopreservation on LAB cells 85
I.3.3. Improving the cryoresistance of LAB 89
I.3.4. Concluding remarks 97

I.4. General insights 98

Part II Materials and Methods 99

II.1. Experimental approach 103
II.2. Bacterial concentrate production 107
II.2.1. Strain and inocula preparation 107
II.2.2. Fermentation 107
II.2.3. Physiological state assessment 113
II.3. Intracellular glass transition temperature assessed by DSC 113
II.4. Membrane fluidity assessed by fluorescence anisotropy 114
II.5. FTIR micro-spectroscopic characterization in aqueous conditions 117
II.6. FTIR spectroscopic measurements during cooling and heating 127
II.7. Fatty acid composition 130
II.7.1. Accelerated Solvent Extraction (ASE) 130
II.7.2. Fatty acid identification by GC-MS 131
II.8. Statistical analyses 132

Part III Results and Discussions 135

III.1. Influence of culture conditions on the technological properties of *Carnobacterium maltaromaticum* CNCM I-3298 starters 137
III.1.1. Context and objectives 138
III.1.2. Abstract 139
III.1.3. Introduction 140
III.1.4. Materials and Methods 145
III.1.5. Results 149
III.1.6. Discussion 153
III.1.7. Key takeaways 161

III.2. Dynamic modeling of *Carnobacterium maltaromaticum* CNCM I-3298 growth and metabolite production, and model-based process optimization 163
III.2.1. Context and objectives 164
III.2.2. Abstract 165
III.2.3. Introduction 166
III.2.4. Materials and methods 171

III.2.5. Dynamic model 173
III.2.6. Results 181
III.2.7. Conclusions 190
III.2.8. Nomenclature 191
III.2.9. Key takeaways 193

III.3. Insights into lactic acid bacteria cryoresistance using FTIR micro-spectroscopy and other analytical approaches 195
III.3.1. Context and objectives 196
III.3.2. Abstract 197
III.3.3. Introduction 198
III.3.4. Materials and Methods 203
III.3.5. Results 213
III.3.6. Discussion 227
III.3.7. Conclusions 233
III.3.8. Key takeaways 234

Conclusions 235

Perspectives 239

References 242

Annexes 267
Annex A-II.5: An introduction to Fourier Transform Infrared Spectroscopy for the analyses of biological samples 268
Annex A-III.1: Supplementary data of Chapter III.1 283
Annex A-III.2: Supplementary data of Chapter III.2 285
Annex A-III.3: Supplementary data of Chapter III.3 290

Resumé substantiel en français 300

List of Figures

PART I – LITERATURE REVIEW

Chapter I.1.

Figure I.1-1: (A) Schematic representation of the growth (dotted line) and acidification activity (solid line) of LAB in a TopCryo® TTI label stored at 8 °C, inducing a color shift when a specific pH is reached; **(B)** the color shift's kinetic dependence on the average temperature profile: at 4 °C the color shift takes place later than at 8 °C. 32

Figure I.1-2: Diagram of industrial LAB concentrate and LAB-based TTI label production steps 36

Figure I.1-3: Simulation of different, realistic storage conditions used to evaluate LAB-based TTI performance. Adapted from Ellouze et al. 2010 and 2011. 42

Figure I.1-4: Schematic representation of biological TTI parametrization strategies and their expected potential shelf-life extension ranges. The ✓ marks the only parametrization strategy currently used in commercialized LAB-based TTI 44

Chapter I.2.

Figure I.2-1: Electron micrograph of *Carnobacterium maltaromaticum* DSM 20730 cells, taken from Schillinger and Holzapfel (1995) 52

Figure I.2-2: Schematic illustration a Gram-positive bacterium cell envelope (cell wall + cell membrane). Credit: Augustin Lerebours (reproduced with permission). 56

Figure I.2-3: Bacterial membrane lipid classification, adapted from Meneghel et al., 2017. 58

Figure I.2-4: Schematic representation of different fatty acyl chain conformations found in biological membranes. Adapted from Fonseca et al., 2019. 58

Figure I.2-5: The different levels of protein organization. Adapted from https://www.genome.gov/genetics-glossary/Protein 60

Figure I.2-6: Schematic representation of a bacterial growth curve, indicating various growth phases. Adapted from Garrison and Huigens 2017 66

Chapter I.3.

Figure I.3-1: Product temperature profile and principal phenomena taking place during freezing. **Tn** (°C): nucleation temperature; **Tf** (°C): freezing temperature; **Tg'** (°C): glass transition temperature of the maximally cryocentrated medium. Adapted from Beal and Fonseca (2015). 74

Figure I.3-2: State diagram of a solute-water mixture frozen at two different cooling rates: **(i)** very slow (<10 °C/min), leading to increasing ice fractions and maximal solute cryo-concentration (green arrow) and **(ii)** very high (e.g., by immersion in liquid nitrogen) (red arrow). The red dashed arrow represents the instability of a product frozen at very high cooling rates followed by storage in a laboratory freezer (-80 °C): ice re-crystallization occurs during storage, leading to increasing solute concentrations. 76

Figure I.3-3: Schematic representation of the physical events taking place during the freezing of a cryoprotected LAB cell. Temperature indications correspond to measurements carried out on L. bulgaricus cells cryoprotected in a 20 % sucrose solution. Adapted from Fonseca et al. 2016 80

Figure I.3-4: Schematic representation of a membrane lipid transition from a disordered liquid-crystalline phase (acyl chains freely adopting gauche conformations) to an ordered gel phase (acyl chains in all-trans conformations). Adapted from Borchman et al. 1991. 82

Figure I.3-5: Schematic illustration of membrane lateral phase separation upon cooling, causing protein aggregation. All phospholipid types (O, □, △) start off in a fluid, disorganized state **(A)**; all phospholipids of the same type rigidify upon reaching their transition temperature and tend to aggregate **(B)**; proteins are excluded from the rigid domains and aggregate in the domains that have remained fluid **(C)**. Adapted from Tablin et al. 2001. 84

PART II – MATERIALS AND METHODS

Figure II.2-1: Bioreactor and probes used in this study 108

Figure II.2-2: Growth and acidification rate of a C. maltaromaticum fermentation carried out under control conditions (pH 7, 30 °C), illustrating harvest time determination 109

Figure II.2-3 : Counting of *C. maltaromaticum* colonies grown on Plate Count Agar for 48 h at 30 °C.....112

Figure II.2-4: Schematic illustration of the Cinac® system and dtpH1.5 measurements.....112

Figure II.5-1 : (a) photo of the iN10 micro-spectroscope used in this study; **(b)** photo of the custom-made demountable sample holder; **(c)** schematic representation of the CaF_2 micro-chamber, adapted from Meneghel et al. 2020 116

Figure II.5-2: (a) a captioned image of the sample chamber taken by the FTIR microscope, illustrating the diluent and bacterial suspension sides separated by a strip of Mylar film; **(b)** IR spectrum taken on the diluent side; **(c)** IR spectrum taken on the bacterial suspension side.....118

Figure II.5-3: Illustration of the water subtraction procedure using Matlab R2014a (version 8.3.0.532). **(a)** raw sample spectrum and diluent spectrum recorded on C. maltaromaticum cells with the Nicolet iN10 IR microscope (Thermo Scientific, USA); **(b)** diluent spectrum multiplied by a range of coefficients; **(c)** result of the subtraction between the raw sample spectrum and a scaled diluent spectrum leading to the same Amide I/Amide II area ratio as dried cells; **(d)** enlargement of the Amide I and II bands where area ratio is shown.....120

Figure II.5-4: Illustration of the spectral data processing steps before analyses. Water subtracted spectra of *C. maltaromaticum* CNCM I-3298 (blue), *L. bulgaricus* ATCC 11842 (red) and *L. bulgaricus* CFL1 (green) are used as an example. **a,b** and **c** are three distinct spectral regions analyzed by Principal Component Analysis. ..122

Figure II.5-5: Illustration of the additional spectral processing applied to the 1800 – 1370 cm^{-1} region, harboring information on protein secondary structures. **(a)** Normalized spectra; **(b)** Secondary derivative of the normalized spectra showing the Amide I band components; **(c)** enlargement of the Amide I band where α-helix and β-sheet band intensities are shown.....126

Figure II.6-1: Peak positions of ν_sCH_2 vibration bands arising from *C. maltaromaticum* cells, plotted against their acquisition temperature. Raw data (blue dots) were fitted with a curve based on a continuous piecewise function. The maximum of the first derivative of the fitted curve was used to determine the lipid phase transition temperature during cooling (Ts).....128

Figure II.6-2: Peak of the bending and libration combination band of water (νH_2O), as a function of temperature. The upshift from approximately 2150 to 2200 cm^{-1} during cooling, determines the water nucleation temperature (Tn).....128

PART III – RESULTS AND DISCUSSION

Chapter III.1.

Figure III.1-1: Diagram of experimental approach applied to quantify the effect of fermentation temperature, pH and harvest time on viability and acidification activity of *C. maltaromaticum* CNCM I-3298 concentrates: **(A)** Frozen starter production process; **(B)** Range of pH and temperatures tested; **(C)** Harvest time determination; **(D)** Cell growth properties measured throughout fermentation; **(E)** Biological properties of cell concentrates measured before freezing and after freeze-thawing. 144

Figure III.1-2: dtpH1.5 values predicted by the regression model versus dtpH1.5 values measured. The corresponding coefficient of determination (R^2 = 0.8734) indicated adequate prediction of acidification activity in a TTI-like medium. 148

Figure III.1-3 : Response surface representations of the effect of fermentation pH and harvest time on the dtpH1.5 values of *C. maltaromaticum* CNCM I-3298 concentrates produced at 30 °C **(A)**, 20 °C **(B)** and 37 °C **(C)**. *experimental data points employed in the model at the given temperatures.....150

Figure III.1-4: dtpH1.5 values of *C. maltaromaticum* CNCM I-3298 concentrates harvested at increasing times of fermentation, carried out at different values of pH and temperature. Fermentation conditions leading to best (full green arrow) and worst (empty red arrow) acidification activities are indicated, as well as the reference conditions corresponding to the TopCryo® commercial TTI (dashed, empty blue arrow). The range of acidification activities leading to technologically similar shelf-lives to the control is signaled by dotted lines. Harvests done before stationary phase are of no industrial interest. 154

Figure III.1-5: Experimental dtpH1.5 (in min) values of all *C. maltaromaticum* CNCM I-3298 concentrates produced following the experimental design, as a function of their viability (in logCFU mL^{-1}). R^2 = 0.4654.....158

Chapter III.2.

Figure III.2-1: Mixed-acid fermentation pathway likely used by *C. maltaromaticum* to ferment trehalose. End products are shown in blue. ACK, acetate kinase; ADH, acetaldehyde dehydrogenase; LDH, lactate dehydrogenase; PFL, pyruvate formate lyase; PTA, phosphate acetyltransferase; PYK, pyruvate kinase; TreH, neutral trehalase. Adapted from (Andersson and Rådström 2002; Laursen et al. 2006; Ward 2015; Gänzle 2015; Zhang et al. 2019). 168

Figure III.2-2: Operating conditions of *C. maltaromaticum* CNCM I-3298 fermentation experiments 170

Figure III.2-3: : (a) Example of inhibition factor I_X as a function of C_I for different n values and K_{IX}=0,2 mol.L^{-1} . **(b)** Example of enzymatic activation factor E_A as a function of t for different r values and t_{lag}=5 h. 174

Figure III.2-4: Typical evolution of the relative production rate over time..... 176

Figure III.2-5: Evolution of concentrations over time for experiment F10 (T=30 °C, pH=8). Comparison between model (continuous line, using parameters from tables 1 and 2) and experimental data (symbols). The error bars for data represent the biological standard deviation, calculated from three independent repetitions of the run F01..... 182

Figure III.2-6: Response surfaces for model parameters, calculated with globally adjusted β coefficients in Eq. III.2-17..... 184

Figure III.2-7: Comparison between experimental variability and average RMSE values for concentrations computed using parameters determined for each experiment (**Table III.2-2**) and the response surface models (Table III.2-TS2 and Equation III.2-17). 186

Chapter III.3.

Figure III.3-1: Diagram of the experimental approach used in this study and the main investigated parameters. The asterisks (*) and (**) indicate that the corresponding results for *L. bulgaricus* ATCC 11842 and *L. bulgaricus* CFL1 cells were taken from Meneghel et al. (2017) and Meneghel et al. (2020), respectively. 202

Figure III.3-2: Illustration of the spectral data processing steps: pre-processing of (**a**) raw FTIR spectra of *C. maltaromaticum* CNCM I-3298 (blue), *L. bulgaricus* ATCC 11842 (red) and *L. bulgaricus* CFL1 (green), to obtain (**b**) sample spectra after

atmospheric suppression and water subtraction; and post-processing of resulting spectra including normalization and baseline correction (EMSC: extended multiplicative scatter correction) of four spectral regions (**c, d, e, f**) and further principal component analysis (PCA). 208

Figure III.3-3: Biological activity loss (culturability loss determined by plate counts method and acidifying activity loss determined with the Cinac system, median values) of *C. maltaromaticum* CNCM I-3298 (CM), *L. bulgaricus* ATCC 11842 (ATCC) and *L. bulgaricus* CFL1 (CFL1) cells following two freeze-thaw cycles. Letters (a, b, c) represent statistical differences between samples at a 95 % confidence level.....212

Figure III.3-4: Biological activity loss (culturability loss determined by plate counts method and acidifying activity loss determined with the Cinac system, median values) of *C. maltaromaticum* CNCM I-3298 (CM), *L. bulgaricus* ATCC 11842 (ATCC) and *L. bulgaricus* CFL1 (CFL1) cells following two freeze-thaw cycles. Letters (a, b, c) represent statistical differences between samples at a 95 % confidence level.....215

Figure III.3-5: Peak positions of the symmetric CH_2 stretching vibration band (ν_sCH_2) arising from *C. maltaromaticum* CNCM I-3298 (CM, blue circles), *L. bulgaricus* ATCC 11842 (ATCC, red circles) and *L. bulgaricus* CFl1 (CFL1, green circles) upon cooling of fresh cells suspended in a 25 % sucrose solution. Data points correspond to the medians of three replicates for each strain and the error bars to the associated interquartile ranges. The temperature range of water nucleation (Tn) is highlighted. Dotted curves indicate the first derivatives of the symmetric CH_2 stretching vibration band (ν_sCH_2), and the maximum of each curve corresponds to the lipid transition temperature Ts reported in Table 3 for each microorganism. 216

Figure III.3-6 : Principal component analysis (PCA) of FTIR spectra of fresh *C. maltaromaticum* CNCM I-3298 (CM, blue circles), *L. bulgaricus* ATCC 11842 (ATCC, red circles) and *L. bulgaricus* CFL1 (CFL1, green circles) cells in an aqueous environment, in the 3016 cm^{-1} to 2800 cm^{-1} range: **a** PC1 versus PC2 score plots explaining 81 % and 4 % of the variance, respectively. **b** Loading plot of PC1, separating CM from ATCC and CFL1: positive peaks in PC1 characterized C. maltaromaticum, whereas negative peaks characterized L. bulgaricus ATCC and CFL1 cells **c** Mean FTIR spectra of fresh cells used for the PCA. The characteristic absorption bands arising from fatty acid chains are indicated. 218

Figure III.3-7: Principal component analysis (PCA) of FTIR spectra of fresh *C. maltaromaticum* (CM, blue circles), *L. bulgaricus* ATCC 11842 (ATCC, red circles) and *L. bulgaricus* CFL1 (CFL1, green circles) cells in an aqueous environment, in the 1800 cm^{-1} to 1370 cm^{-1} range: **a** PC1 versus PC2 score plots explaining 87 % and 7 % of the variance, respectively. **b, c** Loading plots of the PC1 and PC2 axis, respectively.

Positive peaks in PC1 characterized *C. maltaromaticum* and *L. bulgaricus* ATCC 11842 cells, whereas negative peaks characterized *L. bulgaricus* CFL1 cells. Positive peaks in PC2 characterized *C. maltaromaticum* cells, whereas negative peaks characterized *L. bulgaricus* ATCC 11842. **d** Mean second derivatives of the FTIR spectra of fresh cells used for the PCA. The characteristic absorption bands arising from esters and nucleic acids, protein secondary structures (α-helix, β-sheets) and Amide II are indicated. **e** Mean ratios of the α-helix and β-sheets band intensities at respectively 1654 cm^{-1} and 1637 cm^{-1} of the derived spectra measured in fresh (dark bars) and thawed (light bars) cells**.** Letters (a, b, c, d) represent statistical differences between samples at a 95 % confidence level. 220

Figure III.3-8 : Principal component analysis (PCA) of FTIR spectra of fresh *C. maltaromaticum* CNCM I-3298 (CM, blue circles), *L. bulgaricus* ATCC 11842 (ATCC, red circles) and *L. bulgaricus* CFL1 (CFL1, green circles) cells in an aqueous environment, in the 1367 cm^{-1} to 975 cm^{-1} range: **a** PC1 versus PC2 score plots explaining 87 % and 10 % of variance, respectively. **b, c** Loading plots of the PC1 and PC2 axis, respectively. Positive peaks in PC1 characterized L. bulgaricus ATCC 11842 and CFL1 cells, whereas negative peaks characterized *C. maltaromaticum* cells. Positive peaks in PC2 characterized *C. maltaromaticum* and *L. bulgaricus* ATCC 11842 and CFL1 cells, whereas negative peaks characterized *L. bulgaricus* CFL1 cells. **d** Mean FTIR spectra of fresh cells used for the PCA. The Amide III region and the characteristic absorption bands of PO_2^- , as well as the sugar rings region are indicated**.** 222

Figure III.3-9: Principal component analysis (PCA) of FTIR spectra of fresh and thawed *C. maltaromaticum* CNCM I-3298 (CM, blue circles), *L. bulgaricus* ATCC 11842 (ATCC, red circles) and *L. bulgaricus* CFL1 (CFL1, green circles) cells in an aqueous environment, in the 1200 cm^{-1} to 975 cm^{-1} range: **a** PC1 versus PC3 score plot explaining 75 % and 2 % of variance, respectively. **b** loading plot of PC3, indicating separation of *L. bulgaricus* ATCC 11842 and *L. bulgaricus* CFL1 thawed cells from fresh cells, shifting to negative values of PC3 after freeze-thawing. **c** Mean second derivatives of the FTIR spectra of fresh and thawed cells used for the PCA. The characteristic symmetric absorption band of PO_2^- and sugar rings are indicated**.** 224

Figure III.3-10: Schematic representation of the behavior of the three LAB cells following freezing from the culture temperature to -80°C, considering the major physical events taking place: membrane lipid phase transition at Ts, ice nucleation at Tn, intracellular glass transition of cryoprotected cells at Tg'i and glass transition of the extracellular medium (20 % sucrose in saline water) at Tg'e. 226

Figure III.3-11: Effect of the membrane fatty acid composition on the survival rate of LAB after freezing, according to the literature (Gilliland and Speck 1974; Smittle

et al. 1974; Goldberg and Eschar 1977; Broadbent and Lin 1999; Gómez-Zavaglia et al. 2000; Fernandez et al. 2000; Béal et al. 2001; Wang et al. 2011; Gautier et al. 2013; Meneghel et al. 2017). The survival rate is presented as a function of (**a**) the ratio (UFA/SFA) between the unsaturated fatty acids (UFA) and the saturated fatty acids (SFA) and (**b**) the cyclic fatty acid (CFA) content expressed as a percentage of total membrane fatty acids. The data is grouped according to the CFA content: CFA lower than 10 % (orange circles), CFA values between 10 and 20 % (dark grey circles), and CFA values higher than 20 % (light grey circles).....228

ANNEXES

Annex II.5

Figure II.5-A1: Representation of the electromagnetic spectrum as a function of wavelength (m), frequency (Hz) and energy (eV), with an emphasis on the infrared region, and specifically on the mid-infrared region between 4000 and 400 cm^{-1}. Adapted from Hielscher, 2009.....268

Figure II.5-A2. Illustration of the three vibrational modes of a water molecule: symmetric stretching (ν_s), asymmetric stretching (ν_{as}) and bending (δ).....272

Figure II.5-A3: FTIR spectrum of pure water. The stretching modes of water giving rise to an absorption band between 3500 and 3000 cm^{-1}, the libration and bending combination band around 2200 cm^{-1} and the bending mode around 1650 cm^{-1}(Verma et al. 2018).....272

Figure II.5-A4: Block diagram of a FTIR spectrometer. Adapted from Meneghel et al. 2017.....274

Figure II.5-A5: Schematic illustration of the two main acquisition modes suitable for biological applications. Inspired by Barker et al. 2014.....276

Figure II.5-A6: Infrared spectra of a phospholipid (dimyristoylphosphatidylcholin), nucleic acid (calf thymus desoxyribonucleic acid), protein (collagen type I) and carbohydrate (glycogen), illustrating the most prominent IR absorption features of cells. Adapted from Lasch and Naumann (2015).....279

Figure II.5-A7: Chemical structures of a nucleic acid (ribonucleotide), a teichoic acid repeat unit, a phospholipid, a polypeptide and a carbohydrate (glycogen). In green highlights are bonds mainly contributing to the Amide vibration bands. In blue highlights are bonds contributing to the CH_2 stretching bands of lipids. In yellow highlights are the bonds contributing to C=O stretching band of esters in nucleic acids and phospholipids, respectively. In purple highlights the bonds

contributing to the PO_2 stretching band of phosphate groups (found in phospholipids, nucleic acids and teichoic acids). In pink highlights are the bonds contributing to the C-O stretching bands of carbohydrates.....280

Annex III.2

Figure III.2-A1 : Comparison between model parameters determined for each experiment (Table III.2-2) and parameters computed with the response surface models (equation III.2-17 using coefficients in Table III.2-A1).....286

Figure III.2-A2: Evolution of final concentrations (left) and batch-average productivities (right) with temperature and pH for biomass, formic acid and acetic acid.....288

Annex III.3

Figure III.3-A1: PC2 loading plot of the principal component analysis (PCA) of FTIR spectra in the 3016 – 2800 cm^{-1} region presented in Figure 6 of the results section (ATCC: *L. bulgaricus* ATCC 11842; CFL1: *L. bulgaricus* CFL1).....297

Figure III.3-A2: Principal component analysis (PCA) of FTIR spectra of fresh and thawed *C. maltaromaticum* CNCM I-3298 (CM), *L. bulgaricus* ATCC 11842 (ATCC) and *L. bulgaricus* CFL1 (CFL1) cells, acquired in an aqueous environment in the 3016 cm^{-1} to 2800 cm^{-1} region: **a** PC1 versus PC2 score plots explaining 67 % and 11 % of variance, respectively; **b** PC1 versus PC3 score plots explaining 67 % and 4 % of variance, respectively; **c** loading plot of PC1, separating mainly CM from ATCC and CFL1 and indicating the heterogeneity provoked by freeze-thawing on L. bulgaricus cells and homogeneity of CM; **d** Mean spectra of the fresh and thawed cells used for the PCA. The characteristic absorption bands arising from fatty acid chains are indicated.....298

Figure III.3-A3: Principal component analysis (PCA) of FTIR spectra of fresh and thawed *C. maltaromaticum* CNCM I-3298 (CM), *L. bulgaricus* ATCC 11842 (ATCC) and *L. bulgaricus* CFL1 (CFL1) cells, acquired in an aqueous environment in the 1800 cm^{-1} to 1370 cm^{-1} range: **a** PC1 versus PC2 score plots explaining 82 % and 10 % of variance, respectively; **b** loading plot of PC1, separating mainly CM and ATCC from CFL1; **c** loading plot of PC2, indicates the changes in absorption bands from fresh to thawed cells; **d** Mean second derivatives of the spectra of fresh and thawed cells used for the PCA. The characteristic absorption bands arising from the protein backbone vibrations (Amide I and Amide II) and carboxyl groups of esters and nucleic acids are indicated.....299

List of Tables

PART I – LITERATURE REVIEW

Chapter I.1

Table I.1-1 : Examples of TTI devices that have been taken to market, their different categories and basic functioning principles. 32

Table I.1-2: A few studies reported on the development of various LAB-based TTI systems to monitor the quality and safety of perishable foods using different LAB strains. 34

Table I.1-3: Shelf-life (in days) of the TopCryo® TTI label range offered by Cryolog, as a function of storage temperatures 35

Chapter I.2

Table I.2-1: Culture conditions found in literature involving *Carnobacterium maltaromaticum* 54

Table I.2-2: Effect of culture conditions on the physiological state of LAB proposed for LAB-based TTI. 63

Chapter I.3

Table I.3-1 : Reported work on the investigation of cellular component modifications that have been related to an increase of the LAB survival rate following freezing or frozen storage 88

PART II – MATERIALS AND METHODS

Table II.2-1 : Compositions of main culture media and cryoprotectant solutions used in this work 106

Table II.5-1 : Assignment of main infrared vibrational bands in the 3000 – 975 cm^{-1} region of the infrared spectra of bacterial cells, according to literature. Bold references are works carried out on microorganisms. 124

PART III – RESULTS AND DISCUSSION

Chapter III.1

Table III.1-1: Culture conditions applied in published research involving *Carnobacterium maltaromaticum*. 140

Table III.1-2: Regression analysis of the acidification activity (dtpH1.5, in min) of *C. maltaromaticum* CNCM I-3298 cells harvested at increasing times during fermentations carried out at different temperatures and pH. 148

Table III.1-3: Regression analysis of viability (in CFU mL^{-1}) of *C. maltaromaticum* CNCM I-3298 cells harvested at increasing times during fermentations carried out at different temperatures and pH. 150

Table III.1-4: Mean-centered regression analysis of the acidification activity (dtpH1.5) of *C. maltaromaticum* CNCM I-3298 cells harvested at increasing times during fermentations carried out at different temperatures and pH. 154

Chapter III.2

Table III.2-1: Model parameters independent of operating conditions, determined from the experimental data of the experiment F10 (T=30 °C, pH=8) with tlag=10 h. 180

Table III.2-2: Model parameters determined for each experiment by nonlinear regression. 180

Table III.2-3: Optimal conditions for growth and production of metabolites according to the developed model. In bold: targeted metabolite for each set of operating conditions. Final concentrations and productivities calculated with initial conditions: $[X]_0$=80 $mmol.L^{-1}$, $[S]_0$=100 $mmol.L^{-1}$, $[F, A, L, E]_0$=0. 188

Chapter III.3

Table III.3-1: Reported work on the investigation of cellular components modifications that have been related to an increase of the LAB survival rate following freezing or frozen storage 198

Table III.3-2: Membrane fatty acid composition (relative percentages) of *C. maltaromaticum* CNCM I-3298, *L. bulgaricus* ATCC 11842 and *L. bulgaricus* CFL1

and cells. Values for *L. bulgaricus* ATCC 11842 and *L. bulgaricus* CFL1 were recalculated from raw data available from Meneghel et al. (2017). 214

Table III.3-3: Main parameters characterizing membrane lipid phase transition of *C. maltaromaticum* CNCM I-3298, *L. bulgaricus* ATCC 11842 and *L. bulgaricus* CFL1 cells obtained by monitoring the peak position of $\nu_s CH_2$ around 2850 cm^{-1} (Ts and $\nu_s CH_2$) and the upshift of the vibration water band from approx. 2100 to 2220 cm^{-1} during cooling (Tn) (**Fig. III.3-5**) 216

Table III.3-4: Summary of the markers of LAB cryoresistance put forward in this study, according to the analytical method employed 232

ANNEXES

Annex III.1

Table III.1-A1: dtpH1.5 (in min) and viability (in CFU mL^{-1}) measurements of freeze thawed *Carnobacterium maltaromaticum* CNCM I-3298 concentrates produced according to the culture conditions of the experimental design presented in Figure III.1-1 (B and C).....283

Annex III.2

Table III.2-A1: dtpH1.5 (in min) and viability (in CFU mL^{-1}) measurements of freeze thawed *Carnobacterium maltaromaticum* CNCM I-3298 concentrates produced according to the culture conditions of the experimental design presented in Figure III.1-1 (B and C).....285

Table III.2-A2: Response surface coefficients fitted to experimental data by multiple regression.....285

Table III.2-A3: Quality of fit of the model with parameters computed with the response surface models.....287

Annex III.3

Table III.3-A1: Assignments of main vibrational bands of the 3016—975 cm^{-1} region of the infrared spectra of the studied LAB, according to literature.....291

Table III.3-A2: Biological activity losses (culturability loss determined by plate counts method and acidification activity loss determined with the Cinac system (Corrieu et al. 1988)) following multiple freeze-thaw cycles of *C. maltaromaticum*

CNCM I-3298, *L. bulgaricus* ATCC 11842 and *L. bulgaricus* CFL1 and cells. For every freeze-thaw cycle, the loss was calculated versus the previous freeze-thaw cycle, as described in the Materials and Methods section of the manuscript. L. bulgaricus strains were protected with 20 % sucrose in saline water (weight ratio protective solution: cells = 1:1) and C. maltaromaticum with 20 % trehalose in saline water (weight ratio protective solution:cells = 1:2)……296

Table III.3-A3: Comparison of biological activity losses following one freeze-thaw cycle of *C. maltaromaticum* CNCM I-3298 cells protected with sucrose in similar conditions as *L. bulgaricus* ATCC 11842 and *L. bulgaricus* CFL1 strains (ratio cells:protective solution 1:1) and with trehalose at two different ratios (1:1 and 1:2)……297

Abbreviations & Nomenclature

Abbreviations

ATCC	American Type Culture Collection
ATR	Attenuated Total Reflectance
cFDA	Carboxyfluorescein diacetate
CFA	Cyclic Fatty Acid
CFU	Colony Forming Unit
CNCM	Collection Nationale de Cultures de Microorganismes (Pasteur Institute)
CPA	Cryoprotective Agent
CSP	Cold-Shock Protein
DMSO	Dimethyl sulfoxide
DNA	deoxyribonucleic Acid
DPH	1,6-diphényl-1,3,5-hexatriène
EPS	Exopolysaccharide
FA	Fatty Acid
FTIR	Fourier Transform Infrared Spectroscopy
GC-MS	Gas Chromatography coupled to Mass Spectrometry
HPLC	High Pressure Liquid Chromatography
HSP	Heat-shock Protein
INRAE	National Institute for Agricultural and Environmental research
IR	Infrared radiation
LAB	Lactic Acid Bacteria
MCT	Mercury Cadmium Telluride
MRS broth	Lactobacilli growth medium elaborated by Man, Rogosa and Sharpe in 1960
PG	Phosphatidylglycerol
RNA	Ribonucleic Acid
SFA	Saturated Fatty Acid
SR	Synchrotron Radiation
ssp	Subspecies
TTI	Time-Temperature Integrator
UFA	Unsaturated Fatty Acid

Nomenclature

List of symbols

a_w	Water activity
c	Speed of light (3.8 m s^{-1})
C12:0	Dodecanoic acid (= lauric acid)
C14:0	Tetradecanoic acid (= myristic acid)
C15:0	Pentadecanoid acid
C16:0	Hexadecanoic acid (= palmitic acid)
C16:1	Hexadecenoic acid [e.g., palmitoleic acid (cis-9 unsaturated)]
C17:1	Heptadecenoic acid
C18:0	Octadecanoic acid (= stearic acid)
C18:1	Octadecenoic acid [e.g., oleic acid (cis-9 unsaturated)]
C18:2	Octadecadienoic acid [e.g., linoleic acid (cis-9, cis-12 unsaturated)]
C19:0 cyc	Methylenoctadecanoic acid [e.g., dihydrosterculic acid (9,10 cyclization)]
E_a	Activation energy (J kg^{-1} K^{-1})
h	Plank constant (6.626 10^{-34} J.s)
k	Force constant of a chemical bond (N m^{-1})
M	molar (mol L^{-1})
mOsm	milliosmole
r	Fluorescence anisotropy
T	Temperature (°C)
Tg	Glass transition temperature (°C)
Tg′	Tg for maximally cryo-concentrated solutions (°C)
Tg′e	Extracellular Tg′ (°C)
Tg′i	Intracellular Tg′ (°C)
Tm	Lipid membrane phase transition temperature during heating (°C)
Tn	Water nucleation temperature (°C)
Ts	Lipid membrane phase transition temperature during cooling (°C)
§	Paragraph

Greek letters

δ	IR bending vibration modes
λ	wavenumber (cm^{-1})
ν	IR stretching vibration modes

Foreword

Fermentation is a food preservation method that has been used for centuries. It harnesses the ability of lactic acid bacteria (LAB) – among other microorganisms – to colonize and acidify their environment by producing lactic acid, therefore inhibiting the growth of pathogens and other spoilage micro-organisms. This technological property of LAB is still extensively used today to produce an array of fermented foods, such as yoghurt, cheese, cured meats, sauerkraut or kimchi. The market for LAB concentrates (starter cultures) has been booming, due to the growing selection of functional food products and supplements being developed, such as plant-based yoghurts and cheeses and probiotics (VitaFoods 2020). Additionally, this family of micro-organisms is of great significance in the ever-expanding biotechnological field as it is able to utilize various substrates from renewable resources to produce chemicals of high industrial interest (Mora-Villalobos et al. 2020). In recent years, the acidifying property of LAB is being used in biological time-temperature integrators, to track the shelf-life of perishable foods.

Time-temperature integrators (TTI) work as 'smart-labels' that relay, by an easily interpreted and irreversible sign, the time-temperature history and quality status of the food they are attached to. Biological TTI are usually based on the pH decline of the medium contained within the label, as a result of LAB growth and acidification. In the event of a 'thermal accident' (a more or less significant break of the cold chain), bacteria contained in the label will grow and acidify their environment, causing a color shift and/or an opacification reaction indicating significant alteration. The speed at which the TTI reaches its endpoint is thus dependent upon the growth and acidification kinetics of the strain, in response to a given time-temperature profile.

Cryolog Clock-°T (Nantes, France) is the only company that has ever taken biological TTI to market. Their labels rely on the growth and acidification of *Carnobacterium maltaromaticum* CNCM I-3298, a lactic acid bacterium commonly found in French soft cheeses and other high protein-containing foods such as smoked fish and meats(Cailliez-Grimal et al. 2007; Leisner et al. 2007). In their latest range of labels (TopCryo®), the growth of *C. maltaromaticum* induces a pH decline of the label medium, leading to a color shift from green to red (EU patent no. EP 1 664 334). *Carnobacterium maltaromaticum* concentrates used to inoculate TopCryo® TTI labels are produced like other LAB starters, by a succession of steps: fermentation, concentration, cryoprotection, stabilization (by freezing or freeze-drying) and storage until inoculation. To produce TTI labels, frozen concentrates

are thawed, and a certain volume of cell suspension is mixed into the label medium, depending on desired shelf-life (*i.e.*, low concentrations for long shelf-lives). The labels are then frozen and stored at -80°C until use. For activation, they are thawed at ambient temperature. The shelf-life of these labels are thus dependent on both cell concentration and their acidification activity. The shelf-lives covered by TopCryo® labels range from 30 h to 192 h (8 days) at 4 °C. The 30-hour shelf-life is reached by inoculating the label with the highest possible cell concentration, beyond which the TTI's initial color would no longer be green. The 8-day shelf-life is analogously achieved by inoculating the lowest cell concentration allowing reproducible acidification rates. The color shift response times of 30 hours and 8 days at 4 °C correspond thus respectively to the shortest and longest shelf-life achieved by TopCryo® labels. Many perishable foods, however, display shelf-life durations outside the range offered by Cryolog. Expiry dates for meat products, for example, vary between 3 to 21 days, and those of shellfish between 0.5 to 3 days (Dalgaard, 1995). In a desire to increase the shelf-life range of their TTI labels, Cryolog approached the ProBioSSep research group – in which I carried out most of my PhD work – to explore ways to modulate the growth and acidification activity of *C. maltaromaticum* CNCM I-3298 within their TTI labels.

ProBioSSep, is a research team mainly specialized in studying the production and stabilization of lactic acid bacteria. A lot of their work has been aimed at characterizing the impact of various culture conditions on the physiological state and technological properties of LAB concentrates such as acidification activity, but also resistance to industrial stabilization processes such as freezing and freeze-drying (Velly et al. 2014; Fonseca et al. 2015; Passot et al. 2015; Meneghel et al. 2017).
Among the possible ways of industrially preserving micro-organisms and maintaining their functionalities over long periods of time, freezing is one of the common techniques used today for the stabilization of lactic acid bacteria. Nevertheless, it exposes cells to severe stress that can lead to significant loss of biological activity (viability and acidification activity), depending on bacterial species or strain (Gomez Zavaglia et al. 2000; Fonseca et al. 2001). In the case of *C. maltaromaticum*, however, 11 freeze-thaw cycles were reported to have no significant effect on cell viability, indicating that the strain is extremely cryoresistant (Walker et al. 2006).

A four-year European RISE staff exchange program intitled PREMIUM was initiated in 2017 between five European academic partners and three European industrial partners: this project, coordinated by Fernanda Fonseca of ProBioSSep, is devoted to the study and development of innovative strategies for the long-term preservation of lactic acid bacteria, whilst considering product quality, process conditions and environmental impact (www.inrae.fr/premium). The activities of PREMIUM members are mainly focused on the understanding of the resistance

mechanisms of lactic acid bacteria to various stabilization processes, understanding the protective mechanisms exhibited by oligosaccharide-based cryoprotectants during the stabilization of cells, as well as developing high-throughput analytical tools for the characterization and screening of both cells and cryoprotectants. Among the initial industrial partners was Cryolog Clock-°T, offering *C. maltaromaticum* CNCM I-3298 as a model strain of cryoresistance within the project.

A year and a half into my PhD, Cryolog Clock-T° filed for bankruptcy. At that point, I had quantified the impact of three fermentation parameters (temperature, pH and harvest time) on the acidification activity of *C. maltaromaticum* concentrates, leading to a predictive model for the production of TTI inoculates that could likely expand the shelf-life range offered by Cryolog. Loss of funding from Cryolog, however, resulted in a re-focusing of my research towards the study of *C. maltaromaticum* within the scope of PREMIUM project.

Within this context, my Ph.D. work was initially aimed at improving the performances of *C. maltaromaticum* concentrates for use in biological time-temperature integrators and then the focus was veered towards exploring the cellular mechanisms expressed by *C. maltaromaticum* granting it its exceptional cryoresistance. In this respect, the first objective of my work was to study the physiological state modulation of *C. maltaromaticum* concentrates in response to changes in production conditions. The next objective was to characterize the remarkable cryoresistance of *C. maltaromaticum* cells comparatively to other lactic acid bacteria.

The foundations of my Ph.D. work were thus based on the following starting hypotheses:

- The culture conditions of *C. maltaromaticum* cells have an impact on the physiological state of the produced bacterial concentrates.

- Consequently, the shelf-life range of a biological TTI, such as those developed by Cryolog, can be extended by modulating the growth and acidification kinetics of its inoculum.

- Characterizing *C. maltaromaticum* cells in comparison to other less cryoresistant LAB, with a particular focus on their membrane, a known target of cryoinjury, can shed light on the cryoresistance mechanisms of lactic acid bacteria.

The present manuscript is divided into three main parts: a bibliographical review (**Part I**), a presentation of the experimental approach (**Part II**), a results & discussion section (**Part III**), followed by conclusions & perspectives.

I. The **LITERATURE REVIEW** focuses on the following four axes:
   Time-temperature integrators (**Chapter I.1**); *Carnobacterium maltaromaticum*, as key element of biological time-temperature integrators and model strain of cryoresistance (**Chapter I.2**); the cryopreservation of lactic acid bacteria (**Chapter I.3**).

II. The **EXPERIMENTAL APPROACH** gives a general description of the different methods used and parameters measured to conduct the research, as well as to which part of the results they were relevant to. This is followed by a more detailed description of the materials and methods used.

III. The **RESULTS & DISCUSSION** section presents the achieved results, separated into two main categories: a first category encompassing results around the physiological state modulation of *C. maltaromaticum* (**Chapters III.1 and III.2**) and a second category encompassing those improving our understanding of LAB resistance to freezing (**Chapter III.3**).

   - **CHAPTER III.1** shows the influence of culture conditions on the technological properties of *C. maltaromaticum* CNCM I-3298 starters. This study notably confirmed the strain's high cryoresistance and established a surface response model of the impact of temperature, pH and harvest time on the acidification activity of the produced concentrates.
   - **CHAPTER III.2** presents, through a dynamic growth and metabolite production model, the impact of temperature and pH on the metabolism of *C. maltaromaticum* during fermentation.
   - **CHAPTER III.3** presents the main differences observed between three LAB strains with varying levels of cryoresistance, among which *C. maltaromaticum*, confirming known markers of cryoresistance and proposing new ones.

Finally, the **CONCLUSION & PERSPECTIVES** section gives a summary of the main results of my Ph.D. work as well as perspectives for future research.

Part I
Literature review

I.1. Time-Temperature Integrators

Content

I.1.1. Time-Temperature Integrators (TTI) 31
I.1.1.a. General introduction 31
I.1.1.b. The different working principles of TTI 33
I.1.1.c. A focus on LAB-based TTI 33
I.1.2. Production and performance evaluation of LAB-based TTI 37
I.1.2.a. The industrial production of frozen lactic acid bacteria concentrates 37
(i) Fermentation medium preparation and sterilization 37
(ii) Pre-culture and inoculum preparation 37
(iii) Fermentation 37
(iv) Harvest and cooling 39
(v) Concentration and protection 39
(vi) Stabilization and storage 39
I.1.2.b. The industrial production of a LAB-based TTI label 39
(i) Label medium preparation and sterilization 39
(i) Starter activation and inoculation 39
(ii) Insertion of the medium within labels 41
(iii) Freezing, storage and reactivation 41
I.1.2.c. Performance evaluation of LAB-based TTI 41
I.1.3. Parametrization strategies 45
I.1.3.a. Adjusting initial starter concentrations 45
I.1.3.b. Modulating the physiological state of the selected strain 45
I.1.3.c. Tweaking the label medium's composition 46
(i) pH and chromatic indicators 46
(ii) Nutrient availability 46
(iii) Water activity 47
I.1.3.d. Using different bacterial species or strains, in pure or co-cultures 47
I.1.4. Concluding remarks 49

I.1.1. Time-Temperature Integrators (TTI)

I.1.1.a. General introduction

Most refrigerated perishable foods are not sterile. The microorganisms they contain can multiply, degrade their environment, and often produce unsavory metabolites. Their growth affects the microbiological quality of food and can lead to spoilage. Food quality thus evolves over time, more or less rapidly as a function of a number of parameters such as storage temperature, pH, water activity, gas composition, etc. Among these factors, temperature has the most critical effect on spoilage rates due to the significant temperature changes that can take place during transport and storage. Ensuring cold chain integrity, from production to consumption is therefore crucial to maintain and control the microbiological quality of refrigerated food. In practice, cold chain integrity is not always kept throughout production, distribution, and domestic storage. Breaking the cold chain can affect expected shelf-life, making it difficult to predict the microbiological quality and safety of food at the time of consumption. Food companies are responsible for the safety of products they have either imported, produced, processed, manufactured, or distributed (EFSA Regulation No. 764/2008). Consequently, excessively conservative estimations of shelf-life by actors of the food industry are frequent. They add substantial security margins that lead to considerable waste of perfectly good products. Among the countries of the European Union, annual food waste attributed to date marking issues was estimated to be between 6.9 and 8.9 million tones, across the manufacturing, processing, retail and household sectors (European Commission market study, 2018). The emergence of innovative technologies has therefore been encouraged by the European Union to help reduce food waste, while still ensuring consumer safety. Time-temperature integrators (TTI) can be considered as part of said innovative technologies, by offering a novel approach to improving food safety and preventing spoilage.

TTI are small, cost-effective devices that provide information on the microbiological quality of perishable foods, based on their true time-temperature history along the cold chain. TTI devices relay, by an irreversible and easily detectable sign, the cumulative effect of time and temperature on the food they are tracking. To be able to integrate all breaks of the cold chain during the food's entire lifecycle, and adjust shelf-life information accordingly, TTI generally come in the form of labels attached directly to the food's packaging.

Table I.1-1 : *Examples of TTI devices that have been taken to market, their different categories and basic functioning principles.*

Commercial name / company	Category	Functioning principle
Fresh-Check® and HEATmarker™ (TempTime, New Jersey, USA)	Chemical	Polymerization-based
OnVu® (BASF, Ludwigshafen, DE)	Chemical	Photochromic-based
Freshpoint® (Freshpoint Quality Assurance, Nesher, IS)	Chemical	Photochromic-based
Monitor Mark® (3M, St. Paul, MN, USA)	Physical	Diffusion-based
Tempix® (TEMPIX, Gävle, SE)	Physical	Diffusion-based
Tsenso® (Tsenso, Stuttgart, DE)	Physical	Electronic
Koovea® (Koovea, Montpellier, FR)	Physical	Electronic
CheckPoint® (Vitsab, Limhamn, SE)	Biological	Enzymatic
TopCryo® (Cryolog, Nantes, FR)	Biological	LAB growth

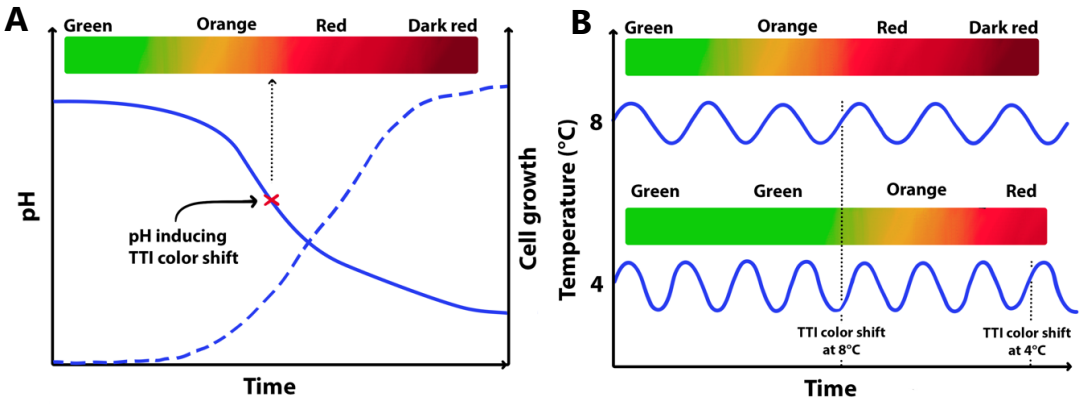

Figure I.1-1: (A) *Schematic representation of the growth (dotted line) and acidification activity (solid line) of LAB in a TopCryo® TTI label stored at 8 °C, inducing a color shift when a specific pH is reached;* ***(B)*** *the color shift's kinetic-dependence on the average temperature profile: at 4 °C the color shift takes place later than at 8 °C.*

I.1.1.b. The different working principles of TTI

Time-Temperature Integrator labels can be divided into three main categories, according to their working principles: chemical, physical or biological (**Table I.1-1**). The first group is comprised of polymerization-based, photochromic-based and oxidation reaction-based systems (Galagan and Su 2008; Salman et al. 2009; Gou et al. 2010). Physical TTIs encompass devices that are diffusion-based (Monitor Mark®, USA), nanoparticle-based, electronic, and so forth (Zweig 2005; Zeng et al. 2010). Biological TTIs are based on enzymatic reactions and/or the use of microorganisms such as yeasts and lactic acid bacteria (LAB) (Wang et al. 2015). Whatever its working principle is, a TTI's response is always strongly correlated to the time-temperature profile, within the tracked product's matrix.
Most of the commercialized TTI today are of the chemical or physical types (**Table I.1-1**), but biological TTI, and more specifically LAB-based TTI, are the ones that actually reproduce the microbiological reactions taking place in food, which lead to spoilage.

I.1.1.c. A focus on LAB-based TTI

The active core of biological time-temperature integrators based on lactic acid bacteria contains three main components: a growth medium, lactic acid bacteria, and a (or several) chromatic indicator(s). With these labels, alteration is generally determined by a progressive color shift brought about by a pH drop of the medium contained within the label, due to the growth and lactic acid production of LAB (**Fig. I.1-1A**). Quality loss kinetics of perishables foods greatly depend on the growth and metabolic activity of the microorganisms they contain which in turn, are heavily influenced by temperature. The influence of temperature on the color shift kinetics of a biological TTI label is illustrated on **Figure I.1-1B**: the endpoint of a TTI label tracking a food product stored, for example, on the door of a household refrigerator (typically 8 °C) will be reached twice as fast as one tracking a similar food product placed at the back of the refrigerator (typically 4 °C).
Microorganisms contained within TTI labels must have similar growth and/or metabolic activity responses to temperature variations, as selected microorganisms contained within the food being tracked (e.g. spoilage LAB, *Listeria monocytogenes*, *Staphylococcus aureus*, etc.). The underlying workings of these labels therefore rely on predictive microbiology: mathematical models of microorganism growth and

Table I.1-2: A few studies reported on the development of various LAB-based TTI systems to monitor the quality and safety of perishable foods using different LAB strains.

LAB used	Design of TTI system	Applicability and performance evaluation when available	References
Lactobacillus sakei	- Laboratory screw-cap bottles containing nutrient rich growth medium, chlorophenol red and microorganisms; - Activation at inoculation of TTI medium; - Color shift from red to yellow, via orange.	- Modelling of TTI evolution isothermally between 0 °C and 16 °C; - Shelf-life studies correlating TTI endpoint with end of minced beef shelf-life.	Vaikousi *et al.* 2008, 2009
Carnobacterium maltaromaticum	- Thin, self-adhesive label containing a gel like growth medium, chromatic indicators and microorganisms; - Activation by rapid freeze-thaw at room temperature; - Color shift from green to red.	- Modelling of the growth and acidification activity of the strain used within the TTI label medium, as a function of temperature, assuring accurate TTI response time; - Shelf-life studies and challenge tests done on ground beef, minced chicken and smoked salmon ensuring that TTI endpoint corresponds to the tracked food's shelf-life.	Ellouze *et al.* 2008, 2010, 2011 Louvet et al. 2005
Weissella cibaria	- Laboratory cell cultureware containing a nutrient rich growth medium, bromothymol purple, methyl red and microorganisms. - Activation at inoculation of TTI medium; - Color shift from purple to yellow.	Strong link between Ea* of the system's pH and color evolution and the quality degradation of ground beef and chicken breast.	Kim *et al.* 2012 Park *et al.* 2013
Weissella koreensis	- Laboratory test tubes containing MRS based growth medium, bromothymol blue, methyl red and microorganisms; - Color shift from green to red, via yellow.	- Strong link between Ea* of TTI system and the Ea of Korean fermented food (kimchi) evolution; - TTI system proposed to indicate ripeness of kimchi.	Lim *et al.* 2014
Lactobacillus ssp.	- Two-dimensional code made of nanobeads containing microorganism immobilized on a nutrient rich base; - Time-temperature effect translated into both a color shift and an easily scannable 2D code; - Must be stored below 5 °C, gradually activated between 5 and 15 °C.	Limited temperature range: 5 to 15 °C.	Lee and Jung 2013
Lactobacillus rhamnosus	- Transparent disk-shaped container including a nutrient rich growth medium, bromothymol green, methyl red and microorganisms.	Proposed for commercial, chilled products.	Lu *et al.* 2013

* Ea: The Arrhenius activation energy parameter, quantifying a reaction's dependency to temperature

metabolic activity as a function of various environmental conditions (temperature, pH, water activity, etc.). Examples of studies reported on the development of LAB-based TTI systems to monitor the quality and safety of perishable foods using different strains and various designs are presented in **Table I.1-2**. Although a few different examples of LAB-based TTI prototypes can be found in literature, only three have been taken to market to date: eO®, TRACEO® and TopCryo®. All three were developed and commercialized by Cryolog Clock-T° (Nantes, France) and rely on the growth of *Carnobacterium maltaromaticum*. The present chapter will thus use Cryolog's latest self-adhesive label, TopCryo®, as a concrete example to describe the design principle of a LAB-based TTI in more detail.

TopCryo® was patented in 2005 (Louvet et al. 2005) as a device intended to monitor the quality of thermosensitive products. Their active core contains chromatic pH indicators and a gel-like growth medium inoculated with *Carnobacterium maltaromaticum* CNCM I-3298 cells, a psychrotrophic lactic acid bacterium. TopCryo® labels are meant to operate within a temperature range of 2 °C to 12 °C, whilst integrating breaks of the cold chain. *C. maltaromaticum* cells contained within the label multiply and acidify the growth medium. The acidification results in a color shift from bright green (pH > 8) to deep red (pH < 6.5), more or less rapidly, depending on the label's time-temperature history (**Fig. I.1-1B**). TopCryo® labels are designed to cover different shelf-lives, ranging from 30 hours to 8 days (192 hr) at 4 °C (**Table I.1-3**), depending on the type of food that needs to be tracked.

Table I.1-2: Shelf-life (in days) of the TopCryo® TTI label range offered by Cryolog, as a function of storage temperatures.

TopCryo®	Storage temperature				
label range	2°C	3°C	4°C	8°C	12°C
TopCryo® B	2.1	1.5	1.3	0.8	0.5
TopCryo® C	3.2	2.4	2.0	1.1	0.8
TopCryo® D	4.7	3.5	3.0	1.7	1.0
TopCryo® E	5.9	4.7	4.0	2.3	1.3
TopCryo® F	7.7	5.9	5.0	2.4	1.7
TopCryo® G	9.0	7.0	6.0	3.3	1.9
TopCryo® H	10.6	8.2	7.0	3.9	2.3
TopCryo® I	12.2	9.3	8.0	4.4	2.7

Information obtained from the Cryolog website (http://cryolog.com/topcryo), January 2019.

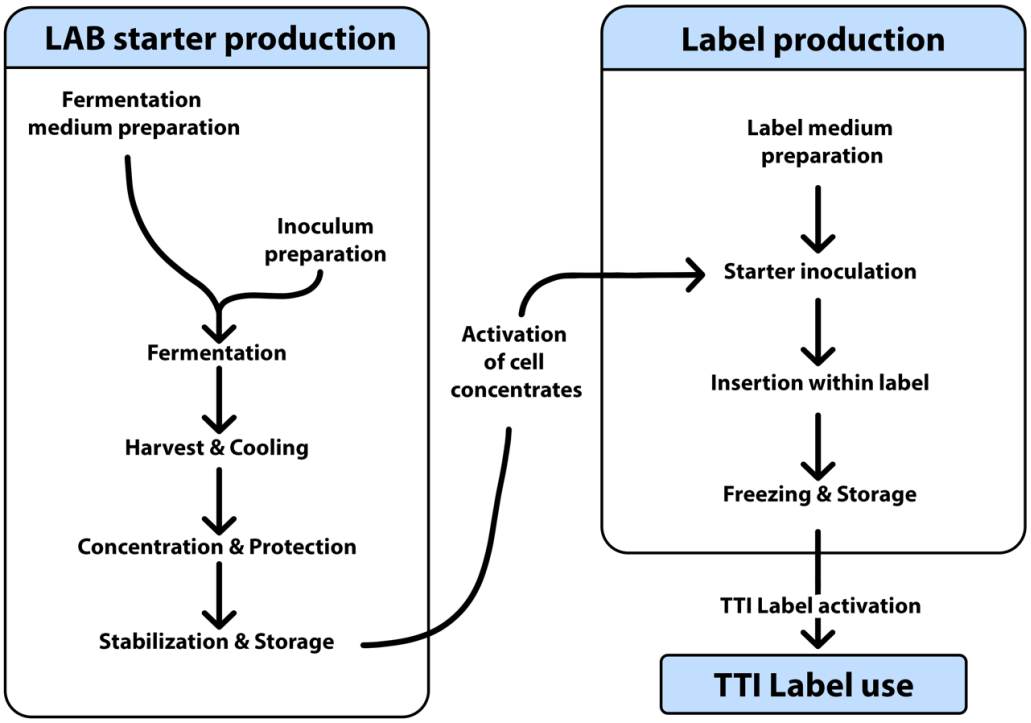

Figure I.1-2: *Diagram of industrial LAB concentrate and LAB-based TTI label production steps*

I.1.2. Production and performance evaluation of LAB-based TTI

Producing a LAB-based TTI involves two main processes: the production of frozen lactic acid bacteria concentrates followed by the production of the TTI labels themselves **(Fig. I.1-2**). The following description of a TTI label production is based on Cryolog's production of TopCryo® labels (personal communication from Cryolog Clock-T°).

I.1.2.a. The industrial production of frozen lactic acid bacteria concentrates

(i) Fermentation medium preparation and sterilization

Lactic acid bacteria have complex nutritional requirements, and their production often demands growth in nutritionally rich media containing one or more carbon sources, nitrogenous compounds, minerals, and vitamins. The fermentation medium is sterilized to avoid contamination of the bacterial culture and its pH is adjusted according to the chosen fermentation protocol.

(ii) Pre-culture and inoculum preparation

Most strains used to inoculate bioreactors are stored frozen (-80°C) or freeze-dried (-20°C or 4°C) and are respectively reactivated by thawing or rehydration. The pre-culture cell suspension is prepared in an adequate growth medium – usually similar or identical to the fermentation medium – then incubated at an optimal temperature for growth. This step can be serially repeated in increasing volumes of growth medium until a high enough cellular concentration is reached.

(iii) Fermentation

This is the key step in the production of LAB concentrates. It is generally done in pure culture and batch mode. The inoculation rate varies between 0.1 and 1% depending on the volume of equipment available and the cultivation times envisaged. The volume of pre-culture inoculated into the bioreactor is determined to obtain an initial cell concentration sufficient to achieve an acceptable latency time. Different parameters are controlled – such as pH, temperature, agitation, and dissolved oxygen partial pressure (pO_2) – and set to values that result in the growth of the highest viable bacterial population (biomass) exhibiting the expected technological properties. Growth and acidification activity are monitored throughout fermentation, by measuring optical density (OD) and the volume of neutralizing agent needed to stabilize the pH at a chosen value, respectively.

(iv) Harvest and cooling

During fermentation, bacteria go through different growth phases at which they exhibit varying physiological states. For use in TTI, the physiological state of LAB is considered to be characterized by cell viability (cultivability) and the acidification activity of the cell concentrates. The time of harvest is therefore a factor impacting the final viability and acidification activity of the harvested cells. The harvested cell suspension is cooled to a temperature that slows down metabolic activity, to preserve the physiological state exhibited by the microorganisms in the bioreactor, at the time of harvest.

(v) Concentration and protection

Centrifugation is used to separate the cells from their culture medium, as well as to concentrate them. The obtained cell pellets are resuspended in a cryoprotectant solution containing various substances such as polyols, polysaccharides and disaccharides, meant to reduce cell damage caused by the following stabilization step and storage.

(vi) Stabilization and storage

This step is aimed at halting metabolic activity and stabilizing cellular structures for the long-term storage of the bacterial concentrates (6 to 24 months), without losing cell viability or acidification activity. Freezing is currently the most used stabilization technique for LAB, although freeze-drying is also industrially practiced. Storage of frozen concentrates is generally done between -50°C and -80°C.

I.1.2.b. The industrial production of a LAB-based TTI label

(i) Label medium preparation and sterilization

The label medium composition is tailored to the desired metabolic activity of the strain that is to grow in the TTI and induce the color shift. In TopCryo®, the label medium is composed of a gel-like nutrient rich medium suitable for the growth of LAB, additives such as glycerol or salts, and food-grade chromatic pH indicators. The medium is then heat sterilized to avoid contamination.

(i) Starter activation and inoculation

The stored frozen starter concentrates (*C. maltaromaticum* CNCM I-3298 cells, in the case of TopCryo®) are thawed, and a precise concentration of reactivated cells is inoculated into the TTI label medium, depending on the targeted shelf-life.

(ii) Insertion of the medium within labels

For TopCryo® labels, this is achieved using a specially designed and patented equipment that seals the medium into self-adhesive labels (Vaillant and Peteuil, 2012).

(iii) Freezing, storage and reactivation

Inoculated labels are inactivated by blast freezing and stored at -40°C until use. Re-activation is achieved by rapid thawing at ambient temperature, upon placing the label on the food to be tracked.

I.1.2.c. Performance evaluation of LAB-based TTI

In many of the studies proposing biological TTI prototypes (**Table I.1-2**), the Arrhenius activation energy (Ea, in kJ/mol.K) indicating temperature sensitivity of the TTI's response is used as the main performance evaluation parameter (Vaikousi et al. 2009, Kim et al. 2012, Lim et al. 2014). According to this approach, a TTI is considered performant if it presents similar Ea response values as the spoilage reaction being tracked. However, relying solely on activation energy values is not sufficient to prove the applicability of a system intended to track the microbiological quality of specific perishable foods. In order to properly evaluate performance and be granted a take-to-market authorization, a LAB-based TTI must undergo rigorous testing similarly to shelf-life date labels: durability studies and challenge tests.

To determine shelf-life, food business operators generally start by consulting predictive microbiological models to estimate the microbiological quality evolution of a product. While these models provide good estimations of spoilage kinetics by taking into account composition and manufacturing processes, they are developed assuming consistent microbial responses in very controlled environments and can thus sometimes fail to accurately predict microbial responses and variations in a complex food matrix. This first shelf-life estimation must therefore be followed by durability studies. Durability studies (or storage tests) are conducted by quantitatively determining growth of target spoilage and pathogenic microorganisms within the food product, under "reasonably foreseeable conditions of distribution, storage and use" (European Commission Regulation No. 2073/2005). A recommended temperature scenario or reference profile is to maintain the food product one third of its estimated shelf-life time at 4 °C and two thirds at 8 °C. For highly perishable foods that may contain pathogens such as *Listeria monocytogenes*, EU guidelines recommend additional challenge tests. Challenge tests are similar to the durability studies mentioned above, with the difference being that specific cold-tolerant pathogens

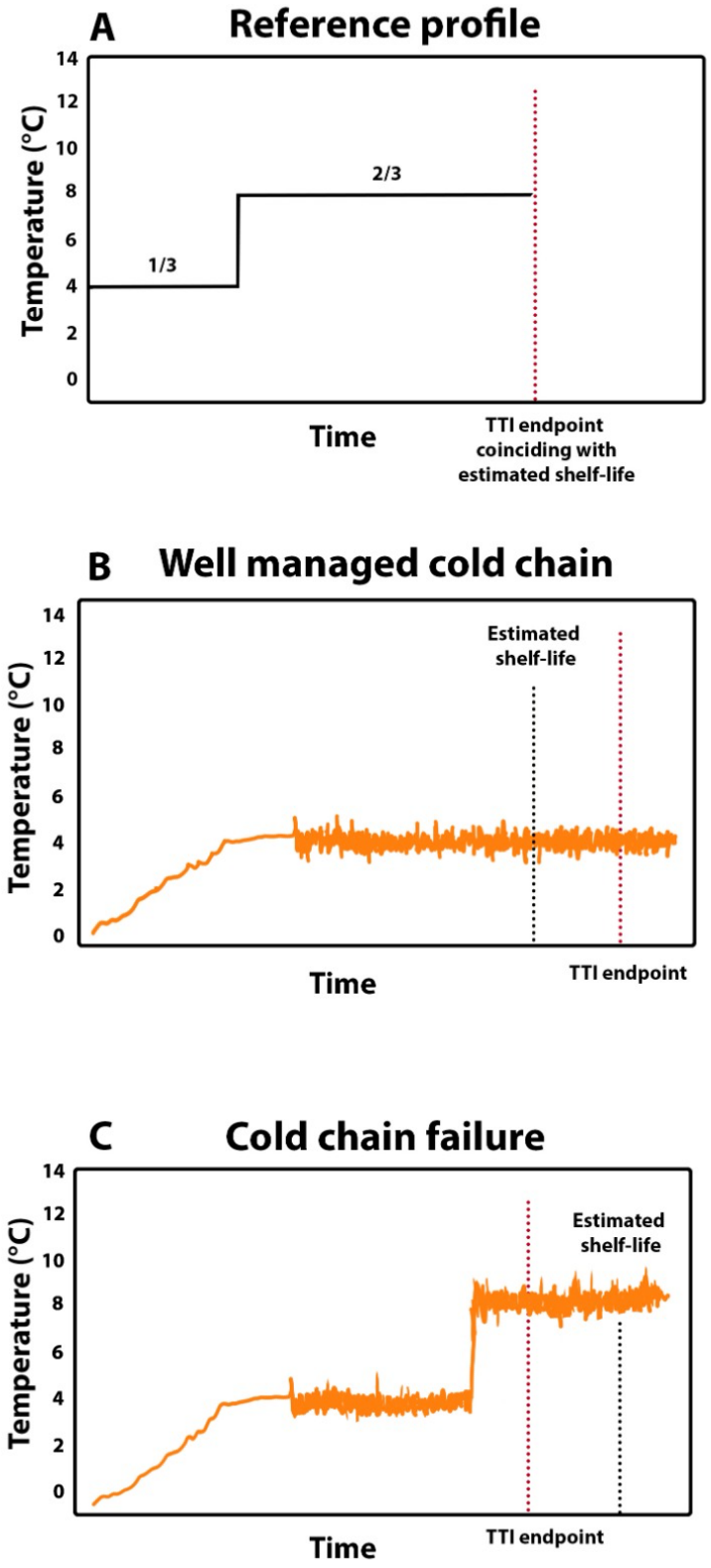

Figure I.1-3: *Simulation of different, realistic storage conditions used to evaluate LAB-based TTI performance. Adapted from Ellouze et al. 2010 and 2011.*

are added to the food product before it is packaged. This is especially important when the microorganism's environment within the food product (chemical characteristics, temperature, a_w, *etc*.) is close to its growth/no growth limit.

The applicability of Cryolog's commercialized TTI was evaluated with both durability studies and challenge tests using ground beef, cooked chicken and smoked salmon (Ellouze et al. 2010, 2011). These food products and their corresponding TTI labels were exposed to three dynamic temperature profiles (**Fig. I.1-3**):

A. A reference profile that was used to estimate shelf-life: one third of the time at 4 °C and the rest of the time at 8 °C;

B. A well-managed cold chain scenario with temperature fluctuations averaging below the reference condition (4°C);

C. A cold-chain failure scenario with temperature fluctuations averaging well above reference condition.

For each temperature profile, the growth of endogenous food microorganisms and added pathogens was evaluated at the end of the estimated shelf-life and the TTI's endpoint (Ellouze et al. 2010, 2011). Results showed that for the first profile (reference profile, **Fig. I.1-3A**), the TTI endpoint coincided with the estimated shelf-life, confirming proper TTI parametrization according to current established guidelines within the food industry. For the second temperature profile (well managed cold chain, **Fig. I.1-3B**), the TTI endpoint came after the estimated shelf-life, but still, before pathogenic or spoilage microorganism levels reached consumption limits. This scenario thus demonstrates how TTI can contribute to reducing food waste. In the third profile (cold-chain failure, **Fig. I.1-3C**), the TTI endpoint was reached before the estimated shelf-life, thus evidencing how the use of TTI can help avoid consumption of potentially spoiled food. Cryolog thus successfully proved their TTI system's ability to integrate the time-temperature history of highly perishable foods and adjust shelf-life information accordingly. This is an example of how such smart devices can contribute to reducing food waste (**Fig. I.1-3B**), without compromising food safety (**Fig. I.1-3C**).

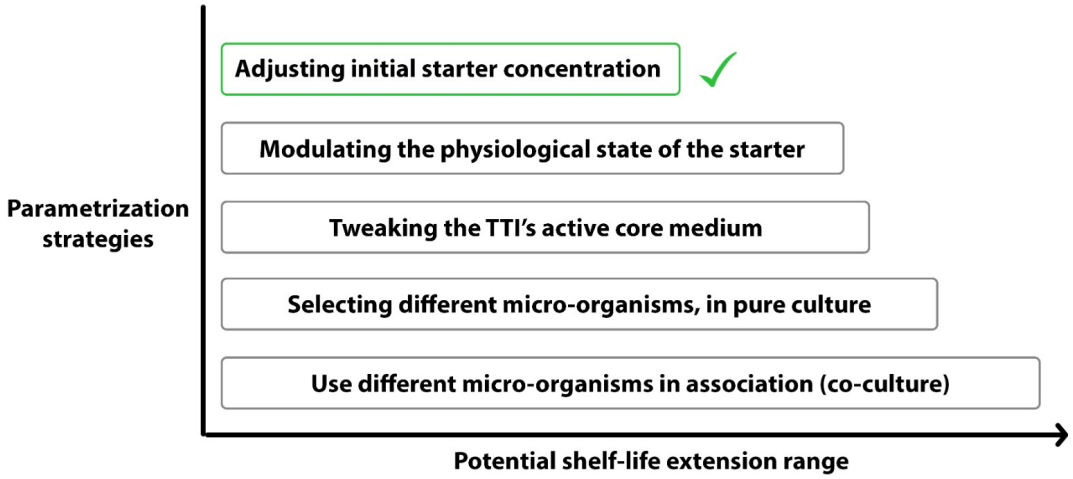

Figure I.1-4: Schematic representation of biological TTI parametrization strategies and their expected potential shelf-life extension ranges. The ✓ marks the only parametrization strategy currently used in commercialized LAB-based TTI

I.1.3. Parametrization strategies

Lactic acid bacteria-based TTI parametrization consists in identifying the production conditions for achieving a target shelf-life. The five different parametrization strategies that can be pursued to modulate the response time of a LAB-based TTI are, in increasing shelf-life range coverage potential (**Fig. I.1-4**): (1) adjusting initial starter concentration; (2) modulating the physiological state of the selected starter; (3) tweaking the label medium's composition; (4) using a different bacterial strain or species in pure culture or (5) using different microorganisms in co-cultures. A more detailed description of each strategy is presented below.

I.1.3.a. Adjusting initial starter concentrations

So far, much of TTI shelf-life modulation – such as the range covered by TopCryo® labels – is achieved by adjusting the initial starter concentration inoculated into the label. There is a linear relationship between initial cell concentration and the label's shelf-life response time. Topcryo®'s 8-day (192 hr) shelf-life at 4 °C (TopCryo® I) is reached by inoculating the lowest *C. maltaromaticum* cell concentration allowing reproducible acidification rates. The 30-hour shelf-life is analogously achieved by inoculating the highest possible cell concentration into the label, beyond which the TTI's initial color would no longer be green. The color shift response times of 30 hours and 8 days at 4 °C correspond thus respectively to the shortest and the longest shelf-life that can be achieve by these labels. However, time-temperature integrators are ideally meant to track the microbiological quality of different food types displaying varying lengths of shelf-lives outside of the range offered by TopCryo®, such as 3 to 21 days for various meats and 0.5 to 3 days for shellfish (Dalgaard, 1995). To be used at a much larger scale, LAB-based TTI are therefore expected to cover a wider shelf-life range than they have been able to cover thus far.

I.1.3.b. Modulating the physiological state of the selected strain

The succession of steps involved in LAB industrial starter production is generally optimized to achieve the highest possible yield of concentrated cells exhibiting high metabolic activities. In productions intended for TTI labels however, other objectives can be pursued: production parameters can be chosen according to the response time needed to be covered by the TTI label. For long shelf-lives, the starters inoculated into the label must indeed harbor slow acidification activities, while high acidification rates lead to labels exhibiting short shelf-lives. As it is known that physiological state

modulation of LAB is highly dependent on their fermentation parameters (temperature, pH, fermentation duration, medium composition, *etc.*) (van de Guchte et al. 2002), these can be changed to favor the production of cells presenting the desired metabolic activity.

I.1.3.c. Tweaking the label medium's composition

(i) pH and chromatic indicators

The initial pH of the TTI medium and the choice of chromatic indicator it contains, greatly influences the time it takes for the color shift to occur. In TopCryo® labels for example, the chromatic pH indicator shifts from green to dark red at pH 6.5. In Vaikousi's proposed prototype (Vaikousi et al. 2008), the pH indicator (chlorophenol red), shifts from red to yellow at pH 5.2. In both TTI systems the higher the initial pH is, the longer it will take for the color shift to occur, at a given acidification rate. At equal initial pH values (*e.g.* pH 8.5), however, the color shift of the TopCryo® label will happen faster than the one of Vaikousi's prototype. Color shift response times can thus be modulated by either increasing or decreasing the initial pH of the label, or by using different chromatic indicators.

(ii) Nutrient availability

Nutrient availability within the TTI label medium could also be a response time modulation lever. Indeed, lactic acid bacteria are known to have many nutritional requirements and their production often demands growth in nutritionally rich environments. Most nutritional studies performed on LAB are focused on maximizing growth rates and/or metabolic activity. In the case of a TTI application, research on nutritional levers that either accelerate, or slow down metabolic activity are both relevant when developing a large range of shelf-life response times. LAB growth requires first and foremost the presence of a carbon source through carbohydrates, their main energy source. The nature of the carbohydrates (monosaccharides, disaccharides, pentoses, hexitols or penitols) varies according to the considered species or strain and sometimes even between strains. It is frequent for a strain to be able to catabolize more than one type of carbohydrate, but its growth and metabolic kinetics will change depending on the available type. In a study aimed at investigating the growth and metabolic performances of *L. sakei* strains on different carbon sources, it was shown that using ribose as a sole carbon source decreased growth and increased acetate production compared to glucose (McLeod et al. 2010). Changing the nature of the carbon source within the TTI label medium can thus have an impact on the growth and/or acidification activity rates of the selected strain, therefore resulting in the

adjustment of the TTI's response time. Nutritional studies have also shown that LAB growth can be stimulated by the addition of ingredients rich in amino acids and small peptides, such as yeast extract or peptone. *C. maltaromaticum* for example exhibits substantially faster growth in milk when it is enriched with 1 g L^{-1} of yeast extract (Edima et al. 2007). Similarly, certain vitamins and nitrogenous bases were shown to stimulate growth, although requirements vary greatly even between strains of the same species. This was clearly evidenced in a study aimed at screening for vitamin and amino acid requirements on 24 *Lactobacillus plantarum* strains, where a very high diversity of requirements between strains was demonstrated (Ruiz-Barba and Jiménez-Díaz 1994). Even if generally time consuming, great potential for TTI shelf-life modulation can thus arise from modifying nutrient availability in the TTI medium.

(iii) Water activity

One of the oldest methods of preventing food spoilage is limiting the available water required for the growth of microorganisms by reducing water activity (a_w). Adjusting the a_w of an aqueous growth medium is often done by the addition of salts, saccharides, or polyols. Glycerol, for example, is miscible with water at any molar ratio and can thus change the a_w of an aqueous solution from 0.0 to 1.0 (Marcolli and Peter 2005). Growth rate and maximum viability reductions, as well as acidification activity modulations are observed in LAB when a_w levels are reduced from 0.99 through 0.95 or 0.93, depending on the species and compounds used to lower water activity (Ruiz-Barba and Jiménez-Díaz 1994).

Tweaking a TTI's medium composition therefore offers many possibilities to modulate a biological TTI's shelf-life response time and consequently, widen the shelf-life range that can be achieved by a single strain. There are however various technological and design constraints linked to label production at industrial scale that must be considered, such as viscosity, cost, consumer behavior, *etc*.

I.1.3.d. Using different bacterial species or strains, in pure or co-cultures

In addition to being dependent on initial cell concentrations, TTI response time evidently relies on the inherent growth and acidification kinetics of the selected lactic acid bacteria. Another strategy to widen the covered range of shelf-life is to switch bacterial species entirely.

Due to their diversity, lactic acid bacteria exhibit very different growth and acidification kinetics, depending on the considered genus, species or strain, on whether they are homo or hetero-fermentative and on their culture conditions. Homofermentative LAB,

such as *Lactobacillus bulgaricus* or *Lactococcus lactis*, are widely used in the dairy industry because they exclusively metabolize sugars into lactic acid (pKa = 3.86), resulting in high acidification activities. Heterofermentative LAB however, tend to have much slower acidification activities because their fermentation of sugars results in numerous other metabolites, including acids that might not have the acidification power of lactic acid, such as acetic acid (pKa = 4.76), butyric acid (pKa = 4.82) or propionic acid (pKa = 4.88) and ethanol. Proportions among different produced metabolites may also vary depending on the microorganism and applied fermentation conditions.

LAB used in biological TTI must however follow certain conditions. They need to grow within the storage temperature range of perishable foods (typically between 0 and 30 °C) and their growth and metabolic activity must be highly dependent on temperature, allowing an accurate monitoring and recording of all temperature variations throughout the product's shelf-life. Additionally, growth must not be inhibited by the pH-indicator of shelf-life. Furthermore, most LAB-based TTI developed to date use psychrotrophic strains that present growth rates similar (or slightly higher) to those of main pathogenic and spoilage bacteria contained within the food being tracked (*e.g. Lysteria monocytogenes)*. This way, the TTI endpoint is attained before the growth of those microorganisms reaches unacceptable levels. All the LAB strains that have been proposed in biological TTI systems (**Table I.1-2**) are commonly found in food or used in the food industry. *Carnobacterium maltaromaticum* is a strain commonly found in French soft cheeses (Cailliez-Grimal et al. 2007). *Lactobacillus sakei* is used in various fermented meats such as *saucisson* (French dry cured sausage). This strain has been shown to inhibit *Listeria monocytogenes* in chicken cold cuts (Katla et al. 2002) and also to present similar kinetic behaviors as many spoilage bacteria of meat products (Vaikousi et al. 2009). *Lactobacillus rhamnosus is* known for its probiotic properties (Saad et al. 2013) and *Weisella cibaria* is commonly isolated from fermented foods and increasingly being investigated to be used as a starter for sourdough and vegetable fermentation (Ricciardi et al. 2009).

An additional approach to further extend TTI response ranges would be to investigate the use of co-cultures. Bacterial cultures applied in food fermentations mostly consist in consortia involving multiple species and/or strains, where each member is affected by the growth and metabolism of the other. A perfect example of this is the yoghurt consortium, consisting of a protocooperation between *Streptococcus thermophilus* and *Lactobacillus delbrueckii subsp. bulgaricus*. In milk fermentation to produce yoghurt, the first microbial exponential growth phase is the

one of *S. thermophilus*, a species that is more tolerant to neutral pH and more effective at metabolizing amino acids and trace elements than *L. bulgaricus* (Sieuwerts 2016). The growth of *S. thermophilus* results in medium acidification, reduction of oxygen and increase of CO_2 concentrations, thereby creating a favorable environment for the more acidophilic, less oxygen tolerant *L. bulgaricus* (Sasaki et al. 2014). The combination potential between two or more microorganisms within a TTI is immense, as microbial interactions are governed by a multitude of molecular and physiological mechanisms. Still, systematic optimization and repeatability studies are required to choose and confirm the applicability of new bacterial species in a biological TTI system. Moreover, the process of acquiring a take-to-market authorization for a single or a combination of species are both long and expensive. Mapping the range of shelf-lives that can be achieved with a selected strain as well as screening new strains and co-culture exploration must therefore be concurrent R&D activities.

I.1.4. Concluding remarks

Time-temperature integrators are devices that are not meant to simply report a temperature limit breach but to translate all inevitable temperature variations experienced by perishable foods, from production to distribution, into an easy-to-read consumer indication. They thus integrate the time and temperature history of the product they are tracking and adjust its shelf-life information accordingly. Among the different types of TTI systems developed to date, biological TTI have the advantage of basing their response upon the same, temperature dependent, microbial growth and metabolic activity that causes food spoilage and end of shelf-life.

A lot of work has yet to be carried out in biological TTI research and in overcoming regulatory obstacles that keep this technology from being fully deployed within the food industry. Furthermore, the only biological TTI system ever taken to market, offers a limited range of shelf-life (30 hours to 8 days, at 4 °C). This shelf-life range is achieved by adjusting the initial starter concentration of the labels. To further extend this range, without changing the bacterial strain used and minimize technological constraints on label production, the most straight forward way would be to modulate the growth and acidifying activity of *C. maltaromaticum* in the TTI label. The following chapter will thus focus on *C. maltaromaticum* and on ways that its acidifying activity could be modulated.

I.2. *Carnobacterium maltaromaticum*

Content

I.2.1. General characteristics 53
I.2.1.a. Taxonomy and known physiological attributes of *C. maltaromaticum* 53
I.2.1.b. Cellular envelope structures and functions in Gram-positive LAB 57
(i) The cell wall 57
(ii) The cytoplasmic membrane 59
I.2.1.c. The intracellular content 61
(i) The cytoplasm 61
(ii) Bacterial DNA, RNA, and plasmids 61
(iii) Cytoplasmic proteins 62
I.2.2. Modulating the technological properties of LAB for industrial applications 62
I.2.2.a. Impact of the fermentation medium composition 64
I.2.2.b. Impact of fermentation temperature and pH 64
(i) Fermentation temperature 64
(ii) Fermentation pH 65
I.2.2.c. Impact of fermentation duration (harvest time) 67
I.2.3. Other useful technological properties of *C. maltaromaticum* 69
I.2.3.a. Potential cheese ripening flora 69
I.2.3.b. Food bio-preservation properties 69
I.2.3.c. A model of lactic acid bacteria cryoresistance 70
I.2.4. Concluding remarks 71

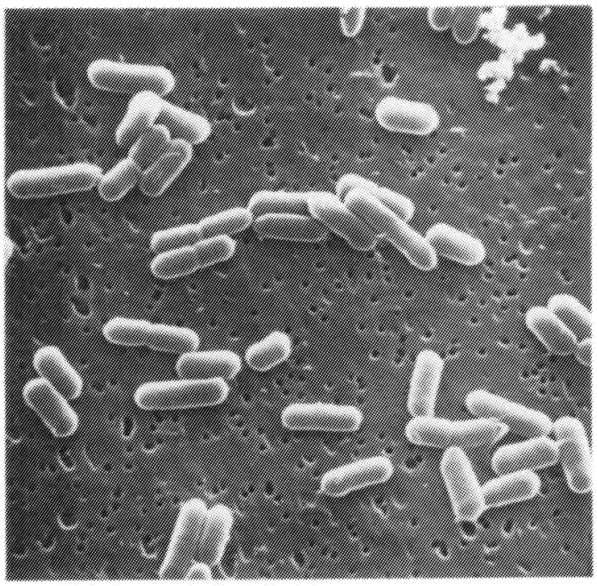

Figure I.2-1: Electron micrograph of Carnobacterium maltaromaticum DSM 20730 cells, taken from Schillinger and Holzapfel (1995)

Formerly thought of as a lactic acid bacterium of poor industrial interest, *Carnobacterium maltaromaticum* has little by little proven to exhibit interesting technological properties such as bacteriocin production and potential role in food bio-preservation (Leisner et al. 2007), or the ability to biosynthesize flavorful compounds (Afzal et al. 2010). In more recent years, *C. maltaromaticum* has proven itself to be a key element of current LAB-based TTI development. Despite a clear industrial potential, a lot is still to be discovered about this strain compared to other LAB strains currently used in the food industry.

I.2.1. General characteristics

I.2.1.a. Taxonomy and known physiological attributes of *C. maltaromaticum*

Carnobacteria are Gram-positive, non-motile, non-sporulating, facultatively anaerobic, catalase negative lactic acid bacteria (Afzal et al. 2010). *Carnobacterium* species form a phylogenetically coherent group on the basis of 16S RNA and can be separated into two ecological groups: 7 species isolated from high protein foods (*C. divergens, C. gallinarum, C. inhibens, C. jeotgali, C. maltaromaticum, C. mobile, C. viridans*) and 5 species isolated from cold environments such as Antarctic ice lakes (*C. alterfunditum, C. funditum, C. antarcticum, C. iners*) and permafrost (*C. pleistocenium*) (Leisner et al. 2007). They are short to medium length, straight, slender rod-shaped cells which generally occur singly or in pairs (**Fig. 1.2-1**). Cell size varies between 0.5 and 0.7 µm in diameter and 1.1 and 3.0 µm in length (Schillinger and Holzapfel 1995).

Carnobacteria are considered to be homofermentative lactic acid bacteria that produce lactic acid from glucose, with pyruvate as a central metabolic intermediate (via the Embden-Meyerhof pathway) (De Bruyn et al. 1987; De Bruyn et al. 1988; Leisner et al. 2007). However, pyruvate may be alternatively converted to acetate, ethanol, formate, and CO_2 (De Bruyn et al. 1988; Schillinger and Holzapfel 1995) under anaerobic conditions and substrate limitation (Gänzle 2015), arising for example at the end of fermentation (Ward 2015). The production of organic acids by Carnobacteria is also strain dependent (De Bruyn et al. 1988; Borch and Molin 1989; Laursen et al. 2006). The first representative of the *Carnobacterium* genus was described in 1983 by Holzapfel and Gerber as *Lactobacillus divergens*; a name suggesting physiological characteristics that "deviate" from other lactobacilli.

Table I.2-1: *Culture conditions found in literature involving* Carnobacterium maltaromaticum.

Strains	Fermentation conditions					References
	Medium	***Atmosphere***	***T (°C)***	***pH***	***Harvest time***	
C. maltaromaticum 3	Yeast extract, proteose peptone, thiamine, glucose	aerobic	25	6.0	NA	Borch and Molin, 1989
C. maltaromaticum LMA 28, LMA 29, LMA 30, DSMZ 20730	TSB-YE broth	aerobic	30	unregulated	NA	Calliez-Grimal *et al.,* 2007; Edima *et al.,* 2008; Rahman *et al.,* 2014, 2016
C. maltaromaticum CNCM I-3298	BHI broth	aerobic	1.75 to 35	5.1 to 10.4	NA	Ellouze *et al.,* 2008
C. maltaromaticum C2, A9b^{+}, A9b^{-}	BHI broth modified with fish peptone	aerobic	25	unregulated	24 h	Dos Reis *et al.,* 2011
C. maltaromaticum LMA 28	TSB-YE broth	aerobic	30	unregulated	End of exponential phase	Afzal *et al.,* 2012
C. maltaromaticum LMA 28	MCGC broth (synthetic minimal medium)	varied DOC 0 % to 90 %	30	6.8	NA	Afzal *et al.,* 2013
C. maltaromaticum (10 strains isolated from vacuum packaged meat)	BHI, lactic acid, sodium acetate	aerobic	30	unregulated (initial pH: 5.4, 6.2, 7.4)	NA	Zhang *et al.,* 2018

One of the deviating characteristics was the ability of the *Carnobacterium* subsp. to grow at high pH levels (pH 9). Additionally, Carnobacteria are inhibited by acetate. They can therefore not grow in the commonly used enumeration media for LAB such as Man, Rogosa and Sharp (MRS) agar, suggesting that their occurrence in foods is likely underreported (Leisner et al. 2007).

Among the *Carnobacteria* species isolated from food, *C. maltaromaticum* and *C. divergens* are considered to have food bio-preservative potential by preventing the growth of *Listeria monocytogenes* – a known psychrotrophic pathogen – in a variety of refrigerated food products (Buchanan and Klawitter 1991; Barakat et al. 2000). Their anti-*Listeria* properties stem from their similar behavior to *L. monocytogenes* towards temperature and pH (microbial competition), in addition to their ability to produce bacteriocins and peptides that are antagonistic to other closely related bacteria (Brillet et al. 2004; Leisner et al. 2007).

Carnobacterium maltaromaticum (formerly known as *Carnobacterium piscicola*) has been commonly found in foods such as dairy, meat, fish and shrimp (Cailliez-Grimal et al. 2007; Leisner et al. 2007). Because of its slow acidifying capabilities compared to commercial starter LAB (Edima et al. 2007), it has generated little industrial interest. The few studies that have performed *C. maltaromaticum* cultures have done so at laboratory scale, in generic LAB culture media and mostly at unregulated pH values, or within a restricted range of pH (pH 6 to pH 6.8) (**Table I.2-1**).

The cardinal values of *C. maltaromaticum* CNCM I-3298 were assessed in brain heart infusion (Ellouze et al. 2008) and while exact values may change depending on the culture medium, they illustrate the broad range of temperature and pH in which *C. maltaromaticum* grows: -5 °C to 36 °C and pH 5 to pH 10. This strain is thus considered psychrotrophic (capable of growing below 7 °C) and alkaliphilic (capable of growing above pH 9). Although *C. maltaromaticum* can cause disease in fish (Leisner et al. 2007), there is only one reported case of *C. maltaromaticum* being involved in human infection (Chmelař et al. 2002). To date, two strains of *C. maltaromaticum* have been authorized for use in or around food: *C. maltaromaticum* CB1, that was classed as GRAS (Generally Recognized as safe, GRN 00159) for ready-to-eat meat products and *C. maltaromaticum* CNCM I-3298, that acquired EFSA (European Food Safety Authority) approval to be used in commercialized TTI.

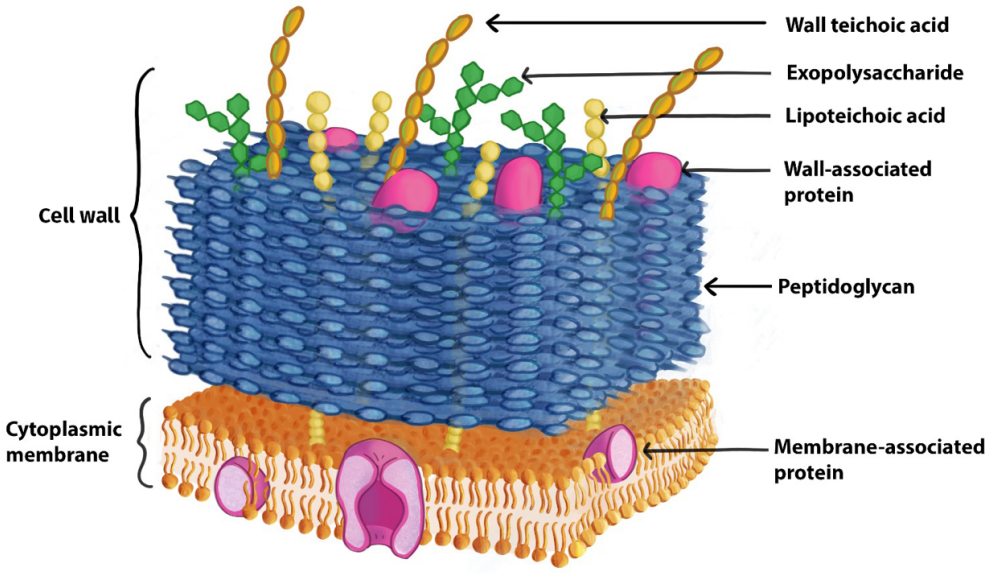

Figure I.2-2: *Schematic illustration a Gram-positive bacterium cell envelope (cell wall + cell membrane). Credit: Augustin Lerebours (reproduced with permission).*

Knowledge of the structure and main physical characteristics of a bacterial strain is of great importance to understand, harness and potentially modulate its interesting technological properties. Although little research has been done on the characterization of a *Carnobacterium maltaromaticum* cell specifically, the main structures of many other lactic acid bacteria have been extensively studied and are thus well known. An overview of these structures is presented in the following paragraphs.

I.2.1.b. Cellular envelope structures and functions in Gram-positive LAB

The cellular envelope of a Gram-positive (G^+) bacteria (**Fig. I.2-2**) is a complex, multilayer structure that serves not only to protect the cell from its surrounding environment but also functions as a surface on which reactions can occur. It is composed of a thick, rigid cell wall on top of a much thinner cytoplasmic membrane.

(i) The cell wall

The cell wall confers mechanical strength and shape to the cell and is mainly composed of peptidoglycan, teichoic acids, proteins, and exopolysaccharides.

The peptidoglycan is a single macromolecule made of glycan chains crosslinked by peptide side branches (Vollmer and Seligman 2010; Misra et al. 2013). In G^+ bacteria it is 20 to 30 nm thick and protects the cell from plasmolyzing or bursting under mild hypertonic or hypotonic environmental conditions (Dmitriev et al. 2005; Misra et al. 2013). Threading through the layers of peptidoglycan, are long anionic acids: teichoic acids. They form a continuum of negative charge extending from the cytoplasmic membrane to the outermost layers of peptidoglycan (Neuhaus and Baddiley 2003). There are two types of teichoic acids: lipoteichoic acids, anchored to the cytoplasmic membrane, and wall teichoic acids, covalently attached to the peptidoglycan and extending through and beyond the cell wall. Together with peptidoglycan, these polymers make up a polyanionic matrix that functions in cation homeostasis (Hughes et al. 1973), in the trafficking of ions, nutrients, proteins and antibiotics (Neuhaus and Baddiley 2003) as well as serve as an anchor for wall proteins (Mazmanian and Schneewind 2002).

Wall proteins are mainly responsible for the controlled synthesis and turnover of the peptidoglycan during cell growth and division (Navarre and Schneewind 1999). In some G^+ pathogens, they are also thought to be important for survival in the infected host (Schneewind et al. 1995).

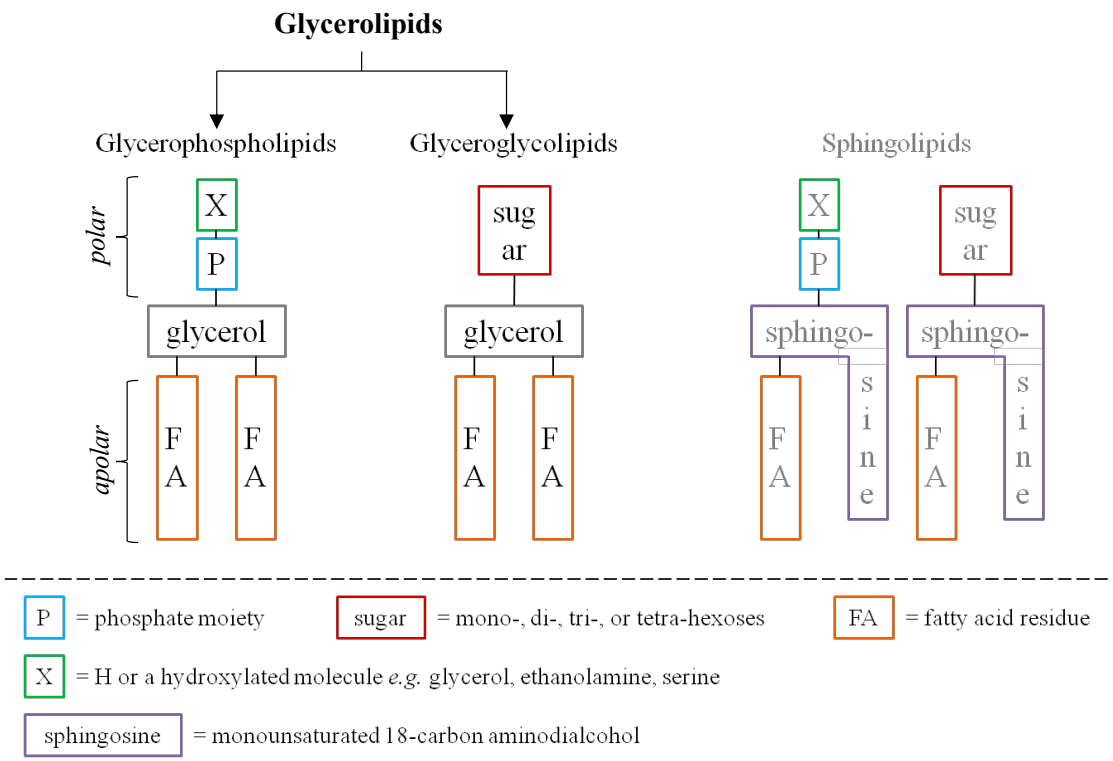

Figure I.2-3: *Bacterial membrane lipid classification, adapted from Meneghel et al., 2017.*

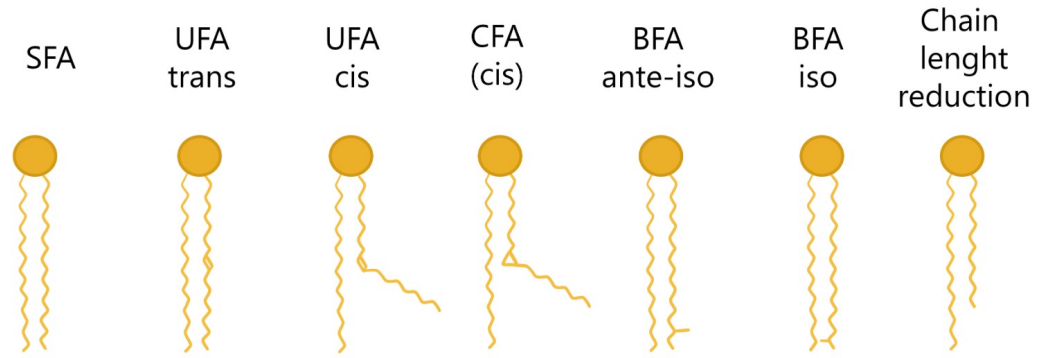

Figure I.2-4: *Schematic representation of different fatty acyl chain conformations found in biological membranes. Adapted from Fonseca et al., 2019.*
FA : fatty acid ; SFA : Saturated FA; UFA: Unsaturated FA; CFA: Cyclic FA; BFA: Branched FA

Exopolysaccharides consist of branched, repeating units of sugars, and sugar derivatives. They are involved in cellular adherence (Dertli et al. 2015), can act as storage units in response to particular environmental stresses (Ates 2015), or protect against dehydration by retaining water molecules at the cell surface (Ophir and Gutnick 1994).

(ii) The cytoplasmic membrane

The cytoplasmic membrane (or cell membrane) is 7 to 9 nm thick and defines the frontier between the extracellular and intracellular compartments of a cell. It acts as a semi-permeable barrier that regulates the movement of substances in and out of the cell and catalyzes exchange reactions, thus maintaining favorable ion and solute gradients for proper growth and metabolic activity. Small, hydrophobic, or uncharged molecules can passively diffuse through the membrane, such as O_2, CO_2, or alcohols. The most commonly accepted structure of the cell membrane is a modified version of the Fluid Mosaic Model by Singer and Nicolson (1972): globular entities (proteins) embedded within a lipid bilayer.

The lipid bilayer is the framework of the cytoplasmic membrane. In many membranes, 50 % of the mass is comprised of lipids (Finne and Matches 1976). These lipids can be separated according to their backbone (**Fig. I.2-3**): those that have a sphingosine backbone, known as sphingolipids, and those that have a glycerol backbone, known as glycerolipids. In prokaryotes, glycerolipids make up the majority of the lipid membrane (Bittman 2013) .

Glycerolipids are amphipathic molecules consisting of a hydrophilic and a hydrophobic region: a polar head group and acyl chains, respectively. Two out of the three hydroxyl groups of the glycerol backbone are replaced by acyl chains and the third by either a sugar or a phosphate group. Those that carry a sugar are called glyceroglycolipids and those that carry a phosphate group are called glycerophospholipids. Classification of glycerophospholipids is based on the small alcohol that is generally joined to the phosphate group: serine, ethanolamine, glycerol, choline, or inositol (Denich et al. 2003). The acyl chains of fatty acids (FA) are mainly composed of an even number of carbons, from 12 to 22. They may be saturated (SFA) or harbor up to two unsaturations (UFA) (**Fig. I.2-4**). Although uncommon, some may exhibit cyclic unsaturation or methyl branching. Fatty acids of 16 and 18 carbons account for more than 60 % of total FA in LAB membranes (Fonseca et al. 2019). It has been extensively reported that the FA composition of a lipid membrane greatly influences its fluidity (Denich et al. 2003; Fonseca et al. 2019).

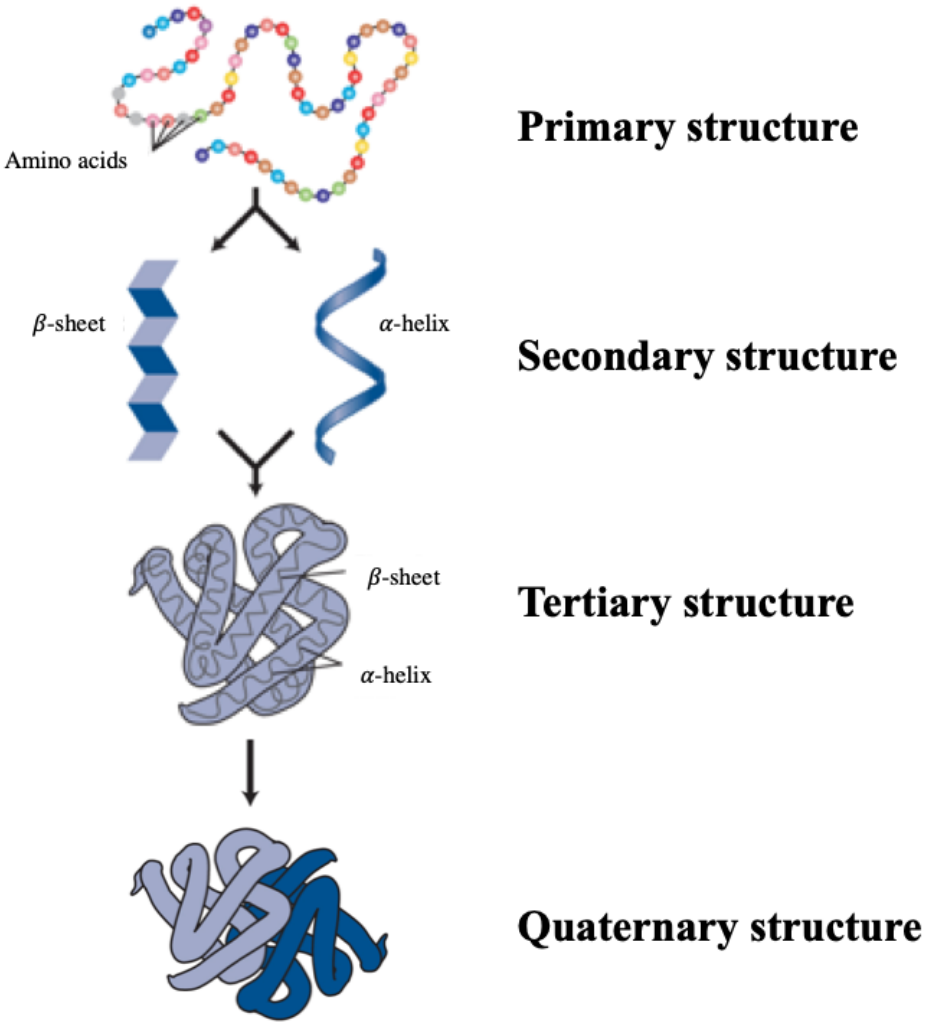

Figure I.2-5: *The different levels of protein organization.*
Adapted from https://www.genome.gov/genetics-glossary/Protein

Membrane proteins constitute close to 50 % of the mass of a cell membrane (Nikaido and Vaara 1985). They can be bound to the surface of the lipid membrane or anchored to the bilayer via one or several transmembrane domains. Membrane proteins are involved in several cellular functions, such as molecular transport, enzymatic reactions, and cellular division as well as quorum sensing and the sensing of environmental perturbations. Like any water-soluble protein, the biological function of a membrane protein is dependent on its four distinct levels of structure (**Fig. I.2-5**). The primary structure refers to the sequences of amino acids in the polypeptide chain, held together by peptide bonds. The secondary structure refers to sub-structures of the polypeptide chain, defined by patterns of hydrogen bonds between peptide groups: α-helix and β-sheets structures. The tertiary structure refers to the folding of the α-helixes and β-sheets into a compact, three-dimensional globular structure. The quaternary structure consists of the association of two or more individual polypeptide chains, operating as a single functional unit. Both the tertiary and quaternary structures are driven by a number of non-covalent interactions such as hydrogen bonding, ionic interactions, Van der Waals forces, or hydrophobic packing. Membrane proteins heavily anchored in the lipid bilayer (integral proteins) are thus generally thought to require a fluid membrane to properly function (Lewis and McElhaney 1998; Uribe and Sampedro 2003).

I.2.1.c. The intracellular content

(i) The cytoplasm

The intracellular compartment of a bacteria contains diffuse nucleic acids, proteins, metabolites, and other essential components unbound to the membrane. All these constituents are encompassed in a solution called the cytoplasm. It is where intracellular transformations take place, such as energy production and synthesis of all cellular components. In comparison to eukaryotic cells, such a human brain cells – exhibiting a total macromolecular concentration of 50 to 100 g/L (Mika and Poolman 2011) – the cytoplasm of a prokaryote is a very crowded and dense solution. For example, the macromolecular concentrations of *E. coli* under isotonic conditions were reported to be 200 g/L of proteins, 75 g/L of RNA and 10 to 20 g/L of DNA (Cayley et al. 1991).

(ii) Bacterial DNA, RNA, and plasmids

Bacterial DNA is generally contained in a single, circular double-stranded molecule called the bacterial chromosome. The chromosome, along with RNA, ribosomes,

and other proteins involved in translation and transcription, form the nucleoid: an irregularly shaped and loose region within the cytoplasm. More genetic material can be found outside the nucleoid, in the form of small, circular, double-stranded DNA molecules called plasmids. They often carry non-essential genes that provide the cell with genetic advantages useful for proper function in hostile environments. Often, these advantages include the ability to catabolize lactose, to produce specific proteases, bacteriocins, and exopolysaccharides, or to resist various bacteriophages and antibiotics (Thomas and Summers 2008).

(iii) Cytoplasmic proteins

Cytoplasmic proteins are as diverse as the roles they serve. They are responsible for all essential biological functions such as biosynthesis, transport, replication, signaling, and even structural support. Depending on their role, localization within the cytosol can vary. Just like membrane proteins, the proper function of cytoplasmic proteins is highly dependent on their environment. Variations in intracellular pH, temperature, osmotic pressure, etc., can compromise their native structure and thus result in loss of functionality.

I.2.2. Modulating the technological properties of LAB for industrial applications

Industrial starter production of LAB is generally optimized for high biomass yields, and cell concentrates displaying high recovery of viability and acidification activity after stabilization and long-term storage. Sometimes, however, other technological properties are desired, such as a specific acidification rate, the production of a specific metabolite, or resistance to a specific stabilization process, etc. These technological properties can be obtained by modifying the physiological state of LAB concentrates, through fermentation parameter adjustments. Among the various fermentation parameters that can be modulated, medium composition, pH, temperature, and time of harvest are those particularly known to affect the physiological state of the produced LAB concentrates (Béal et al. 2001; Wang et al. 2005a; Rault et al. 2008; Rault et al. 2009; Velly et al. 2014; Hansen et al. 2016).

For use in TTI labels, the technological properties of interest for *C. maltaromaticum* starters are their viability and acidification activity within the TTI labels. The reference conditions for industrial production of *C. maltaromaticum* CNCM I-3298 concentrates are 30 °C, pH 7, and a harvest time close to the beginning of the stationary phase. However, little research has been published about the effects of

fermentation conditions on modulating the physiological state of *C. maltaromaticum* concentrates. Some of the few studies that have investigated the effect of fermentation conditions on other potential candidates for LAB-based TTI are shown in **Table I.2-2**.

In a study on *Carnobacterium divergens* – a *Carnobacterium* subspecies often isolate from the same high protein foods as *C. maltaromaticum* – Brillet-Viel and colleagues (2016) aimed at optimizing growth and bacteriocin activity. They investigated the effect of temperature (15 to 30 °C), pH (6.5 to 6.8), and carbohydrate concentration (2 to 20 g/L) on both viability and bacteriocin production. Low temperature and high carbohydrate concentrations had a positive effect on the viability of *C. divergens* whereas the tested range of pH had no significant effect on viability. Nonetheless, low pH values did increase bacteriocin production of *C. divergens*. This research, although not done specifically on *C. maltaromaticum*, demonstrated that fermentation parameters such as temperature, pH, and medium composition are able to affect the growth and metabolite production of a *Carnobacterium* similar to *C. maltaromaticum*.

Table I.2-1: *Effect of culture conditions on the physiological state of LAB proposed for LAB-based TTI.*

LAB strains	Investigated culture conditions	Effect on physiological state	References
Carnobacterium divergens V41	→ Temperature: 15 to 30 °C → pH: 6.5 to 8 → Carbohydrates (2 to 20 g L^{-1})	- Positive effect of low temperature and high carbohydrate concentration on viability; - No effect of tested pH range on viability; - Low pH increased bacteriocin production.	Brillet-Viel et al. 2016
Lactobacillus sakei 23K	Fermentation at optimal growth temperature (26 °C) and upon reaching exponential phase: →Heat shock (HS): 20 min at 42 °C →Cold shock (CS): 20 min at 4 °C	- No difference in viability; - Both HS and CS induced better acidification activity; - Best acidification activity after CS.	Hüfner and Hertel 2008
Lactobacillus rhanmnosus GG *	→ Temperature: 37 °C → pH: unregulated → Glucose (10 to 34 g L^{-1}) → Peptone (8 to 12 g L^{-1})	- Growth favored by high peptone concentrations; - Lactic acid production yields favored by high glucose concentration.	Mel et al. 2008
Weisella cibaria DBPZ1006 *	→ Temperature: 10 to 45 °C → pH: 4 to 8 → a_w: 0.935 to 0.994	Maximum growth rate achieved at 36.3 °C, pH 6.6 and a_w of 0.994	Ricciardi et al. 2009

I.2.2.a. Impact of the fermentation medium composition

Nutritionally rich media is needed to grow LAB, as they are incapable of synthesizing many amino acids and vitamins. The physiological state of LAB concentrates is therefore highly dependent on the composition of their growth medium.

The carbon source that has been reported for the culture media of *C. maltaromaticum* is glucose, or any polymeric carbohydrate containing a glucose moiety such as lactose or trehalose (Leisner 1992). From glucose, *C. maltaromaticum* was shown to produce lactic acid and acetic acid. Because of its low beta-galactosidase activity, its ability to metabolize galactose (the other sugar moiety of lactose) is compromised, resulting in slow growth and acidification rates in milk compared to commercial starters such as *Lc. lactis* and *S. thermophilus* (Edima et al. 2008). However, the addition of 1g/L of yeast-extract in milk improved growth and acidification performance of *C.* maltaromaticum, resulting in enhanced milk coagulation. Tweaking the fermentation medium composition of a *C. maltaromaticum* culture can thus lead to physiological changes.

During the aerobic growth of *C. maltaromaticum* in laboratory media, acetic acid production can exceed lactic acid production (Borch and Molin 1989). It has been suggested that by replacing glucose with ribose, the amount of acetic acid produced is increased relative to lactic acid (Leisner 1992). The pKa of acetic acid (4.76) is close to one unit higher than the pKa of lactic acid (3.86), which makes acetic acid about ten times less acidic than lactic acid. The acidification power of *C. maltaromaticum* cells grown in a culture medium containing ribose as only carbon source, should therefore be weaker than the acidification power of cells grown in a glucose-based medium. The carbon source of the fermentation medium for the production of *C. maltaromaticum* concentrates could thus be chosen depending on the desired acidification activity exhibited by the harvested cells.

I.2.2.b. Impact of fermentation temperature and pH

(i) Fermentation temperature

In a study aimed at improving the fermentation of raw sausage by stress conditioning *Lactobacillus sakei* starters, cold-stressed cells were reported to exhibit enhanced acidification activity (Hüfner and Hertel 2008). Exponentially growing cells of *L. sakei* 23K produced at their optimal growth temperature (26 °C), were subjected to a 20 min

cold-stress treatment at 4 °C. The resulting harvested cells were then inoculated into sausage batter and acidification kinetics were monitored. Cells that were subjected to cold stress prior to inoculation were able to reduce the pH of the meat down to pH 5.0 approximately 30 hours quicker than untreated cells. Since enzyme-catalyzed reactions slow down as temperature decreases, the authors suggest that more glycolytic enzymes must be produced, to compensate for a slower metabolism (or glycolytic capacity), resulting in increased acidification activity performance of the harvested *L. sakei* cells exposed to cold stress.

The adaptive response of LAB to temperature downshift has been linked to the production of cold-induced proteins (Panoff et al. 1994; Wouters et al. 1999b). In a study investigating the effect of low-temperature stress on *Lactococcus lactis*, the maximal glycolytic activity measured in cells at 30 °C was increased 2.5-fold following a cold stress treatment at 10 °C (Wouters et al. 2000). Analysis of the cold adapted cells showed an upregulation of the histidyl phosphor-carrier protein (HPr), a protein linked to glycolysis regulation (Deutscher et al. 2006). An upregulation of HPr was also reported during the cold acclimation of *Lactococcus piscium* at 5 °C (Garnier et al. 2010).

Exposure to heat stress has similarly been shown to induce changes in LAB. In a study investigating the effect of heat shock on the cryoresistance of *Lactococcus lactis* subsp. *lactis* and *cremoris*, cells exposed to a 25 min heat shock at 42 °C (*L. lactis* subsp. *lactis*) or 39 °C (*L. lactis* subsp. *cremoris*) exhibited increased resistance to freezing. The improved resistance was linked to the production of stress-induced proteins. Cells exposed to heat-stress produce heat-shock proteins (HSPs), which are believed to assist in protein folding, assembly and transport (Varmanen and Savijoki 2011).

(ii) Fermentation pH

A study aimed at developing a medium for the selective enumeration of *C. maltaromaticum*, showed that its viability did not vary significantly at pH values ranging from 5 to 9 (Edima et al. 2006). This suggests that the pH at which *C. maltaromaticum* cells are grown does not affect the viability of the harvested cells. However, this study did not investigate any other technological property of the cells, such as their acidification activity or their ability to recover after a stabilization process. It is generally known that acid adaptation systems in LAB promote synthesis of stress proteins associated with physiological changes and improved resistance (Lorca and de Valdez 2001; van de Guchte et al. 2002). In research investigating the influence of

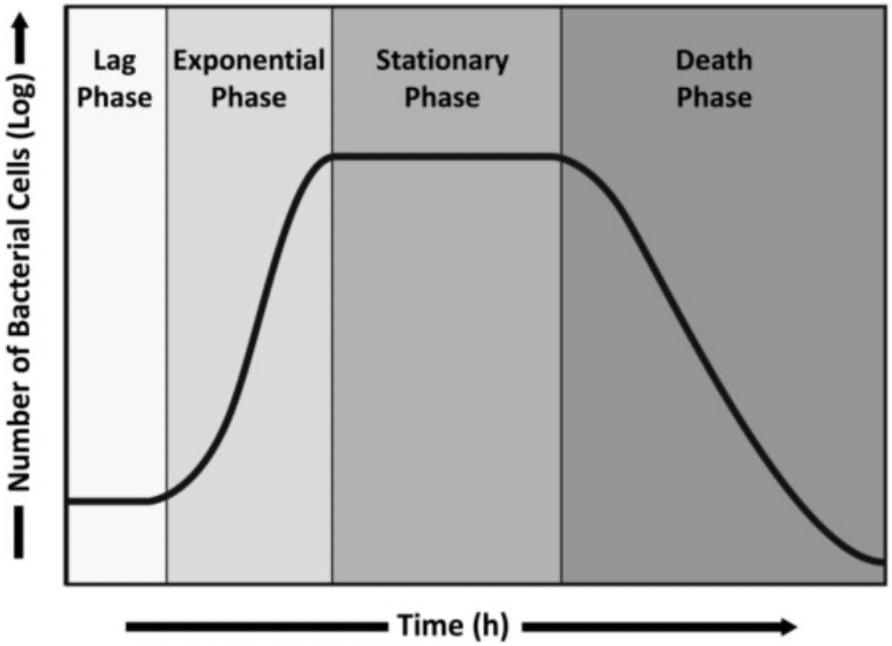

Figure I.2-6: *Schematic representation of a bacterial growth curve, indicating various growth phases. Adapted from Garrison and Huigens 2017*

fermentation pH on growth, viability and specific acidification activity of *Lactococcus lactis* DGCC1212 (Hansen et al. 2016), highest viable cell counts were measured for fermentations carried out at pH 6.5 and pH 7.5 but highest specific acidification activity was reached for cells produced at pH 5.5. This work, along with the work of Brillet-Viel (2016) on *Carnobacterium divergens* indicate that low pH may modulate the metabolic activity of harvested concentrates.

Interestingly, in a few studies examining the effect of fermentation pH on the physiological state of LAB concentrates, the effect of pH was strongly tied to harvest time (Rault et al. 2009; Hansen et al. 2016).

I.2.2.c. Impact of fermentation duration (harvest time)

During fermentation, bacteria go through four distinct growth phases (**Fig. I.2-6**) at which they acquire various physiological traits.

The initial phase is the lag phase, where the cells, newly inoculated in the fermentation medium, adjust their metabolism to their new environment. They are thus metabolically active, but no growth is observed. When the cells have adjusted and are ready to undertake all the biological reactions necessary for cell division, cellular growth starts.
Then comes the exponential or log phase: a time during which growth is exponential. Metabolic activity is at its highest and cell concentration doubles after each generation time. Eventually, cell growth then enters its stationary phase, where the number of dividing cells equals the number of dying cells thus resulting in no overall growth. Fast accumulation of waste products (*e.g.* metabolites such as lactic acid) during the exponential growth phase creates less favorable conditions for proper metabolic activity and can directly provoke starvation or energy depletion, irrespective of the extracellular amount of substrate. The availability of certain essential substrates has indeed been linked to cell environmental conditions (Konings et al. 1997).
As metabolites continue to accumulate and nutrients become less available, the number of dying cells continues to rise and cells enter their death phase. In the death phase, the number of living cells decreases exponentially, and cell population experiences a sharp decline. The physiological state of bacterial concentrates is therefore greatly dependent on the growth phase at which they were harvested.

Organic acids such as lactic acid or acetic acid are major products of carbohydrate metabolism in lactic acid bacteria. However, their accumulation in the fermentation medium also inhibits growth (Piard and Desmazeaud 1991). The inhibition caused by these acids is due to the solubility of their non-dissociated form within the cytoplasmic membrane. Once inside the cell, the acids dissociate into an anion and a proton (because the intracellular pH tends to be higher than their pKa) and are no longer able to diffuse freely across the cell membrane. This influences the transmembrane pH gradient and decreases the amount of energy available for cell growth (Othman et al. 2017; Pinhal et al. 2019)

In pH-controlled fermentations, the amount of non-dissociated acids is dependent on the pH set-point: the lower the pH set-point is, the more non-dissociated acid will be present in medium and the more stressful the environment will be for the cells. A low concentration of non-dissociated lactic acid was proposed by Hansen and colleagues (2016) as an explanation for the higher active cell count measured in *Lc. lactis* cultured at pH 7.5 compared to pH 6.5 and pH 5.5. However, increasing harvest times resulted in a decrease of acidification for pH 7.5 and pH 6.5 cultures, but not for pH 5.5 cultures, suggesting that low pH may have a protective effect on the stress induced by increasing harvest times. Similarly, Rault and coworkers (2009) reported that fermentations carried out at pH 5 resulted in *L. bulgaricus* cells exhibiting a more robust physiological state (high viability and acidification activity) throughout growth, than fermentations carried out at pH 6. Cells grown at pH 6 and harvested at increasing times resulted in viability decrease and acidification activity variations. The stress associated with increasing harvest times is therefore likely dependent on the pH set-point of the fermentation.

Entry into stationary phase has been shown to result in the development of a general stress-resistant state (van de Guchte et al. 2002). A few studies have reported that if harvest extended up to six hours into the stationary phase, LAB cells are exposed to stressful conditions that in turn can prepare them to cope better with the different stresses arising from freezing and freeze-drying steps (Fonseca et al. 2001; Carvalho et al. 2004; Rault et al. 2010; Velly et al. 2014). For example, increasing the harvest time of *Lc. lactis* TOMSC161 from early stationary phase up to six hours of stationary phase did not affect viability or acidification activity but did result in a decrease of acidification activity loss after freeze-drying by 50 % (Velly et al. 2014).

The time of harvest thus appears as a key parameter to be considered in the modulation the physiological state of LAB concentrates, especially as it relates to its resistance to stabilization processes.

I.2.3. Other useful technological properties of *C. maltaromaticum*

I.2.3.a. Potential cheese ripening flora

C. maltaromaticum was found to be present in many French soft cheeses (Cailliez-Grimal et al. 2007). Its growth in milk does not result in coagulation and does not inhibit or compete with starter LAB such as *Lc. lactis* and *S. thermophilus* (Edima et al. 2008). Though its growth is arrested below pH 5 (the pH at which most soft cheeses are drained), its viability is not affected. The growth of *C. maltaromaticum* in cheese can resume towards the end of ripening, when more favorable conditions are met, such as cold storage (around 14 °C) and high pH values (around pH 8) (Afzal et al. 2010). At this point, *C. maltaromaticum* can take over the maturation of the cheese and produce aromatic substances that – as its name suggests – give a malty flavor, such as 3-methylbutanal (Miller et al. 1974; Leisner et al. 2007).

I.2.3.b. Food bio-preservation properties

The potential of *C. maltaromaticum* in food bio-preservation comes from its ability to produce bacteriocins as well as the similar growth and metabolic kinetics it has to *Listeria monocytogenes* (Leisner et al. 2007).

In a study investigating the effect of piscicolin 126 – a bacteriocin produced by *Carnobacterium piscicola* JG126 – on the growth of *L. monocytogenes* in milk and camembert cheese, significant inhibition of *L. monocytogenes* growth was reported, without affecting the starter cultures (Wan et al. 1997). The antimicrobial activity exerted by bacteriocins is the result of pore formation, dissipation of membrane potential, and leakage of intracellular substances (Suzuki et al. 2005; Drider et al. 2006).

The shelf-life of a vacuum-packed cold-smoked salmon was successfully extended by inoculation of *Carnobacteria* demonstrating no bacteriocin activity (Leroi et al. 1996). The anti-listeria properties, in this case, could be partly due to glucose depletion (Buchanan and Bagi 1997; Nilsson et al. 2004). In conditions that are favorable for the growth of both microorganisms, *C. maltaromaticum* is able to

metabolize glucose faster than *L. monocytogenes* and thus deplete the environment of the necessary carbon source for growth (Buchanan and Klawitter 1991; Mathieu et al. 1994).

I.2.3.c. A model of lactic acid bacteria cryoresistance

The distribution of Carnobacteria in the natural environment such as polar lakes and permafrost as well as in foods, suggests that *C. maltaromaticum* could exhibit good cryoresistance. This was confirmed in a study investigating the freeze-thaw tolerance of bacterial soil communities that overwinter (Walker et al. 2006). *C. maltaromaticum* showed no significant viability loss after three freeze-thaw cycles and only 1 log CFU/mL after 12 freeze-thaw cycles. Twenty-eight cycles were needed to observe a loss of viability of two to three orders of magnitude.
The industrial practices of Cryolog Clock-T° for the production of TopCryo® TTI labels inoculated with *C. maltaromaticum* CNCM I-3298, disregard any effect of freezing and freeze-thawing on the cells' physiological state: no significant differences were observed between the viability or acidification activity of fresh and thawed cells.

The ability to survive freezing is an important attribute for a LAB used industrially, as cryopreservation is one of the most widely used stabilization technique in the industrial production of LAB concentrates (Béal and Fonseca 2015). However, freezing tolerance is highly dependent on strain (Fonseca et al. 2000; Rault et al. 2007; Meneghel et al. 2017) and on how the cryopreservation process is conducted. More understanding about the physical events that take place during freezing and how those might affect cells, could help explain how some LAB strains are more cryoresistant than others. *C. maltaromaticum* could thus be a model strain of cryoresistance among lactic acid bacteria and further research might reveal markers of cryoresistance that could be promoted in other, more cryosensitive strains.

I.2.4. Concluding remarks

Carnobacterium maltaromaticum has been commonly isolated from various foods and research has come some way towards understanding certain aspects regarding its potential in cheese maturation and in food bio-preservation. As seen in the previous chapter, *C. maltaromaticum* has additionally proven itself to be a key element in the only LAB-based TTI that was ever taken to market. However, no studies have been published on the industrial production of *C. maltaromaticum* concentrates and the effect of various fermentation parameters on their physiological state. More work needs to be done understanding and characterizing this species to fully exploit its technological properties. Furthermore, *C. maltaromaticum* is an ideal model strain of cryoresistance for cryobiology research. No work has explored the cellular mechanisms expressed by *C. maltaromaticum* granting it its exceptional cryoresistance. The following chapter will thus focus on the physical events that take place during freezing, and their varying effect on LAB cells.

I.3. Cryopreservation of lactic acid bacteria

Content

I.3.1. Physical events taking place during the cryopreservation of LAB 75
I.3.1.a. The freezing and frozen storage of a sucrose solution 75
I.3.1.b. Cooling kinetics 77
I.3.1.c. Main physical events occurring during the freezing, frozen storage and thawing of cryoprotected LAB concentrates 81
(i) The lipid membrane phase transition 81
(ii) Ice formation and cryo-concentration 81
(iii) Intra- and extracellular vitrification 83
(iv) Thawing 83
I.3.2. Stresses and damages induced by cryopreservation on LAB cells 85
I.3.2.a. Thermal stress 85
I.3.2.b. Osmotic stress 87
I.3.3. Improving the cryoresistance of LAB 89
I.3.3.a. Identifying markers of cryoresistance 89
(i) Cellular markers involving membrane properties 89
(ii) Cellular markers involving protein synthesis and other cellular components 91
I.3.3.b. Changing fermentation and post-fermentation conditions to favor markers of cryoresistance 92
(i) Changing environmental conditions during fermentation 92
(ii) Changing environmental conditions at the end of fermentation 93
I.3.3.c. Using cryoprotective solutions and controlling freezing, storage, and thawing protocols 95
(i) Cryoprotection 95
(ii) Freezing, storage and thawing protocols 96
I.3.4. Concluding remarks 97
I.4. General insights 98

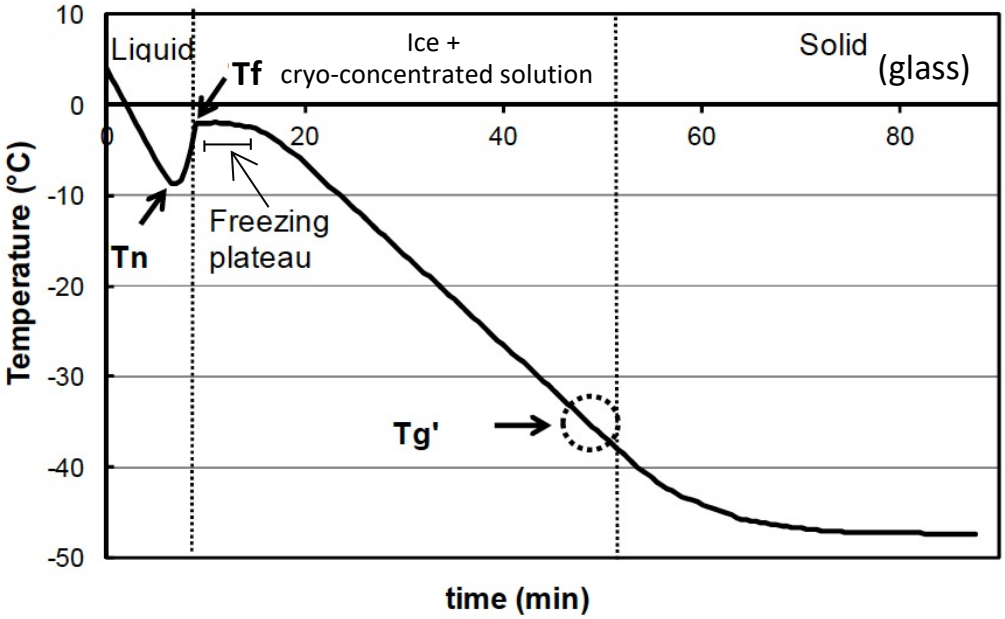

Figure I.3-1: *Product temperature profile and principal phenomena taking place during freezing.* ***Tn*** *(°C): nucleation temperature;* ***Tf*** *(°C): freezing temperature;* ***Tg'*** *(°C): glass transition temperature of the maximally cryocentrated medium. Adapted from Beal and Fonseca (2015).*

I.3.1. Physical events taking place during the cryopreservation of LAB

Cryopreservation of LAB entails the freezing and storage of cells at temperatures generally below -50 °C (typically around -80 °C). Cryopreserved LAB can be stored frozen over long periods of time – ranging from a few months to several years – with limited loss of viability or any other technological function. This stabilization technique, although widely used industrially, is nevertheless a stressful process for bacteria. It can affect their physical and biological properties, leading to cell damage and in some cases, to cell death. To limit the negative effects of freezing on cellular components, LAB cells undergoing cryopreservation are usually suspended in an aqueous solution containing cryoprotective agents.

The next section will describe the main physical events occurring during the freezing and thawing of a 20 % sucrose solution, commonly encountered in LAB cryopreservation (Béal and Fonseca 2015). It will be followed by a description of the consequences these physical events have on LAB cellular structures and biological activity.

I.3.1.a. The freezing and frozen storage of a sucrose solution

During the cryopreservation of a sucrose solution resulting in a state change from liquid to solid, several intermediate events take place. These events will be illustrated in **Figures I.3-1 and I.3-2**. A cryoprotective solution containing 20 % sucrose will be used as an example.

Figure I.3-1 presents the temperature variation of the sucrose solution being cooled from 5 °C to -50 °C, as a function of time. At any temperature below the solution's freezing temperature (Tf), water can nucleate. The temperature at which water nucleates is called the water nucleation temperature (Tn). When ice forms, the exothermic nature of water crystallization results in a temperature increase until reaching a plateau at Tf – called the freezing plateau – before temperature decrease resumes. As ice forms, the solute concentration of the unfrozen phase increases. The concomitant decrease of temperature and increase of solute concentration, results in a rapid increase in the viscosity of the medium. When the solution is maximally cryo-concentrated, it changes to an amorphous solid, glassy state. The temperature at which this happens is the glass transition temperature (Tg').

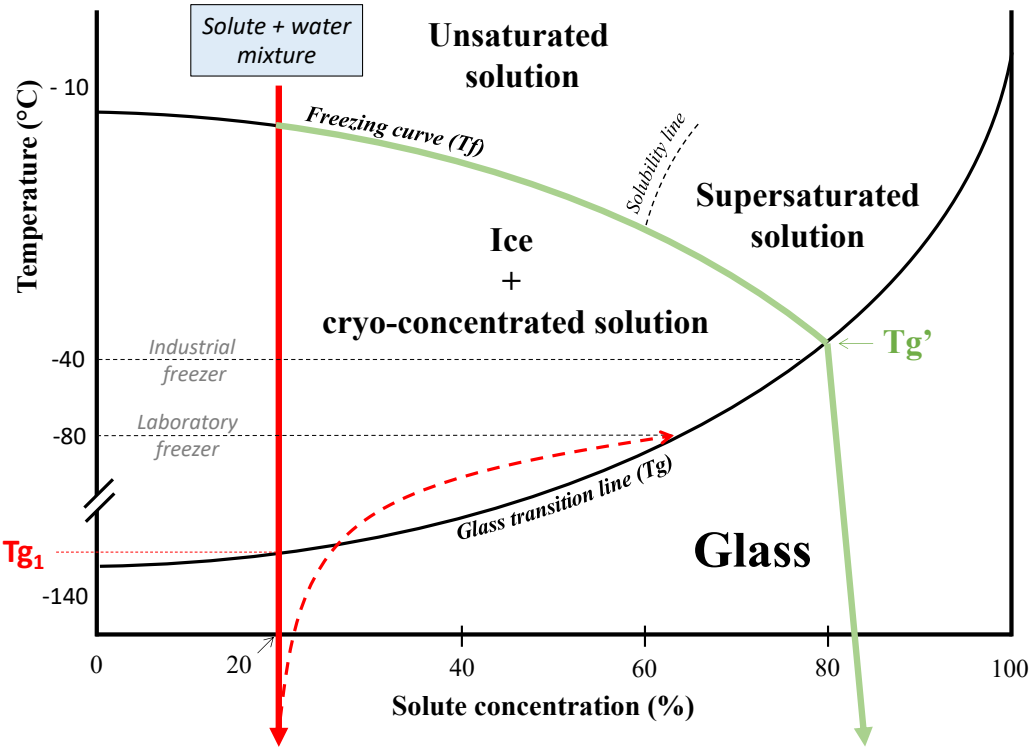

Figure I.3-2: *State diagram of a solute-water mixture frozen at two different cooling rates:* ***(i)*** *very slow (< 10 °C/min), leading to increasing ice fractions and maximal solute cryo-concentration (green arrow) and* ***(ii)*** *very high (e.g., by immersion in liquid nitrogen) (red arrow). The red dashed arrow represents the instability of a product frozen at very high cooling rates followed by storage in a laboratory freezer (-80 °C): ice re-crystallization occurs during storage, leading to increasing solute concentrations.*

The phase diagram presented in **Figure I.3-2** illustrates the two extreme freezing scenarios that can happen with a 20 % sucrose solution undergoing cryopreservation in an industrial or laboratory setting.
The first scenario (green arrow) involves applying slow cooling rates (e.g., <10 °C/min) to favor ice formation, leading to a maximally cryo-concentrated matrix (approximately 80 % sucrose) that transitions to an amorphous glassy state at Tg' (*approx.* -42 °C). The sample can then be stored and remain stable in a laboratory (-80 °C) or industrial freezer (*approx.* -50 °C).
The second scenario (red arrow) entails rapid cooling of the solution by immersion in liquid nitrogen. The very high cooling rate (~2600 °C/min) results in no ice formed as the sample rapidly finds itself at -196 °C, much below its glass transition temperature (Tg_1). Once frozen, the sample can either be kept in liquid nitrogen or be stored in a freezer (e.g., between -80 and -50 °C).

If storage is carried out in liquid nitrogen or any other temperature below Tg_1, the diffusion of water molecules through the glassy matrix is greatly hindered by extremely high viscosity (10^{12} to 10^{14} Pa.s). The amorphous solid state of the matrix inhibits ice formation, which favors long term stability. If storage occurs above Tg_1, the medium will be in an unstable, viscous liquid state where ice recrystallization can occur. As ice forms, the unfrozen fraction of the medium will cryo-concentrate until its viscosity is high enough that it transitions into a glassy state. For example, if a 20 % sucrose solution was rapidly cooled by immersion in liquid nitrogen, and then stored in a laboratory freezer at -80 °C (i.e., above its glass transition temperature), the medium will cryoconcentrate during storage as ice formation continues, and then turn to glass once a sucrose concentration of approximately 65 % is reached (dashed red arrow).

I.3.1.b. Cooling kinetics

By influencing the physical events that occur during the freezing and frozen storage of a cryoprotective solution, freezing rates also influence the damage mechanisms involved in cellular cryo-injury.
According to the two-factor hypothesis put forward by Mazur and colleagues (1970 and 1972), low cooling rates (<10 °C/min) favor injuries induced by high solute concentrations, while high cooling rates (>100 °C/min) favor those induced by intracellular ice formation. However, the two-factor hypothesis was largely considered based on observations of eukaryotic cells. No intracellular ice has ever been evidenced in LAB cells when freezing is carried out in a cryoprotective solution, regardless of applied cooling rates (Fonseca et al. 2006).

While several studies on LAB cryopreservation showed that high cooling rates lead to better viability upon thawing, than slow cooling rates (Baumann and Reinbold 1966; Tsvetkov and Shishkova 1982; Morice et al. 1992; Fonseca et al. 2001), the same cannot be said for all LAB species or strains (Smittle et al. 1972; Péter and Reichart 2001). For example, frozen *L. rhamnosus* GG concentrates, are usually prepared at very high cooling rates by immersion in liquid nitrogen with limited loss of technological function (Volkert et al. 2008), but the same method used on *L. bulgaricus* leads to low survival (6 to 27%, depending on the strain) (Smittle et al. 1972; Fonseca et al. 2006). It has also been demonstrated by Fonseca *et al.* (2006) that the effect of high cooling rates on the quality of cryopreserved LAB concentrates is dependent on subsequent storage temperatures. In their study, samples cryoprotected with glycerol and frozen at high rates by immersion in liquid nitrogen, presented minimum loss of biological activity (viability and acidification activity) only when stored at -80 °C. When stored at -20 °C, those samples presented maximum loss of biological activity and scanning electron microscopy images showed that cells were plasmolyzed. Furthermore, due to the difficulties in controlling rapid cooling, resulting in variable ice crystal sizes, high cooling rates have also been reported to increase variability in the quality of the cryopreserved cells (Smittle et al. 1972). Reference microorganism collections such as the American Type Culture Collection (ATCC) or the German Collection of Microorganisms and Cell Cultures (DSMZ) as well as some authors (De Paoli 2005; Prakash et al. 2013; She and Petti 2015) thus recommend that microorganisms be frozen at slow and controlled cooling rates. Research is however still needed to elucidate LAB responses to slow cooling in order to optimize cryopreservation protocols.

The cellular stresses and damages induced by cryopreservation presented from now on, will thus focus on those ensued by slow cooling rates, in a cryoprotective solution.

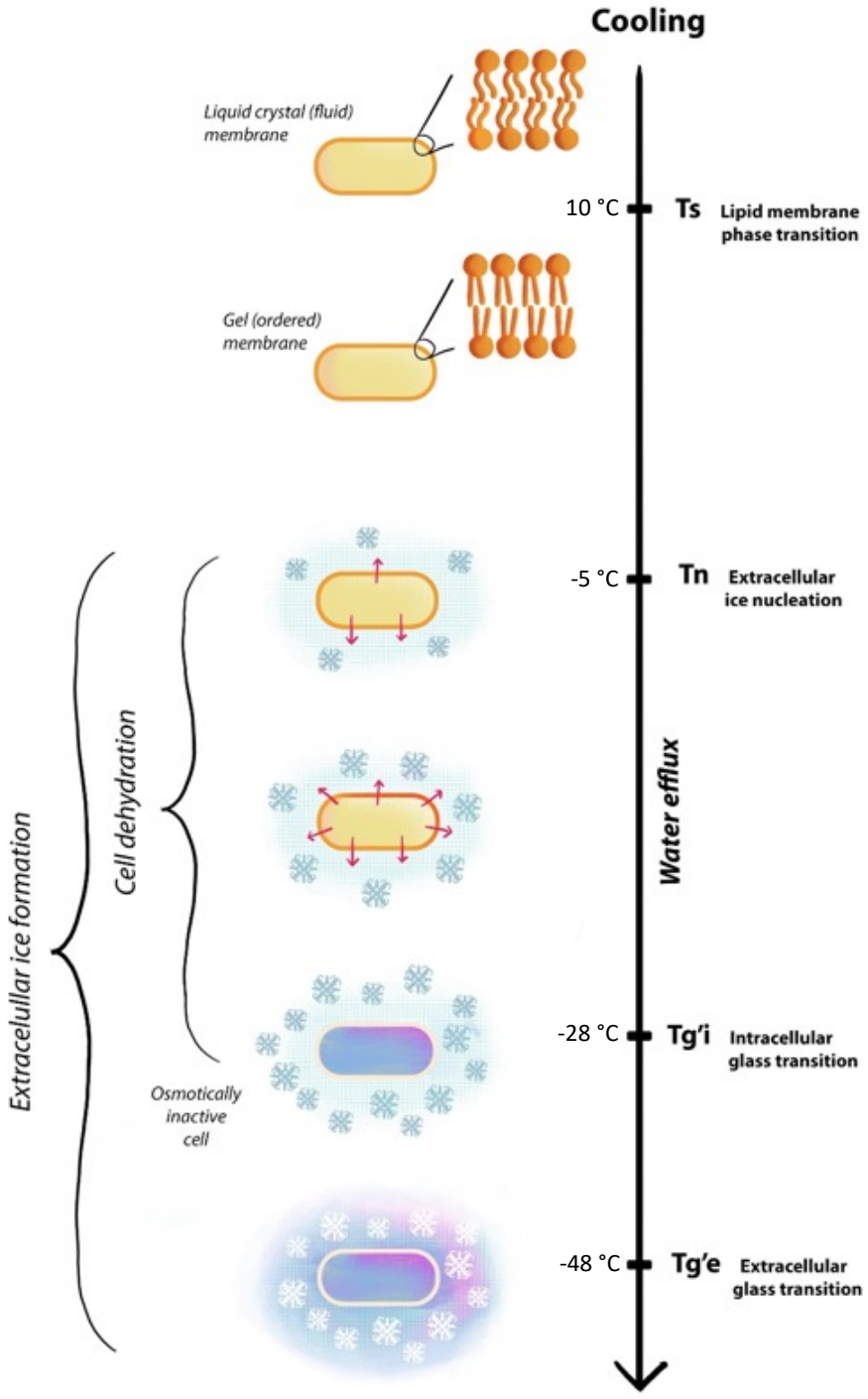

Figure I.3-3: *Schematic representation of the physical events taking place during the freezing of a cryoprotected LAB cell. Temperature indications correspond to measurements carried out on* L. bulgaricus *cells cryoprotected in a 20 % sucrose solution. Adapted from Fonseca* et al. *2016*

I.3.1.c. Main physical events occurring during the freezing, frozen storage and thawing of cryoprotected LAB concentrates

The sequence of physical events that take place during the freezing of cryoprotected LAB cells at a slow cooling rate, is depicted in **Figure I.3-3** and described below. The physical changes undergone by the cells are a direct consequence of the physical events taking place in the extracellular medium (i.e., the cryoprotective solution), which were described previously (**§ I.3.1.a**).

(i) The lipid membrane phase transition

As temperature decreases, the organization of lipid acyl chains goes from a disorganized and fluid "liquid crystalline" phase, to a more organized and rigid "gel" phase (Denich et al. 2003). This membrane solidification occurs at the lipid phase transition temperature (Ts), and mainly depends on fatty acids composing the membrane. Above their solidification temperature, acyl chains present minimal van der Waals interactions with neighboring chains, resulting from their methyl groups freely adopting gauche rotamers (Lewis and McElhaney 2013) (**Fig. I.3-4, left**). In the liquid crystalline phase, lipid bilayers are disordered and fluid structures. Below their solidification temperatures, acyl chains adopt an all-trans conformation (**Fig. I.3-4, right**), thus facilitating lipid packing and ultimately rigidifying the membrane. Lipids carrying saturated and/or long chain fatty acid residues undergo phase transition at higher temperatures than those carrying unsaturated and/or short chain residues (Denich et al. 2003). The lipid membrane phase transition is the result of the lipid phase transitions of all lipids constituting the membrane.

Depending on the LAB population undergoing cryopreservation, membrane lipid phase transition can happen either before or after the beginning of extracellular ice formation. For example, *L. bulgaricus* CFL1 cells grown in either MRS broth or a Whey-based medium, were shown to exhibit a membrane phase transition during cooling at either 22 °C or – 8 °C, respectively (Gautier et al. 2013).

(ii) Ice formation and cryo-concentration

Ice formation begins at the water nucleation temperature (Tn) of the extracellular medium. As extracellular ice grows, the suspending medium cryoconcentrates and external osmolarity increases. Water is drawn out of the cells to maintain osmotic equilibrium between the intra- and extracellular compartments, causing cell dehydration and shrinkage.

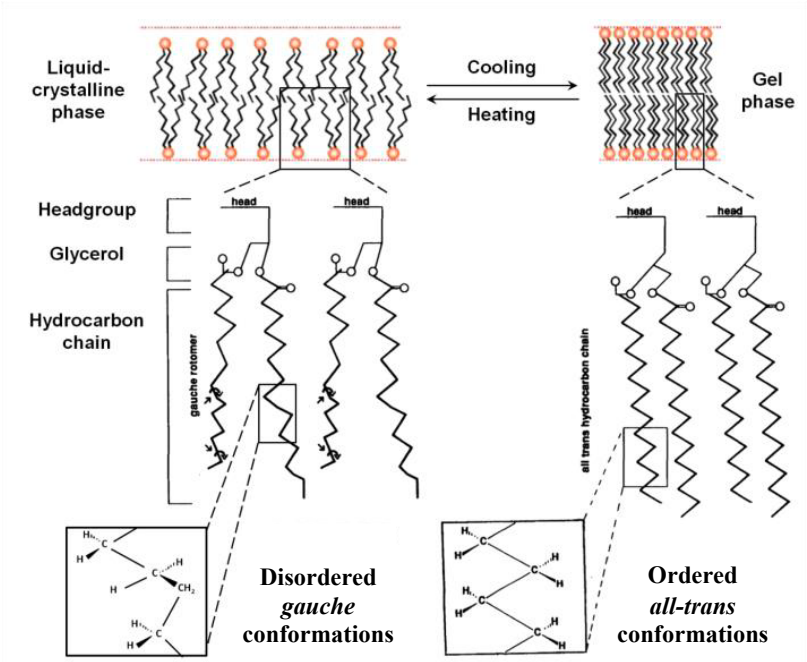

Figure I.3-4: *Schematic representation of a membrane lipid transition from a disordered liquid-crystalline phase (acyl chains freely adopting gauche conformations) to an ordered gel phase (acyl chains in all-trans conformations). Adapted from Borchman et al. 1991.*

(iii) Intra- and extracellular vitrification

The vitrification of the intracellular compartment as well as the extracellular medium being frozen at a slow rate, happens at respectively Tg'i and Tg'e.

As cells dehydrate and shrink, their cytoplasm maximally cryoconcentrates and vitrifies at Tg'i. The intracellular compartment then becomes osmotically inactive and no longer responds to the increasing osmolarity of the extracellular compartment. The latter, on the other hand, continues to cryo-concentrate as more ice forms until, in-turn, vitrifying at Tg'e.

Below Tg'e, the whole cell suspension has turned to glass and all diffusion driven reactions are hindered. LAB concentrates can then be stored frozen for a few months up to several years, with limited changes in their viability and/or metabolic activity, assuming that storage temperatures were kept below Tg'e.

Both Tg'i and Tg'e, are dependent on cell size and the composition of the suspending medium (Clarke et al. 2013; Fonseca et al. 2016). Generally, Tg'i is higher than Tg'e since the intracellular compartment is densely packed with macromolecules and thus presents very high viscosity (Mika and Poolman 2011).

(iv) Thawing

If a slow freezing rate was initially applied (<10 °C/min), and a final thawed temperature above the lipid phase transition temperature is reached, all the physical events described during the freezing process happen in reverse order during thawing. Assuming storage was carried out below Tg'e, the first physical event brought about by thawing is the transition of the extracellular matrix from an amorphous glassy state, back to a rubbery, super saturated solution. As temperature continues to increase, the intracellular compartment transitions from an osmotically inactive, vitrified state, to an osmotically active viscous liquid state. As extracellular ice melts, water flows back into the cells and cell volume gradually increases until reaching its original size. When all the ice has melted, the cells are suspended in their initial medium exhibiting favorable osmolarity. Finally, as temperatures exceed the lipid membrane phase transition temperature during heating (Tm, or melting temperature), the lipid membrane transitions back from a rigid gel state to a fluid crystalline state.

Cells able to withstand the sequence of physical events encountered during freezing, storage and thawing without severe injury, regain full cellular function and are thus re-activated.

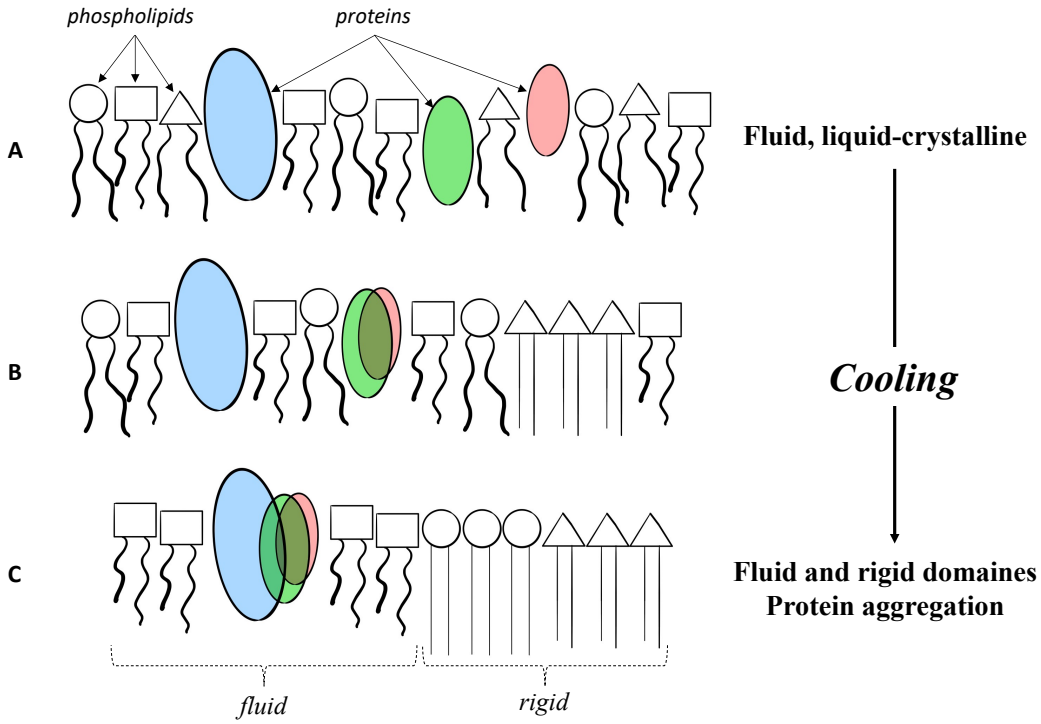

Figure I.3-5: *Schematic illustration of membrane lateral phase separation upon cooling, causing protein aggregation. All phospholipid types (O, □, Δ) start off in a fluid, disorganized state* ***(A)****; all phospholipids of the same type rigidify upon reaching their transition temperature and tend to aggregate* ***(B)****; proteins are excluded from the rigid domains and aggregate in the domains that have remained fluid* ***(C)****. Adapted from Tablin et al. 2001.*

I.3.2. Stresses and damages induced by cryopreservation on LAB cells

During cryopreservation, LAB cells suffer different kinds of stresses resulting from the physical events described previously. Thermal stress (due to severe temperature variations) can induce protein denaturation as well as membrane damage due to modifications of membrane fluidity. Osmotic stress (due the cryoconcentration of the extracellular matrix) leads to water efflux and cell shrinkage, which then results in increased intracellular osmolarity. Water efflux through a rigid membrane and cell shrinkage both also lead to mechanical stress on the membrane which can then result in membrane damage. Finally, oxidative stress can lead to oxidation of cellular lipids and proteins (Fonseca et al. 2003). This oxidative stress was evidenced before freezing et during frozen storage at high subzero temperatures (*e.g.,* -20 °C) (Fonseca et al. 2003). Nonetheless, studies carried out on LAB cells and other bacteria, have shown that thermal and osmotic stresses are the two stresses most involved in cell damage during freezing and thawing (Fonseca et al. 2006; Moussa et al. 2008; Simonin et al. 2015; Meneghel et al. 2017). They will thus be described in more detail below.

I.3.2.a. Thermal stress

The main target of temperature-induced cellular alterations is the cellular membrane (Rault et al. 2007; Cao-Hoang et al. 2010). The lipid membrane phase transitions that occur during cooling (Ts), or heating (Tm), happen over a temperature range dependent on the specific thermodynamic properties of each lipid composing the membrane. During cell membrane phase transition (**Fig. I.3-5**), individual lipids that have already transitioned from a disordered state to an ordered state, will tend to aggregate, resulting in the coexistence of fluid and rigid domains (**Fig. I.3-5B**) (Quinn 1985; Beney and Gervais 2001). This is thought to cause membrane leakage and lateral phase separation of membrane components such as proteins (Drobnis et al. 1993; Tablin et al. 2001). The exclusion of proteins from the rigid parts of the lipid membrane (**Fig. I.3-5C**) results in protein aggregation and eventually leads to their inactivation (Letellier et al. 1977; Tablin et al. 2001). Furthermore, the native conformation of some proteins is dependent on various hydrophobic interactions whose stability peak between 30 and 80 °C and become weaker at both lower and higher temperatures (Chandler 2005; van Dijk et al. 2015). Cold temperatures alone, even above freezing, have been shown to cause protein denaturation (Dias et al. 2010).

I.3.2.b. Osmotic stress

In a study investigating the relative impact of cold and osmotic stress on *L. bulgaricus*, the latter was evidenced as having the most significant impact (Meneghel et al. 2017).

Osmotic dehydration and cell volume reduction induced by the cryoconcentration of the extracellular medium brings about mechanical constraints on the cell membrane. The low compressibility of lipid membranes limits the capacity of cells to shrink passed a certain volume, thus forcing the cellular membrane to wrinkle, leading to membrane permeabilization in *E. coli* (Beney et al. 2004). Permanent deformation and loss of membrane integrity attributed to osmotic stress was also shown in LAB (Murga et al. 2000; Rault et al. 2007; Gautier et al. 2013). Plasmolysis was directly observed through electron microscopy in freeze-thawed *L. bulgaricus* CFL1 cells and in cells stored frozen at temperatures above Tg'e (Fonseca et al. 2006). Osmotic dehydration, similarly to cooling, has furthermore been shown to cause membrane rigidification and membrane phase separation, due to the lyotropic behavior of individual lipids (Laroche and Gervais 2003; Beney et al. 2004). Since a rigid membrane is less permeable to water than a fluid membrane (Stubbs 1983), water efflux through a membrane that exhibits higher rigidity likely induces additional mechanical stress on the membrane.

Increased external osmolarity can also lead to changes in pH and intracellular concentrations. Excessive concentrations of any non-permeating solute can cause membrane permeability alterations (Meryman 1968). Increased osmolarity both inside and outside of the cell can cause protein denaturation in the intracellular compartment and the cell membrane (Sleator and Hill 2002). This is why between Tg'i and Tg'e, even as the intracellular compartment is osmotically inactive, the cell membrane can still incur damage due to the high osmolarity of the extracellular matrix (Fonseca et al. 2016).

It is likely that cell injury or death caused by cryopreservation stems from a combination of all the above-mentioned stresses. Each stress can show varying relative importance, depending on the physiological characteristics of the considered strain, and the applied cryopreservation protocol. Cell resistance to a cryopreservation process can be improved by modulating fermentation parameters (culture medium, temperature, pH, etc.), as well as various cryopreservation parameters (cryoprotectant formulation, freezing and thawing rates, storage temperature).

Table I.3-1 : *Reported work on the investigation of cellular component modifications that have been related to an increase of the LAB survival rate following freezing or frozen storage*

Cell components or properties	LAB and conditions	Methods	Possible link to cryoresistance	References
Lipid membrane				
Lipid phase transition	*L. bulgaricus* CFL1 grown in MRS or whey-based culture media	Dynamic FTIR measurements (during cooling (Ts) and heating (Tm) between +50 °C and -50 °C) in aqueous conditions (3000 - 2800 cm^{-1} region)	**Lower lipid phase transition temperature** (Ts=-8 °C vs 22 °C); **higher position of $vsCH_2$** in frozen range (2850.5 cm^{-1} vs 2849.5 cm^{-1} at -48 °C)	(Gautier et al. 2013)
	L. bulgaricus CFL1 and *L. bulgaricus* ATCC 11842		**Lower lipid phase transition temperature** (Ts= 5.7 °C vs 13.8 °C); **higher position of $vsCH_2$** in frozen range (2850 cm^{-1} vs 2849.5 cm^{-1} at -48 °C)	(Meneghel et al. 2017)
Fluidity	*L. bulgaricus* CFL1 grown in MRS or whey-based culture media	Fluorescence anisotropy, synchrotron UV fluorescence microscopy	Increased fluidity at 0 °C (TMA-DPH anisotropy 0.120 vs 0.330 vs 0.250), no rigid lipid domains	(Passot et al. 2014)
	L. bulgaricus CFL1 and *L. bulgaricus* ATCC 11842 whey-based culture media	Fluorescence anisotropy	Increased fluidity at 0 C° (DPH anisotropy 0.250 vs 0.280)	Meneghel et al. 2017)
Fatty acid composition	*L. bulgaricus* NSC1, NSC2, NSC3 and NSC4 grown with or with Tween 80	Extracted lipids analysed by gas chromatography	**Higher UFA/SFA** (1.14 vs 0.7) and **higher CFA** content (17.05 % vs 4.2 %)	(Smittle et al. 1974)
	Lactobacillus ssp. A-12, *S. lactis* grown with or without Tween 80		Lactobacillus: **Higher UFA/SFA** (1.15 vs 0.65) and **higher CFA content** (19 % vs 10.7 %); *S. lactis*: **Higher UFA/SFA** (1.1 vs 0.3)	(Goldberg and Eschar 1977)
	Streptococci (AC1, AC11, E8, ML1) grown without and with controlled pH		**Higher UFA/SFA** (1.48 vs 1.06)	(Gilliland and Speck 1974)
	Lc. lactis ssp. *lactis* (MM210 and FG2), *Lc. lactis* ssp. *cremoris* (MM160 and MM310): heat (HS) or cold (CS) shock		HS: **Lower UFA/SFA** (0.65 vs. 0.82) and **higher CFA** content (23.25 % vs 16.12 %) CS: **Higher UFA/SFA** (1.09 vs 0.82)	(Broadbent and Lin 1999)
	L. acidophilus CRL 640 grown at different temperatures		**Lower CFA** content (5.7 % vs 16.9 %) Higher content of glycolipids	(Murga et al. 2000)
	S. thermophilus CFS2 grown under different conditions		**Higher UFA/SFA** (1.43 / 1.45)	(Beal et al. 2001)
	L. bulgaricus (CIDCA 331, CIDCA 332, CIDCA 333, ATCC 9659), *L. lactis* (CIDCA 123, CIDCA 133), *L. helveticus* ATCC 15807, *L. acidophilus* CIDCA 134		*L. bulgaricus*: **Higher UFA/SFA** (2.26 vs 1.24) and **lower CFA** content (0.4 % vs 18 %) Other strains: **Lower UFA/SFA** (1.2 vs 2.35) and **higher CFA** content (17.4 % vs 2 %)	(Gomez Zavaglia et al. 2000)

UFA: unsaturated fatty acids; SFA: saturated fatty acids; CFA: cyclic fatty acids; temperature; Ts: temperature of lipid phase transition during cooling (s, solidification); Tm, temperature of lipid phase transition during heating (m, melting); $vsCH_2$: the position of the symmetric CH_2 stretching band of fatty acids acyl chains at approximately 2850 cm^{-1} (DPH: 1,6-diphenyl-1,3,5-hexatriene/hydrophobic probe ; TMA-DPH: 1-[4 (trimethylamino) phenyl]-6-phenyl-1,3,5-hexatriene/amphiphilic probe; PCR: polymerase chain reaction; MALDI-TOF: Matrix Assisted Laser Desorption Ionization - Time of Flight; FTIR: Fourier transform infrared; SR: synchrotron radiation

I.3.3. Improving the cryoresistance of LAB

Cryoresistance varies depending on bacterial species or strain and on various production parameters. These include growth conditions, cryoprotective additives as well as cooling, thawing and storage protocols. Cellular markers that favor cryoresistance have been identified by investigating cellular characteristics discriminating cryoresistant LAB populations from cryosensitive ones. Some of these markers have been induced in natively cryosensitive populations by controlling fermentation and post-fermentation conditions. Cryoresistance can also be improved further, by using cryoprotective solutions and controlling freezing, storage and thawing protocols.

I.3.3.a. Identifying markers of cryoresistance

Table I.3-1 present studies that have investigated cellular markers discriminating cryo-resistant LAB populations from cryo-sensitive ones, to identify those that may be involved in cryoresistance mechanisms. Characteristics linked to the more cryo-resistant populations are indicated, as well as analytical methods used.

(i) Cellular markers involving membrane properties

Since the cell membrane appears to be the primary target of freeze-injury (Murga et al. 2000; Murga et al. 2001; Rault et al. 2007; Gautier et al. 2013), a lot of research on LAB cryoresistance has been geared towards characterizing lipid membrane properties involved in cryoresistance mechanisms (**Table I.3-1**).
Membrane fluidity is usually determined by quantifying the fluorescence anisotropy of a probe such as diphenylhexatriene (DPH), inserted in the lipid bilayer (Passot et al. 2014; Velly et al. 2015; Meneghel et al. 2017). Lipid phase transition temperatures can additionally be measured *in situ* and during freezing or thawing, by using FTIR spectroscopy (Oldenhof et al. 2005; Gautier et al. 2013; Fonseca et al. 2016). These analytical methods have shown that cryoresistant populations exhibit higher membrane fluidity and lower Ts than cryosensitive populations (Gautier et al. 2013; Passot et al. 2014; Meneghel et al. 2017). The lower the Ts of a cell membrane is, the more fluid it remains along the freezing process and the easier water can diffuse through it, thus limiting membrane damage.

Table I.3-1 (continued): *Reported work on the investigation of cellular component modifications that have been related to an increase of the LAB survival rate following freezing or frozen storage*

Cell components or properties	LAB and conditions	Methods	Possible link to cryoresistance	References
Lipid membrane				
Fatty acid composition (continued)	*L. acidophilus* RD758 grown under different pH and temperature	Extracted lipids analyzed by gas- chromatography coupled to mass spectrometry	**Higher CFA** content (11-12% vs 4-8%)	(Wang et al. 2005a)
	L. acidophilus RD758, cold adaptation		**Higher UFA/SFA** (0.22 vs 0.18) and **higher CFA** content (3.1 % vs 2.5 %)	(Wang et al. 2005b)
	L. acidophilus RD758 exposed to nutrient starvation		**Higher UFA/SFA** (0.18 vs 0.15) and **higher CFA** content (2.25 vs 1.62)	(Wang et al. 2011)
	L. bulgaricus CFL1 grown in MRS or whey-based culture media		**Higher UFA/SFA** (1.6 vs 0.5) and **higher CFA** content (14 % vs 2%)	(Gautier et al. 2013)
	L. bulgaricus CFL1 and *L. bulgaricus* ATCC 11842 in whey-based culture media		**Higher UFA/SFA** (1.04 vs 0.69)	(Meneghel et al. 2017)
Proteins				
	Lc. lactis ssp. lactis (MM210 and FG2), *Lc. lactis ssp. cremoris* (MM160 and MM310): heat (HS) or cold (CS) shock	Addition of erythromycin in the growth medium	Requirement of stress-induced proteins for improving resistance to freezing	(Broadbent and Lin 1999)
	Lc. lactis (M474, M392) exposed to cold shock	DNA sequence analysis through PCR amplification and cloning	Presence of a gene encoding for cold-shock proteins	(Kim and Dunn 1997)
	L. plantarum NC8 mutants	Generation of mutant strain overproducing cold-shock proteins (CspL, CspP, and CspC)	Increased production of a cold-shock protein (CspP)	(Derzelle et al. 2003)
	L. acidophilus RD758 exposed to cold stress	Proteome analysis through 2D electrophoresis and MALDI-TOF	Upregulation of cold-shock proteins involved in carbohydrate and energy metabolisms and in pH homeostasis	(Wang et al. 2005b)
	L. bulgaricus CFL1 exposed to acid stress	Proteome analysis through 2D electrophoresis	Upregulation of 11 proteins and downregulation of 10 proteins	(Streit et al. 2008)
	L. bulgaricus CFL1 grown in MRS or whey-based culture media	SR-FTIR micro-spectroscopy of dried cells (1800 - 1300 region)	High content of alpha-helical proteins and low content of beta-sheet proteins	(Passot et al. 2015)
	L. bulgaricus CFL1 and *L. bulgaricus* ATCC 11842 whey-based culture media	FTIR micro-spectroscopy in aqueous conditions (1800 - 1300 cm^{-1} region)	Low content of alpha-helical proteins and high content of beta-sheet proteins	(Meneghel et al. 2020)
Cell wall components				
	L. bulgaricus CFL1 grown in MRS or whey-based culture media	SR-FTIR micro-spectroscopic measurement of dried cells (1300 – 900 cm^{-1} region)	Higher absorbance of PO_2^- groups (1253 - 1238 cm^{-1})	(Passot et al. 2015)
	L. bulgaricus CFL1 and *L. bulgaricus* ATCC 11842 whey-based culture media	FTIR micro-spectroscopic measurement in aqueous conditions (1360 -975 cm^{-1} region)	Lower absorbance of complex sugar rings (1076 - 1052 cm^{-1}) and PO_2^- groups (1222 - 1200 cm^{-1})	(Meneghel et al. 2020)

Membrane fluidity and phase transition temperatures are membrane properties mainly governed by the fatty acid composition of lipid membranes, and more specifically, largely by the ratio of unsaturated over fatty acid content (UFA/SFA) (Fonseca et al. 2019). The characterization of the fatty acid composition of bacterial membranes involves the extraction and methylation of cell fatty acids, followed by their identification and quantification using gas chromatography generally coupled with mass spectrometry (GC-MS). As expected, cryoresistant LAB populations were widely reported to have higher contents of unsaturated over saturated fatty acids compared to cryosensitive ones (Smittle et al. 1974; Gilliland and Speck 1974; Goldberg and Eschar 1977; Broadbent and Lin 1999; Gomez-Zavaglia et al. 2000; Béal et al. 2001; Wang et al. 2005; Wang et al. 2011; Gautier et al. 2013; Meneghel et al. 2017).

Although cyclic fatty acids (CFA) seem to be involved in cryoresistance and lipid membrane property modulations, their effect remains unclear and contradictory. Some studies have associated better cryoresistance to high CFA contents (Smittle et al. 1974; Goldberg and Eschar 1977; Broadbent and Lin 1999; Gomez-Zavaglia 2000; Wang et al. 2005; Gautier et al. 2013), while others have associated it to low CFA contents (Murga et al. 2000; Gomez-Zavaglia et al. 2000). Similarly, some authors believe CFAs contribute to membrane fluidity (Machado et al. 2004; Zhang and Rock 2008), while others have reported a membrane fluidity decrease with increasing CFA content (Li et al. 2009; Velly et al. 2015). More research thus seems necessary to understand the role of CFA in membrane fluidity and cryoresistance.

In a few studies, only minor modifications of the membrane fatty acid composition were observed (Béal et al. 2001; Wang et al. 2005b; Wang et al. 2011), indicating that other cellular components and mechanisms are likely involved in LAB cryoresistance.

(ii) Cellular markers involving protein synthesis and other cellular components

Studies investigating the proteome of cryoresistant vs cryosensitive LAB populations, have used genomic (Kim and Dunn 1997; Derzelle et al. 2003), proteomic (Streit et al. 2008 ; Wang et al. 2011) and FTIR micro-spectroscopic (Passot et al. 2015; Meneghel et al. 2020) approaches (**Table 1.3-2**). These studies have linked improved cryoresistance to changes in protein synthesis, and more specifically to the production of cold-shock proteins (Kim and Dunn 1997; Derzelle et al. 2003). These proteins are believed to improve cryo-resistance by maintaining efficient transcription and translation under low positive temperatures (Wouters et al. 1999a; Derzelle et al. 2003; Keto-Timonen et al. 2016).

By cryoconcentrating the extracellular compartment, freezing likely induces changes in molecular interactions in and around the cell wall (**Fig. I.2-2**). The main cell wall components in Gram-positive bacteria are the peptidoglycan and teichoic acids. Both are believed to play an important role in maintaining membrane integrity (Neuhaus and Baddiley 2003; Dmitriev et al. 2005; Misra et al. 2013).

Two *L. bulgaricus* populations presenting varying levels of cryoresistance were reported to exhibit significant differences in the molecular composition of their cell wall (Passot et al. 2015; Meneghel et al. 2020). Both studies were done using FTIR micro-spectroscopy. The first one, carried out on dried samples of *L. bulgaricus* CFL1, revealed increased absorption of bands associated to phosphodiester containing components, such as teichoic acids, in the cryoresistant population (grown in MRS instead of a whey-based medium). However, to avoid potential bias induced by sample drying Meneghel et al. (2020) developed an FTIR micro-spectroscopic approach enabling the accurate exploitation of the entire mid-infrared region of bacterial cells, in aqueous conditions. Their study of cryoresistant *L. bulgaricus* ATCC 11842 and cryosensitive *L. bulgaricus* CFL1 using the novel FTIR approach, revealed on the contrary that a higher contribution of bands associated to phosphodiesters, characterized the cryosensitive strain. Though the cell wall seems to likely be involved in LAB cryoresistance, further investigation is necessary to better understand its role in cryoresistance mechanisms.

I.3.3.b. Changing fermentation and post-fermentation conditions to favor markers of cryoresistance

The modulation of membrane fatty acid composition or synthesis of stress proteins can be induced by changing bacterial production parameters while cells are still metabolically active. Many studies have thus focused on identifying fermentation medium compositions, temperature, pH or harvest time as well as post-fermentation treatments that increase LAB cryoresistance.

(i) Changing environmental conditions during fermentation

Fermentation medium

Changing the fermentation medium of LAB can lead to changes in cell membrane properties and other cellular components, including protein content and cell wall compositions. Adding sodium oleate (Tween 80) to the fermentation medium of *L. bulgaricus* cells was reported to improve cryoresistance by increasing the UFA and CFA contents of their lipid membrane (Smittle et al. 1974). Higher contents of UFA and CFA was also reported in *L. bulgaricus* cells grown in MRS compared to a Whey-based medium, and linked to lower lipid membrane phase transition temperatures upon freezing and thawing, resulting in higher cryoresistance (Gautier et al. 2013).

The growth of *L. bulgaricus* cells in MRS was also reported to lead to higher membrane fluidity (Passot et al. 2014), higher contents of cell proteins presenting α-helix structures and of charged polymers such as teichoic acids that constitute the Gram-positive bacterial wall (Passot et al. 2015).

Fermentation temperature

Fermentation temperature was reported to be a strong lever for improving cryoresistance of LAB, by modulating their fatty acid composition and proteome.
Growth of *L. acidophilus* under sub-optimal fermentation temperatures (*i.e.,* temperatures below the optimal temperature for growth), has been reported in several papers to lead to changes in membrane fatty acid composition, resulting in improved cryoresistance (Murga et al. 2000; Murga et al. 2001; Wang et al. 2005c). The improved cryoresistance of *L. acidophilus* CRL 640 cells grown at 25 °C instead of 40 °C was linked to an increase in C18:2 and C16:0 contents and a concomitant decrease of C14:0 and cycC19:0 (Murga et al. 2001). The increased cryoresistance of *L. acidophilus* RD758 grown at 30 °C instead of 42 °C was also ascribed to changes in membrane fatty acid composition but was additionally linked to changes in protein synthesis (Wang et al. 2005). Some of the upregulated proteins included ribosomal protein S2 and the GTPase TrmE, which facilitate translation at low temperature. Among the downregulated proteins were glutamate N-acetyltransferase, pyruvate dehydrogenase and elongation factor, involved in amino acid biosynthesis, glycolysis and protein translation, respectively, thus indicating a general metabolism reduction at 30 °C.

Fermentation pH

Carrying out fermentations at lower pH values has been reported to be another interesting lever for improving LAB cryoresistance (Béal *et al.* 2015). Controlling the fermentation pH of *L. acidophilus* RD758 cells at a sub-optimal value (pH 5 instead of pH 6), was reported to modify their fatty acid composition in a way that favored cryoresistance (Wang *et al.* 2005a). The C16:0, C18:1 and cycC19:0 relative contents were increased in cells grown at pH 5 compared to pH 6, to the detriment of C14:0 and C18:0. These changes in membrane fatty acid composition led to a UFA/SFA increase. These results confirm those previously reported by Béal *et al.* (2001) with *S. thermophilus* CFS2, indicating that cells exhibited higher UFA/SFA when fermentation was carried out at pH 5.5 instead of pH 6.0.

(ii) Changing environmental conditions at the end of fermentation

Cooling and acidification before harvest

The cold incubation of *L. acidophilus* RD748 (8 h at 26 °C) and *L. plantarum* L67 (6 h at 5°C) prior to harvest was shown to improve their cryoresistance (Wang et al. 2005c; Song et al. 2014). In the case of *L. acidophilus*, authors reported a slight increase in UFA/SFA (0.18 to 0.22) and in the relative cycC19:0 fatty acid

concentrations (2.5 to 3.1%). Moreover, an increased synthesis of four proteins involved in stress response was observed. In the case of *L. plantarum*, the authors linked the cells improved cryoresistance to the induction of 24 proteins, 13 of which were identified to be mainly involved in cell growth, energy metabolism and stress response.
Other authors also demonstrated that cold adaptation prior to freezing could similarly improve the cryoresistance of *Lc. lactis* (Kim et al. 1999; Broadbent and Lin 1999), *L. bulgaricus* (Panoff et al. 2000) and *E. faecalis* (Thammavongs et al. 1996). In addition to the effect of cold incubation, the effect of acid shock prior to harvest was demonstrated to improve the cryoresistance of *L. bulgaricus* CFL1 (Streit et al. 2008). Authors reported changes in the synthesis of 21 proteins involved in energy metabolism, nucleotide and protein synthesis and stress response.

Harvest time
Increasing the harvest time of *L. bulgaricus* CFL1 from exponential growth phase to stationary or late-stationary phase was reported improve cryoresistance (Rault et al. 2009). This improvement was linked to changes in membrane fatty acid composition, demonstrated by an increase in C16:0 and cycC19:0 and a decrease in C18:1, as well as changes in protein synthesis (Rault et al. 2010). Proteins involved in nucleotide metabolism, transcription and translation processes were down-regulated, while those involved in energy, amino acids, and lipid metabolisms as well as stress proteins were up-regulated.
In *L. acidophilus* and *L. plantarum*, stationary phase harvest resulted in improved cryoresistance (Lorca and de Valdez 1999; Péter and Reichart 2001), which could be explained by a significant up-regulation of proteins related to survival under nutrient starvation as well as general stress response proteins (Lorca and de Valdez 2001; Cohen et al. 2006).

Nutrient starvation
Nutrient starvation, a stress that happens to be the most frequent type of stress provoking entry into stationary growth phase (van de Guchte et al. 2002), was also shown to improve cryoresistance of LAB. An 18-hour lactose starvation of *L. acidophilus* RD748 prior to harvest, induced a physiological response resulting in an improved ability to resist freezing and frozen storage (Wang et al. 2011a). This improved cryoresistance was linked to an up-regulation of proteins involved in energy metabolism and pH homeostasis, and a down-regulation of proteins involved in transcription and translation processes and biosynthesis amino acids, proteins, and other cell wall components. Furthermore, these starved cells also showed an increase in branched, unsaturated, and cyclic fatty acids in membrane lipids, likely contributing to their improved cryoresistance.

I.3.3.c. Using cryoprotective solutions and controlling freezing, storage, and thawing protocols

Once cells are harvested, they are chilled and concentrated. Their metabolic activity is thus slowed down, and physiological state degradation is minimized. Further improvement of LAB cryoresistance can be achieved, in the absence of any active metabolism. This can be done by using cryoprotective additives and by optimizing freeze-thawing and storage conditions.

(i) Cryoprotection

Suspending freshly harvested cells in a cryoprotective solution prior to freezing, significantly reduces the damaging effects of freezing and extends the range of optimal freezing operating conditions.

The most common cryoprotective agents (CPAs) currently used in LAB cryopreservation include:

- Mono- and disaccharides, such as sucrose (Cárcoba and Rodríguez 2000; Berner and Viernstein 2006; Wang et al. 2019a) trehalose (Cárcoba and Rodríguez 2000; Giulio et al. 2005) and lactose (Cárcoba and Rodríguez 2000);
- Polyols such as inositol (Péter and Reichart 2001) and glycerol (Fonseca et al. 2000; Fonseca et al. 2001; Fonseca et al. 2003; Wang et al. 2019);
- Amino acids and peptides, such as glutamate and betain (Fonseca et al. 2003)
- Vitamins, such as ascorbic acid (Fonseca et al. 2003)
- Complex media such as meat extract (Cárcoba and Rodríguez 2000) and skimmed milk (Berner and Viernstein 2006; Wang et al. 2019)

The protective mechanisms exerted by cryoprotectants are still not fully understood and depend on the nature of the CPAs they contain and their ability to permeate the cell membrane (Béal and Fonseca 2015). Four main mechanisms of action identified are described below.

<u>Preventing intracellular ice formation</u>

CPAs induce water efflux from the cell, thus favoring cell dehydration and shrinkage and ultimately avoiding the risk of intracellular ice. CPA that can permeate through

the cell membrane prevent intracellular ice formation by lowering the freezing point inside the cell through increased hydrogen bonds with water molecules (Fonseca et al. 2003).

Increasing the extracellular glass transition temperature

The extracellular glass transition temperature of a cryoprotected cell suspension mostly depends on the nature and concentration of the CPAs used. The glass transition temperature of the extracellular medium (Tg'e) can thus be increased by the addition of certain CPA, allowing the maintenance of an amorphous medium around the cells, at higher temperatures. Disaccharides and high molecular weight molecules such as maltodextrins, have been shown to significantly increase the Tg'e of a cryoprotected LAB suspension, thus allowing higher storage temperatures (Béal and Fonseca 2015).

Protecting the cytoplasmic membrane

Some CPA (such as sucrose or trehalose) are thought to protect the lipid membranes during freezing by direct interaction with membrane phospholipids through hydrogen bonding with polar headgroups (Crowe et al. 1984; Lambruschini et al. 2000; Lairion and Disalvo 2007). Other CPA are thought to protect the cell membrane by modifying the lipid structure and transition temperature. Dimethyl sulfoxide (DMSO) and glycerol, for example, were shown to reduce the acyl chain packing of model mammalian cells (human foreskin fibroblasts) during freezing (Ragoonanan et al. 2010).

Limiting oxidation damage

The use of CPA that exhibit antioxidant properties (*i.e.,* prevent oxidation reactions by scavenging reactive oxygen species), can be effective in limiting oxidation of cellular lipids and proteins. Sodium ascorbate, for example, was shown to be effective in limiting oxidation damage during frozen storage of *L. bulgaricus* (Fonseca et al. 2003).

(ii) Freezing, storage and thawing protocols

As mentioned previously, in the paragraph about cooling rates for bacterial concentrates (**§ I.3.2**), if high cooling rates are applied, the extracellular matrix does not have time to maximally cryo-concentrate, and a significant amount of water vitrifies to form a glassy matrix instead of crystalizing to form ice. In that case, the glass transition temperature of the extracellular matrix (Tg'e) is very low and the

frozen concentrate must be stored at a temperature below Tg'e to avoid ice recrystallization and other diffusion reactions leading to cell damage (Cárcoba and Rodríguez 2000; Fonseca et al. 2001; Fonseca et al. 2006). The stability provided by cryopreservation is thus highly dependent on storage temperature. If storage is conducted at a temperature above the extracellular glass transition temperature, and not all unbound water had crystalized during the freezing stage, undesired ice re-crystallization may occur and cause plasmolysis of LAB cells (Fonseca et al. 2006) (**Fig. I.3-2**).

If slow cooling rates are applied, these phenomena are avoided, and protocols are better controlled and thus more repeatable. Furthermore, storage can be carried out at higher temperatures (*e.g.,* -40 °C, assuming the Tg'e of the cryoprotective solution used is higher than -40 °C), thus reducing energy costs of storage and frozen transport. When slow cooling rates are applied and storage is carried out at higher temperatures (-20°C), cell damage is mainly cause by osmotic stress (because the extracellular matrix maximally cryoconcentrates) and oxidative stress (Fonseca et al. 2003). A better understanding of these mechanisms is still needed to improve LAB cryopreservation protocols under these conditions.

Thawing by immersion of the frozen sample in a warm water bath (between 30 and 42°C, depending on the considered strain) until all ice has melted, is widely applied (De Paoli 2005; Smith et al. 2008; Prakash et al. 2013). Immersion in a warm water bath results in a fast rate of thawing (~110 °C/min), minimizing the time the cells are exposed to stressful conditions before being suspended back in their initial medium exhibiting favorable osmolarity. Applying fast thawing rates is all the more important if fast cooling rates were applied, to limit ice recrystallization (Baumann and Reinbold 1966).

I.3.4. Concluding remarks

Cryopreservation is a challenging stabilization process for LAB cells. Freezing, frozen storage and thawing can induce significant degradation of cellular structures, resulting in loss of LAB technological function or death. Modulating various parameters during the production of cryopreserved LAB concentrates has proven to be powerful in modifying membrane compositions, protein synthesis or vitrification temperatures, in favor of increased cryoresistance. Not all LAB populations, however, respond to a cryopreservation process in the same way. Comparing the cellular characteristics of fresh and thawed LAB populations

presenting different cryoresistance levels, would improve knowledge on cellular mechanisms of cryoresistance and cryoinjury. Most studies have limited their investigation of the effects of cryopreservation on LAB to a reduced number of species and to at most two cellular structures at a time (the effect on the lipid membrane composition and proteins synthesis). Few studies have looked at all the cellular structures in conjunction. The only studies that have, have used FTIR micro-spectroscopy, and only one study (Meneghel et al. 2020) has done so on live cells, in aqueous conditions.

I.4. General insights

In the first part of this review, we have seen that biological TTI are promising tools that can help improve food safety and prevent a lot of food waste. However, more research and development has yet to be carried out before they can be fully deployed within the food industry. The main obstacle is the reduced range of shelf-life current biological TTI can offer. In the second part of this review, we have seen that modulating the growth and acidification kinetics of *C. maltaromaticum* concentrates – the only microorganism ever used in TTI development, so far – could be an important step towards increasing shelf-life range. However, there is a lack of knowledge on the characterization and optimization of *C. maltaromaticum* growth and metabolite production, both in a bioreactor to produce concentrates; and in an environment similar to the one inside biological TTI labels. It is thus necessary to gain more insight into the effect of culture conditions on *C. maltaromaticum* in order to design strategies for the production of *C. maltaromaticum* concentrates with physiological responses of interest to biological TTI. In the last part of this review, we have seen that cryopreservation is a stressful stabilization process that can lead to loss of technological function and death of lactic acid bacteria. However, it is a stabilization process that does not seem to impact the technological function of *C. maltaromaticum* concentrates. A thorough characterization of *C. maltaromaticum* cells along with other LAB species and strains presenting varying levels of cryoresistance could help gain more insight into lactic acid bacteria cryoresistance markers.

Part II
Materials and Methods

Content

II.1. Experimental approach 103
II.2. Bacterial concentrate production 107
II.2.1. Strain and inocula preparation 107
II.2.2. Fermentation 107
II.2.2.a. Equipment 107
II.2.2.b. Preparation and culture conditions 109
II.2.2.c. Monitoring of fermentation kinetics 111
II.2.2.d. Concentration and protection 111
II.2.2.e. Stabilization, storage and re-activation 111
II.2.3. Physiological state assessment 113
II.2.3.a. Viability (culturability) 113
II.2.3.b. Acidification activity 113
II.3. Intracellular glass transition temperature assessed by DSC 113
II.3.1.a. Equipment 113
II.3.1.b. Sample preparation 114
II.3.1.c. Essay procedure 114
II.4. Membrane fluidity assessed by fluorescence anisotropy 114
II.4.1.a. Equipment 114
II.4.1.b. Sample preparation and staining 114
II.4.1.c. Essay procedure 115
II.5. FTIR micro-spectroscopic characterization in aqueous conditions 117
II.5.1.a. Equipment 117
II.5.1.b. Sample preparation 119
II.5.1.c. Spectra acquisition 119
II.5.1.d. Spectra pre-processing: atmospheric suppression and water subtraction 121
II.5.1.e. Spectra post-processing and statistical analysis 123
II.6. FTIR spectroscopic measurements during cooling and heating 127
II.6.1.a. Equipment 127
II.6.1.b. Sample preparation 127
II.6.1.c. Spectra acquisition 129
II.6.1.d. Spectra analysis 129

II.7. Fatty acid composition 130
II.7.1. Accelerated Solvent Extraction (ASE) 130
II.7.1.a. Equipment 130
II.7.1.b. Sample preparation 130
II.7.1.c. Extraction method 130
II.7.2. Fatty acid identification by GC-MS 131
II.7.2.a. Equipment and configuration 131
II.7.2.b. Sample preparation 131
II.7.2.c. Identification and quantification 131
II.8. Statistical analyses 132
II.8.1.a. Stepwise descending multiple regression analyses 132
II.8.1.b. Principal Component Analyses 132
II.8.1.c. ANOVA 132
II.8.1.d. Kruskal-Wallis tests 133

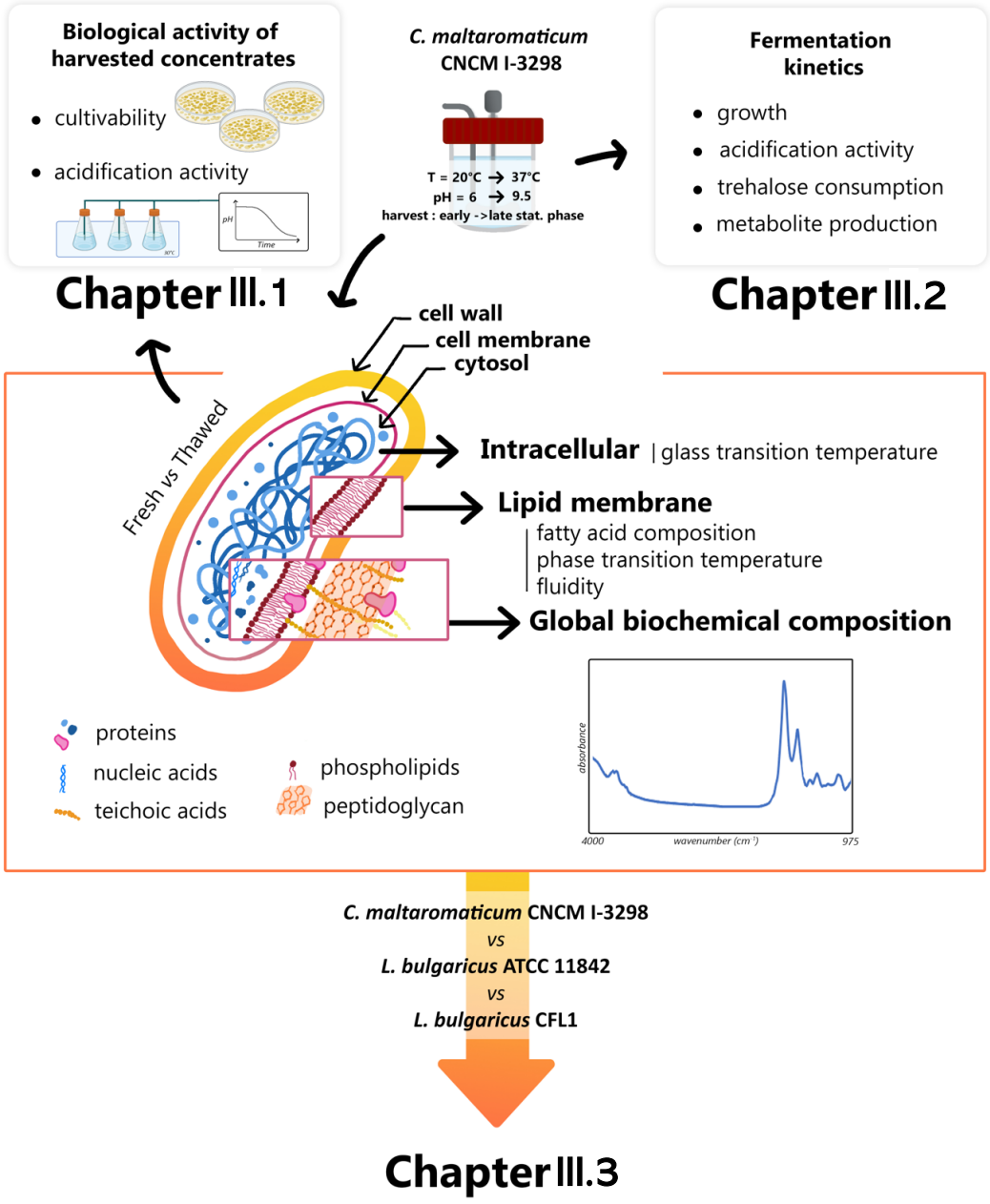

Figure II.1-1: *Schematic overview of the experimental approach carried out in this work.*

II.1. Experimental approach

The objectives of this project were structured around three main parts: **(i)** design strategies for the production of *Carnobacterium maltaromaticum* concentrates with physiological responses of interest to biological TTIs; **(ii)** characterize these concentrates in order to link their physiological responses (cultivability, acidification activity and resistance to stabilization) to biophysical and biochemical properties and **(iii)** compare these properties to those of two other LAB strains, presenting lower cryoresistances, in order to search for markers of cryoresistance and cryoinjury.

A schematic overview of the experimental approach carried out in this work is presented in **Figure II.1-1**. Only the main measurements related to the different chapters of the *Results & Discussion* part of this manuscript are mentioned in the figure.

1/ First, *C. maltaromaticum* CNCM I-3298 concentrates were produced under varying temperatures (20 °C to 37 °C) and pH (pH 6 to pH 9.5) and harvested at increasing times from early to late stationary growth phase. This was done in the hope of changing the acidification activity of the harvested concentrates, without loss of cultivability or any other technological function (*e.g.,* resistance to freezing).

2/ Biological activity measurements were carried out on fresh and thawed harvested concentrates, to quantify the impact of fermentation temperature, pH and harvest time on *C. maltaromaticum*. This led to a predictive model for the production of cell concentrates presenting a broad range of acidification activities. This work was published in a peer-reviewed journal [*Appl Microbiol Biotechnol*, 2019, 126(5):1468-1479] and is presented in **CHAPTER III.1** of the *Results & Discussion* section.

3/ The fermentation kinetics (growth, acidification activity, substrate consumption and metabolite production) of *C. maltaromaticum* cultivated under different temperatures and pH values were monitored. This enabled the development of a

dynamic model for the growth and bioconversion of *C. maltaromaticum* CNCM I-3298, in collaboration with Dr. Cristian Puentes (Associate Professor at *École Centrale de Paris*). This work was published in a peer-reviewed journal [*Foods*, 2021, 10(8):1922-1945] and is presented in **CHAPTER III.2** of the *Results & Discussion* section.

4/ Finally, because of its exceptional cryoresistance, *C. maltaromaticum* CNCM I-3298 was used as a model strain of cryoresistance in a search for markers of cryoresistance and cryoinjury in lactic acid bacteria. The characteristics of fresh and thawed *C. maltaromaticum* cells were compared to those of two other LAB strains: *L. bulgaricus* ATCC 11842 and *L. bulgaricus* CFL1. A thorough characterization of these strains involved the assessment of their intracellular glass transition temperature, their lipid membrane properties (fatty acid composition, phase transition temperature and fluidity) and their global biochemical composition. This work was submitted for publication in a peer-reviewed journal (*Analytical and Bioanalytical Chemistry* journal) and is presented in **CHAPTER III.3** of the *Results & Discussion* section.

A detailed description of all materials and methods used throughout this project, is presented in the following.

Table II.2-1 *: Compositions of main culture media and cryoprotectant solutions used in this work*

	Quanity ***(g/kg of water)***	**Ingredients**	**Suppliers**
Fermentation medium	10	Proteose peptone	Oxoid; Waltham, MA, USA
	5	Yeast extract	Humeau; La-Chapelle-sur-Erdre, France
	5	Tween 80	VWR; Leuven, Belgium
	40	Trehalose	Treha™; Tokyo, Japan
	0.41	MgSO4	Merck; Darmstadt, Germany
	0.056	MnSO4	Merck; Darmstadt, Germany
Trehalose based cryoprotectant (20%)	200	Trehalose	Treha™; Tokyo, Japan
	9	NaCl	VWR; Leuven, Belgium
Cinac medium (acidification activity measurements)	10	Proteose peptone	Oxoid; Waltham, MA, USA
	5	Yeast extract	Humeau; La-Chapelle-sur-Erdre, France
	5	Tween 80	VWR; Leuven, Belgium
	15	Trehalose	Treha™; Tokyo, Japan
	60	Glycerol	VWR; Leuven, Belgium
	0.41	MgSO4	Merck; Darmstadt, Germany
	0.056	MnSO4	Merck; Darmstadt, Germany

II.2. Bacterial concentrate production

II.2.1. Strain and inocula preparation

The strain studied throughout this work was *Carnobacterium maltaromaticum* CNCM I-3298 (National Collection of Cultures of Microorganisms, Pasteur Institute, France). Stock cultures were stored at -80 °C in milk (EPI Ingredients, Ancenis, France) supplemented with 15 % (wt/wt) glycerol (VWR, Leuven, Belgium). Re-activation of cells was done by thawing 1 mL cryotubes of stock culture in a 30 °C water bath for 3 min.

Re-activated bacterial suspensions were pre-cultured twice in the fermentation medium (see **Table II.2-1** for detailed composition), before being used to inoculate the bioreactor.

Ten milliliters of sterilized medium (121 °C for 20 min) were inoculated with 100 µL of thawed stock culture and incubated at 30 °C for 13 to 16 h, until the beginning of stationary growth phase (see **Fig. I.2-6**). One milliliter of the resulting culture was transferred into 50 mL of fresh medium before being incubated for 11 h under the same conditions, until the beginning of stationary growth phase. No stirring was applied to the pre-cultures. The resulting culture was used to inoculate the bioreactor.

II.2.2. Fermentation

II.2.2.a. Equipment

C. maltaromaticum was cultured in a 4 L bioreactor (Minifors 1; Infors HT, Bottmingen, Switzerland) with a working volume of 3.5 L. Cell growth was monitored by an 880 nm infra-red probe (Excell210; CellD, Roquemaure, France). pH was monitored using a Mettler Toledo pH probe (InLab Reach 325, Mettler Toledo; Colombus, OH, USA) **(Fig. II.2-1)**.

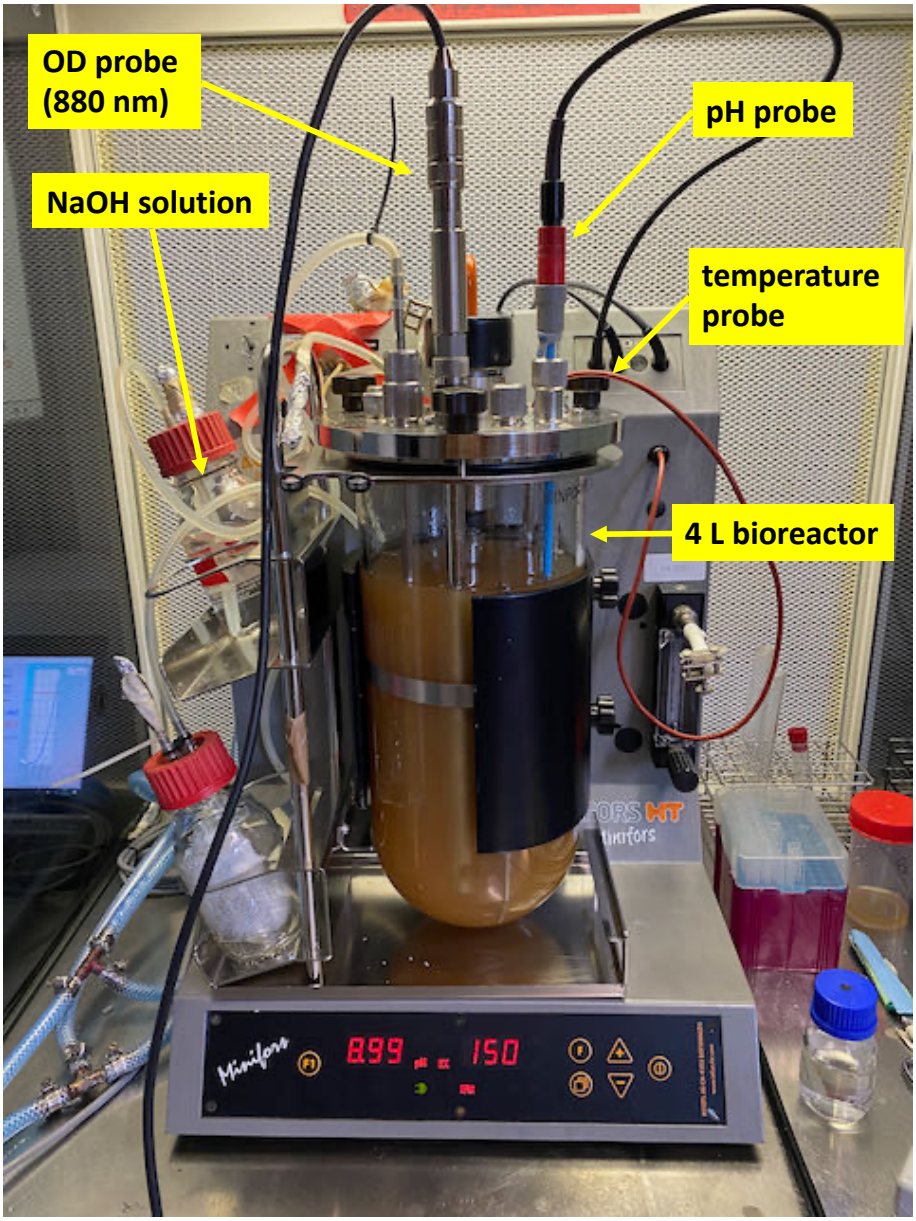

Figure II.2-1: *Bioreactor and probes used in this study*

II.2.2.b. Preparation and culture conditions

The pH of the fermentation medium (**Table II.2-1**) was adjusted to the desired value with 5N NaOH solution (VWR, Pennsylvania, USA) prior to sterilization at 121°C for 20 min. After cooling, the sterilized culture medium was introduced into the bioreactor under a laminar flow hood. The pH value of the sterilized medium was verified and adjusted again, when necessary, with 5N NaOH or 0.01N H_2SO_4 solution. Inoculation was performed at an initial concentration of approximately 10^7 CFU mL^{-1}, corresponding to 28 mL of an inocula exhibiting an optical density of 0.7 (at 600 nm). An agitation speed of 150 rpm was applied for culture homogenization. Temperature and pH were set and maintained at different values: 20 °C to 37 °C and pH 6 to 9.5, according to the experimental plan presented in Chapter III.1. of the *Results & Discussion* section. pH was controlled by the automatic addition of 5N NaOH. The consumption rate of NaOH (dV/dt, in $mL.min^{-1}$), controlled and monitored using the IRIS NT V5 software (Infors AG, Bottmingen, Switzerland), was used to determine maximum acidification rate **(Fig. II.2-2)**. The time at which the maximum acidification rate was reached, considered as the beginning of the stationary growth phase. Cells were harvested at varying times of fermentation between the beginning of stationary growth phase (t = 0 h) and up to t = 10 h into stationary phase.

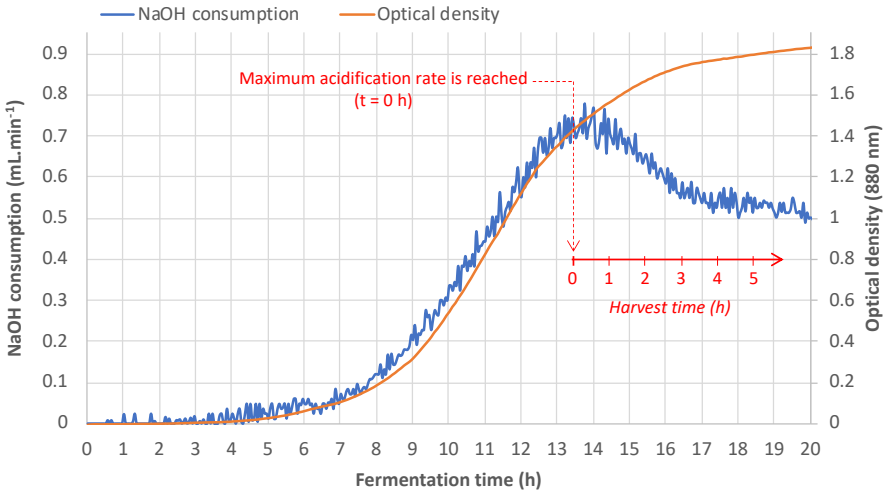

Figure II.2-2: *Growth and acidification rate of a* C. maltaromaticum *fermentation carried out under control conditions (pH 7, 30 °C), illustrating harvest time determination*

.

II.2.2.c. Monitoring of fermentation kinetics

Cell growth and acidification activity were monitored throughout fermentation. Substrate and metabolite concentrations were determined by high-performance liquid chromatography (HPLC, Waters Associates, Millipore; Molsheim, France). Before HPLC analysis, approximately 10 mL of each sample was centrifuged at 16 000 *g* for 30 min at 4 °C, and the supernatant was filtered through 0.22 µm pores (Sartorius Stedim, Biotech, Göttingen, Germany). Analyses were made using a cation exchange column (Aminex Ion Exclusion HPX-87 300 9 78 mm; Biorad, Richmond, VA, USA) at 35 °C. Mobile phase was 0.005 $mol.L^{-1}$ of H_2SO_4 and flow rate was set at 0.6 $ml.min^{-1}$ (LC-6A pump; Shimadzu, Courtaboeuf, France).

II.2.2.d. Concentration and protection

Harvested cell suspensions were concentrated by centrifugation (Avanti® J-E centrifuge; Beckman Coulter; Fullerton, CA) at 2 635 *g* for 10 min at 4 °C. Resulting cell pellets were then re-suspended in a cryoprotective solution at a ratio of 1 : 2 (1 g of concentrated cells in 2 g of cryoprotectant) prior to freezing. The cryoprotectant was a 20 % trehalose-based solution (**Table II.2-1**), sterilized at 121 °C for 20 min.

II.2.2.e. Stabilization, storage and re-activation

One milliliter of cryoprotected cell suspensions were distributed in 1 mL cryotubes (Sarstedt; Nümbrecht, Germany) and then frozen to -80 °C at a cooling rate of approximately 4 $°C.min^{-1}$. Frozen cells samples were stored at -80 °C from 24 h to several months. Re-activation of frozen cells was carried out by thawing the cryotubes in a 30 °C water bath for 3 min.

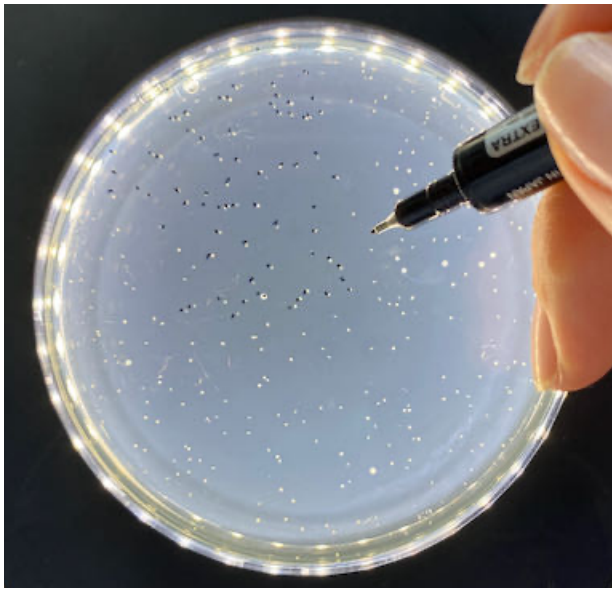

Figure II.2-3 : *Counting of* C. maltaromaticum *colonies grown on Plate Count Agar for 48 h at 30 °C*

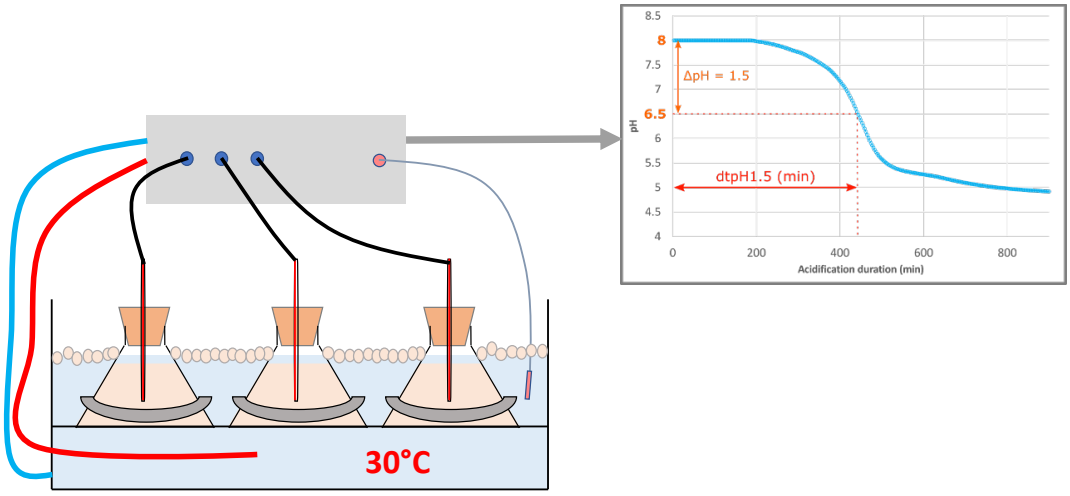

Figure II.2-4: *Schematic illustration of the Cinac® system and dtpH1.5 measurements*

II.2.3. Physiological state assessment

II.2.3.a. Viability (culturability)

Cell viability was measured using the agar plate count method. Fresh or re-activated cell suspensions were serially diluted in saline water, plated into Plate Count Agar (Biokar Diagnostics, Paris, France) and aerobically incubated at 30 °C for 48 h **(Fig. II.2-3)**. Plate counts between 30 and 300 colony forming units (CFU) were kept for cell concentration evaluation. Cell plate counts were expressed in $CFU.mL^{-1}$ and results were obtained in triplicate.

II.2.3.b. Acidification activity

Acidification activity was measured using the Cinac® system (Corrieu et al. 1988). The medium employed for Cinac® measurements is detailed in **Table II.2-1**. After the medium's pH value was adjusted to pH 8.0 with 5N NaOH, it was sterilized at 121 °C for 20 min and then aseptically distributed into 150 mL flasks. Each flask was inoculated with 15 µL of fresh or re-activated bacterial suspensions and incubated in a 30 °C water bath **(Fig. II.2-4)**. For each sample, acidification activity was characterized by dtpH1.5 (in min), corresponding to the time it took for pH to drop by 1.5 units. Thus, the lower the value of dtpH1.5, the higher the acidification activity. The dtpH1.5 descriptor was chosen because a pH drop of 1.5 upH (from pH 8.0 to pH 6.5) is what caused TopCryo® labels to shift from bright green to dark red. Acidification activities were measured in triplicate.

II.3. Intracellular glass transition temperature assessed by DSC

Intracellular glass transition temperatures, Tg'i, was determined by differential scanning calorimetry DSC) as described previously (Fonseca et al 2016; Clarke et al. 2013).

II.3.1.a. Equipment

A power compensation calorimeter (Diamond, Perkin Elmer LLC, Norwalk, CT, USA, equipped with a liquid nitrogen cooling accessory, CryoFill, Perkin Elmer) was used.

II.3.1.b. Sample preparation

After washing the cells three times with peptone water (1 g L^{-1}), about 20 to 50 mg of cell pellet by centrifugation (14 000 x g for 3 min) was scanned following cooling to -100°C and heating to 20°C at 10 °C min^{-1}. Cell concentrations were typically 10^8 to 10^{10} mL^{-1}. An empty pan was used as a reference.

II.3.1.c. Essay procedure

Temperature calibration was performed using cyclohexane (crystal-crystal transition at −87.1 °C) and mercury (melting point at −38.6 °C). The glass transition temperatures of the intracellular contents (Tg'i, °C) and the protective solutions (extracellular medium) (Tg'e, °C) were calculated from the first derivative of the heat flow recorded during warming (Fonseca et al. 2016; ASTM Standard Method E 1356-08(2014)).

II.4. Membrane fluidity assessed by fluorescence anisotropy

II.4.1.a. Equipment

Membrane fluidity of *C. maltaromaticum* was assessed by steady-state fluorescence anisotropy, using a 1,6-diphenyl-1,3,5-hexatriene (DPH) fluorescent probe. Steady-state fluorescence anisotropy (r) of *C. maltaromaticum* cells was measured in a photoluminescence spectrometer (FLS1000, Edinburgh Instruments, Serlabo Technologies, France).

II.4.1.b. Sample preparation and staining

Stock solutions of DPH (6 mM, Sigma-Aldrich; St. Louis, MO, USA) were prepared in dimethylsulfoxide (DMSO, Sigma-Aldrich; St. Louis, MO, USA). The staining procedure described by Bouix and Ghrobal 2017 with minor modifications was applied. 50 µL samples of either fresh or freeze-thawed cell suspension of Carnobacterium, were washed three times with 50 mM 2-[N-morpholino]ethanesulfonic acid buffer (MES) (Sigma-Aldrich, L'Isle d'Abeau, France) containing 10 mM of glucose, and adjusted at pH 5.5 with KOH (30%). The bacterial pellets obtained after three washes were diluted in 1 mL of the same buffer to reach approximately 10^7 cells.mL^{-1}. Ten µL of DPH 6 mM, were added to

1 mL of cell suspension at 10^7 cells·mL^{-1}. Just before use, DPH solution was sonicated for 10 min at 20 Hz. After addition of the dye, the cell suspension was vortexed for 1 min, and incubated 3 min in darkness at 30 °C prior to centrifugation (14,000×g for 90 sec). The pellet was re-suspended in 3 mL of the protective solution tested (sucrose or trehalose) loaded into a stirred quartz cuvette.

II.4.1.c. Essay procedure

The excitation and emission wavelengths of the spectrometer were respectively set at 360 and 430 nm. Polarizers were located on the excitation source and on the photomultiplier tube to measure anisotropy. Measurements were carried out at different sample temperatures ranging from 42 °C to 0 °C using a Peltier-based temperature-controlled cuvette holder (LFI-3751, Wavelength electronics; Bozeman, MT, USA and Luma 40, Quantum Northwest, WA, USA). Fluoracle® software (Edinburg Instruments, UK) was used to perform and analyze the fluorescence anisotropy measurements at different temperatures (at 5°C interval, automatically performed in batch mode). Temperature dynamics were performed on three bacterial cultures.

Steady state anisotropy (**r**) was calculated according to the following equation (Eq. II.4-1):

$$r = \frac{I_{vv} - G \times I_{vh}}{I_{vv} + 2G \times I_{vh}} \qquad \text{(II.4-1)}$$

Where $\boldsymbol{I_{vv}}$ and $\boldsymbol{I_{vh}}$ represent the fluorescence intensity obtained with the vertical excitation and vertical or horizontal emissions, respectively. G is a correlation factor accounting for the polarization bias in the detection system and is equal to I_{hv}/I_{hh} (the fluorescence intensity obtained with the horizontal excitation and vertical emission over the one obtained with the horizontal excitation and horizontal emission). Fluorescence anisotropy is inversely proportional to membrane fluidity: the more rigid a membrane becomes, the higher its anisotropy value (***r***) will be.

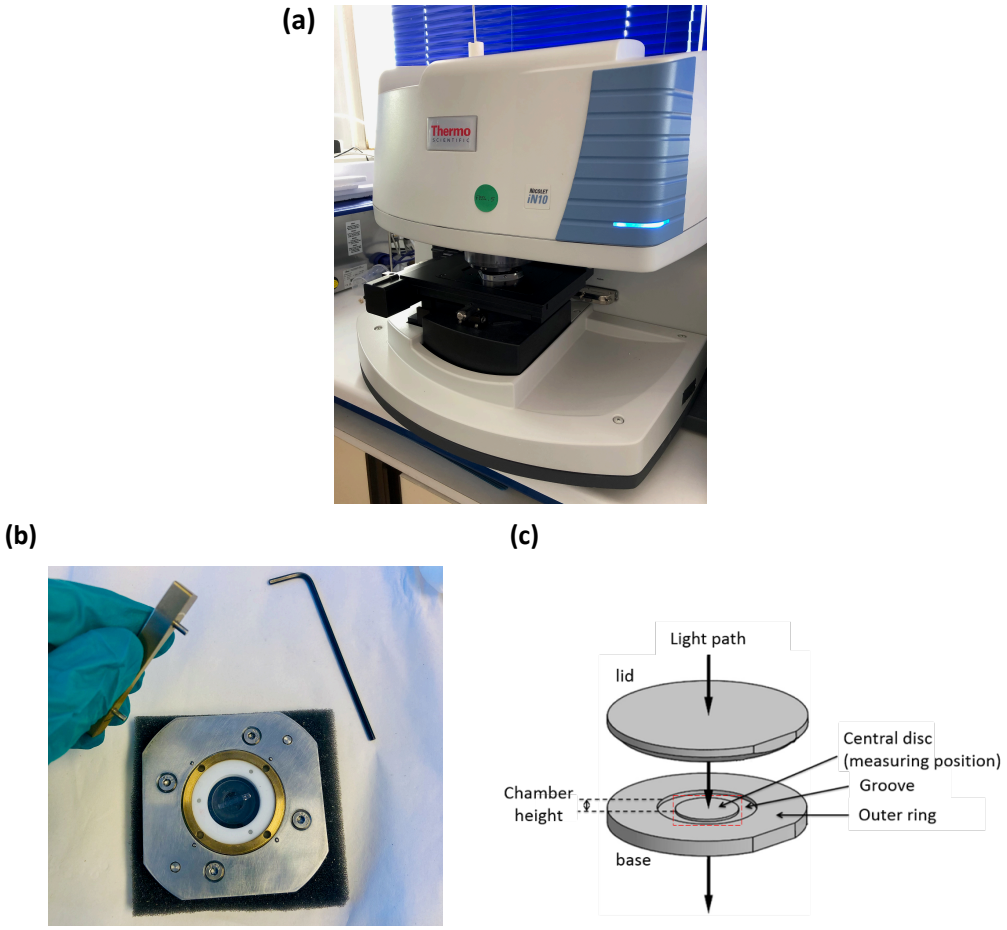

Figure II.5-1 : (a) *photo of the iN10 micro-spectroscope used in this study;* ***(b)*** *photo of the custom-made demountable sample holder;* ***(c)*** *schematic representation of the* CaF_2 *micro-chamber, adapted from Meneghel et al. 2020*

II.5. FTIR micro-spectroscopic characterization in aqueous conditions

Infrared spectroscopy is a powerful tool for the characterization of biological samples (**see Annex II.5**). It provides information on molecules present in a sample, in the form of more or less complex spectra. The interpretation of these spectra reveals the chemical components that constitute the analyzed sample. The FTIR micro-spectroscopic approach used in this work to characterize bacterial samples in aqueous conditions is presented in the following. A more detailed description of this method has been published by Meneghel *et al.* (2020).

II.5.1.a. Equipment

The infrared microscope used in this study was a Nicolet iN10 (Thermo Fisher Scientific, Madison, WI, USA) **(Fig. II.5-1a)** equipped with a custom-made demountable sample holder, developed by Meneghel and colleagues (2020) **(Fig. II.5-1b)**. The sample holder was able to maintain a CaF_2 micro-chamber (Hellma Analytics, Paris, France) **(Fig. II.5-1c)** tightly closed, to limit water evaporation for the duration of the measurements. The CaF_2 micro-chamber height (path length) of 5.8 µm ± 0.8 µm was accurately determined by counting the complete peak to peak interference fringes appearing on spectra.

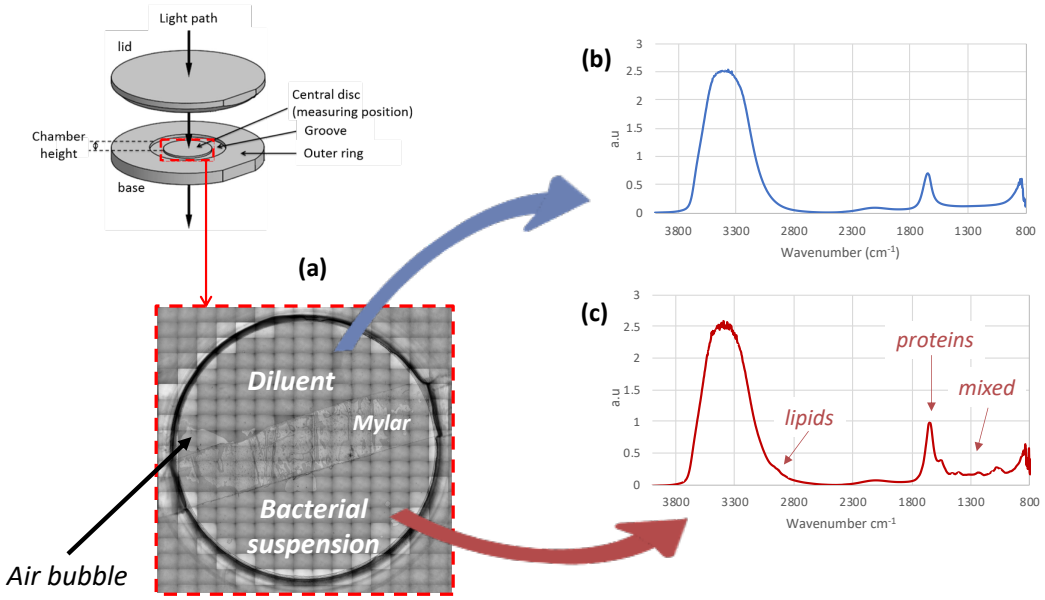

Figure II.5-2: (a) *a captioned image of the sample chamber taken by the FTIR microscope, illustrating the diluent and bacterial suspension sides separated by a strip of Mylar film;* ***(b)*** *IR spectrum taken on the diluent side;* ***(c)*** *IR spectrum taken on the bacterial suspension side.*

II.5.1.b. Sample preparation

Carnobacterium maltaromaticum cell samples were washed three times in saline water then centrifuged at 16 100 *g* for 5 min. A very small amount (the tip of a 200 µL pipette cone: ~0.5 to 1 µL) of the resulting cell pellet was deposited on one side of the chamber, separated from the diluent side (containing ~1 µL of saline water) by a 2.5 µm thick strip of Mylar® film (GoodFellow; Lille, France), as shown on **Figure II.5-2a**.

II.5.1.c. Spectra acquisition

Spectra acquisition and pre-processing was performed using the OMNIC software (version 8.1; Thermo Fisher Scientific; Madison, WI, USA). Each acquired spectrum was obtained from 128 co-added scans in the mid-IR region, between 4000 and 900 cm^{-1} at a resolution of 4 cm^{-1}.

For each bacterial sample, three different sets of spectra were acquired at 50 x 50 µm aperture, on multiple points across three different regions of the sample chamber **(Fig. II.5-2a)**: (i) the background spectrum, acquired in an air bubble, (ii) the diluent spectra, acquired along three separate areas of the diluent side **(Fig. II.5-2b)** and (iii) the sample spectra, acquired along three separate areas of the bacterial suspension side **(Fig. II.5-2c)**.

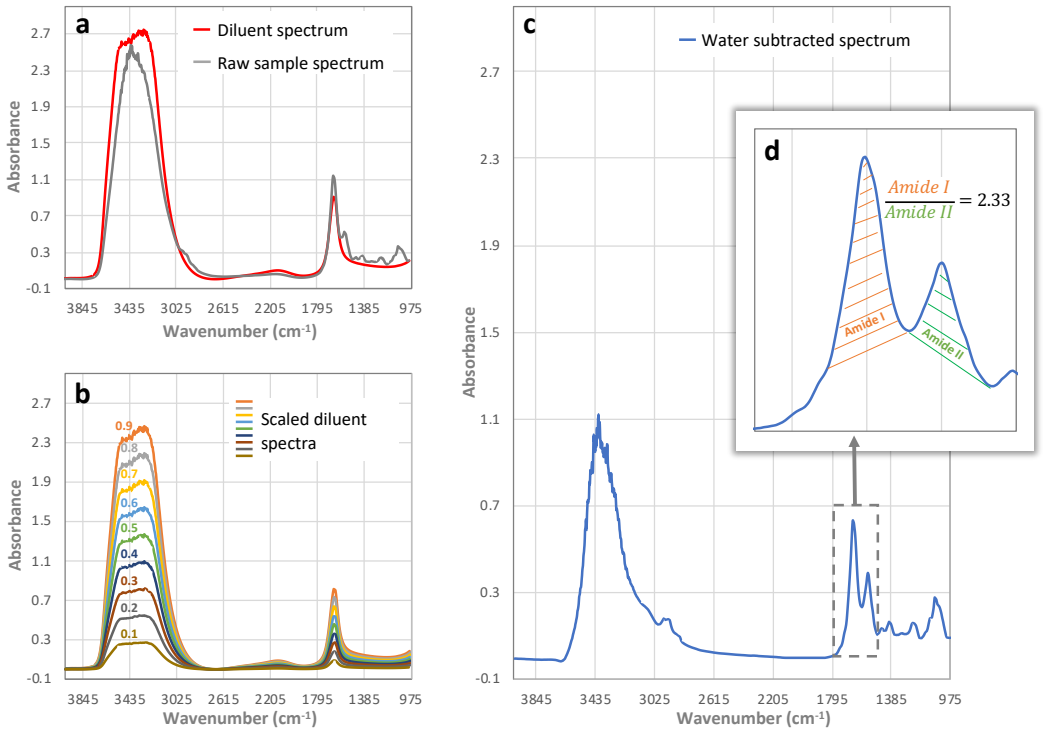

Figure II.5-3: *Illustration of the water subtraction procedure using Matlab R2014a (version 8.3.0.532).* ***(a)*** *raw sample spectrum and diluent spectrum recorded on* C. maltaromaticum *cells with the Nicolet iN10 IR microscope (Thermo Scientific, USA);* ***(b)*** *diluent spectrum multiplied by a range of coefficients;* ***(c)*** *result of the subtraction between the raw sample spectrum and a scaled diluent spectrum leading to the same Amide I/Amide II area ratio as dried cells;* ***(d)*** *enlargement of the Amide I and II bands where area ratio is shown.*

II.5.1.d. Spectra pre-processing: atmospheric suppression and water subtraction

Automatic atmospheric suppression was applied to all spectra using the Omnic software in order to remove residual spectral contributions from water vapor and carbon dioxide. Approximately 45 to 50 spectra per biological sample were exported for water subtraction.

Removing the spectral contribution of water – in particular the H-O-H bending mode centered around 1 650 cm^{-1}, interfering with the Amide I band of proteins (**Fig.II.5-3a**) – was necessary to access more spectral information in the mid-IR region, and specifically information carried by the Amide I band of proteins.

An in-house Matlab script (version 8.3.0.532, Mathworks, Natick, MA, USA) developed by Meneghel et al. (2020) was used for water subtraction. The script involved removing a scaled diluent spectrum (see **Fig. II.5-3b**) to each of the sample spectra, to obtain a water subtracted spectrum presenting a similar Amide I/II area ratio to those of dried cells (see **Fig. II.5-3c and d**). The Amide I/II ratio of dried *C. maltaromaticum* cells was determined on 176 spectra from three biological replicates of cells produced under controlled conditions (pH7, 30°C). The obtained median value of this ratio was 2.33.

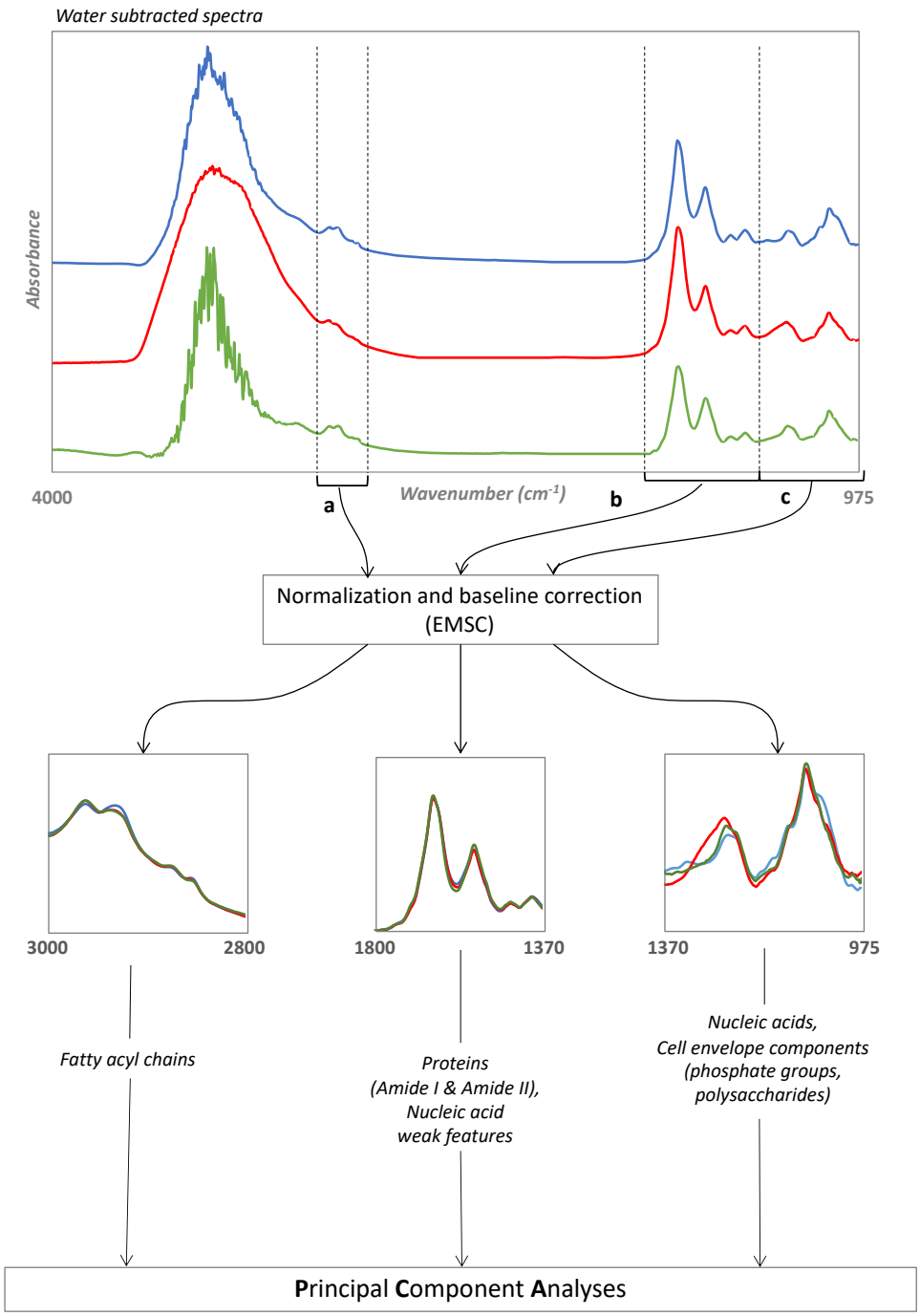

Figure II.5-4: *Illustration of the spectral data processing steps before analyses. Water subtracted spectra of* C. maltaromaticum *CNCM I-3298 (blue),* L. bulgaricus *ATCC 11842 (red) and* L. bulgaricus *CFL1 (green) are used as an example.* ***a, b*** *and* ***c*** *are three distinct spectral regions analyzed by Principal Component Analysis.*

II.5.1.e. Spectra post-processing and statistical analysis

Post-processing of the water subtracted spectra was done using the Unscrambler® X software package (version 10.2, Camo Software AS; Olso, Norway), on three distinct spectral regions:

- 1/ The 3016 – 2800 cm^{-1} region (**Fig. II.5-4a**), where absorption bands arising from the C-H stretching vibrations of $-CH_3$ and $>CH_2$ functional groups can be found. This region therefore contains information on fatty acid chains of the lipid membrane.

- 2/ The 1800 – 1370 cm^{-1} region (**Fig. II.5-4b**), where the Amide I and Amide II bands of proteins are found, as well as bands arising from the C=O vibrations of esters and carboxyl groups. This region therefore carries mainly information on protein secondary structure, fatty acids and nucleic acids.

- 3/ The 1370 – 975 cm^{-1} region (**Fig. II.5-4c**), where the Amide III band of proteins can be found as well as complex vibration bands arising from polysaccharides and phosphodiester groups. This region therefore contains information on proteins, nucleic acids and cell envelope components (peptidoglycan, teichoic acids and phospholipids).

Normalization and baseline corrections were performed in each region using an extended multiplicative scatter correction (EMSC). Resulting spectra were then submitted to Principal Component Analysis (PCA), using the Unscrambler® X software package, to reveal data variance (score plots) and peak positions of interest (loadings). Each region was analyzed separately. The assignment of principal absorption bands was done using data from literature (**Table II.5-1**). The band frequencies are often given as approximations, since the frequency of a bond vibration is highly dependent on the sample's environment (*e.g.,* temperature or water activity), as well as inter- or intra-molecular interactions (*e.g.,* hydrogen bonding interactions with the cell surface or the spatial arrangement of proteins).

Table II.5-1 : Assignment of main infrared vibrational bands in the 3000 – 975 cm^{-1} region of the infrared spectra of bacterial cells, according to literature. Bold references are works carried out on microorganisms.

Main biomolecules	Vibration	Frequency (cm^{-1})	References
Fatty acyl chains (membrane lipids and peptidoglycan → 2930 cm^{-1} (*))	νC=C	~3010/3006/2997	(*)**Naumann et al. 1982; Le Gal et al. 1991;** Arrondo and Goñi 1998**; Naumann 2006;** Movasaghi et al. 2008**; Quilès et al. 2010; Dianawati et al. 2012; Saulou et al. 2013; Lasch and Naumann 2015; Passot et al. 2015**
	$\nu_{as}CH_3$	~2961/2959/2956	
	$\nu_{as}CH_2$	~2921/2925/2918/2930	
	ν_sCH_3	~2875/2874/2872/2867	
	ν_sCH_2	~2854/2852/2850	
	νC=O (esters)	1740/1736/1730	
Nucleic acids, ADN/ARN bases (*weak features of nucleic acids often overlapped by Amide I band of proteins*)	νC=O (esters, carboxylic acids)	~1715/1713	**Naumann et al. 1982; Naumann 2006; Santivarangkna et al. 2007; Quilès et al. 2010; Meneghel et al. 2020**
	νC=O, νC=N, νC=C, δN-H	1715-1680	
Proteins (whole cell: cell wall, cell membrane and cytoplasm)	**Amide I: νC=O**	1700 —1600	
	pleated sheets, β-turns	1695-1662 ~1695/1685/1675	**Naumann 2006;** Barth 2007
	α -helical structures	1657-1648 ~1655/1654/1656	**Naumann 2006;** Barth 2007**; Passot et al. 2015; Meneghel et al. 2020**
	random coiled structures	~1645	**Le Gal et al. 1991**
	β-sheet structures	1641-1623, 1631-1627 ~1637, 1633, 1624	**Le Gal et al. 1991; Naumann 2006;** Barth 2007**; Passot et al. 2015; Meneghel et al. 2020**
	Aspartate, Glutamate $\nu_{as}COO^-$	~1615	**Naumann 2006;** Barth 2007
	Amide II: δN-H, νC-N	1550-1520 ~1542/1540/1550	**Filip et al. 2004; Naumann 2006;** Barth 2007**; Meneghel et al. 2020**
	Amide III: δC-N, νC-N	1400-1200 ~1250, 1235	**Le Gal et al. 1991;** Fu et al. 1994**; Filip et al. 2004;** Cai and Singh 2004**; Naumann 2006;** Barth 2007

ν: stretching, δ: bending, ν_s: symmetric stretching,ν_{as}.: antisymmetric stretching

Table I.4-1 (continued): *Assignment of main infrared vibrational bands in the 3000 – 975 cm^{-1} region of the infrared spectra of bacterial cells, according to literature. Bold references are works carried out on microorganisms.*

Main biomolecules	Vibration	Frequency (cm^{-1})	References
Phosphodiesters, phospholipids (cell membrane), **Teichoic and lipoteichoic acids** (cell wall), **Nucleic acids** (nucleoid)	$\nu_{as}PO_2$ (+ Amide III)	1253-1238, 1250-1220, 1240-1210, ~1243/1238/1218	**Naumann et al. 1982; Naumann 2006;** Movasaghi et al. 2008**; Quilès et al. 2010; Passot et al. 2015; Meneghel et al. 2020**
	$\nu_{s}PO_2$	1095-1075, 1085-1074 ~1096/1085	**Naumann 2006;** Movasaghi et al. 2008**; Kochan et al. 2018; Meneghel et al. 2020**
Polysaccharides, sugar rings (peptidoglycan, cell wall)	νC-O, νC-C, C-O-C deformation, νP-O-C, νP-O-P	1200-900 1155-1130,1112-1100, ~1120, 1060, 1040	**Naumann et al. 1982; Jiang et al. 2004; Naumann 2006;** Movasaghi et al. 2008**; Quilès et al. 2010; Meneghel et al. 2020**
Ribose skelet (RNA), ribosomes, sugars	νC-O ribose, νC-C	994-996,~993	Movasaghi et al. 2008**; Quilès et al. 2010**

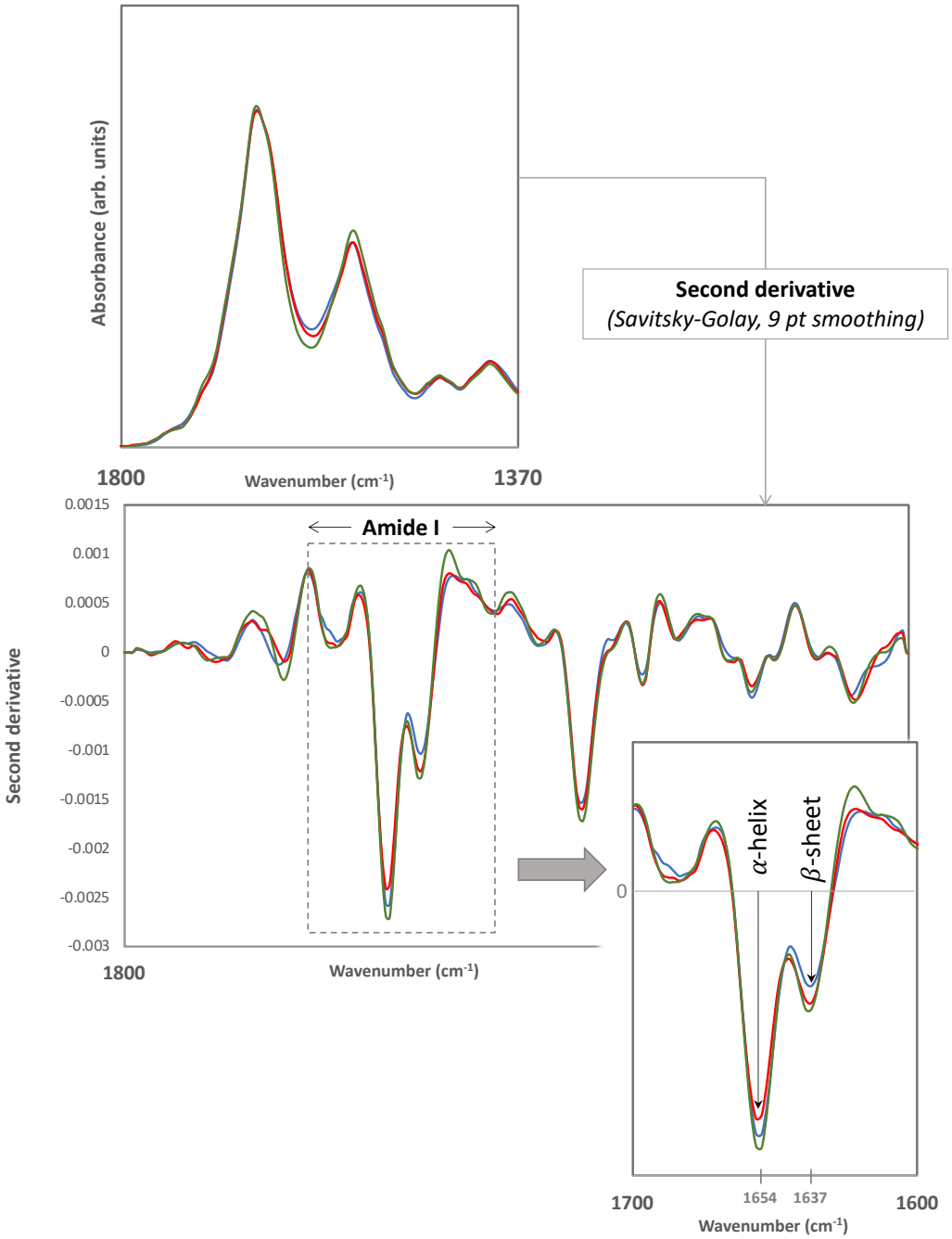

Figure II.5-5: *Illustration of the additional spectral processing applied to the 1800 – 1370 cm^{-1} region, harboring information on protein secondary structures.* ***(a)*** *Normalized spectra;* ***(b)*** *Secondary derivative of the normalized spectra showing the Amide I band components;* ***(c)*** *enlargement of the Amide I band where α-helix and β-sheet band intensities are shown.*

In the 1800 – 1370 region, spectra were further processed to notably enhance and visualize the components of the Amide I band that provide information on the secondary structure of proteins (**Fig. II.5-5**): α-helix and β-sheet bands, respectively found at ~1654 and ~1637 cm^{-1}. This was done by applying the Savitzky-Golay second-order derivative algorithm using a third-degree polynomial and a 9-point smoothing factor. The minima of these derivatives represent the peak positions of corresponding bands on the original spectra. The intensity ratios between the α-helix band peak at 1654 cm^{-1} and the β-sheet band peak at 1637 cm^{-1} in the second derivative spectra of the Amide I region (1700 – 1600 cm^{-1}) was used as a measure for secondary protein structure changes between fresh and thawed cells. To evaluate the significance of the change in α-helix/β-sheet ratio measured in thawed cells compared to fresh cells, ANOVA was performed using the XLSTAT 2018.3 software (Addinsoft, Paris, France).

II.6. FTIR spectroscopic measurements during cooling and heating

The spectra were determined on the cell pellets of thawed, washed bacterial samples, according to the method described below. A more detailed description of the method was done by Gaultier *et al.* 2013

II.6.1.a. Equipment

Measurements were carried out on a Nicolet Magna 750 FTIR spectrometer (Thermo Fisher Scientific; Madison, WI, USA) equipped with a mercury/cadmium/telluric (MCT) detector and a variable temperature stage (Specac Ltd.; Orpington, Kent, UK), as described by Gautier et al. 2013. The optical bench was continuously purged with dry air (Balston; Haverhill, MA, USA) to remove the spectral contribution of water vapor. Temperature was decreased at a rate of 2 °C.min^{-1} by pouring liquid nitrogen into the cell holder. An accurate cooling rate was insured by a thermocouple inserted in a hole provided for that purpose, as close to the sample as possible.

II.6.1.b. Sample preparation

Bacterial samples were washed three times in saline water then centrifuged at 16 100 *g* for 5 min. A small amount of the resulting cell pellet was tightly sandwiched between two calcium fluoride (CaF_2) windows (ISP Optics; Riga, Latvia).

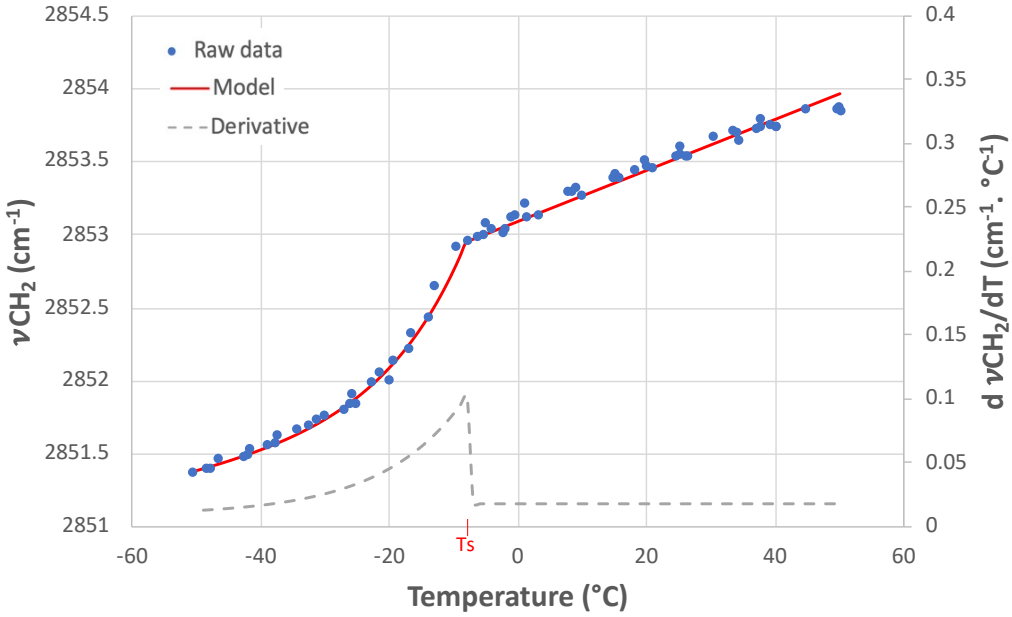

Figure II.6-1: *Peak positions of $\nu_s CH_2$ vibration bands arising from* C. maltaromaticum *cells, plotted against their acquisition temperature. Raw data (blue dots) were fitted with a curve based on a continuous piecewise function. The maximum of the first derivative of the fitted curve was used to determine the lipid phase transition temperature during cooling (Ts).*

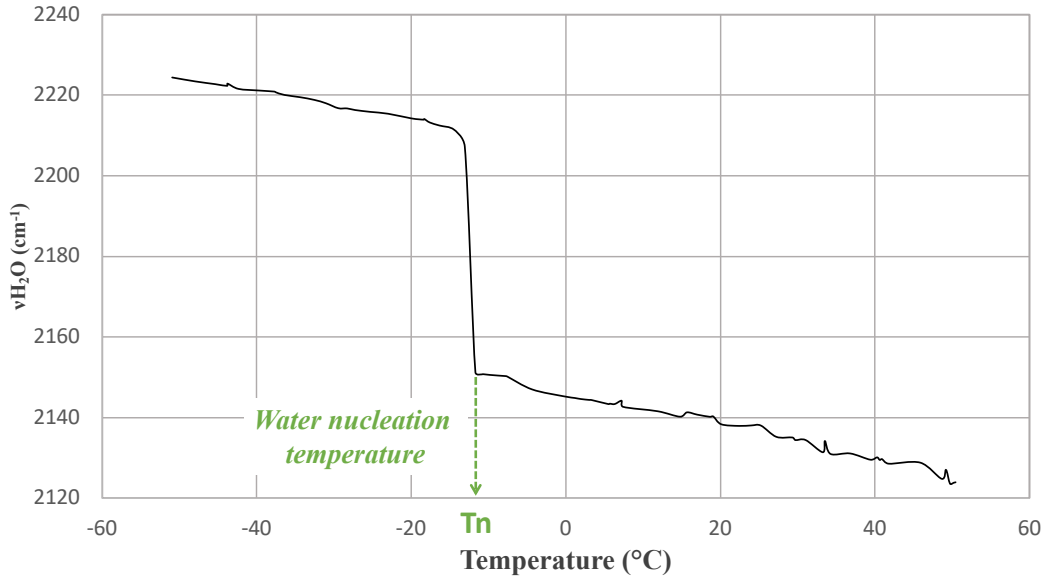

Figure II.6-2: *Peak of the bending and libration combination band of water (νH_2O), as a function of temperature. The upshift from approximately 2150 to 2200 cm^{-1} during cooling, determines the water nucleation temperature (Tn).*

II.6.1.c. Spectra acquisition

Spectra acquisition was performed by the Omnic software (version 7.1, Thermo Fisher Scientific; Madison, WI, USA): 32 co-added scans were collected in the mid-IR region between 4000 and 900 cm^{-1}, every 45 s at a 4 cm^{-1} resolution. Spectra were recorded during cooling from 50 °C to -50 °C and during heating to 120°C.

II.6.1.d. Spectra analysis

The lipid membrane phase transition temperature (Ts) and organization during freezing was studied by monitoring the absorbance band positions of the symmetric CH_2 stretching vibration band (ν_sCH_2) arising from the lipid acyl chains of the cytoplasmic membrane, located around 2850 cm^{-1}.

Spectra analyses were performed using the ASpIR software (Infrared Spectra Acquisition and Processing, INRA; Thiverval-Grignon, France): the peak position of ν_sCH_2 in each spectrum was determined using their second-order derivative and smoothed according to a seven-point Savitsky-Golay algorithm. Each peak was then plotted against the temperature at which they were measured (**Fig. II.6-1**). The ν_sCH_2 peak position *versus* temperature plots arising from *C. maltaromaticum* samples were fitted with a curve based on a continuous piecewise function: a linear function for temperatures above the phase transition temperature during cooling and a sum of linear and exponential functions for temperatures below Ts. Phase transition temperatures during cooling were determined using the maxima of the first-order derivative of the fitted curve.

In addition, ice nucleation was determined by monitoring the peak position upshift from approximately 2 150 cm^{-1} to 2 220 cm^{-1} of the absorption band of the OH libration and bending modes of water (νH_2O) (**Fig. II.6-2**).

II.7. Fatty acid composition

Membrane fatty acid (FA) compositions were determined on the cell pellets of thawed, washed bacterial samples, according to the method described below. A more detailed description of the method was done by Gaultier et al. (2013).

II.7.1. Accelerated Solvent Extraction (ASE)

II.7.1.a. Equipment

Lipid extraction was performed using an accelerate solvent extractor (ASE 350, Dionex; Sunnyvale, CA, USA) and 10 mL stainless steel extraction cells (Thermo Fisher Scientific, Madison, WI, USA). The solvent was evaporated using a vacuum centrifugal evaporator (RC 10-22) combined to a refrigerated trap (RCT 90; Jouan, Saint-Herblain, France).

II.7.1.b. Sample preparation

Frozen cell suspensions were thawed and washed twice in saline solution (9% NaCl). Washed cell pellets were obtained with a final centrifugation at 16 100 x *g* for 10 min at 4°C. Between 0.15 g and 0.20 g of washed cell pellet was then thoroughly mixed using a pestle and mortar, with 2.0 g of diatomaceous earth (Thermo Fisher Scientific, Madison, WI, USA), serving as a dispersant and desiccant. The mix was then introduced into the 10 mL stainless steel extraction cell. The remaining space in the extraction cell was then filled with sand (50-70 µm mesh particle size, Sigma-Aldrich; St. Louis, MO, USA) before being tightly closed.

II.7.1.c. Extraction method

The solvent extraction method comprised three cycles, each using different extraction solvent, containing different *chloroform : methanol* volume ratios (2:1, 1:1, 1:2) at 100 °C and under pressure (10^7 Pa). All resulting extracts of a sample were combined in the same vial. Each vial was then evaporated to dryness and resuspended in equal parts chloroform and potassium chloride solution (8.8 $g.L^{-1}$ of KCl). After vigorous manual shaking, extracts were centrifuged to separate the organic phase from the aqueous phase. The organic phase (containing the lipids) was transferred into 1 mL glass vials and evaporated to dryness in a vacuum

concentrator (Jouan RC10-22, ThermoFisher, Saint Herblain, France) coupled to a cooling unit. The vials, each containing approximately 1 mg of dried lipids, were hermetically stored at -20 °C until GC-MS analysis.

II.7.2. Fatty acid identification by GC-MS

II.7.2.a. Equipment and configuration

Fatty acid identification was carried out using a Hewlett-Packard 6890 gas chromatograph equipped with a capillary column packed with 70 % cyanopropyl polysilphenylene-siloxane BPX70 (60 m x 0.25 mm x 0.25 µm; SGE Analytical Science Pty Ltd.; Victoria, Australia), coupled to a mass selective detector (5973; Agilent Technologies, Avondale, PA, USA).

II.7.2.b. Sample preparation

The dried extracted lipid samples, as well as fatty acid standards (Larodan; Solna, Sweden and Sigma-Aldrich; St. Louis, MO, USA) were resuspended in chloroform (approximately 300 µL of chloroform per milligram of dried lipids). Fifty microliters of the lipid suspension were then transferred to GC-MS vials, to which were added 25 µL of a C9:0 internal standard (Sigma-Aldrich; St. Louis, MO, USA) and 50 µL of the methylation reagent, trimethylsulfonium hydroxide (TMSH, Sigma-Aldrich; St. Louis, MO, USA).

II.7.2.c. Identification and quantification

Identification of the FA methyl esters extracted from bacterial samples was done by comparing their retention time to those of the known standards. Identity confirmation was done using the mass selective detector at a scan rate of 3.14 scans.s^{-1}, with data collected in the range of 33 to 500 amu. The mass spectra of the FA methyl esters were compared with the Wiley 275.L data bank (Hewlett-Packard, Gaithersburg, MD, USA).
Quantification of the FA was calculated using an external calibration performed with serials dilutions of commercial standards, in addition to the C9:0 internal standard. Results were expresses as percentages, over total extracted FA.

II.8. Statistical analyses

II.8.1.a. Stepwise descending multiple regression analyses

(Results Chap. I)

Stepwise descending multiple regression analyses were performed on results presented in chapter I to quantify the effect of independent variables (temperature (X_1), pH (X_2) and harvest time (X_3)) on the culturability and acidification activity (Y) of harvested cell concentrates. These analyses were performed using the MATLAB R2014b software equipped with the Statistics Toolbox (The Mathworks, Inc., Natick, MA). The applied regression model was a second-order polynomial with interactions of the following form

$$Y = \beta_0 + \beta_1 X_1 + \beta_2 X_2 + \beta_3 X_3 + \beta_{11} X_1^2 + \beta_{22} X_2^2 + \beta_{33} X_3^2 + \beta_{12} X_1 X_2 + \beta_{13} X_1 X_3 + \beta_{23} X_2 X_3 \quad \text{(II.8-1)}$$

where β_0, β_i, β_{ii} and β_{ij} are respectively the intercept, linear, quadratic and interaction coefficients. The adequacy of the model was assessed by its coefficient of determination (R^2), a measurement of the percentage of total data variance explained by the model. Regression was initially performed with the complete model. Parameters not significantly different from zero at a 0.05 level were iteratively removed from the model (i.e., set to exactly zero) starting with the one exhibiting the highest coefficient of variation.

II.8.1.b. Principal Component Analyses

(Results Chap. III)

Principal Component Analyses (PCA) were performed on the multivariate data obtained by FTIR micro-spectroscopy, where each wavenumber of a FTIR spectrum is considered a variable. This multivariate data analysis procedure is a powerful chemometric method that reveals the most relevant and discriminating wavenumbers among samples.

II.8.1.c. ANOVA

(***Results Chap. III)***

ANalyses Of VAriance (ANOVA) were used to test whether two or more population means were equal, assuming big sample sizes (n > 30) that follow a

normal distribution. ANOVA were performed using XLSTAT 2020.5 (Addinsoft, Paris, France). Significance levels of 95 % (p-value < 0.05) were considered.

II.8.1.d. Kruskal-Wallis tests

(Results Chap. III)

Kruskal-Wallis is the non-parametric equivalent of one-way ANOVA. The test does not assume a normal distribution of data and compares medians to determine whether samples originate from the same distribution. However, it does not identify pairs or groups of stochastic dominance among the samples. Specific sample groups can be obtained through post-hoc Conover Iman tests.

In this work, Kruskal-Wallis tests followed by post-hoc Conover Iman tests were thus performed on small sample sizes ($3<n<30$). These tests were performed using XLSTAT 2020.5 (Addinsoft, Paris, France) or the Statgraphics software (Statgraphics Technologies, Inc.; The Plaines, VA, USA). Significance levels of 95 % (p-value < 0.05) were considered.

Part III
Results and Discussions

III.1.
Influence of culture conditions on the technological properties of *Carnobacterium maltaromaticum* CNCM I-3298 starters

Content

III.1.1. Context and objectives 138
III.1.2. Abstract 139
III.1.3. Introduction 141
III.1.4. Materials and Methods 145
III.1.4.a. Frozen starter production process 145
(i) Strain and inoculum preparation 145
(ii) Fermentation 145
(iii) Concentration, cryoprotection and freezing 145
III.1.4.b. Experimental design 146
III.1.4.c. Kinetic measurements in the bioreactor: cell growth, acid production and substrate consumption 146
III.1.4.d. Biological properties of starters 147
(i) Viability 147
(ii) Acidification activity in TTI-like medium 147
III.1.4.e. Statistical analysis 147
III.1.5. Results 149
III.1.6. Discussion 153
III.1.7. Key takeaways 161

III.1.1. Context and objectives

Biological Time-Temperature Integrators (TTI) are "smart labels" that relay, by an irreversible color shift, the cumulative effect of time and temperature on the microbial quality of food they are attached to. These labels thus act as a shelf-life indicator of perishables foods. TopCryo® labels, developed by Cryolog Clock-T°, were the only biological TTIs ever taken to market. They were based on the pH decline of the medium contained within the label, as a result of *C. maltaromaticum* growth and acidification. The shelf-life covered by these labels ranged from 30 h to 8 days at 4 °C, depending on the initial cell concentration inoculated into the label medium. Further extension of this shelf-life range, without switching bacterial strains, was the initial main goal of this PhD project, funded by Cryolog Clock-T°. The first investigated strategy was to change the rate at which *C. maltaromaticum* cells acidify the label medium, by changing their physiological state.

Objectives

The purpose of this study was to investigate the effect of a broad spectrum of fermentation parameters (temperature, pH and harvest time), on the technological properties (viability, acidification activity and freeze resistance) of *C. maltaromaticum* concentrates. This intended to reveal the extent of possible shelf-life modifications of a biological time temperature indicator, based *C. maltaromaticum* growth and acidification activity.

The present study was published in March 2019,
in the ***Journal of Applied Microbiology*** (Volume 126, Issue 5 ; p. 1468-1479).
DOI: 10.1111/jam.14223

Authors:
A. Girardeau[1,2], C. Puentes[1], S. Keravec[2], P. Peteuil[2], I.C. Trelea[1], F. Fonseca[1*]

[1] UMR GMPA, AgroParisTech, INRA, Université Paris-Saclay, 78850 Thiverval-Grignon, France
[2] CRYOLOG, R&D department, 44261 Nantes, France
*Corresponding author: Fernanda Fonseca, INRA, UMR 782 Génie et Microbiologie des Procédés Alimentaires (GMPA), F-78 850, Thiverval-Grignon, France. E-mail: fernanda.fonseca@inra.fr

III.1.2. Abstract

Aim: Investigate the effect of a broad spectrum of culture conditions on the acidification activity and viability of *Carnobacterium maltaromaticum* CNCM I-3298, the main technological properties that determine the shelf-life of biological Time-Temperature Integrator labels.

Methods and results: Cells were cultivated at different temperatures (20 to 37 °C) and pH (6 to 9.5) according to a modified central composite design and harvested at increasing times up to 10 h of stationary phase. Acidification activity and viability of freeze-thawed concentrates were assessed in medium mimicking the biological label. Acidification activity was influenced by all three culture conditions, but pH and harvest time were the most influential. Viability was not significantly affected by the tested range of culture conditions.

Conclusions: *C. maltaromaticum* CNCM I-3298 must be cultivated at 20 °C, pH 6 and harvested at the beginning of stationary phase to exhibit fastest acidification activities. However, if slower acidification activities are pursued, the recommended culture conditions are 30 °C, pH 9.5 and a harvest time between 4 to 6 hours of stationary phase.

Significance and impact of the study: Quantifying the impact of fermentation temperature, pH and harvest time has led to a predictive model for the production of biological Time-Temperature Integrators covering a broad range of shelf-lives.

Keywords: acidification activity, fermentation, lactic acid bacteria, stress response, biological TTI

Table III.1-1: *Culture conditions applied in published research involving* Carnobacterium maltaromaticum.

Strains	Fermentation conditions					References
	Medium	***Atmosphere***	***T (°C)***	***pH***	***Harvest time***	
C. maltaromaticum 3	Yeast extract, proteose peptone, thiamine, glucose	aerobic	25	6.0	NA	Borch and Molin, 1989
C. maltaromaticum LMA 28, LMA 29, LMA 30, DSMZ 20730	TSB-YE broth	aerobic	30	unregulated	NA	Cailliez-Grimal *et al.* 2007; Edima *et al.* 2008; Rahman *et al.* 2014, 2016
C. maltaromaticum CNCM I-3298	BHI broth	aerobic	1.75 to 35	5.1 to 10.4	NA	Ellouze *et al.* 2008
C. maltaromaticum C2, A9b^{+}, A9b^{-}	BHI broth modified with fish peptone	aerobic	25	unregulated	24 h	dos Reis *et al.* 2011
C. maltaromaticum LMA 28	TSB-YE broth	aerobic	30	unregulated	End of exponential phase	Afzal *et al.* 2012
C. maltaromaticum LMA 28	MCGC broth (synthetic minimal medium)	varied DOC 0 % to 90 %	30	6.8	NA	Afzal *et al.* 2013
C. maltaromaticum (10 strains isolated from vacuum packaged meat)	BHI, lactic acid, sodium acetate	aerobic	30	unregulated (initial pH: 5.4, 6.2, 7.4)	NA	Zhang *et al.* 2018

NA, not applicable; TSB-YE, tryptone soy broth and yeast extract; BHI, brain heart infusion.

III.1.3. Introduction

Time-Temperature Integrators (TTI) work as 'smart-labels' that relay, by an easily interpreted and irreversible sign, the time-temperature history and quality status of the food they are attached to (Taoukis and Labuza 1989). Biological TTI are usually based on a pH decline of medium contained within the label, as a result of lactic acid bacteria (LAB) growth and acidification. In the event of a "thermal accident" (a more or less significant break of the cold chain), bacteria contained in the label will grow and acidify their environment, causing a color shift and/or an opacification reaction indicating significant alteration (Varlet-Grancher, 2006; Ellouze *et al.*, 2008; Lee and Jung, 2016).

Bacterial strains used for biological TTI must be carefully chosen and configured to closely match the behavior of micro-organisms endogenous to the food being traced. The only biological TTI currently on the market is TopCryo®, produced by Clock-°T (Cryolog, Nantes, Frances). In TopCryo® labels, the growth of *Carnobacterium maltaromaticum* CNCM I-3298 induces a pH decline of the label medium leading to a color shift from green to red (EU patent no. EP 1 664 334). *C. maltaromaticum* concentrates used to inoculate TopCryo® TTI labels are produced like other LAB starters by a succession of steps: fermentation, concentration, cryoprotection, freezing or freeze-drying and storage until inoculation. To produce TTI labels, stored concentrates are freeze-thawed, and a certain volume of cell suspension is mixed into the label medium, depending on desired shelf-life (*i.e.,* low concentrations for long shelf-lives). The labels are then frozen and stored at -80 °C until use. For activation, they are freeze-thawed at ambient temperature. The shelf-life covered by the label is thus dependent on both cell concentration and their acidification activity. Today, TopCryo® covers shelf-lives ranging from 30 h to 192 h (8 days) at 4 °C. To further extend the range of the current commercialized biological TTI without changing the bacterial strain that is currently used, two main strategies can be foreseen to modulate acidification activity: (1) modify the label medium, which would lead to several technological constraints and/or (2) modulate the physiological state of *C. maltaromaticum* CNCM I-3298.

It is known that physiological state modulation of LAB mainly depends on fermentation parameters (medium composition, temperature, pH, harvesting time/growth phase) (Rault *et al.*, 2009; Velly *et al.*, 2014; Brillet-Viel *et al.*, 2016; Hansen *et al.*, 2016). One of the main characteristics of *Carnobacteria* is their psychrotrophic nature and their ability to grow at high pH levels (Edima *et al.*, 2006) . The cardinal values of *C. maltaromaticum* CNCM I-3298 were previously assessed by Ellouze *et al.* (2008) in Brain Heart Infusion (BHI) culture medium (**Table III.1-1**) and using the experimental protocols developed by Pinon *et al.* (2004) and Membré *et al.* (2004).

While exact values may change depending on the culture medium, they illustrate the broad range of temperature and pH at which *C. maltaromaticum* grows: -5 to 36 °C, pH 5 to 10 (Ellouze et al. 2008).

Few studies have been reported on the fermentation of *Carnobacterium maltaromaticum* (**Table III.1-1**) and they mostly concern laboratory fermentations performed in different culture media, at unregulated pH values or restricted range of pH (pH 6 to 6.8). To our knowledge, the impact of fermentation parameters on the physiological state of *C. maltaromaticum* concentrates in conditions close to industrial practices has not yet been reported.

The main objective of this work was therefore to study the effect of three fermentation parameters (temperature, pH and harvest time) on the technological properties, namely viability and acidification activity, of freeze-thawed *C. maltaromaticum* concentrates, in a medium mimicking the TTI label. Mapping the acidification activities of freeze-thawed *C. maltaromaticum* concentrates obtained under a wide range of fermentation conditions would reveal the extent of the possible shelf-life modifications of TopCryo® labels that can be achieved by changing fermentation parameters.

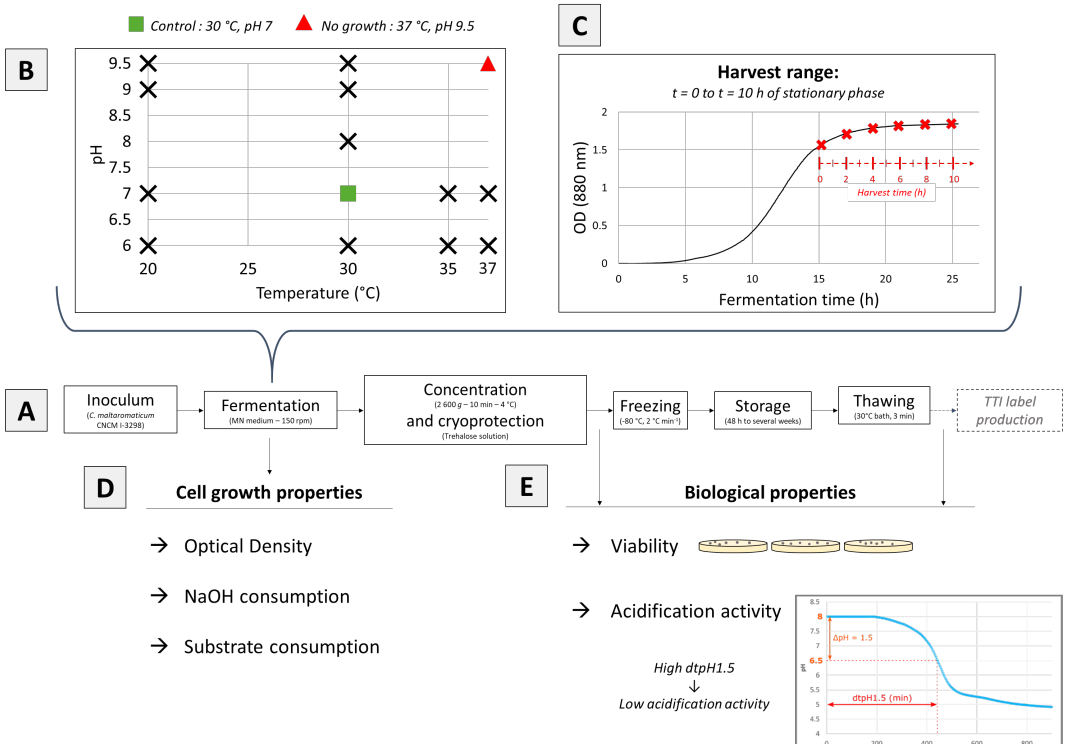

Figure III.1-1: *Diagram of experimental approach applied to quantify the effect of fermentation temperature, pH and harvest time on viability and acidification activity of C. maltaromaticum CNCM I-3298 concentrates:* ***(A)*** *Frozen starter production process;* ***(B)*** *Range of pH and temperatures tested;* ***(C)*** *Harvest time determination;* ***(D)*** *Cell growth properties measured throughout fermentation;* ***(E)*** *Biological properties of cell concentrates measured before freezing and after freeze-thawing.*

III.1.4. Materials and Methods

III.1.4.a. Frozen starter production process

An overview of the starter production process is given in **Figure III.1-1A**.

(i) Strain and inoculum preparation

Stock culture of *Carnobacterium maltaromaticum* CNCM I-3298 was stored at -80 °C in milk (EPI Ingredients, Ancenis, France) supplemented with 15 % (wt/wt) glycerol (VWR, Leuven, Belgium). Inocula were grown in a medium (referred to as MN medium) composed of the following ingredients (g kg^{-1}) : trehalose (Treha™; Tokyo, Japan), 40.0; proteose peptone (Oxoid; Waltham, MA, USA), 20.0; yeast extract (Humeau; La-Chapelle-sur-Erdre, France), 5.0; Tween 80 (VWR; Leuven, Belgium), 20.0; $MnSO_4$ (Merck; Darmstadt, Germany), 0.41 and $MgSO_4$ (Merck; Darmstadt, Germany), 0.056. The medium was sterilized at 121°C for 20 min. 10 mL of sterilized medium was inoculated with 100 µL of stock culture and incubated for 13 to 16 h at 30 °C. 1 mL of the resulting culture was transferred into 50 mL of fresh medium before being incubated for 11 h under the same conditions. The resulting culture was used to inoculate the bioreactor.

(ii) Fermentation

The MN medium was also used as the fermentation culture medium. After adjusting pH to the desired value with NaOH solution (VWR, Pennsylvania, USA) the medium was sterilized at 121 °C for 20 min, cooled down to ambient temperature and introduced into a 3.5 L working volume bioreactor (Minifors, Infors HT, Bottmingen, Switzerland). The pH value of the sterilized medium was verified and adjusted again when necessary with NaOH or H_2SO_4 solution. The inoculation was performed at an initial concentration of approximately 10^7 CFU mL^{-1}. An agitation speed of 150 rpm was applied for culture homogenization. Temperature and pH were set at different values varying between 20 and 37 °C and pH 6 and 9.5, according to the experimental design presented in **Figure III.1-1B**. pH was controlled by the automatic addition of 5N NaOH.

(iii) Concentration, cryoprotection and freezing

Cells were harvested at increasing times of fermentation, starting at the beginning of stationary phase (t = 0 h) and up to t = 10 h into stationary phase. Harvested cell suspensions were concentrated by centrifugation (Avanti® J-E centrifuge; Beckman Coulter; Fullerton, CA) at 2 635 *g* for 10 min at 4 °C. Resulting cell pellets were then re-suspended in a cryoprotective solution at a ratio of 1 : 2 (1 g of concentrated cells : 2 g of protective solution) prior to freezing.

The protective solution was composed of 200 g L^{-1} of trehalose (Treha™; Tokyo, Japan) and 9 g L^{-1} of NaCl and sterilized at 121 °C for 20 min. Cryoprotected cell suspensions were distributed in 1 mL cryotubes (Sarstedt; Nümbrecht, Germany) prior to freezing at -80 °C. Re-activation was carried out by thawing the frozen cell suspensions in a 30 °C water bath for 3 min.

III.1.4.b. Experimental design

A modified central composite experimental design (**Fig. III.1-1B and 1C**) was carried out to investigate the effect of three fermentation parameters (temperature, pH and harvest time) on acidification activity and viability. The experimental ranges chosen for temperature were 20 °C to 37 °C, 6 to 9.5 for pH (**Fig. III.1-1B**) and up to 10 hours after the beginning of stationary phase, for harvest time (**Fig. III.1-1C**). These ranges were chosen according to the cardinal values of *C. maltaromaticum* determined by Ellouze *et al.* (2008) and preliminary tests. The range of fermentation conditions tested were aimed at creating the largest possible scope of moderately stressful conditions that would change the physiological state of *C. maltaromaticum*, while still allowing enough growth to reach a cell concentration compatible with industrial application (> 1 g L^{-1}).

III.1.4.c. Kinetic measurements in the bioreactor: cell growth, acid production and substrate consumption

The cell growth and acidification activity were monitored throughout fermentation (**Fig. III.1-1D**). Cell growth was monitored by an infra-red probe (Excell210, CellD, Roquemaure, France) continuously measuring absorbance at 880 nm (data acquisition every minute). Acidification activity in the bioreactor was determined according to the volume of NaOH solution injected into the bioreactor to maintain a constant pH (data acquisition every minute) with the IRIS NT V5 software (Infors, AG, Bottmingen, Switzerland). NaOH consumption rate (dv/dt, in mL min^{-1}) was used to determine the maximum acidification rate. Trehalose concentrations were determined by high-performance liquid chromatography (HPLC, Waters Associates, Millipore; Molsheim, France) in order to verify that carbon source was not depleted (i.e. absence of supplementary stress from carbon source starvation). Before HPLC analysis, each sample was centrifuged at 16 000 *g* for 30 min at 4 °C then filtered through 0.22 µm pores (Sartorius stedim, Biotech; Göttingen, Germany). Analyses were made using a cation exchange column (Aminex Ion Exclusion HPX-87 300x7.8 mm, Biorad, Richmond, USA) at 35 °C. Mobile phase was 0.005 M H_2SO_4 and flow rate was set at 0.6 mL min^{-1} (LC-6A pump, Shimadzu, Courtaboeuf).

III.1.4.d. Biological properties of starters

(i) Viability

Cell viability was measured using the agar plate count method (**Fig. III.1-1E**). Thawed cell suspensions were diluted in saline water then plated into Plate Count Agar (Biokar Diagnostics, Paris, France) and aerobically incubated at 30 °C for 48 h. The cell plate counts were expressed in UFC mL^{-1} and results were obtained in triplicate.

(ii) Acidification activity in TTI-like medium

Acidification activity was measured using the CINAC system (Corrieu *et al.*, 1988). The measurements were performed at 30 °C, in a growth medium similar to the one used in TopCryo® labels. The medium contained the following ingredients (g kg^{-1}) : glycerol (VWR; Leuven, Belgium), 60.0; trehalose (Treha™; Tokyo, Japan), 15.0; proteose peptone (Oxoid; Waltham, MA, USA), 10.0; yeast extract (Humeau; La-Chapelle-sur-Erdre, France), 5.0; Tween 80 (VWR; Leuven, Belgium), 5.0; $MnSO_4$ (Merck; Darmstadt, Germany), 0.41 and $MgSO_4$ (Merck; Darmstadt, Germany), 0.056. The medium was sterilized at 121 °C for 20 min before being aseptically distributed into 150 mL flasks. Each flask was inoculated with 15 µL of fresh or thawed bacterial suspensions. For each sample, the acidification activity was characterized as the time necessary for a pH drop of 1.5 upH, namely dtpH1.5 (in min) (**Fig. III.1-1E**). Thus, the shorter the value of the dtpH1.5 descriptor was, the higher the acidification activity was. Acidification activities were measured in triplicate.

III.1.4.e. Statistical analysis

Student's paired t-tests were performed using the XLSTAT 2018.3 software (Addinsoft, Paris, France) to evaluate the effect of freezing on viability (in CFU mL^{-1}) and on acidification activity (dtpH1.5, in min). Stepwise descending multiple regression analyses were performed to quantify the effect of independent variables (temperature (X_1), pH (X_2) and harvest time (X_3)) on viability and acidification activity (Y) using the MATLAB R2014b software equipped with the Statistics Toolbox (The Mathworks, Inc., Natick, MA). The applied regression model was a second-order polynomial with interactions of the following form:

$$Y = \beta_0 + \beta_1 X_1 + \beta_2 X_2 + \beta_3 X_3 + \beta_{11} X_1^2 + \beta_{22} X_2^2 + \beta_{33} X_3^2 + \beta_{12} X_1 X_2 + \beta_{13} X_1 X_3 + \beta_{23} X_2 X_3 \quad \text{(III.1-1)}$$

β_0, β_i, β_{ii} and β_{ij} are respectively the intercept, linear, quadratic and interaction coefficients. The adequacy of the model was assessed by its coefficient of determination (R^2), a measurement of the percentage of total data variance

Table III.1-2: *Regression analysis of the acidification activity (dtpH1.5, in min) of* C. maltaromaticum *CNCM I-3298 cells harvested at increasing times during fermentations carried out at different temperatures and pH.*

Term	Estimated coefficient (β)	*Min*	*Max*
Intercept	299.99	*265.21*	*334.77*
X_3 *(harvest time)*	-21.05	*-28.39*	*-13.72*
X_1 X_2 *(temperature x pH)*	0.3623	*0.2091*	*0.5154*
X_2 X_3 *(pH x harvest time)*	3.697	*2.669*	*4.726*
X_2^2*(pH x pH)*	1.178	*0.8414*	*1.516*
$R^2 = 0.8734$		*95% confidence interval*	

(X_1: fermentation temperature; X_2: fermentation pH; X_3: harvest time) (Eq. III.1-1)

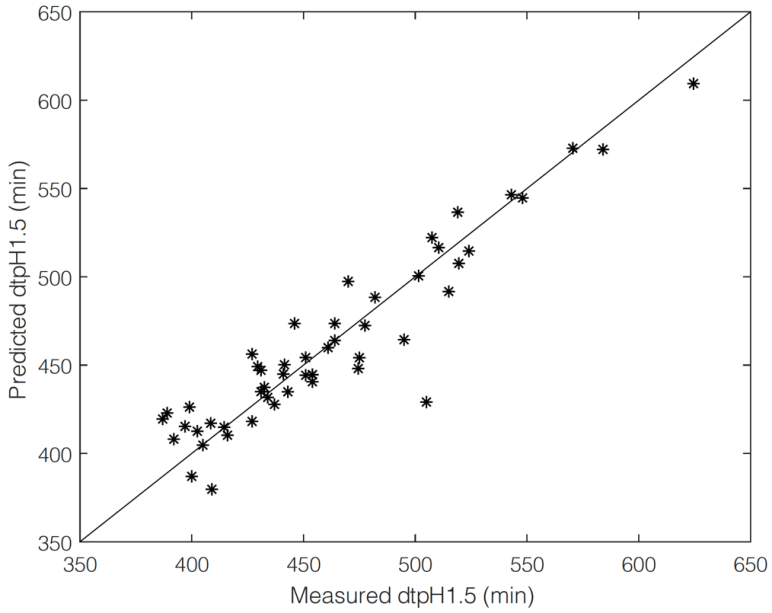

Figure III.1-2: dtpH1.5 values predicted by the regression model versus dtpH1.5 values measured. The corresponding coefficient of determination (R^2 = 0.8734) indicated adequate prediction of acidification activity in a TTI-like medium.

explained by the model. Regression was initially performed with the complete model. Parameters not significantly different from zero at a 0.05 level were iteratively removed from the model (i.e., set to exactly zero) starting with the one exhibiting the highest coefficient of variation. Response surface plots were generated from the fitted quadratic polynomial equations obtained in order to visually assess the relationships between variables and responses.

III.1.5. Results

Effect of freezing on the viability and acidification activity of *Carnobacterium maltaromaticum* CNCM I-3298

The reported freeze-thaw resistance of *C. maltaromaticum* (Walker *et al.*, 2006) was corroborated in this work by measuring the viability (in UFC mL^{-1}) and acidification activity (dtpH1.5, in min) of cells produced in reference conditions (pH7, 30°C), before and after freezing. Student's paired t-tests were conducted to compare the viability and acidification activity of cells before and after freezing. Cells produced at pH 7 and 30°C displayed no significant loss of viability or acidification activity after being freeze-thawed ($n = 6$, p-value > 0.05). Moreover, similar freeze-thaw resistance was exhibited by cells produced in two extreme fermentation conditions (pH 9, 30°C and pH 6, 30°C). All the following measurements of viability and acidification activity were thus performed on freeze-thawed concentrates.

Effect of fermentation conditions (temperature, pH and harvest time) on the acidification activity of TTI label starters.

All residual concentrations of trehalose measured at each harvest time were above 1.3 g L^{-1}, thus confirming that biomass had not been subjected to carbon starvation, regardless of applied fermentation parameters. The effects of fermentation temperature, fermentation pH and harvest time on the acidification activity (dtpH1.5, in min) of the freeze-thawed concentrates were examined in a culture medium close to the TTI label medium. The dtpH1.5 descriptor used in this study for assessing the acidification activity changes, is the main technological property of the produced cell concentrates. It varied between 392 ± 4 min and 625 ± 2 min, depending on the culture conditions. Low dtpH1.5 values corresponded to high acidification activities. Results of the stepwise multiple regression analysis are summarized in **Table III.1-2**. They enabled quantification of the linear, quadratic, and interactive effects of three independent fermentation variables on dtpH1.5, the main technological property of the produced cell concentrates. The model explains more than 87 % of dtpH1.5 variability, according to the coefficient of determination (R^2) (**Table III.1-2**). Consequently, the model adequately predicts acidification activity of the TTI label starters, as a function of their fermentation temperature and pH as well as the time at which they were harvested. The accuracy of the model

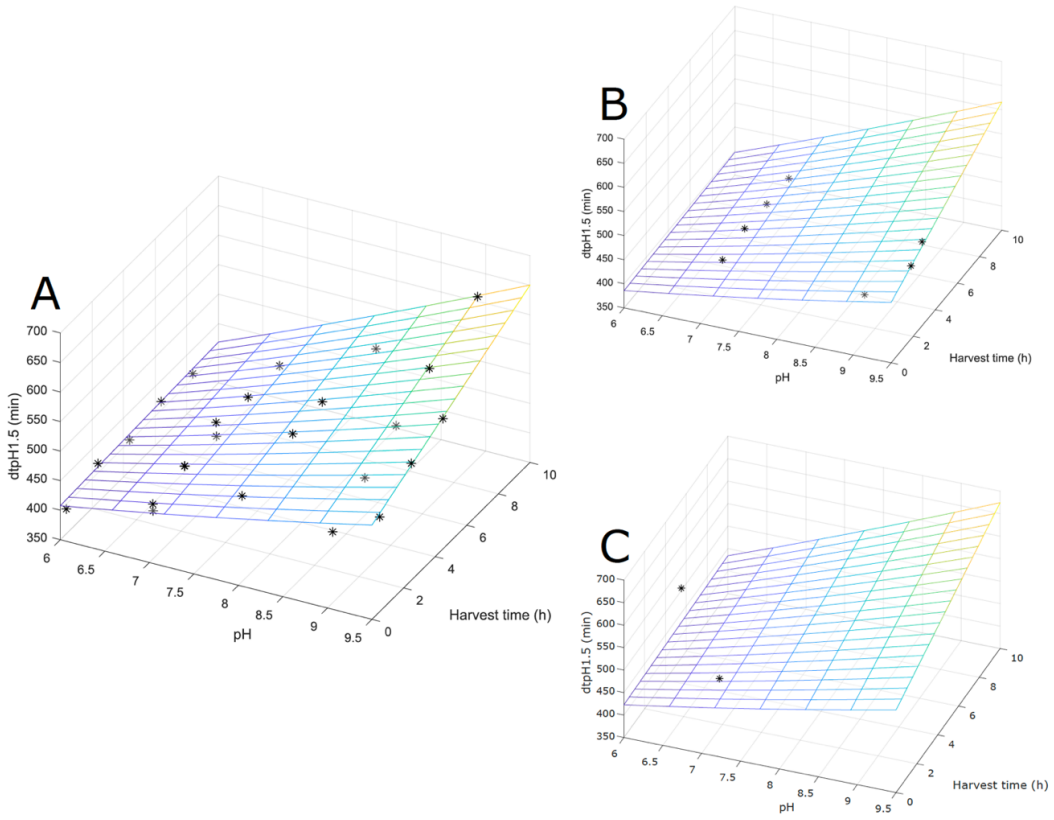

Figure III.1-3 : *Response surface representations of the effect of fermentation pH and harvest time on the dtpH1.5 values of C. maltaromaticum CNCM I-3298 concentrates produced at 30 °C* ***(A)****, 20 °C* ***(B)*** *and 37 °C* ***(C)****. *experimental data points employed in the model at the given temperatures.*

Table III.1-3: *Regression analysis of viability (in CFU mL^{-1}) of C. maltaromaticum CNCM I-3298 cells harvested at increasing times during fermentations carried out at different temperatures and pH.*

Term	Estimated coefficient ($.10^{11}$) (β)	*Min ($.10^{11}$)*	*Max ($.10^{11}$)*
Intercept	4.25	*3.37*	*5.13*
X_2^2 *(pH x pH)*	-0.0414	*-0.0564*	*-0.0265*
R^2 = 0.454		95 % confidence interval	

(X_2: fermentation pH) (Eq. III.1-1)

and possible outliers can be visualized in **Figure III.1-2**, where the 51 predicted versus measured values of dtpH1.5 are plotted.

Figure III.1-3 shows response surfaces generated with the model for fermentations carried out at 30 °C (**A**), 20 °C (**B**) and 37 °C (**C**), enabling visual assessment of the conjugated effect of fermentation pH and harvest time on dtpH1.5. The limited influence of temperature can be observed through the nearly identical shapes of the response surfaces at both ends of the temperature range (**Fig III.1-3., B and C**). At all temperatures, dtpH1.5 increased with both pH and harvest time in the considered range. According to the model, for fermentations carried out at 30 °C (**Fig. III.1-3, A**), highest acidification activity (lowest dtpH1.5: 407 min) could be achieved with cells cultured at pH 6 and harvested at the beginning of stationary phase (harvest time = 0 h). Lowest acidification activity (highest dtpH1.5: 650 min) could be achieved with cells cultured at pH 9.5, 30 °C (**Fig. III.1-3, A**) and harvested after 10 hours of stationary phase (harvest time = 10 h). Cultivating cells at 20 °C instead of 30 °C would lead to higher acidification activities (lower dtpH1.5) (**Fig. III.1-3, B**) and inversely when cultivating them at 37 °C (**Fig. III.1-3, C**). At pH 9.5 and 37 °C, no growth was observed experimentally. The complete data set used to generate the model is available in supporting information (**Table III.1-A1**).

Effect of fermentation conditions on viability (CFU mL^{-1})

The viability of freeze-thawed concentrates assessed by the agar plate count method varied between 3.1 10^{10} CFU mL^{-1} and 4.0 10^{11} CFU mL^{-1} for all applied fermentation conditions, similarly to the range measured in the industrial production of *C. maltaromaticum* CNCM I-3298 concentrates at reference conditions. Stepwise descending multiple regression analyses were performed to investigate the effect of the fermentation conditions on the viability (in CFU mL^{-1}) of the freeze-thawed cell concentrates produced according to the experimental design. Results are summarized in **Table III.1-3** and the complete data set used to generate the model is available in supporting information (**Table III.1-A1**).
Only 45 % of viability measurements were explained by the quadratic effect of fermentation pH and the effect of the other design variables were not significant at a 0.05 level. Despite the slight influence of pH on viability, the poor coefficient of determination (R^2) level suggests that the range of fermentation parameters applied in the experimental design had a limited influence on the viability of the harvested cells, compared to the variability of the measurement.

III.1.6. Discussion

Industrial starter production is generally optimized for obtaining high biomass yields and concentrated cells displaying high acidification activity and viability upon long term storage. However, the utilization of *Carnobacterium maltaromaticum* starters for producing biological TTI labels involves different challenges. TTI labels are meant to be used as a tool to measure food shelf-life that can largely vary according to the food type: 3 to 21 days for various meats and 0.5 to 3 days for shellfish, under modified atmosphere packaging, at 4 °C (Dalgaard, 1995). To extend food shelf-life ranges, the physiological state modulation of a strain through fermentation condition adjustment, appears to be a path worth pursuing. For use in TTI labels, physiological state of *Carnobacterium maltaromaticum* starters can mainly be associated with acidification activity and viable cell concentration. The objective of this work was thus to map the range of acidification activity and viability that can be covered by *Carnobacterium maltaromaticum* CNCM I-3298, by modifying fermentation conditions. It was also aimed at modeling the relationship between fermentation conditions and the physiological state of concentrated cells in order to develop a useful tool for producing TTI labels corresponding to a broadened range of shelf-lives.

All tested fermentation conditions led to biomass yields superior to the threshold for industrial production (1 g L^{-1}). All other production steps (concentration, cryoprotection and freezing) were very close to those currently used in industrial production of *C. maltaromaticum* concentrates for biological TTI labels, thus making the direct industrial application of results from this study possible.

As expected, freezing had no significant effect on viability or acidification activity of *C. maltaromaticum* CNCM I-3298 concentrates. This is not surprising, given the psychrotrophic nature of *Carnobacteria* and their distribution in the natural environment (Leisner et al. 2007). In previous work investigating the freeze-thaw tolerance of bacterial soil communities that overwinter, *C. maltaromaticum* showed no significant viability losses after three freeze-thaw cycles and only 1 log CFU mL^{-1} after 12 freeze-thaw cycles. 28 cycles were needed to observe a loss of viability of two to three orders of magnitude (Walker *et al*., 2006). *C. maltaromaticum*'s resistance to freezing could be in part due to their small size (Fonseca *et al*., 2000; Dumont *et al*., 2004). The low sensitivity of small LAB has been related to their resulting high cell surface area to volume (SA/V) ratio, thus facilitating water efflux from the cell during freezing (Fonseca *et al*., 2000; Dumont *et al*., 2004). Cell sizes of *Carnobacteria* vary between 0.5 and 0.7 µm in diameter and 1.1 and 3.0 µm in length (Schillinger and Holzapfel 1995), making them relatively small rods with a SA/V ratio of 3.2 to 4.9 $µm^{-1}$. They are similar to the size of *Lactobacillus delbrueckii* subsp. *lactis* (0.83 µm in diameter, 3.3 µm in length, SA/V ratio of 5.4 $µm^{-1}$), a rod reported to be resistant to freeze-thawing (Fonseca *et al*., 2000).

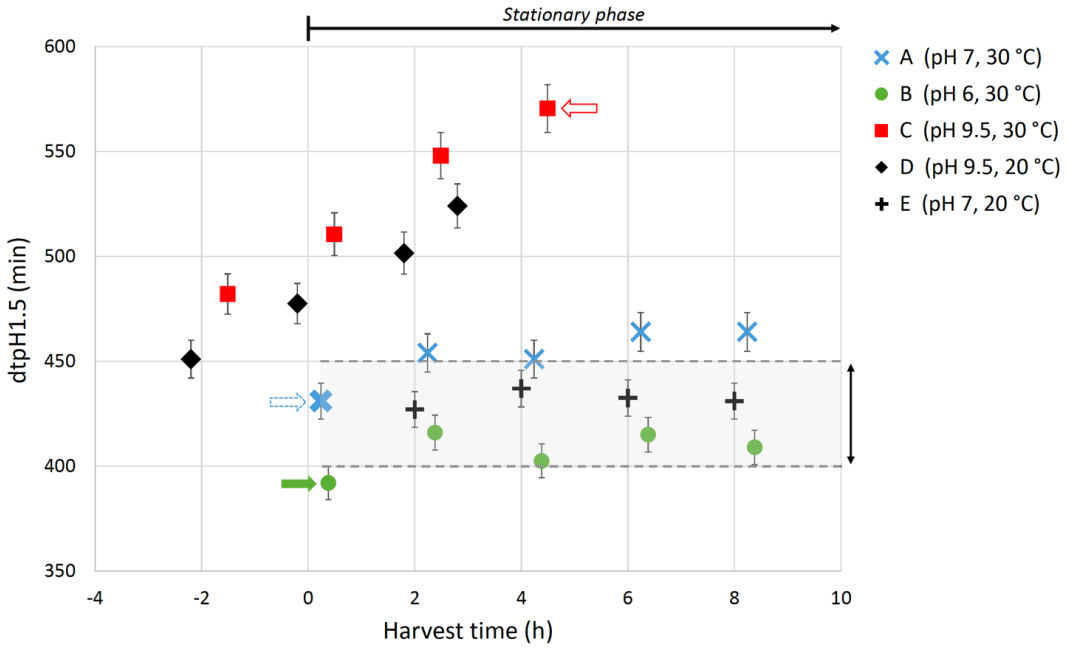

Figure III.1-4: *dtpH1.5 values of* C. maltaromaticum *CNCM I-3298 concentrates harvested at increasing times of fermentation, carried out at different values of pH and temperature. Fermentation conditions leading to best (full green arrow) and worst (empty red arrow) acidification activities are indicated, as well as the reference conditions corresponding to the TopCryo® commercial TTI (dashed, empty blue arrow). The range of acidification activities leading to technologically similar shelf-lives to the control is signaled by dotted lines. Harvests done before stationary phase are of no industrial interest.*

Table III.1-4: *Mean-centered regression analysis of the acidification activity (dtpH1.5) of C. maltaromaticum CNCM I-3298 cells harvested at increasing times during fermentations carried out at different temperatures and pH.*

Variables	Mean-centered coefficients	*Min*	*Max*
Harvest time	**-1.8048**	**-2.4338**	**-1.1758**
Temperature x pH	**0.2891**	**0.1669**	**0.4114**
pH x harvest time	**2.2180**	**1.6012**	**2.8349**
pH^2	**0.4440**	**0.3169**	**0.5712**

This strain presented similar freeze-thaw resistance to small *Streptococci* and much higher resistance than *Lactobacillus delbrueckii* spp. *bulgaricus* CFL1, respectively exhibiting high (10 to 11 μm^{-1}) and low (2.9 μm^{-1}) SA/V ratios. Furthermore, the freeze-thaw resistance of *C. maltaromaticum* CNCM I-3298 concentrates was certainly enhanced in our study by the addition of trehalose before freezing, a sugar known to be an effective cryoprotectant (de Antoni *et al.*, 1989). *C. maltaromaticum*'s resistance to freeze-thawing confirmed previous work (Walker *et al.* , 2006) and supported industrial practices that directly assesses acidification activity and viability on freeze-thawed concentrates, thus inferring that the physiological states of the cells are similar before and after freezing.

Fermentation temperature, pH and harvest time are known factors that affect LAB starter quality (van de Guchte et al. 2002). In this study, *Carnobacterium maltaromaticum* CNCM I-3298 exhibited significant sensitivity to all three factors. Extreme acidification activities of *C. maltaromaticum* concentrates achieved in this study are presented in **Figure III.1-4** as a function of harvest time in order to help visually illustrate the effect of each factor and facilitate comparison with control conditions (**Fig. III.1-4, fermentation A**). The reference conditions for industrial production of *C. maltaromaticum* concentrates were 30 °C, pH 7 and a harvest time close to the beginning of stationary phase, as indicated by the dashed arrow in **Figure III.1-4**. Reference fermentation conditions led to starters exhibiting intermediate acidification activities (dtpH1.5 = 440 min). Highest acidification activity values (i.e. lowest dtpH1.5) were measured in cells produced at pH 6, 30 °C and harvested at the beginning of stationary phase (F**ig. III.1-4, fermentation B**). Lowest acidification activity values (i.e. highest dtpH1.5) were measured for those produced at pH 9.5, 30 °C and harvested after 4 hours of stationary phase (**Fig. III.1-4, fermentation C**).

The mean-centered coefficients of the model describing the effect temperature, pH and harvest time on acidification activity are presented in T**able III.1-4**. Measurement units are different between the three culture parameters (temperature in °C, pH in upH and harvest time in h) and the response variable (dtpH1.5 in min). The mean-centered analysis makes it possible to reduce coefficients to the same scale in order to rank the influence of the culture variables on dtpH1.5. The variable that is most influent on dtpH1.5 is thus the interactive variable between pH and harvest time (2.218) and the least influent is the interactive variable between pH and temperature (0.289) (**Table III.1-4**).

Although the effect of temperature evidenced in **Table III.1-4** only appears through the interaction variable with pH, its moderate effect can still be observed in **Figure III.1-4**. There is indeed a positive influence of low temperature on acidification activity (**Fig. III.1-4, fermentations A *vs* E and C *vs* D**).

Low temperature was also reported to induce high acidification activity in both *Lactobacillus sakei* (Hüfner and Hertel 2008), another psychrotrophic LAB, and *Lactococcus lactis* (Wouters et al. 2000). The adaptive response of LAB to temperature downshift has been linked to the production of cold induced proteins (Panoff *et al.*, 1994; Wouters *et al.*, 1999). During cold acclimation of *Lactococcus piscium* CNCM I-4031 at 5 °C, Garnier *et al.* (2010) detected an upregulation of the histidyl phosphor-carrier protein (HPr), a protein that has been linked to glycolysis regulation (Deutscher *et al.*, 2006). The cold induction of the HPr protein has likewise been observed in *Lactococcus lactis* (Wouters et al. 2000), *Bacillus subtilis* (Graumann et al. 1997) and *Lactobacillus sakei* (Marceau et al. 2004). When lowering temperatures, enzyme-catalyzed reactions slow down. As suggested by Hüfner and Hertel (2008), it can thus be expected that cold induces higher production of glycolytic enzymes, to compensate for slower metabolism (glycolytic capacity) at low temperatures. In their study on *Lc. lactis*, Wouters *et al.* (2000) observed an increase of the maximal glycolytic activity by 2.5 fold following a temperature downshift. We could consequently speculate that an increase in the production of certain proteins (such as HPr) in *C. maltaromaticum* CNCM I-3298 during growth at sub-optimal temperatures (i.e. 20 °C) would lead to an increased acidification activity of the harvested cells at higher temperatures (i.e. 30 °C), such as those used for the industrial quality control in TTI-like medium.

A strong effect of pH on the acidification activity of *C. maltaromaticum* can be observed in **Figure III.1-4**. During this study, highest acidification activity values were measured in cells produced at pH 6 (**Fig. III.1-4, fermentation B**) and lowest in those produced at pH 9.5 (**Fig. III.1-4, fermentations C and D**). This is corroborated by the mean-centered coefficient value attached to the quadratic effect of pH presented in **Table III.1-4**. It is generally known that acid adaptation systems in LAB promote synthesis of stress proteins associated with improved stress resistance (Lorca and de Valdez 2001). The positive effect of low pH on acidification activity observed in this work supports a study aimed at optimizing cell growth and bacteriocin activity of *Carnobacterium divergens* V41 where low pH (i.e. pH 6.5 compared to pH 8) was also shown to improve metabolic activity (Brillet-Viel et al. 2016). Low pH may thus favor metabolic activity in all *Carnobacteria*.

Remarkably, in this study the negative effect of high pH on acidification activity is greatly enhanced by increasing harvest times, as can be observed for pH 9.5 (**Fig. III.1-4, fermentations C and D**). The interaction between pH and harvest time displays the highest mean-centered coefficient value (2.218, **Table III.1-4**), thus appearing to be the most influent variable on the dtpH1.5 descriptor. In the studied parameter range, it notably outweighs the seemingly positive effect of increased harvest time on dtpH1.5 brought about by the negative value of its coefficient: -1.805 (**Table III.1-4**). The interaction between pH and harvest time on acidification activity was reported to have a similar effect on *Lactococcus lactis*

concentrates produced during batch fermentation (Hansen et al. 2016). Highest acidification activities were achieved at low pH (pH 5.5) and the negative effect of increasing harvest times during stationary phase was only seen at high pH (pH 6.5 and 7.5). In their study, Hansen *et al.* (2016) correlated low *Lc. lactis* acidification activities with decreasing cell sizes observed upon entry into stationary phase during fermentations carried out at pH 6.5 and 7.5, but not at pH 5.5. Shrinkage has been generally linked to nutrient starvation (Hochman 1997), the most frequent type of stress provoking entry into stationary phase (van de Guchte et al. 2002). Interestingly, a mechanism reported to favor cell survival after nutrient depletion is the production of extra ATP through the arginine deiminase (ADI) pathway (Arena *et al*., 1999; Stuart *et al*., 1999), that happens to partly be induced by acid stress (de Angelis and Gobbetti, 2004). The production of ATP by the ADI pathway is due to arginine catabolism and the production of NH_3. This helps restore optimal intracellular pH during acid stress (Marquis et al. 1987). The ADI pathway is present in both *Lc. Lactis* (Budin-Verneuil et al. 2003) and *C. maltaromaticum* (Leisner, *et al.*, 1994) and in *Lactobacillus bulgaricus*, a strain that also exhibited more stable acidification activities during stationary phase at pH 5 compared to pH 6 (Rault *et al*., 2009). It is known that the availability of certain essential substrates is linked to cell environmental conditions (Konings et al. 1997). The negative, but still moderate effect of stationary phase when pH is low could therefore also be explained by a decreased availability of certain substrates, rather than complete depletion. Consequently, at low pH the acidification activity increase (or its maintenance) of *C. maltaromaticum*, *Lc. lactis* and *Lb. bulgaricus* during stationary phase could be explained by a less critical nutritional deprivation, in addition to the induction of the ADI pathway.

All TopCryo® labels are currently inoculated with *C. maltaromaticum* starters produced by fermentations carried out in control conditions and always harvested at the same culture time (**Figure III.1-4**). Maximum range of shelf-life covered by these labels at 4 °C is 30 h to 192 h. Concentrates produced during fermentations carried out at 30 °C, pH 6 (**Fig. III.1-4, fermentation B**) and harvested at beginning of stationary phase, could potentially reduce the lower limit of TopCryo®'s range by 2 h (-7 % of the current lower limit). On the other hand, concentrates produced at 30 °C, pH 9.5 (**Fig III.1-4, fermentation C**) and harvested 4 h into stationary phase could increase the upper limit of the range by 68 h (+35% of the current upper limit). The shelf-life range of TopCryo® is presently achieved by inoculating the labels with varying cell concentrations (i.e. lower cell concentrations for longer shelf-lives and higher cell concentrations for shorter shelf-lives). The difference in acidification activities observed today in TopCryo® labels is thus directly correlated to viable cell concentration. It was therefore important to confirm that the acidification activity modulation presented in this study was not due to gain or loss of starter cell viability. To this end, the influence of the three studied fermentation parameters on viability was analyzed using the same stepwise multiple regression

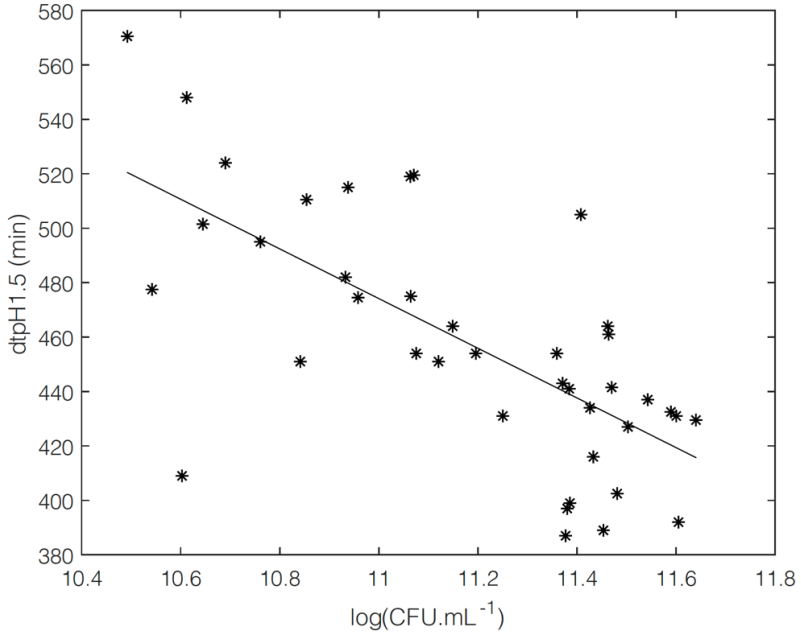

Figure III.1-5: *Experimental dtpH1.5 (in min) values of all C. maltaromaticum CNCM I-3298 concentrates produced following the experimental design, as a function of their viability (in logCFU mL^{-1}). R^2 = 0.4654*

analysis method as the one used for the acidification activity descriptor (dtpH1.5). As expected for psychrotrophic micro-organisms, the range of tested temperatures did not show any significant effect on viability, and neither did harvest time. The only parameter to have an effect on viability was pH, but it only explained 45 % of data (**Table III.1-3**). It is important to note that due to the intrinsic variability of the plate count agar method, it is common practice to only consider viability variations above 0.3 log CFU mL^{-1} as significant. The variability of this method was particularly critical here as cultures of *Carnobacteria* cells can be present in single, pair or short chains (Schillinger and Holzapfel 1995). Furthermore, cell chain length is dependent on culture conditions and can significantly affect CFU counts. However, given that plate count variability in this study was under 0.3 log, it can safely be suggested that cell viability was not significantly affected by the applied fermentation conditions. This is substantiated by a study aimed at developing a medium for the selective enumeration of *C. maltaromaticum*, where viability did not vary significantly at pH values ranging from 5 to 9 (Edima *et al.*, 2006). Edima *et al.* (2008) reported that although growth stops under pH 5.0, *C. maltaromaticum* is able to sustain its viability at an even lower pH (pH 4.0 in coculture with *Lc. lactis*). It is therefore not surprising that the viability of *C. maltaromaticum* CNCM I-3298 would not be significantly impacted by the range of pH tested in this experimental design. Furthermore, the results of this work are in agreement with a more recent study investigating the impact of the same three fermentation conditions (pH, temperature and harvest time) on the physiological state of *Lc. lactis* at different steps of starter production (Velly *et al.*, 2014). The authors also observed no significant change in *Lc. lactis* viability, regardless of applied fermentation conditions.

To further explore the possible link between acidification activity and viability, dtpH1.5 measurements of concentrates produced in the experimental design were plotted against their viability (**Figure III.1-5**). A downward trend can be observed, indicating as expected, that as viable cell concentration increases, dtpH1.5 values decrease (i.e. acidification activity increases). However, this trend explains less than 47 % of variability (R^2 = 0.4654). For example, for a dtpH1.5 value of 480 min, corresponding cell viabilities ranged between 10.6 and 11.5 log CFU mL^{-1}. Likewise, for a cell viability of 11.4 log CFU mL^{-1}, corresponding dtpH1.5 values ranged between 380 and 510 min. Consequently, the changes in acidification activity can be mainly attributed to the physiological state modulation induced by the application of sub-lethal fermentation conditions, and not simply by gain or loss of cell viability.

This study has evidenced that the acidification activity of *Carnobacterium maltaromaticum* CNCM I-3298 concentrates can be modulated by applying sub-lethal stress conditions during the fermentation step of production. Although fermentation temperature, pH and harvest time all influenced acidification activity,

pH and harvest time were identified to be the most efficient modulation parameters for the production of concentrates exhibiting extreme acidification activities. This work has led to the development of a simple tool in form of a response surface model that can quantify the acidification activity exhibited by *C. maltaromaticum* CNCM I-3298 concentrates according to the applied values of fermentation parameters.

In future work, intracellular pH measurements as well as an integrative approach combining cell membrane characterization (fluidity and lipids composition) and proteomics should offer a better understanding of the mechanisms responsible for the physiological changes induced by sub-lethal stress conditions during fermentation of *Carnobacterium maltaromaticum*.

Acknowledgements: This work was supported by Clock-°T (Cryolog, Nantes, France). This project has also received funding from the European Union's Horizon 2020 research and innovation program under grant agreement N° 777657. The authors thank Dr Marie-Nöelle Leclercq-Perlat for the HPLC analyses.

Conflict of Interest: No conflict of interest to declare.

III.1.7. Key takeaways

→ The range of fermentation parameters applied had no effect on the freeze resistance and limited effect on the viability of *C. maltaromaticum* concentrates.

→ Fermentation temperature, pH and harvest time all influenced the acidification activity of the concentrates, with pH and harvest time identified as being the most influential.

→ Concentrates exhibiting the fastest acidification activity were cultured at 20 °C, pH 6 and harvested at the beginning of stationary phase. These concentrates could potentially reduce the lower limit of the TopCryo® range by 7 % (-2 h).

→ Concentrates exhibiting the slowest acidification activity were cultured at 30 °C, pH 9.5 and harvested after 4 to 6 hours of stationary phase. These concentrates could potentially increase the limit of the TopCryo® range by 35% (+68 h).

→ This study led to the development of a predictive model for the production of *C. maltaromaticum* concentrates exhibiting specific acidification activities, according to the applied values of fermentation parameters.

III.2.
Dynamic modeling of *Carnobacterium maltaromaticum* CNCM I-3298 growth and metabolite production, and model-based process optimization

Content

III.2.1. Context and objectives 164
III.2.2. Abstract 165
III.2.3. Introduction 167
III.2.4. Materials and methods 171
III.2.4.a. Fermentation 171
(i) Culture medium and bacterial strain 171
(ii) Bioreactor and parameter control 171
III.2.4.b. Kinetic measurements 172
(i) Cell growth 172
(ii) Total acid production 172
(iii) Substrate consumption and metabolite production 172
III.2.5. Dynamic model 173
III.2.5.a. Model formulation 173
III.2.5.b. Model parameter identification 177
III.2.5.c. Response surface model for parameter dependence on fermentation conditions 179
III.2.6. Results 181
III.2.6.a. Model parameter identification 181
III.2.6.b. Response surface model for parameter dependence on fermentation conditions 185
III.2.6.c. Model Validation 187
III.2.6.d. Model-Based optimization of fermentation operating conditions for industrial use 189
III.2.7. Conclusions 190
III.2.8. Nomenclature 191
III.2.9. Key takeaways 193

III.2.1. Context and objectives

Carnobacteria were formerly thought of as lactic acid bacteria of poor industrial interest because of their slow acidifying capabilities compared to other LAB. Little to no studies have therefore been published on the industrial production of *C. maltaromaticum* concentrates. The previous chapter presented, to the best of our knowledge, the first study investigating the effect of fermentation parameters on the physiological state of *C. maltaromaticum* concentrates. However, there is still a lack of knowledge on the impact of key fermentation parameters such as temperature and pH, on *C. maltaromaticum* growth and production of metabolites in a bioreactor. This knowledge is necessary to optimize industrial processes involving the growth and acid synthesis of *C. maltaromaticum* cells, which could then help further improve the development and parametrization of a biological TTI like TopCryo®.

Objectives

The purpose of the present study was to offer a dynamic model for the growth of *C. maltaromaticum* CNCM I-3298 and production of the four main metabolites (formic acid, acetic acid, lactic acid and ethanol), in batch culture.

In the framework of this project, as initially planned with Cryolog Clock-T°, this model (valid in a pH-regulated fermenter) should have been extended to work in an unregulated pH environment (depending on the produced acids and the buffering capacity of the medium). The extended model would have been used to predict the color shift of the label, as a function of its time-temperature history. A model-based design would have considerably reduced the experimental work necessary to develop new labels exhibiting a wide range of shelf lives.

The present study was published in August 2021,
in ***Foods*** (Volume 10, Issue 8 ; p. 1922).
DOI: 10.3390/foods10081922

Authors:
Cristian Puentes[1,2], Amélie Girardeau[1], Stephanie Passot[1], Fernanda Fonseca[1] and I-C Trelea[1,*]

[1] INRAE, AgroParisTech, UMR SayFood, Université Paris-Saclay, F-78850 Thiverval-Grignon, France; cristian.puentes@centralesupelec.fr (C.P.); amelie.girardeau@inrae.fr (A.G.); stephanie.passot@inrae.fr (S.P.); fernanda.fonseca@inrae.fr (F.F.)
[2] CentraleSupélec, LGPM, Université Paris-Saclay, F-91192 Gif-sur-Yvette, France
[*]Correspondence: ioan-cristian.trelea@inrae.fr; Tel.: +33 1 30 81 54 90

III.2.2. Abstract

Carnobacterium maltaromaticum is a species of lactic acid bacteria found in dairy, meat, and fish, with technological properties useful in food biopreservation and flavor development. In more recent years, it has also proven to be a key element of biological time–temperature integrators for tracking temperature variations experienced by perishable foods along the cold-chain. A dynamic model for the growth of *C. maltaromaticum* CNCM I-3298 and production of four metabolites (formic acid, acetic acid, lactic acid, and ethanol) from trehalose in batch culture was developed using the reaction scheme formalism. The dependence of the specific growth and production rates as well as the product inhibition parameters on the operating conditions were described by the response surface method. The parameters of the model were calibrated from eight experiments, covering a broad spectrum of culture conditions (temperatures between 20 and 37 °C; pH between 6.0 and 9.5). The model was validated against another set of eight independent experiments performed under different conditions selected in the same range. The model correctly predicted the growth kinetics of *C. maltaromaticum* CNCM I-3298 as well as the dynamics of the carbon source conversion, with a mean relative error of 10% for biomass and 14% for trehalose and the metabolites. The paper illustrates that the proposed model is a valuable tool for optimizing the culture of *C. maltaromaticum* CNCM I-3298 by determining operating conditions that favor the production of biomass or selected metabolites. Model-based optimization may thus reduce the number of experiments and substantially speed up the process development, with potential applications in food technology for producing starters and improving the yield and productivity of the fermentation of sugars into metabolites of industrial interest.

Keywords: *Carnobacterium maltaromaticum*; Modeling; Microbial growth; Optimization; Fermentation

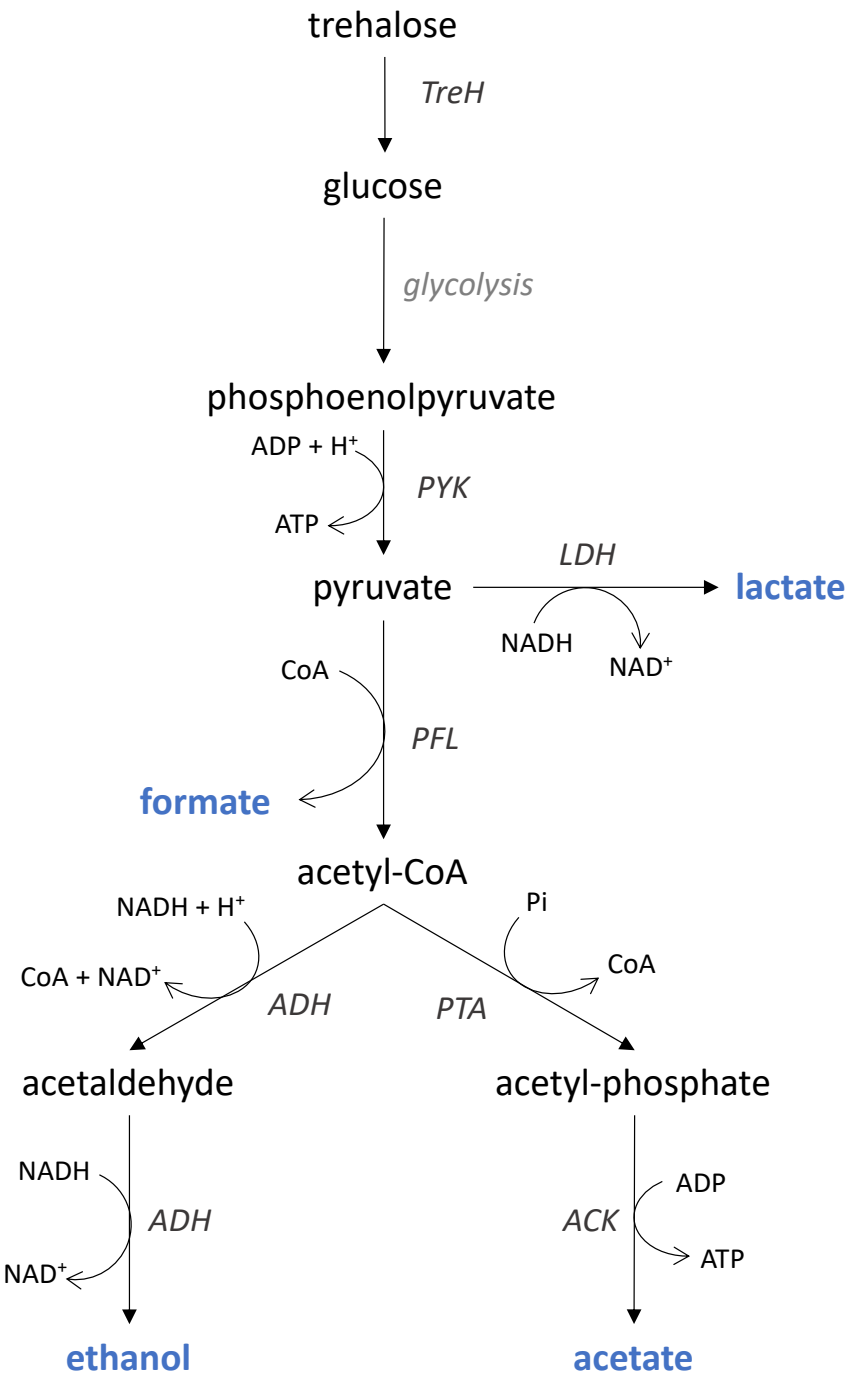

Figure III.2-1: Mixed-acid fermentation pathway likely used by C. maltaromaticum to ferment trehalose. End products are shown in blue. ACK, acetate kinase; ADH, acetaldehyde dehydrogenase; LDH, lactate dehydrogenase; PFL, pyruvate formate lyase; PTA, phosphate acetyltransferase; PYK, pyruvate kinase; TreH, neutral trehalase. Adapted from (Andersson and Rådström 2002; Laursen et al. 2006; Ward 2015; Gänzle 2015; Zhang et al. 2019)

III.2.3. Introduction

Carnobacterium maltaromaticum is a psychrotropic species of lactic acid bacteria widely found in food such as dairy products, fish and meat. It is a gram positive, facultative anaerobic bacterium, able to grow at alkaline pH (up to 9.6) (Edima et al. 2007; Afzal et al. 2010). In the food industry, *C. maltaromaticum* has potential applications related to health protection and organoleptic properties. These include the biopreservation of food, by inhibiting the growth of foodborne pathogens such as *Listeria* sp. in cold conditions, and the development of flavor in ripened cheese varieties (Cailliez-Grimal et al. 2007; Edima et al. 2007; Afzal et al. 2010). This lactic acid bacterium may also be used as biological indicator in time-temperature integrators (TTI); 'smart-labels' that monitor the time-temperature history of chilled products throughout the cold chain (Taoukis and Labuza 1989; Ellouze et al. 2008). Concentrates of the strain CNCM I-3298 have been selected as inoculum for TopCryo® labels, the only biological TTI that has been taken to market to date. A pH decline of the label medium, associated with bacterial growth, produces an irreversible color change from green to red as an indication to the consumer about the spoilage of the food to which the TTI is attached (Girardeau et al. 2019). In these applications, *C. maltaromaticum* concentrates produced by fermentation may be used alone or in association with other microorganisms. Some experimental studies on *C. maltaromaticum* fermentation in different culture conditions have been reported in the literature (Borch and Molin 1989; Cailliez-Grimal et al. 2007; Ellouze et al. 2008; dos Reis et al. 2011; Afzal et al. 2012; Afzal et al. 2013; Rahman et al. 2014; Rahman et al. 2016; Zhang et al. 2018; Girardeau et al. 2019). The effect of temperature and pH on the acidifying activity was evaluated and modelled by Girardeau et al. (2019). However, there is a lack of knowledge on the characterization and optimization of Carnobacteria growth and production of various metabolites such as acids or flavor compounds in bioreactor.

Carnobacteria are considered to be homofermentative lactic acid bacteria that produce lactic acid from glucose, with pyruvate as a central metabolic intermediate (via the Embden-Meyerhof pathway) (De Bruyn et al. 1987; De Bruyn et al. 1988; Leisner et al. 2007). However, pyruvate may be alternatively converted to acetate, ethanol, formate, and CO_2 (De Bruyn et al. 1988; Schillinger and Holzapfel 1995) under anaerobic conditions and substrate limitation (Gänzle 2015), arising for example at the end of fermentation (Ward 2015). The production of organic acids by Carnobacteria is also strain dependent (De Bruyn et al. 1988; Borch and Molin 1989; Laursen et al. 2006). A recent study reported that lactic, formic and acetic acids are key organic acids produced by *C. maltaromaticum* in a meat juice medium (Zhang et al. 2019), indicating that this microorganism has the enzymatic machinery to perform mixed-acid fermentation (**Figure III.2-1**).

.

For optimization purposes, modeling has proven to be a powerful tool, enabling the exploration of a wider range of operating conditions while minimizing cost, compared to the experimental approach (Levisauskas et al. 2003; Antelo et al. 2012; Kiparissides et al. 2015; Balsa-Canto et al. 2016; Sánchez-Castañeda et al. 2018; Sinner et al. 2019). To our knowledge, the only dynamic model dealing with *C. maltaromaticum* strains has been published by Ellouze et al. (2008). That research was oriented towards a biological TTI setting associated to a sausage-like packaging instead of a bioreactor and taking into account lactic acid as single metabolite.

The aim of this study is thus to develop and validate a dynamic model predicting the impact of fermentation conditions (temperature and pH) on the growth and bioconversion fermentation dynamics of *C. maltaromaticum* CNCM I-3298, using trehalose as carbon source and considering the four main identified metabolites: formic acid, acetic acid, lactic acid and ethanol. This study was conducted as part of a research project on the production and conservation of *C. maltaromaticum* concentrates. In that context, the growth of *C. maltaromaticum* was tested in different sugars: glucose, maltose, mannitol, and trehalose, with similar growth rates. Trehalose was chosen in this study because this molecule is known for its ability to protect cells during bacterial stabilization processes (freeze-drying in particular). Therefore, the residual trehalose (not consumed during fermentation) could be used as cryoprotectant after production of bacterial concentrates.

The model development involved four major steps, presented in Section III.2.5: derivation of the main governing equations based on the known mixed-acid fermentation pathway, mass balances and kinetic rate expressions (Section III.2.5.a), parameter identification for each fermentation experiment (Section III.2.5.b), construction of response surfaces of the calibrated parameters as a function of temperature and pH (Section III.2.5.c), and final validation of the complete model. The resulting model is shown to be a useful tool to determine the optimal conditions for producing bacterium concentrates in bioreactors and to assess the productivity of the bioconversion fermentation of sugars into metabolites of potential industrial interest (Section III.2.6.d).

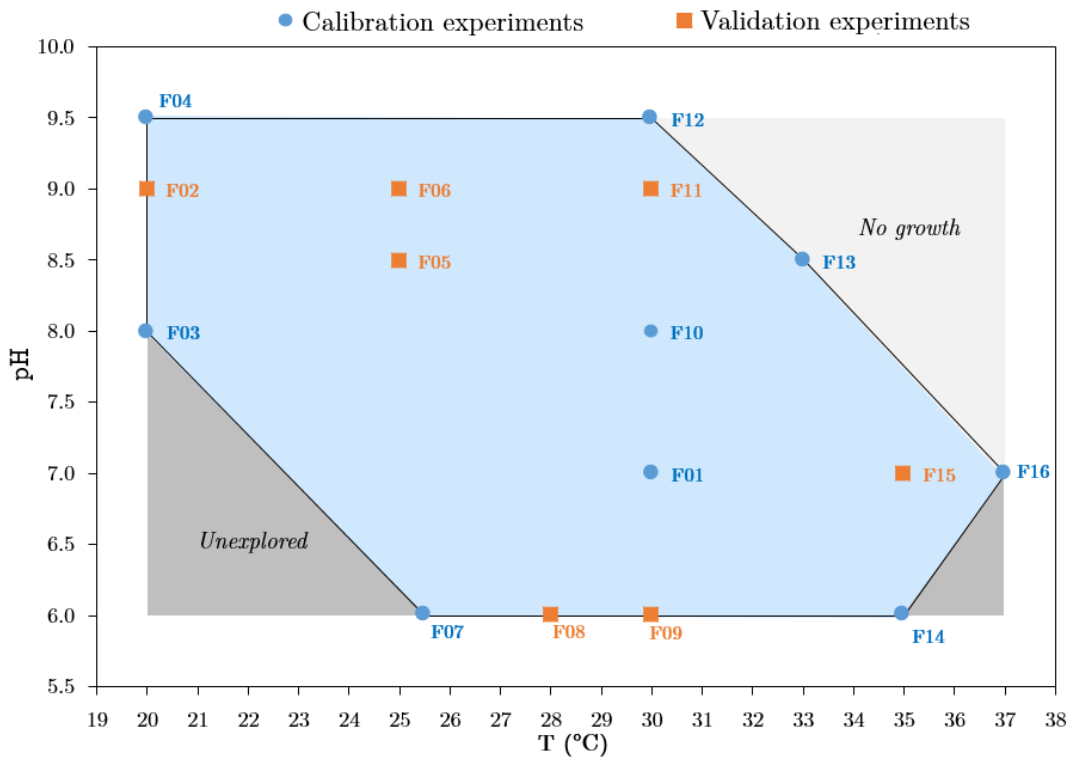

Figure III.2-2: *Operating conditions of* C. maltaromaticum *CNCM I-3298 fermentation experiments*

III.2.4. Materials and methods

Data used to calibrate and validate the model were partially reported in a previous study, in which a modified central composite experimental design was carried out to study the effect of operating conditions on the technological properties of *C. maltaromaticum* CNCM I-3298 (Girardeau et al. 2019). Sixteen lab-scale fermentations (hereafter named F01 to F16) were performed using a wide range of regulated operating conditions (**Figure III.2-2**): temperature between 20 and 37 °C and pH between 6.0 and 9.5.
Fermentation durations varied between 20 h and 45 h and the initial conditions were: for biomass (X_0) 0.077 $mol_C \cdot L^{-1}$, trehalose (S_0) between 0.091$mol \cdot L^{-1}$ and 0.107 $mol \cdot L^{-1}$ and medium volume (V_0) 3.5 L. The main fermentation settings and the kinetic measurements are reported below.

III.2.4.a. Fermentation

(i) Culture medium and bacterial strain

The fermentation medium was composed of the following ingradients for 1 kg of final solution: 40 g of trehalose (Treha™; Tokyo Japan), 10 g of proteose peptone (Oxoid; Waltham, MA, USA); 5 g of yeast extract (Humeau; La-Chapelle-sur-Erdre, France); 5 g of Tween 80 (VWR; Leuven, Belgium); 0.41 g of $MgSO_4$ (Merck; Darmstadt, Germany); 0.056 g $MnSO_4$ (Merck; Darmstadt, Germany) and water to reach a total of 1 kg of solution. All medium components were sterilized together at 121 °C, for 20 min. Fermentations were carried out on *C. maltaromaticum* CNCM I-3298 pre-cultures. Pre-cultures were prepared by inoculating 10 mL of sterilized fermentation medium with 100 µL of *C. maltaromaticum* CNCM I-3298 stock culture and incubated for 13 to 16 h at 30 °C. One milliliter of the resulting culture was transferred into 50 mL of fresh medium and then incubated again for 11 h under the same conditions. The resulting culture was then used to inoculate the bioreactor. Inoculation was performed at an initial concentration of approximately 10^7 CFU mL^{-1}.

(ii) Bioreactor and parameter control

The bioreactor (Minifors, Infors HT, Bottmingen, Switzerland) had a total volume of 5 L and was equipped with a heat mantle and a cryostat for temperature control. It contained 3.5 L of fermentation medium, inoculated with an initial cell concentration of approximately 10^7 CFU·mL^{-1}. Initial pH was adjusted to the desired value with 5 N NaOH or 0.01 N H_2SO_4 solutions. During fermentation, pH was controlled by automatic addition of 5 N NaOH. Culture homogenization was performed with an agitation device set at 150 rpm. Temperature and pH were set according to the investigated operating conditions mentioned above (**Figure III.2-2**).

III.2.4.b. Kinetic measurements

(i) Cell growth

Cell growth was monitored using an infra-red probe (Excell210, CellD, Roquemaure, France) continuously measuring absorbance at 880 nm and storing data every minute. The absorbance data were calibrated in dry weight. Dry cell weight was determined by filtering 10 mL of bacterial suspension (straight out of the bioreactor) through a 0.20 µm polyethersulfone membrane (Supor®, PALL Biotech, Saint-Germain-en-Laye, France). The filter was then dried for 24 h at 80 °C. Measurements were obtained in triplicate. Mass concentrations were finally converted to $mol_C.L^{-1}$ (carbon-mol of biomass per liter) assuming the simplified unit-carbon biomass formula $CH_{1.8}O_{0.5}$ (Battley 1960).

(ii) Total acid production

Total acid production was determined according to the volume of NaOH solution injected into the bioreactor to maintain a constant pH. The pH was regulated/controlled to set values using the IRIS NT V5 software (Infors, AG, Bottmingen, Switzerland).

(iii) Substrate consumption and metabolite production

Trehalose consumption and metabolite production were determined using high-performance liquid chromatography (HPLC, Waters Associates, Millipore; Molsheim, France). HPLC was performed on culture media samples of a few mL, aseptically retrieved from the bioreactor at different times during fermentation and filtered through 0.22 µm pores (Sartorius stedim, Biotech; Göttigen, Germany). Analyses were made using a cation exchange column (Aminex Ion Exclusion HPX-87 300x7.8 mm, Biorad, Richmond, USA) at 35 °C. Mobile phase was 0.0005 M H_2SO_4 and flow rate was set at 0.6 mL^{-1} (LC-6A pump, Shimadzu, Courtaboeuf, France).

HPLC analysis showed that *C. maltaromaticum* CNCM I-3298 produces not only lactic acid but also formic acid, acetic acid and ethanol in variable proportions according to the fermentation conditions.

III.2.5. Dynamic model

The mathematical model is a set of ordinary differential equations implemented in MATLAB R2018b (the MathWorks Inc. Natick, MA). Model parameters and response surface coefficients were identified by nonlinear regression analysis using the Statistic and Machine Learning Toolbox of MATLAB.

III.2.5.a. Model formulation

The dynamic model developed in this study combines biochemical knowledge about the metabolism of the selected bacterium and mass balances of the main compounds: substrate, biomass and identified metabolites. Expressions of specific growth and metabolite production rates include substrate limitation, product inhibition phenomena and time lags due to microbial metabolism adaptation (Bastin and Dochain 1990). The surface response method was used to express the empiric dependence of some model parameters on operating conditions. The model assumed the bioreactor is perfectly stirred and were no differences between individual cells. It is thus unsegregated and zero-dimensional, predicting average spatial concentrations (Bailey 1998).

Seven state variables were considered: six volume concentrations (biomass [X], trehalose [S], formic acid [F], acetic acid [A], lactic acid [L], and ethanol [E], **Figure III.2-1**), and the culture medium volume (V). This latter variable varies continuously with the addition of base (NaOH) for pH control but also changes in a discrete way due to periodic sampling for biological and chemical analysis.

Mass balances for the considered metabolites resulted in the following set of differential equations:

$$\frac{d[X]}{dt} = \mu_X[X] - \frac{Q}{V}[X] \quad \text{(III.2-1)}$$

$$\frac{d[F]}{dt} = \pi_F[X] - \frac{Q}{V}[F] \quad \text{(III.2-2)}$$

$$\frac{d[A]}{dt} = \pi_A[X] - \frac{Q}{V}[A] \quad \text{(III.2-3)}$$

$$\frac{d[L]}{dt} = \pi_L[X] - \frac{Q}{V}[L] \quad \text{(III.2-4)}$$

$$\frac{d[E]}{dt} = \pi_E[X] - \frac{Q}{V}[E] \quad \text{(III.2-5)}$$

$$\frac{d[A_T]}{dt} = \frac{d[F]}{dt} + \frac{d[A]}{dt} + \frac{d[L]}{dt} \quad \text{(III.2-6)}$$

$$\frac{d[S]}{dt} = -\left(\frac{\mu_X}{Y_{X/S}} + \frac{\pi_F}{Y_{F/S}} + \frac{\pi_A}{Y_{A/S}} + \frac{\pi_L}{Y_{L/S}} + \frac{\pi_E}{Y_{E/S}}\right)[X] - \frac{Q}{V}[S] \quad \text{(III.2-7)}$$

$$\frac{dV}{dt} = Q \quad \text{(III.2-8)}$$

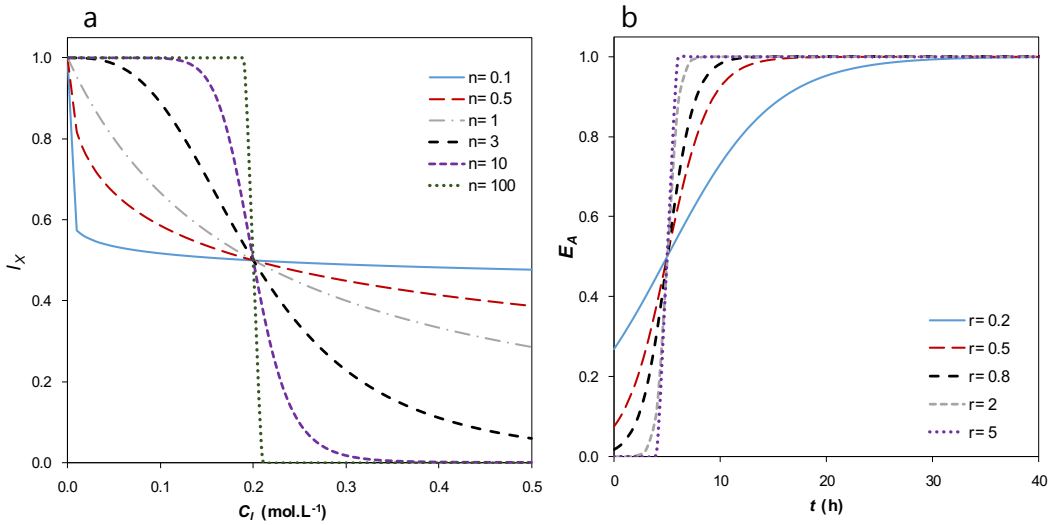

Figure III.2-3: : (a) *Example of inhibition factor I_X as a function of C_I for different n values and K_{IX}=0,2 mol.L^{-1} .* ***(b)*** *Example of enzymatic activation factor E_A as a function of t for different r values and t_{lag}=5 h.*

where μ_X is the specific growth rate (h^{-1}), π_F, π_A, π_L, π_E the specific productions rates of four metabolites (h^{-1}) and $Y_{X/S}$, $Y_{F/S}$, $Y_{A/S}$, $Y_{L/S}$, $Y_{E/S}$ the yield of biomass and metabolites with respect to the substrate ($mol.mol^{-1}$). Q is the experimentally measured rate of NaOH solution ($L.h^{-1}$) added for pH control throughout fermentation.

In Eq. III.2-6, $[A_T]$ is the total acid concentration, defined as the sum of formic, acetic and lactic acid concentrations. These compounds are assumed to be mainly responsible for the pH change of the liquid medium.
Specific growth and production rates were defined using the Monod law to account for substrate limitation, modified with product inhibition and enzymatic adaptation factors (Monod 1942; Levenspiel 1980; Baranyi and Roberts 1994):

$$\mu_X = \mu_{max,X} I_X E_A \frac{[S]}{K_{SX} + [S]} \quad \text{(III.2-9)}$$

$$\pi_m = \pi_{max,m}\, I_m E_A \frac{[S]}{K_{Sm} + [S]} \qquad m = F, A, L, E \quad \text{(III.2-10)}$$

In these equations, I_X and I_m are inhibition factors that depend on the inhibitor concentration. They vary between 1 and 0. Inhibition increases with the inhibitor concentration and its effect on the specific rate is maximal when the corresponding factor is 0. In this model, a progressive inhibition factor of the following form was used (Aiba and Shoda 1969; Claret et al. 1993):

$$I_X = \frac{1}{1 + \left(\frac{C_I}{K_{IX}}\right)^n} \quad \text{(III.2-11)}$$

$$I_m = \frac{1}{1 + \left(\frac{C_I}{K_{Im}}\right)^p} \qquad m = F, A, L, E \quad \text{(III.2-12)}$$

K_{IX} and K_{Im} represent characteristic concentrations of the inhibitors ($mol.L^{-1}$) such that the corresponding rates (μ_X and π_m) are reduced by a factor of two compared to the absence of inhibitor, *n* and *p* are shape factors and C_I is the concentration of the inhibitor. Since all the metabolites are produced in similar proportions and no biochemical knowledge about their relative inhibiting nature is available, C_I was simply defined as the sum of the 4 metabolite concentrations:

$$C_I = [F] + [A] + [L] + [E] \quad \text{(III.2-13)}$$

To illustrate the role of the shape factor *n*, **Figure III.2-3a** depicts the evolution of I_X with C_I for different *n* values and a lag-time of 5 h. A more or less sharp change in the inhibition factor occurs around the characteristic inhibitor concentration, $C_I=K_{IX}$. The significance of the shape factor *p* is similar.

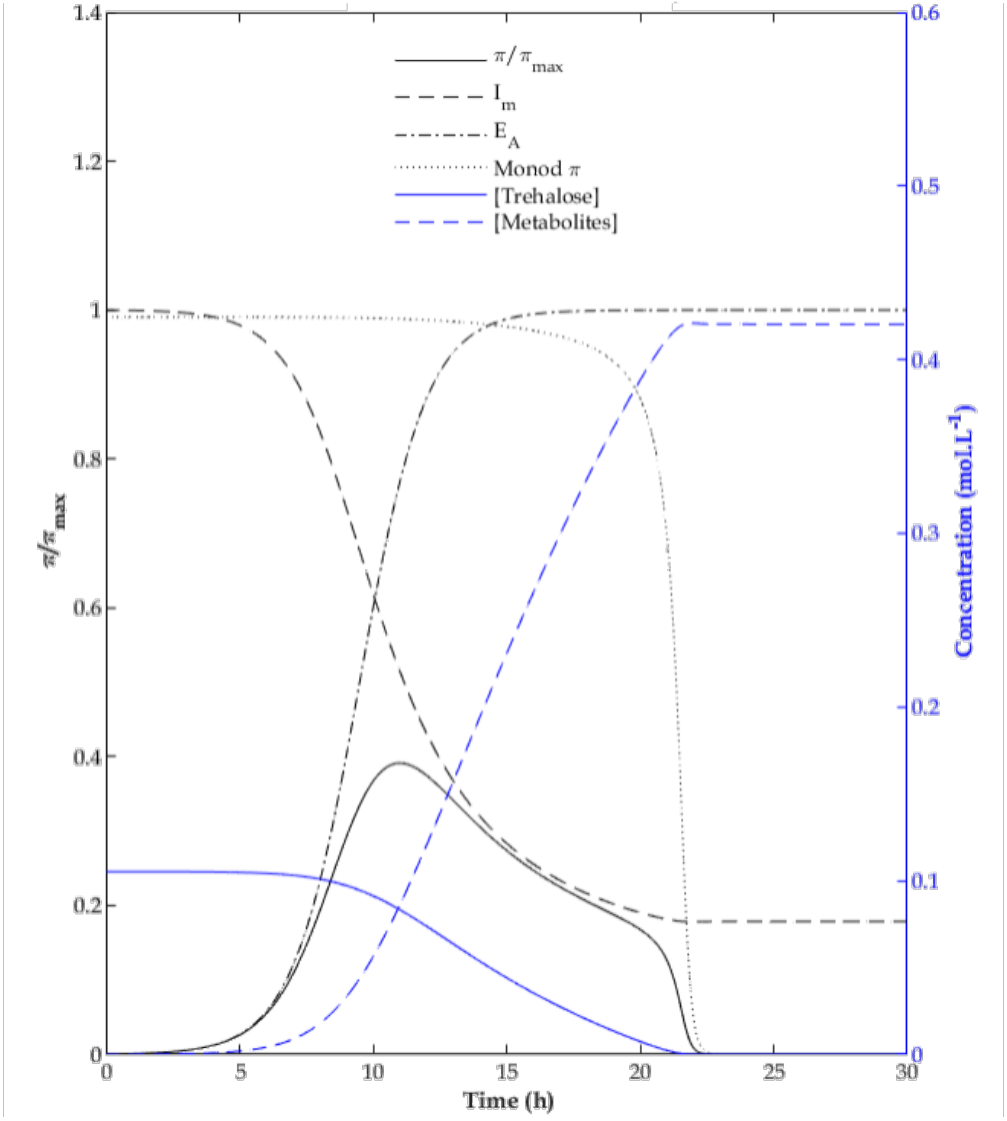

Figure III.2-4: *Typical evolution of the relative production rate over time*

The enzymatic adaptation factor E_A, is an empirical representation of the lag time, a period of adaptation to the culture environment where the microorganism produces new enzymatic machinery(Monod 1949; Baranyi 1998; Rolfe et al. 2012). Based on the shape of experimental data, the following equation was proposed:

$$E_A = \frac{1}{1 + \exp\left(-r\left(t - t_{lag}\right)\right)} \quad \text{(III.2-14)}$$

where t_{lag} (h) is the lag time experimentally observed. **Figure III.2-3b** shows that E_A is an increasing function of time, tending to 1 when $t \gg t_{lag}$. In analogy with *n*, *r* is a shape factor that describes the gradual transition from the lag phase to the active phase of growth. A higher value of *r* implies a steeper change of E_A around $t=t_{lag}$.

To illustrate the features of the proposed model, a representation of the dimensionless specific growth and production rates (μ/μ_{max} and π/π_{max}) over time is depicted in **Figure III.2-4**. The dynamic behavior of both variables is similar given the similarity of Eqs. 1 to 5. The specific rates achieve a maximum value in the active growth phase, and they are zero when $t \ll t_{lag}$ and when the substrate is depleted. The shape of the curve is defined by three factors: in the increasing region (0 to 10 h in **Figure III.2-4**), the dominant effect is enzyme activation E_A (Eq. III.2-14); in the slowly decreasing region (10 to 20 h) the rate is controlled by inhibition (Eqs. III.2-11 or 12), whereas in the sharply decreasing region (20 to 22 h) it is controlled by substrate limitation, corresponding to the Monod-like factor in Eqs. III.2-9 or 10.

III.2.5.b. Model parameter identification

The system of kinetic equations for a single fermentation experiment includes 24 parameters: five yield coefficients, five inhibition parameters, five growth/production rates, five Monod-like saturation constants, three shape factors and one lag time. Due to a limited number of experimental data and to facilitate the identification procedure, a single value was adopted for the inhibition parameter (K_{Im}) and the Monod saturation constant (K_{Sm}) of the 4 identified metabolites. Moreover, 10 parameters were fixed for all experiments: the shape factors, the yield coefficients, the Monod saturation constants (K_{SX} and K_{Sm}). For each fermentation, lag time was determined by graphical readout. This simplification of fixing parameters independent of operating conditions is supported by two assumptions often used in the literature: (1) metabolite production yields are constant and therefore independent of culture conditions (Bouville 2007) and (2) the saturation constant of the Monod model depends only on the nature of the substrate (Monod 1942; Monod 1949), which is the same in all experiments of this study.

The remaining group of seven parameters ($\mu_{max,X}$, $\pi_{max,F}$, $\pi_{max,A}$, $\pi_{max,L}$, $\pi_{max,E}$, K_{IX}, K_{Im}) were identified for each fermentation of the experimental design by nonlinear regression. Here, the Levenberg-Marquardt algorithm (Seber and Wild 2003), was used to minimize the sum of squares of the errors between experimental and predicted concentrations. However, since the ranges and the number of measurements were slightly different among the metabolites, the values compared in the least squares function were normalized by dividing by their maximum value and were weighted by the relevant number of experimental measurements.

The quality of the model representation was quantified with two error indicators, defined as follows:

Root mean square error:

$$RMSE = \left[\frac{1}{N}\sum_{i=1}^{N}\left(C_{\boldsymbol{model,i}} - \boldsymbol{C_{exp,i}}\right)^{\mathbf{2}}\right]^{1/2} \qquad \text{(III.2-15)}$$

Relative mean error (as a percentage):

$$RME = \frac{1}{N}\sum_{i=1}^{N}\frac{\left|C_{model,i} - C_{exp,i}\right|}{C_{exp,max} - C_{exp,min}} \cdot 100\% \qquad \text{(III.2-16)}$$

where N is the number of available measurements, C_{model} and C_{exp} are respectively the values of the concentration variables calculated with the model and measured experimentally.

III.2.5.c. Response surface model for parameter dependence on fermentation conditions

Nonlinear regression was performed to model the relationship between the 7 parameters of the dynamic model specific to each experiment and the fermentation operating conditions, namely temperature (T) and pH. The regression model had a similar form for all parameters, the logarithm of the parameter being expressed as a second-order polynomial with interaction:

$$Log_{10}Par_i = \beta_{0i} + \beta_{1i}T + \beta_{2i}pH + \beta_{3i}T^2 + \beta_{4i}pH^2 + \beta_{5i}TpH \qquad \text{(III.2-17)}$$

The regression coefficients (β) for all parameters depending on operating conditions ($\mu_{max,X}$, $\pi_{max,F}$, $\pi_{max,A}$, $\pi_{max,L}$, $\pi_{max,E}$, K_{IX}, K_{Im}) were simultaneously computed by least-squares optimization based on all available concentration measurements.

Table III.2-1: *Model parameters independent of operating conditions, determined from the experimental data of the experiment F10 (T=30 °C, pH=8) with tlag=10 h.*

Parameter	Constant value
$Y_{X/S}$ ($mol_C.mol^{-1}$)	6.9
$Y_{F/S}$ ($mol.mol^{-1}$)	5.6
$Y_{A/S}$ ($mol.mol^{-1}$)	3.8
$Y_{L/S}$ ($mol.mol^{-1}$)	7.0
$Y_{E/S}$ ($mol.mol^{-1}$)	4.7
K_{SX} ($mol.L^{-1}$)	0.001
K_{Sm} ($mol.L^{-1}$)	0.001
n	3
p	1
r (h^{-1})	0.8

Table III.2-2: *Model parameters determined for each experiment by nonlinear regression.*

Fermentation		μ_{maxX} (h^{-1})	π_{maxF} (h^{-1})	π_{maxA} (h^{-1})	π_{maxL} (h^{-1})	π_{maxE} (h^{-1})	KI_X ($mol.L^{-1}$)	KI_m ($mol.L^{-1}$)
F01	Value	0.224	0.152	0.064	0.215	0.078	0.117	0.069
	Standard error	0.003	0.003	0.003	0.005	0.001	0.004	0.003
F02	Value	0.096	0.122	0.064	0.053	0.064	0.143	0.142
	Standard error	0.021	0.012	0.007	0.006	0.006	0.083	0.036
F03	Value	0.164	0.137	0.064	0.131	0.072	0.099	0.102
	Standard error	0.012	0.009	0.004	0.009	0.005	0.006	0.013
F04	Value	0.078	0.063	0.031	0.072	0.034	0.144	0.092
	Standard error	0.012	0.004	0.002	0.004	0.002	0.047	0.016
F05	Value	0.130	0.130	0.060	0.196	0.070	0.160	0.100
	Standard error	0.005	0.002	0.002	0.004	0.001	0.004	0.004
F06	Value	0.094	0.129	0.063	0.159	0.063	0.163	0.092
	Standard error	0.001	0.002	0.001	0.003	0.001	0.003	0.002
F07	Value	0.074	0.028	0.010	0.089	0.022	0.122	0.139
	Standard error	0.002	0.001	0.001	0.004	0.002	0.005	0.004
F08	Value	0.060	0.055	0.024	0.126	0.048	0.149	0.060
	Standard error	0.002	0.002	0.000	0.003	0.002	0.001	0.002
F09	Value	0.071	0.097	0.048	0.114	0.071	0.108	0.044
	Standard error	0.009	0.007	0.004	0.010	0.006	0.021	0.007
F10	Value	0.220	0.230	0.100	0.300	0.120	0.193	0.091
	Standard error	0.051	0.013	0.007	0.022	0.007	0.044	0.015
F11	Value	0.121	0.127	0.060	0.116	0.066	0.179	0.133
	Standard error	0.004	0.007	0.004	0.005	0.003	0.006	0.003
F12	Value	0.132	0.155	0.082	0.076	0.086	0.043	0.059
	Standard error	0.010	0.026	0.003	0.002	0.006	0.002	0.007
F13	Value	0.147	0.162	0.077	0.219	0.092	0.164	0.106
	Standard error	0.006	0.006	0.002	0.008	0.004	0.009	0.003
F14	Value	0.047	0.045	0.020	0.112	0.032	0.140	0.130
	Standard error	0.005	0.004	0.001	0.006	0.003	0.016	0.007
F15	Value	0.160	0.180	0.080	0.330	0.110	0.260	0.170
	Standard error	0.056	0.013	0.008	0.030	0.010	0.022	0.010
F16	Value	0.110	0.110	0.050	0.200	0.070	0.320	0.280
	Standard error	0.003	0.004	0.002	0.007	0.003	0.051	0.104

In this way, the accuracy and standard errors of the coefficients were statistically acceptable, due to a large number of degrees of freedom: several hundreds of concentration data were used to estimate 42 coefficients. Initial guesses for these coefficients were obtained using Eq. III.2-17 and parameter values determined separately for each experiment.

In this procedure, two sets of data from the experimental design were defined as indicated in **Figure III.2-2**: eight calibration experiments, located in extreme positions of the experimental domain, used simultaneously for coefficients (β) estimation, and eight validation experiments, only used a posteriori to verify the accuracy of the complete dynamic model.

III.2.6. Results

III.2.6.a. Model parameter identification

The values of the parameters that are independent of operating conditions, summarized in **Table III.2-1**, were determined from the experimental data of experiment F10. This run is placed on a central position in the composite experimental design (T=30 °C, pH=8) (**Figure III.2-2**). Monod saturation constants are usually difficult to determine from batch experiments because the number of measurements is typically very low in the substrate limitation zone. Saturation constants were thus fixed to a common value with a typical order of magnitude (Owens and Legan 1987). As for yields, they were found to differ from the theoretical ones defined through standard stoichiometric reactions of anabolism and catabolism. These differences can be due to other reactions involving the carbon substrate, whose products were not analytically measured and not considered in the model.
After fixing the parameters in **Table III.2-1** for the whole set of experiments, the group of seven adjustable parameters of the model ($\mu_{max,X}$, $\pi_{max,F}$, $\pi_{max,A}$, $\pi_{max,L}$, $\pi_{max,E}$, K_{IX}, K_{Im}) were identified for each run by nonlinear regression.

The parameters obtained by this procedure are summarized in **Table III.2-2**. Standard errors were computed from the variance-covariance matrix of the nonlinear optimization algorithm. These errors represent between 5 % and 13 % of the value of the identified parameters, a reasonable uncertainty level for a biological model.
For the whole set of experiments, the prediction errors are reported in **Annex Table III.2-A1**. Except for some runs for variables S, F and A, all RME were lower than 15 %. Also, the average RMSE and RME values for each concentration are of the same order of magnitude as the experimental variability, here defined as the biological repeatability for run F01, for which 3 independent replicates were performed.

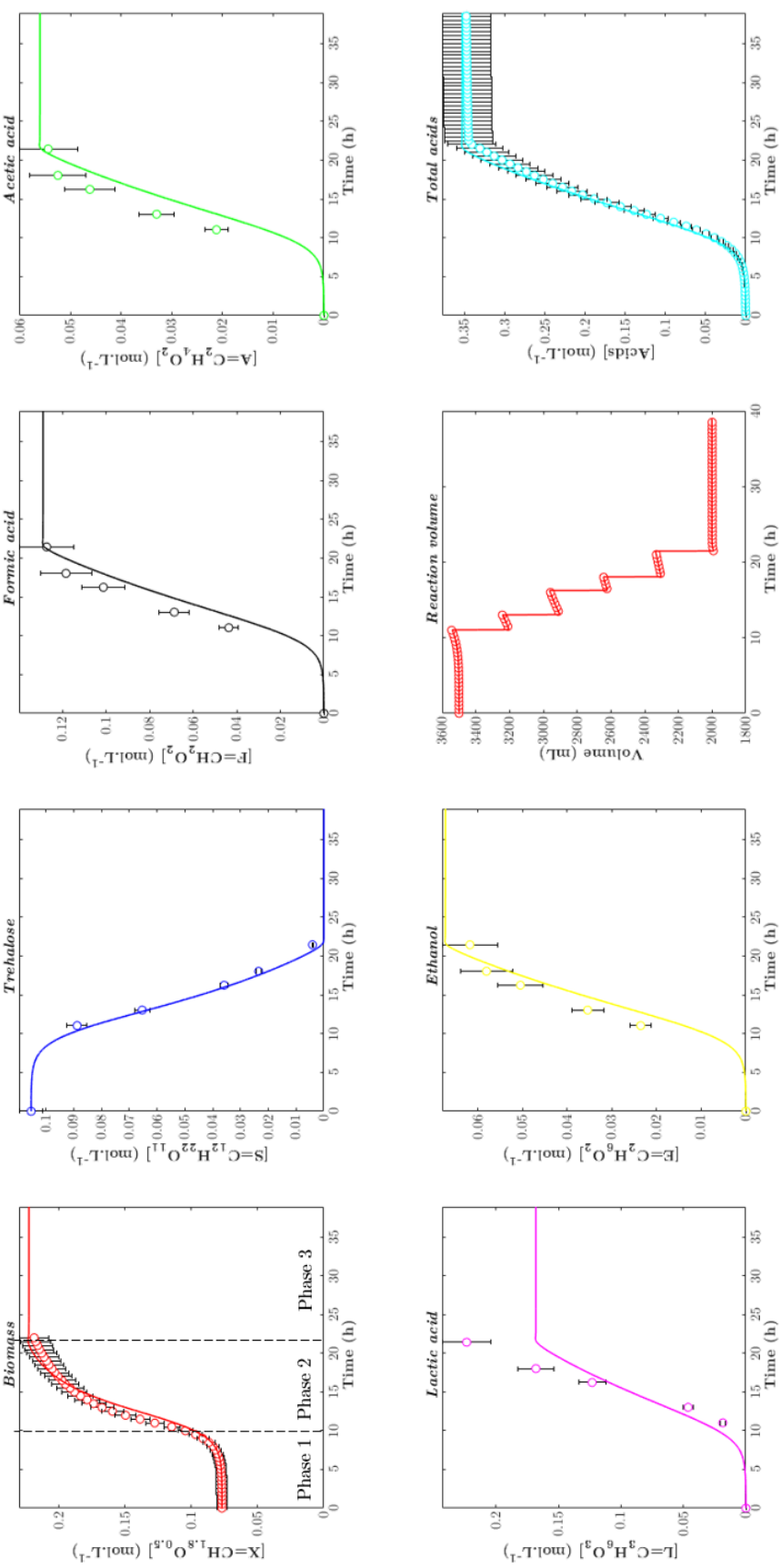

Figure III.2-5: *Evolution of concentrations over time for experiment F10 (T=30 °C, pH=8). Comparison between model (continuous line, using parameters from tables 1 and 2) and experimental data (symbols). The error bars for data represent the biological standard deviation, calculated from three independent repetitions of the run F01.*

These results validate the formulation and accuracy of the proposed model, for the operating conditions included in the experimental design.

In the specific case of reference run F10, a comparison between the model simulation (using the corresponding parameters from **Table III.2-2**) and experimental data is depicted in **Figure III.2-5**.
Three growth phases are apparent in **Figure III.2-5**: a lag phase (phase 1, between 0 and 10 h), a phase of active growth, substrate consumption and metabolite production (phase 2, between 10 h and 21 h), and a final phase where concentrations do not change over time, owing to the depletion of the carbon source or growth inhibition by metabolites (phase 3, after 21 h). Regarding culture volume evolution, as already mentioned, the discrete variations at regular intervals are due to sampling for analysis of the culture medium and gradual increase is due to NaOH addition for pH control. One can also observe that the four metabolites are produced simultaneously, with no gap for the growth dynamics. The metabolites are thus primary end products generated during a single trophophase (Madigan et al. 2006). This justifies the choice of a global inhibitor concentration (Eq. III.2-13), which includes four correlated concentrations.

In consideration of the visual fit from **Figure III.2-5**, the model representation is reasonably satisfactory. The most pronounced discrepancy between the model and experimental data appears for lactic acid, for which the model predicts a lower concentration before substrate depletion.

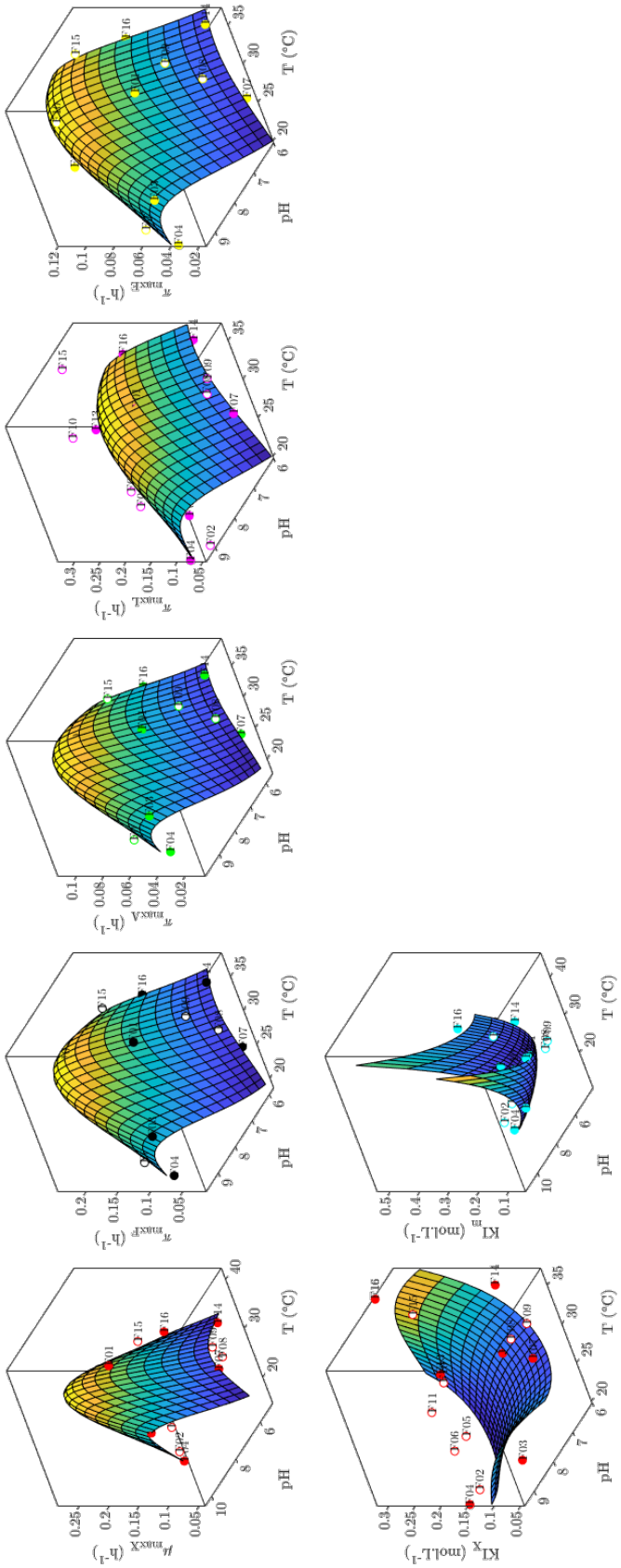

Figure III.2-6: *Response surfaces for model parameters, calculated with globally adjusted β coefficients in Eq. III.2-17*

III.2.6.b. Response surface model for parameter dependence on fermentation conditions

Model parameters were expressed as a function of temperature and pH, according to the surface model (Eq. 17). The values of the β regression coefficients were adjusted globally using the whole set of calibration data.

The resulting response surfaces for the 7 model parameters are plotted in **Figure III.2-6**. For the five kinetic parameters, (i.e., the maximum specific growth and production rates) the response surfaces have the same convex shape, with a well-defined maximum value at intermediate T and pH conditions. These maxima likely indicate the optimal temperatures and pH for cellular growth as well as the enzymatic activity catalyzing each of the reactions leading to the production of the different metabolites (**Figure III.2-1**).

Concerning the inhibition concentrations, the response surface for K_{Im} has a concave shape with a local minimum whereas that of K_{IX} resembles a saddle surface. For this latter case, the surface shape indicates that for every pH there is a T where K_{IX} is minimal and for every T there is a pH where K_{IX} is maximal. Both K_{Im} and K_{IX} represent the combined effect of several inhibiting metabolites (Eq. III.2-11 to 13) with potentially different inhibition mechanisms.

For completeness, the final values of the regression coefficients of Eq. III.2-17 for the seven adjustable parameters of the dynamic model are reported in **Annex Table III.2-A2**. All coefficients in Eq. 17 for each model parameter were significantly different from zero at a 0.05 level. A comparison between the parameter values determined for each experiment, (section III.2.6.a) and the parameter values computed with Eq. III.2-17 (from globally adjusted β coefficients) is depicted in **Annex Figure III.2-A1**. The goodness of the fit was assessed through the coefficient of determination, R2. This coefficient is higher than 0.89 for six out of seven model parameters, which is a high threshold for biological data. In the case of K_{Im}, only 66 % of the variance of this parameter is explained by variables T and pH. The remaining 34 % could be associated with inherent experimental variability and factors not included in the model, for instance transient variability of the inhibition and kinetics parameters and actual dependence of the fixed parameters (**Table III.2-1**) with T and pH (Rodríguez et al. 2008). From a more general point of view, differences from experimental data could be due to features that are not represented by the mathematical model such as population segregation, internal pH variability and concentration gradients in the culture medium (Bellgardt 2000; González-Cabaleiro et al. 2015).

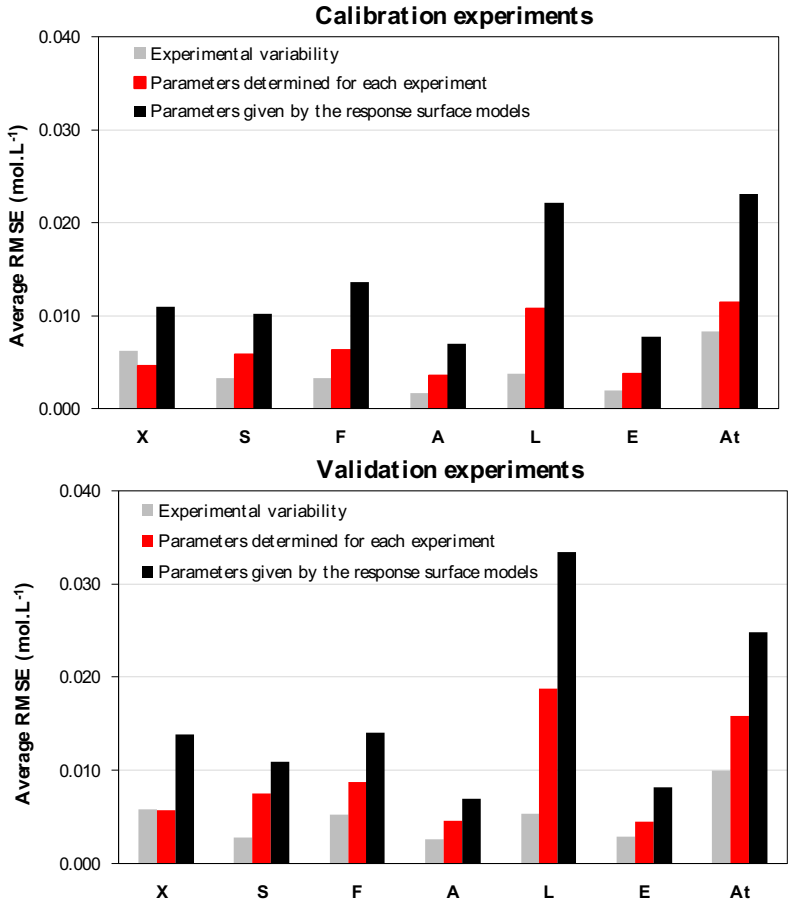

Figure III.2-7: *Comparison between experimental variability and average RMSE values for concentrations computed using parameters determined for each experiment (**Table III.2-2**) and the response surface models (Table III.2-A2 and Equation III.2-17).*

III.2.6.c. Model Validation

The ability of the dynamic model including the parameters calculated from operating conditions (Eq. III.2-17) to predict data of independent experiments was assessed with the set of validation experiments.
A comparison between the average RMSE values obtained in Section III.2.6.a (determined for each experiment) and Section III.2.6.b (calculated from operating conditions) for calibration and validation sets is depicted in **Figure III.2-7**. In most cases RMSE values were higher than the corresponding experimental variabilities indicating that more complex models could capture additional phenomena not included in the present model, such as dependence of yields, saturation constants or lag time (**Table III.2-1**) on operating conditions. As one might expect, RMSE was generally lower for the calibration experiments than for the validation experiments, not used for parameter determination. However, the relative difference remained small (less than 30 %) indicating a satisfactory ability of the developed model to predict time evolution of the considered biomass, substrate, and metabolites in new conditions within the explored experimental range.

It also appears in **Figure III.2-7** that average RMSE values with parameters given by the response surface model (**Table III.2-A3**) are about 50% higher than with parameters determined separately for each experiment (**Table III.2-A1**), for both calibration and validation sets. This result could be expected since in the global calibration step, data from 8 independent experiments were combined as a whole for the least squares estimation, with a detrimental effect on the individual representation of each experiment. However, results with the parameters calculated from operating conditions are the most useful for engineering purposes since they enable a quick prediction of growth and metabolites production dynamics, based on the selected combination of temperature and pH.

In light of this quantitative analysis, the prediction accuracy of the empirical dynamic model coupled to the regression model may be considered satisfactory within the operating domain covered in this study.

Table III.2-3: *Optimal conditions for growth and production of metabolites according to the developed model. In bold: targeted metabolite for each set of operating conditions. Final concentrations and productivities calculated with initial conditions:* $[X]_0=80\ mmol.L^{-1}$, $[S]_0=100\ mmol.L^{-1}$, $[F, A, L, E]_0=0$.

(A) Target: ↑ maximal concentration, ↓ minimal concentration.

A. Target		T (°C)	pH	Final concentrations ($mmol.L^{-1}$)						Final productivities ($mmol.L^{-1}.h^{-1}$)					
				X	F	A	L	E	A_T	X	F	A	L	E	A_T
Biomass	B ↑	20.0	7.8	**227**	129	56	177	73	363	6.56	3.73	1.61	5.11	2.09	10.46
Formic acid	F ↑	28.0	9.5	133	**176**	89	123	94	387	1.68	2.20	1.12	1.54	1.18	4.86
Acetic acid	A ↑	28.0	9.5	133	176	**89**	123	94	387	1.68	2.20	1.12	1.54	1.18	4.86
Lactic acid	L ↑	37.0	6.0	180	95	42	**296**	72	433	1.68	2.20	1.12	1.54	1.18	4.86
Ethanol	E ↑	37.0	9.5	118	147	77	128	**139**	352	2.35	2.90	1.54	2.54	2.76	6.98
Ethanol	E ↓	27.0	7.6	217	143	62	166	**68**	372	6.93	4.57	1.98	5.31	2.16	11.86
Total acids	A_T↑	37.0	6.0	180	95	42	296	72	**433**	3.33	1.76	0.77	5.48	1.33	8.01
Total acids	A_T↓	37.0	9.5	118	147	77	128	139	**352**	2.35	2.90	1.54	2.54	2.76	6.98

(B) Target: ↑ maximal productivity, ↓ minimal productivity.

B. Target		T (°C)	pH	Final concentrations ($mmol.L^{-1}$)						Final productivities ($mmol.L^{-1}.h^{-1}$)					
				X	F	A	L	E	A_T	X	F	A	L	E	A_T
Biomass	B ↑	33.5	7.5	199	139	64	178	73	382	**7.49**	5.25	2.41	6.71	2.77	14.38
Formic acid	F ↑	34.5	8.0	178	148	71	163	82	381	6.77	**5.61**	2.70	6.18	3.12	14.48
Acetic acid	A ↑	35.0	8.1	172	148	72	161	85	381	6.49	5.58	**2.71**	6.06	3.21	14.35
Lactic acid	L ↑	37.0	7.1	188	123	58	215	78	395	6.60	4.31	2.04	**7.54**	2.73	13.89
Ethanol	E ↑	37.0	8.3	158	144	73	162	97	378	5.57	5.08	2.56	5.70	**3.43**	13.34
Ethanol	E ↓	28.0	6.0	175	108	41	278	78	427	2.14	1.32	0.50	3.38	**0.95**	5.20
Total acids	A_T↑	35.5	7.7	184	139	67	177	81	384	7.16	5.41	2.59	6.90	3.13	**14.90**
Total acids	A_T↓	25.0	9.5	146	173	88	126	87	386	1.71	2.03	1.03	1.48	1.02	**4.53**

III.2.6.d. Model-Based optimization of fermentation operating conditions for industrial use

Optimal conditions for growth and metabolite production of *C. maltaromaticum* calculated using the developed model are summarized in **Table III.2-3**. Two optimization criteria were considered: final concentrations and final productivities calculated for a 99.9% substrate consumption.

For a detailed representation of the evolution of final concentrations and productivities for biomass and metabolites with temperature and pH, the reader is referred to **Annex Figure III.2-A2**. As a general trend, the highest productivities were obtained around 35 °C and pH 7.5, although the exact optimal conditions depended on the considered metabolite (**Table III.2-3**). No general trend was readily apparent for the maximization of the final concentrations.

These data can be useful to optimize industrial processes involving the growth of *C. maltaromaticum* cells in a trehalose-based substrate. A first application consists in producing *C. maltaromaticum* concentrates, regardless of metabolite production. In this case two conditions of cultivation appear advisable: 20 °C and pH 7.8 to maximize concentration (227 $mmol_C \cdot L^{-1}$) or 33.5 °C and pH 7.5, in order to maximize productivity (7.49 $mmol_C \cdot L^{-1} \cdot h^{-1}$) and thus the biomass production per unit of time, at the expense of a 12% reduction of the final biomass concentration (199 $mmol_C \cdot L^{-1}$).

A second application deals with the development and parametrization of time-temperature integrators (TTI), labels in which a pH decline, associated with acids synthesis, entails an irreversible color change from green to red. Modulating the acidifying activity of C. maltaromaticum allows thus a reliable shelf-life estimation of different food products. Long shelf-lives can be tracked using TTI composed of concentrates exhibiting low acidifying activities (minimal production of total acids), while short shelf-lives can be tracked using concentrates exhibiting high acidifying activities. In the scenario of maximizing acidifying activity, the production of total acids must be favored and thus fermentation should be carried out at two possible conditions: 37.0 °C and pH 6.0 to maximize their final concentration (433 $mmol \cdot L^{-1}$) or 35.5 °C and pH 7.7 to maximize their productivity (14.90 $mmol \cdot L^{-1} \cdot h^{-1}$). Under these conditions, the biomass production decreases respectively by 20% and 4% with respect to its optimal values. If the objective is on the contrary to minimize acidifying activity, two conditions can be envisaged to favor the lowest production of total acids: 37.0 °C and pH 9.5 for a final concentration of 352 $mmol \cdot L^{-1}$ or 25.0 °C and pH 9.5 for a final productivity of 4.53 $mmol \cdot L^{-1} \cdot h^{-1}$. Under these conditions, the mean biomass production would decrease respectively by 48% and 77% with respect to the maximal values.

Data from **Table III.2-3A** show that the conditions to minimize the total acids concentration (37 °C et pH 9.5) coincide with those to maximize the ethanol concentration (the non-acidifying metabolite, 139 mmol.L^{-1}) and lead to a lactic acid concentration close to its minimal value (128 mmol.L^{-1} versus the minimum around 120 mmol.L^{-1}). Conversely, when the production of total acids is maximized, the lactic acid concentration is also maximal (296 mmol.L^{-1}) and that of ethanol is close to its minimum (72 mmol.L^{-1} versus 68 mmol.L^{-1}).

Furthermore, it should be noted that the condition 27°C and pH 7.6 leads both to a good biomass productivity (6.93 mmol·L^{-1}·h^{-1} versus the maximum 7.49 mmol·L^{-1}·h^{-1}) and a low total acids concentration (372 mmol.L^{-1} versus the minimum 352 mmol.L^{-1}). Cultivation at this condition turns out be advantageous to ally a high biomass production and a relatively low total acidification.

III.2.7. Conclusions

The dynamic model developed in this study is able to predict with satisfactory accuracy the growth of *C. maltaromaticum* CNCM I-3298 (average error of 10 %) as well as the conversion of trehalose into four primary metabolites (average error of 14 %), in a wide range of conditions of temperature and pH. The interpolation capability of the model was verified with a set of 8 independent validations experiments for which the average relative error is 13 %.

This model constitutes a useful tool for optimizing *C. maltaromaticum* cultures. Based on two easily measurable parameters, pH and temperature, it could be implemented in industrial applications of food technology to define optimal growth and metabolite production conditions with various objectives such as the maximization of biomass for production of bacterium concentrates, or the maximization or minimization of the acidifying activity.

Further work is required to incorporate the effect of other culture parameters, such as aeration, nutrient concentrations, or the use of a different carbon source, which may modify growth kinetics and metabolite production. Also, it would be relevant to deepen the understanding of inhibition mechanisms of the metabolites to give more biological significance to the associated parameters in the model.

Moreover, this model could be extended to predict the growth and acidifying kinetics of *C. maltaromaticum* in an environment where temperature varies in an arbitrary but known way and pH is not controlled but depends on the produced acids and the buffer characteristics of the medium. Such an environment is, for example, the cell growth medium within a time-temperature integrator (TTI), a label to monitor the preservation of food products through tracking of the cold chain.

III.2.8. Nomenclature

A	Acetic acid
E	Ethanol
F	Formic acid
L	Lactic acid
S	Carbon substrate (trehalose)
X	Biomass
E_A	Enzymatic activation factor
C ($mol \cdot L^{-1}$)	Concentration (in the calculation of errors and the definition of the inhibition factors)
[i] ($mol \cdot L^{-1}$)	Concentration of species i (substrate, metabolite, biomass) in the culture medium (in the system of differential equations)
I_m	Production inhibition factor of metabolite m
I_X	Biomass growth inhibition factor
K_{Im} ($mol \cdot L^{-1}$)	Concentration for 50% production rate inhibition of metabolite m
K_{IX} ($mol_C \cdot L^{-1}$)	Concentration for 50% growth rate inhibition of biomass
K_{Sm} ($mol \cdot L^{-1}$)	Concentration of production rate saturation of metabolite m
K_{SX} ($mol_C \cdot L^{-1}$)	Concentration of biomass growth rate saturation
mol_C	Carbon-mol of biomass
n	Shape factor of the growth inhibition function
p	Shape factor of the production inhibition function
pH	Potential of Hydrogen
Q ($L \cdot h^{-1}$)	Rate of base addition for pH control
r	Shape factor of the enzymatic activation function
T (K)	Temperature
TTI	Time-temperature indicator
RMSE	Root-mean square error
RME	Relative mean error
SE	Standard error
t (h)	Time
t_{lag} (h)	Lag time
V (L)	Culture medium volume
$Y_{i/S}$ (mol·mol-1)	Yield of product i on substrate S
$Y_{X/S}$ ($mol_C \cdot mol^{-1}$)	Biomass yield on substrate S
μ_X (h^{-1})	Specific growth rate
$\mu_{max,X}$ (h^{-1})	Maximal specific growth rate
π_m (h^{-1})	Specific production rate of metabolite m
$\pi_{max,m}$ (h^{-1})	Maximum specific production rate of metabolite m

Author Contributions: Conceptualization, C.P., A.G., F.F. and C.T.; methodology, C.P., A.G., F.F. and C.T.; software, C.P. and C.T.; validation, C.P., A.G., S.P., F.F. and C.T.; formal analysis, C.P. and C.T.; investigation, C.P. and A.G.; resources, F.F. and C.T.; data curation, C.P. and A.G.; writing—original draft preparation, C.P. and A.G.; writing—review and editing, C.P., A.G., S.P., F.F. and C.T.; visualization, C.P., A.G. and C.T.; supervision, S.P., F.F. and C.T.; project administration, S.P., F.F. and C.T.; funding acquisition, S.P. and F.F. All authors have read and agreed to the published version of the manuscript.

Funding: This work has received funding from the European Union's Horizon 2020Marie Skłodowska-Curie research and innovation program under grant agreement no. 777657.

Data Availability Statement: The data presented in this study are available on request from the corresponding author. The data are not publicly available due to ongoing research project.

Acknowledgments: The authors thank Dr Marie-Nöelle Lecercq-Perlat for the HPLC analyses.

Conflicts of Interest: The authors declare no conflict of interest. The funders had no role in the design of the study; in the collection, analyses, or interpretation of data; in the writing of the manuscript, or in the decision to publish the results.

III.2.9. Key takeaways

→ The developed model can predict the growth and metabolite production of *C. maltaromaticum* CNCM I-3298 with satisfactory accuracy, in a culture medium containing similar nutrients as that of the TopCryo® TTI label medium and within a large range of temperature (20 to 37 °C) and pH (6.0 to 9.5).

→ The model can be used as a tool to optimize the culture of *C. maltaromaticum* in a trehalose-based substrate, by determining operating conditions that favor the production of biomass or selected metabolites, for industrial applications other than TTI label development.

→ The model can serve as a base for the development of an extended model predicting the growth and acidifying kinetics of *C. maltaromaticum* in an environment where temperature is known but varies, and where pH is not controlled. Such an environment is for example, what *C. maltaromaticum* cells experience within a TTI label.

III.3.
Insights into lactic acid bacteria cryoresistance using FTIR micro-spectroscopy and other analytical approaches

Content

III.3.1. Context and objectives 196
III.3.2. Abstract 197
III.3.3. Introduction 198
III.3.4. Materials and Methods 203
III.3.4.a. Bacterial strains, growth conditions, freezing and thawing protocols 203
III.3.4.b. Biological activity assessment of cell samples 203
III.3.4.c. Characterization of the cytoplasmic membrane 204
III.3.4.d. Statistical analysis 211
III.3.5. Results 212
III.3.6. Discussion 227
III.3.7. Conclusions 233
III.3.8. Key takeaways 234

III.3.1. Context and objectives

Growth under sub-lethal stress conditions was shown to have a significant impact on the physiological state of *C. maltaromaticum* (**Chapter III.1 and III.2**) and yet did not seem to affect strain's ability to recover its biological activity after freeze-thaw (**Chapter III.1**). This revealed that the strain presents robust cryoresistance mechanisms, making it an interesting model for cryobiology research. No work has so far explored the cellular mechanisms expressed by *C. maltaromaticum*, granting it such resistance to freezing. Following the loss of funding from Cryolog Clock-T° a year and a half into the PhD project (due to bankruptcy), the focus was switched from modeling the growth and metabolite production of *C. maltaromaticum* under an unregulated pH (extension of the model presented in Chapter 2), to further investigating the strain's cryoresistance mechanisms compared to other LAB.

A novel FTIR micro-spectroscopic approach had recently been developed, enabling the accurate exploitation of the entire mid-infrared region of bacterial cells in aqueous conditions (Meneghel *et al.* 2020). This approach was used to investigate the biochemical characteristics of *L. bulgaricus* ATCC 11842 and *L. bulgaricus* CFL1, two lactic acid bacteria presenting different cryoresistance levels. Their FTIR measurements were however carried out on fresh cells only, so the impact of freezing on the biochemical properties of cells has not yet been explored. Comparing the biochemical characteristics of fresh and thawed populations would reveal potential differences in cryoinjury between the studied strains.

Objectives

Search for markers of LAB cryoresistance by comparing the biophysical and biochemical characteristics of three strains exhibiting varying cryoresistance levels: *C. maltaromaticum* CNCM I-3298, *L. bulgaricus* ATCC 11842 and *L. bulgaricus* CFL1.

The present study was submitted for publication in September 2021,
in the **Analytical and Bioanalytical Chemistry** journal.

Authors:
Amelie Girardeau, Stephanie Passot, Julie Meneghel, Stephanie Cenard, Pascale Lieben, Ioan-Cristian Trelea, Fernanda Fonseca,*

Université Paris-Saclay, INRAE, AgroParisTech, UMR SayFood, 78850, Thiverval-Grignon, France
*Correspondance email: fernanda.fonseca@inrae.fr

III.3.2. Abstract

Freezing is widely used for bacterial cell preservation. However, resistance to freezing can greatly vary depending on bacterial species or growth conditions. Our study aims at identifying cellular markers of cryoresistance based on the comparison of three lactic acid bacteria (LAB) exhibiting different tolerance to freezing: *Carnobacterium maltaromaticum* CNCM I-3298, *Lactobacillus delbrueckii* subsp. *bulgaricus* ATCC 11842, and *Lactobacillus delbrueckii* subsp. *bulgaricus* CFL1.

A thorough characterization of their cytoplasmic membrane properties was carried out by measuring their fatty acid composition, membrane fluidity, and lipid phase transition upon cooling from 50 °C to -50 °C. Vitrification temperatures of the intra- and extra-cellular compartments were also quantified by differential scanning calorimetry. Additionally, the cell biochemical characterization was carried out using a recently developed Fourier transform infrared (FTIR) micro-spectroscopic approach allowing the analysis of live bacteria in an aqueous environment.

The multivariate analysis of the FTIR spectra of fresh and thawed cells enabled the discrimination of the three bacteria according to their lipid, protein, and cell wall peptidoglycan components. It also revealed freezing-induced modifications of these three cellular components and an increase in bacteria heterogeneity for the two strains of *L. bulgaricus*, the freeze-sensitive bacteria. No cellular damage was observed for *C. maltaromaticum*, the freeze-resistant bacteria. Comparison of the results obtained from the different analytical methods confirmed previously reported cryoresistance markers and suggested new ones, such as changes in the absorbance of specific infrared spectral bands. FTIR microspectroscopy could be used as a rapid and non-invasive technique to evaluate the freeze-sensitivity of LAB.

Keywords: Lactic acid bacteria – Freezing – Membrane properties – Infrared spectroscopy – cryoresistance markers

Table III.3-1: Reported work on the investigation of cellular components modifications that have been related to an increase of the LAB survival rate following freezing or frozen storage

Cell components or properties	LAB and conditions	Methods	Possible link to cryoresistance	References
Lipid membrane				
Fatty acid composition	*L. bulgaricus* NSC1, NSC2, NSC3 and NSC4 grown with or with Tween 80	Extracted lipids analysed by gas chromatography	**Higher UFA/SFA** (1.14 vs 0.7) and **higher CFA** content (17.05 % vs 4.2 %)	Smittle et al. 1974
	Lactobacillus ssp. A-12, *S. lactis* grown with or without Tween 80		Lactobacillus: **Higher UFA/SFA** (1.15 vs 0.65) and **higher CFA content** (19 % vs 10.7 %); *S. lactis*: **Higher UFA/SFA** (1.1 vs 0.3)	Goldberg and Eschar 1977
	Streptococci (AC1, AC11, E8, ML1) grown without and with controlled pH		**Higher UFA/SFA** (1.48 vs 1.06)	Gilliland and Speck 1974
	Lc. lactis ssp. *lactis* (MM210 and FG2), *Lc. lactis* ssp. *cremoris* (MM160 and MM310): heat (HS) or cold (CS) shock		HS: **Lower UFA/SFA** (0.65 vs. 0.82) and **higher CFA** content (23.25 % vs 16.12 %) CS: **Higher UFA/SFA** (1.09 vs 0.82)	Broadbent and Lin 1999
	L. acidophilus CRL 640 grown at different temperatures		**Lower CFA** content (5.7 % vs 16.9 %) Higher content of glycolipids	Fernandez et al. 2000
	S. thermophilus CFS2 grown under different conditions		**Higher UFA/SFA** (1.43 / 1.45)	Béal et al. 2001
	L. bulgaricus (CIDCA 331, CIDCA 332, CIDCA 333, ATCC 9659), *L. lactis (*CIDCA 123, CIDCA 133*), L. helveticus* ATCC 15807, *L. acidophilus* CIDCA 134		*L. bulgaricus*: **Higher UFA/SFA** (2.26 vs 1.24) and **lower CFA** content (0.4 % vs 18 %) Other strains: **Lower UFA/SFA** (1.2 vs 2.35) and **higher CFA** content (17.4 % vs 2 %)	Gómez-Zavaglia et al. 2000
	L. acidophilus RD758 grown under different pH and temperature	Extracted lipids analysed by gas- chromatography coupled to mass spectrometry	**Higher CFA** content (11-12% vs 4-8%)	Wang et al. 2005a
	L. acidophilus RD758, cold adaptation		**Higher UFA/SFA** (0.22 vs 0.18) and **higher CFA** content (3.1 % vs 2.5 %)	Wang et al. 2005b
	L. acidophilus RD758 exposed to nutrient starvation		**Higher UFA/SFA** (0.18 vs 0.15) and **higher CFA** content (2.25 vs 1.62)	Wang et al. 2011
	L. bulgaricus CFL1 grown in MRS or whey-based culture media		**Higher UFA/SFA** (1.6 vs 0.5) and **higher CFA** content (14 % vs 2%)	Gautier et al. 2013
	L. bulgaricus CFL1 and *L. bulgaricus* ATCC 11842 in whey-based culture media		**Higher UFA/SFA** (1.04 vs 0.69)	Meneghel et al. 2017

UFA: unsaturated fatty acids; SFA: saturated fatty acids; CFA: cyclic fatty acids; temperature; Ts: temperature of lipid phase transition during cooling (s, solidification); Tm, temperature of lipid phase transition during heating (m, melting); νsCH_2: the position of the symmetric CH_2 stretching band of fatty acids acyl chains at approximately 2850 m^{-1} (DPH: 1,6-diphenyl-1,3,5-hexatriene/hydrophobic probe ; TMA-DPH: 1-[4 (trimethylamino) phenyl]-6-phenyl-1,3,5-hexatriene/amphiphilic probe; PCR: polymerase chain reaction; MALDI-TOF: Matrix Assisted Laser Desorption Ionization - Time of Flight; FTIR: Fourier transform infrared; SR: synchrotron radiation

III.3.3. Introduction

Lactic acid bacteria (LAB) concentrates are widely used today in the food industry to produce various fermented products such as yoghurt, cheese, or kimchi, as well as in the health industry to produce probiotics. Freezing is one of the most employed LAB preservation techniques and a critical step in the production of LAB concentrates. It is nonetheless a stressful stabilization process that can lead to cell damage and death.

During freezing, LAB cells are mainly exposed to cold and osmotic stresses, leading to lipid membrane rigidification, cell dehydration, and volume reduction (Fonseca et al. 2016; Meneghel et al. 2017). The cell dehydration and volume reduction induced by the cryoconcentration of the extracellular medium bring about mechanical constraints on the cell membrane and lead to permanent deformation and loss of membrane integrity (Fernandez et al. 2000; Rault et al. 2007; Gautier et al. 2013). Furthermore, protein damage induced by freezing has been reported (Passot et al. 2015). The cellular freezing-induced damage can be influenced by the addition of protective additives (Cárcoba and Rodriguez 2000; Fonseca et al. 2003; Wang et al. 2019b), as well as cooling, thawing, and storage protocols (Fonseca et al. 2001; Fonseca et al. 2006).

Cryoresistance of LAB can be increased by inducing active cell responses to cold and osmotic stresses when cells are exposed to changes in culture conditions during fermentation (temperature, pH, nutrients) (**Table III.3-1**) (Fonseca et al. 2019). Cryoresistance varies also depending on bacterial species or strain (Gómez-Zavaglia et al. 2000; Fonseca et al. 2001). Several studies, reported in **Table III.3-1**, have investigated the modifications of cellular components that have been related to an increase of the bacterial survival rate following freezing or frozen storage. The analytical methods applied for characterizing those components are also listed in **Table III.3-1**.

More than 70 % of the reported studies focused on the role of the cytoplasmic membrane on LAB cryoresistance and evidenced the key role of its fatty acid composition. In most works, an improvement of cell viability or acidifying activity after freezing was related to an increase in the ratio between unsaturated fatty acids (UFA) and saturated fatty acids (SFA) (Gilliland and Speck 1974; Smittle et al. 1974; Goldberg and Eschar 1977; Broadbent and Lin 1999; Gómez-Zavaglia et al. 2000; Gautier et al. 2013; Meneghel et al. 2017), and/or an increase in the cyclic fatty acids (CFA) content of the membrane (Smittle et al. 1974; Goldberg and Eschar 1977; Broadbent and Lin 1999; Gómez-Zavaglia et al. 2000; Wang et al. 2005b; Gautier et al. 2013). However, the effect of CFA on LAB cryoresistance remains unclear, since few authors have associated better cryoresistance with a reduction in CFA contents (Gómez-Zavaglia et al. 2000; Fernandez et al. 2000). Three studies that deeper investigated the membrane properties of *L. bulgaricus* CFL1 and ATCC 11842, related the increase of the UFA/SFA ratio to a decrease of lipid membrane phase transition

Table III.3-1 (continued): *Reported work on the investigation of cellular components modifications that have been related to an increase of the LAB survival rate following freezing or frozen storage*

Cell components or properties	LAB and conditions	Methods	Possible link to cryoresistance	References
Lipid membrane				
Lipid phase transition	*L. bulgaricus* CFL1 grown in MRS or whey-based culture media	Dynamic FTIR measurements (during cooling (Ts) and heating (Tm) between +50 °C and -50 °C) in aqueous conditions (3000 - 2800 cm^{-1} region)	**Lower lipid phase transition temperature** (Ts=-8 °C vs 22 °C); **higher position of vsCH₂** in frozen range (2850.5 cm^{-1} vs 2849.5 cm^{-1} at -48 °C)	Gautier et al. 2013
	L. bulgaricus CFL1 and *L. bulgaricus* ATCC 11842		**Lower lipid phase transition temperature** (Ts= 5.7 °C vs 13.8 °C); **higher position of vsCH₂** in frozen range (2850 cm^{-1} vs 2849.5 cm^{-1} at -48 °C)	Meneghel et al. 2017
Fluidity	*L. bulgaricus* CFL1 grown in MRS or whey-based culture media	Fluorescence anisotropy, synchrotron UV fluorescence microscopy	Increased fluidity at 0 °C (TMA-DPH anisotropy 0.120 vs 0.330 vs 0.250), no rigid lipid domains	Passot et al. 2014
	L. bulgaricus CFL1 and *L. bulgaricus* ATCC 11842 whey-based culture media	Fluorescence anisotropy	Increased fluidity at 0 C° (DPH anisotropy 0.250 vs 0.280)	Meneghel et al. 2017
Proteins				
	Lc. lactis ssp. lactis (MM210 and FG2), *Lc. lactis ssp. cremoris* (MM160 and MM310): heat (HS) or cold (CS) shock	Addition of erythromycin in the growth medium	Requirement of stress-induced proteins for improving resistance to freezing	Broadbent and Lin 199)
	Lc. lactis (M474, M392) exposed to cold shock	DNA sequence analysis through PCR amplification and cloning	Presence of a gene encoding for cold-shock proteins	Kim and Dunn 1997
	L. plantarum NC8 mutants	Generation of mutant strain overproducing cold-shock proteins (CspL, CspP, and CspC)	Increased production of a cold-shock protein (CspP)	Derzelle et al. 2003
	L. acidophilus RD758 exposed to cold stress	Proteome analysis through 2D electrophoresis and MALDI-TOF	Upregulation of cold-shock proteins involved in carbohydrate and energy metabolisms and in pH homeostasis	Wang et al. 2005b
	L. bulgaricus CFL1 exposed to acid stress	Proteome analysis through 2D electrophoresis	Upregulation of 11 proteins and downregulation of 10 proteins	Streit et al. 2008
	L. bulgaricus CFL1 grown in MRS or whey-based culture media	SR-FTIR micro-spectroscopy of dried cells (1800 - 1300 region)	High content of alpha-helical proteins and low content of beta-sheet proteins	Passot et al. 2015
	L. bulgaricus CFL1 and *L. bulgaricus* ATCC 11842 whey-based culture media	FTIR micro-spectroscopy in aqueous conditions (1800 - 1300 cm^{-1} region)	Low content of alpha-helical proteins and high content of beta-sheet proteins	Meneghel et al. 2020
Cell wall components				
	L. bulgaricus CFL1 grown in MRS or whey-based culture media	SR-FTIR micro-spectroscopic measurement of dried cells (1300 – 900 cm^{-1} region)	Higher absorbance of PO_2^- groups (1253 - 1238 cm^{-1})	Passot et al. 2015
	L. bulgaricus CFL1 and *L. bulgaricus* ATCC 11842 whey-based culture media	FTIR micro-spectroscopic measurement in aqueous conditions (1360 -975 cm^{-1} region)	Lower absorbance of complex sugar rings (1076 - 1052 cm^{-1}) and PO_2^- groups (1222 - 1200 cm^{-1})	Meneghel et al. 2020

temperature (Ts) following cooling (Ts from 14 / 22 °C to -6 / -8 °C measured by FTIR spectroscopy) and to an increase of membrane fluidity at 0 C° (determined by fluorescence anisotropy) (Gautier et al. 2013; Passot et al. 2014; Meneghel et al. 2017). Consequently, when approaching ice nucleation, the membrane of freeze-resistant cells is in a more fluid and flexible state than the membrane of freeze-sensitive cells and thus better withstands the mechanical constraints following water escape from the cell and the resulting cell shrinkage caused by ice nucleation and ice crystals growth. However, minor modifications of the membrane fatty acids composition were observed in few studies (Béal et al. 2001; Wang et al. 2005d; Wang et al. 2011b), indicating that other cellular components and mechanisms are involved in LAB cryoresistance. Studies investigating the proteome of cryoresistant versus cryosensitive LAB populations, have also linked improved resistance to changes in protein synthesis (Kim and Dunn 1997; Derzelle et al. 2003; Wang et al. 2005b; Streit et al. 2008), and more specifically to the production of cold-shock proteins (Kim and Dunn 1997; Derzelle et al. 2003). These proteins are believed to improve cryoresistance by maintaining efficient transcription and translation under low positive temperatures (Wouters et al. 1999a; Derzelle et al. 2003; Keto-Timonen et al. 2016).
In more recent years, FTIR micro-spectroscopy has emerged as a powerful tool to assess biochemical changes in microorganisms caused by stress conditions (Al-Qadiri et al. 2008b; Al-Qadiri et al. 2008a; Lu et al. 2011; Saulou et al. 2013; Pénicaud et al. 2014; Passot et al. 2015). A study investigating the FTIR spectral features of dried samples of two *L. bulgaricus* CFL1 populations presenting different cryoresistance levels, revealed potential markers of cryoresistance related to cellular lipids, protein secondary structures, and cell wall components (Passot et al. 2015). To avoid potential bias induced by sample drying, Meneghel et al. (Meneghel et al. 2020), developed an FTIR micro-spectroscopic approach enabling the accurate exploitation of the entire mid-infrared region of bacterial cells in aqueous conditions. This was achieved using a custom-built sample chamber and a specifically developed water subtraction program, able to greatly reduce the spectral contribution of water.

In this study, we aimed to complete the work of Meneghel et al. (Meneghel et al. 2017; Meneghel et al. 2020) by applying the developed FTIR approach to obtain the biochemical composition of fresh and thawed samples of *L. bulgaricus* ATCC 11842, *L. bulgaricus* CFL1and *C. maltaromaticum* CNCM I-3298. The latter was included in this research because it is an extremely cryoresistant LAB reported to present no viability loss after 11 freeze-thaw cycles (Walker et al. 2006). Moreover, *C. maltaromaticum* was shown to maintain its cryoresistance despite changes in growth conditions (temperature, pH, and harvest time) (Girardeau et al. 2019). The membrane fatty acid composition, lipid membrane phase transition following freezing, membrane fluidity following cooling, and intracellular glass transition temperature were also measured to extend the range of markers of cryoresistance.

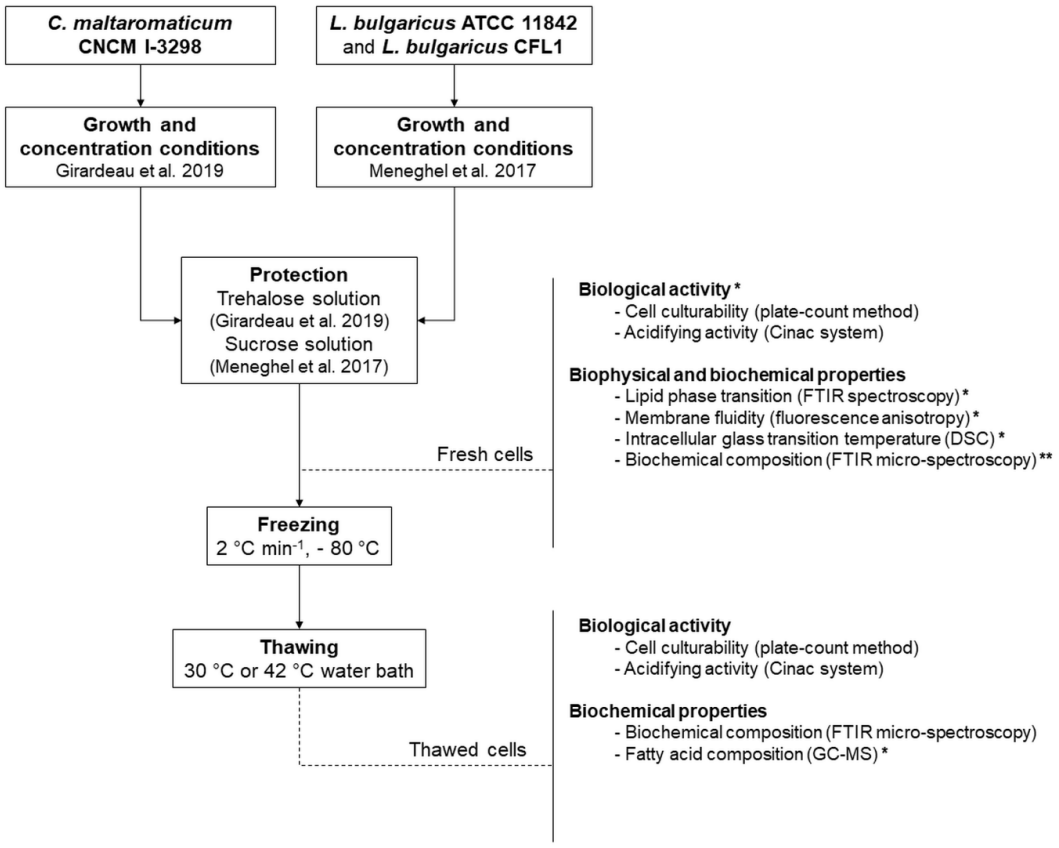

Figure III.3-1: *Diagram of the experimental approach used in this study and the main investigated parameters. The asterisks (*) and (**) indicate that the corresponding results for L. bulgaricus ATCC 11842 and L. bulgaricus CFL1 cells were taken from Meneghel et al. (2017) and Meneghel et al. (2020), respectively.*

III.3.4. Materials and Methods

The experimental approach and various methods used are shown in **Figure III.3-1**. Unless otherwise indicated, all measurements were performed on three independent bacterial cultures, for each strain. For the experimental methods followed by asterisks in Figure 1, the corresponding data for *L. bulgaricus* strains were taken from Meneghel et al. (2017 and 2020).

III.3.4.a. Bacterial strains, growth conditions, freezing and thawing protocols

Three strains of lactic acid bacteria were used in this study: *Carnobacterium maltaromaticum* CNCM I-3298 (Pasteur Institute, Paris, France), *Lactobacillus delbrueckii* subsp. *bulgaricus* CFL1 (CIRM-BIA; Rennes, France) and *Lactobacillus delbrueckii* subsp. *bulgaricus* ATCC 11842 (Manassas, VA, USA).
The *C. maltaromaticum* strain was cultivated and frozen according to the procedure described by Girardeau et al. (Girardeau et al. 2019), and the *L. bulgaricus* strains, according to the procedures described by Meneghel et al. (2017). After centrifugation (**Fig. III.3-1**), cell pellets of *C. maltaromaticum* and *L. bulgaricus* were re-suspended in a trehalose solution (20 % wt in saline water) at a weight ratio of 1:2 (1 g of cell pellet and 2 g of cryoprotective solution), or in a sucrose solution (20 % wt in saline water) at a weight ratio of 1:1, respectively. All cryopreserved bacterial concentrates were stored a minimum of 24 h at -80 °C. Thawing was carried out using a water bath set to 30 °C for *C. maltaromaticum* and 42 °C for the *L. bulgaricus* strains. Several freeze-thaw cycles were applied to better assess differences in biological activity recovery.
To determine a potential effect of the protective conditions applied that differed between *L bulgaricus* (Meneghel et al. 2017) and *C. maltaromaticum* (Girardeau et al. 2019), the biological activity recovery of *C. maltaromaticum* was also investigated for cell pellets re-suspended in a sucrose solution (20 % wt in saline water) at a weight ratio of 1:2 and 1:1 (cell pellet weight: protective solution weight).

III.3.4.b. Biological activity assessment of cell samples

(i) Culturability

Cell viability was measured using the agar plate count method. Fresh or thawed cell suspensions were diluted in saline water, then plated into an agar growth medium: Plate Count Agar (Biokar Diagnostics, Paris, France) for *C. maltaromaticum* and MRS Agar (Biokar Diagnostics, Paris, France) for the *L. bulgaricus* strains. Incubation was carried out at the strain's respective optimal temperatures for growth (30 °C for *C. maltaromaticum* and 42 °C for *L. bulgaricus*), for 48 h. The cell plate counts were expressed in $CFU.mL^{-1}$ and results were obtained in triplicate.
Culturability loss after each freezing cycle (FC) (in $log[CFU.mL^{-1}]$) was calculated using the following equation (Eq. III.3-1):

$$Culturability\ loss\ after\ the\ FC(i) = \log \frac{[CFU\ mL^{-1}]_{thawed\ cells\ after\ FC(i)}}{[CFU\ mL^{-1}]_{thawed\ cells\ after\ FC(i-1)}} \quad \text{(III.3-1)}$$

For the first freezing cycle (i=1), $[CFU.mL^{-1}]_{\text{thawed cells after FC(i-1)}}$ corresponds to the cell concentration in the fresh sample.

(ii) Acidifying activity

Acidifying activity measurements were carried out using the Cinac system (AMS; Frepillon, France) according to the procedure described by Girardeau et al. (Girardeau et al. 2019) for *C. maltaromaticum* cells and according to Meneghel et al. (Meneghel et al. 2017) for the *L. bulgaricus* cells. Briefly, flasks containing 150 mL of sterile culture medium were pre-warmed to the optimal temperature for growth of each of the studied strains. Following the inoculation of a flask with a precise volume of cryoprotected bacterial suspension (15 µL for *C. maltaromaticum* suspensions or 100 µL for *L. bulgaricus* suspensions), their pH was continuously monitored every 3 min until the end of acidification. Measurements were obtained in triplicate. The minimum of the first-order derivative of the acidifying curves represents the time required for the bacterial suspension to reach its maximum acidifying rate and was used as a discriminating descriptor between fresh and thawed cells within each strain (tm, in min). The higher the tm value was, the lower the acidifying activity was.

Acidifying activity (AA) loss after each freezing cycle (FC) (in min) was quantified as follows:

$$AA\ loss\ after\ FC(i) = tm_{thawed\ cells\ after\ FC(i)} - tm_{thawed\ cells\ after\ FC(i-1)} \quad \text{(III.3-2)}$$

For the first freezing cycle (i=1), $tm_{\text{thawed cells after FC(i-1)}}$ corresponds to the tm value of the fresh sample.

III.3.4.c. Characterization of the cytoplasmic membrane

(i) Membrane lipid extraction and gas chromatrography: fatty acid (FA) composition

Membrane fatty acid (FA) composition of *C. maltaromaticum* was determined on the cell pellets of thawed, washed bacterial samples, according to the method detailed by Meneghel et al. (Meneghel et al. 2017). Briefly, lipid extraction was performed using an accelerated solvent extractor (ASE 350, Dionex; Sunnyvale, CA, USA), using a chloroform/methanol-based extraction method. The obtained lipids were then mixed with a C9:0 internal standard (Sigma-Aldrich; St. Louis, MO, USA)

and methylated using trimethylsulfonium hydroxide (TMSH, Sigma-Aldrich; St. Louis, MO, USA). FA identification and quantification was carried out on a Hewlett-Packard 6890 gas chromatograph (GMI; Ramsey, MI, USA) coupled to a mass spectrometer (5973, Agilent Technologies; Avondale, PA, USA). Results were expressed as relative FA percentages.
Fatty acid compositions of the *L. bulgaricus* strains were recalculated from raw data available from Meneghel et al. (Meneghel et al. 2017).

(ii) Steady-state fluorescence anisotropy: membrane fluidity

Membrane fluidity of *C. maltaromaticum* was assessed by steady-state fluorescence anisotropy, using a 1,6-diphenyl-1,3,5-hexatriene (DPH) fluorescent probe. The method described by Meneghel et al. (Meneghel et al. 2017), with minor modifications, was applied. Stock solutions of DPH (6 mM, Sigma-Aldrich; St. Louis, MO, USA) were prepared in dimethylsulfoxide (DMSO, Sigma-Aldrich; St. Louis, MO, USA).
Briefly, 50 µL of cryoprotected bacterial sample were washed three times in MES – KOH buffer (50 mM, pH 5.5) supplemented with 10 mM glucose. The bacterial pellets obtained after three washes were diluted in 1mL of the same buffer to reach approximately 10^7 cells.mL^{-1}. Ten µL of DPH 6 mM, were added to 1 mL of cell suspension. Just before use, DPH solution was sonicated for 10 min at 20 Hz. After addition of the dye, the cell suspension was vortexed for 1 min, and incubated 3 min in darkness at 30 °C before centrifugation (14,000 × g for 90 sec). The pellet was re-suspended in 3 mL of a 25 % (w/w) of sucrose solution and loaded into a stirred quartz cuvette.
Steady-state fluorescence anisotropy (r) of *C. maltaromaticum* cells were measured in a photoluminescence spectrometer (FLS1000, Edinburgh Instruments, Serlabo Technologies, France). The excitation and emission wavelengths were respectively set at 360 and 430 nm. Polarizers were located on the excitation source and on the photomultiplier tube to measure anisotropy.
Anisotropy values were obtained at different sample temperatures ranging from 42 °C to 0 °C using a Peltier-based temperature-controlled cuvette holder (LFI-3751, Wavelength electronics; Bozeman, MT, USA and Luma 40, Quantum Northwest, WA, USA). Since the anisotropy values of *L. bulgaricus* strains (taken from Meneghel et al. (Meneghel et al. 2017)) were obtained on a different equipment (Fluorolog-3 spectrofluorometer, Jobin-Yvon Horiba), a control measurement was carried out on each *L. bulgaricus* strain using the same equipment and protocol than those used for *C. maltaromaticum*. The results were similar regardless of the equipment used.

(iii) FTIR spectroscopy measurements: membrane lipid phase transition

The membrane lipid phase transition of cells during freezing was studied using FTIR spectroscopy, by measuring the position of the symmetric CH_2 stretching vibration band ($\nu_s CH_2$) located around 2850 cm^{-1} and arising from the lipid acyl chains of the

cytoplasmic membrane. The peak position and shape of the O-H libration and bending combination band of water (νH_2O) located around 2200 cm^{-1} was simultaneously monitored to determine ice nucleation temperatures (Tn).
Measurements were carried out on a Nicolet Magna 750 FTIR spectrometer (Thermo Fisher Scientific; Madison, WI, USA) equipped with a variable temperature stage (Specac Ltd.; Orpington, Kent, UK), as described by Meneghel et al. (Meneghel et al. 2017). The optical bench was continuously purged with dry air (Balston; Haverhill, MA, USA) to remove the spectral contribution of water vapor.
Concentrated and protected bacterial samples of *C. maltaromaticum* were washed two times in saline water, re-suspended in a 25 % (w/w) sucrose solution for 15 min at room temperature, before being centrifuged at 16,100 × g for 5 min, according to the preparation applied by Meneghel et al. (Meneghel et al. 2017) for the *L. bulgaricus* samples. A small amount of the resulting cell pellet was tightly sandwiched between two calcium fluoride (CaF_2) windows (ISP Optics; Riga, Latvia). Temperature was decreased from 50 °C to -50 °C at a rate of 2 °C.min^{-1} by pouring liquid nitrogen into the cell holder. An accurately controlled cooling rate was insured by a thermocouple inserted as close as possible to the sample. Spectra acquisition was performed throughout cooling by the Omnic software (version 7.1, Thermo Fisher Scientific; Madison, WI, USA): 32 co-added scans were collected in the mid-IR region between 4000 and 900 cm^{-1}, every 45 s at a 4 cm^{-1} resolution. The lipid phase transition (Ts) values of the *L. bulgaricus* strains were taken from Meneghel et al. (2017), and their ν_sCH_2 values at the frozen state (-48°C) were obtained from the corresponding raw data.
Spectra analyses were performed using the ASpIR software (Infrared Spectra Acquisition and Processing, INRAE; Thiverval-Grignon, France): the peak positions of ν_sCH_2 and νH_2O in each spectrum were determined using their second-order derivatives. Second order derivatives were calculated and smoothed according to a seven-point Savitsky-Golay algorithm. The obtained peak frequencies were then plotted against the temperature at which they were measured.
The ν_sCH_2 plots arising from the *L. bulgaricus* samples were fitted with a curve based on an asymmetric sigmoid transition function and the first derivative was calculated. The maximum of the first derivative of the fitted curves was taken as the lipid membrane phase transition temperature (Ts, lipid solidification following freezing, in °C). In the case of *C. maltaromaticum* samples, plots were fitted with a curve based on a continuous piecewise function: a linear function for temperatures above Ts and a sum of linear and exponential functions for temperatures below Ts.

(iv) DSC measurements: intracellular glass transition temperature

The intracellular glass transition temperature (Tg'i, °C) was determined by differential scanning calorimetry DSC) as described previously (Clarke et al. 2013; Fonseca et al. 2016; Meneghel et al. 2017). A power compensation calorimeter (Diamond, Perkin Elmer LLC, Norwalk, CT, USA), equipped with a liquid nitrogen cooling accessory (CryoFill, Perkin Elmer) was used. Cell pellets of *C.*

maltaromaticum obtained after harvest were washed three times with peptone water (1 $g.L^{-1}$). About 20–50 mg of a washed cell pellet obtained by centrifugation (14,000 × g for 3 min) was scanned following cooling to -100°C and heating to 20°C at 10 °C.min^{-1} with an acquisition rate of 5 points per second (Pyris software 13.1, Perkin Elmer). Cell concentrations were typically 10^8–10^{10} cells per mL. An empty pan was used as a reference. Temperature calibration was performed using cyclohexane (crystal-crystal transition at −87.1 °C) and mercury (melting point at −38.6 °C).

Additionally, the washed cell pellet with peptone water was resuspended in a sucrose cryoprotective solution (20 % in saline water), incubated for 30 min and then centrifuged. The resulting sucrose protected *C. maltaromaticum* pellet was also analysed to enable the comparison with *L. bulgaricus* results (Meneghel et al. 2017).

The first derivative of the heat flow curve recorded during the warming step was calculated and smoothed (50 points smoothing). The glass transition temperature of the intracellular content (Tg'i) was calculated as the maximal value of the peak observed in the first derivative curve. The values of intracellular temperatures of the *L. bulgaricus* strains as well as the value of the extracellular glass transition temperature (Tg'e, °C) (protective sucrose solution) were taken from Meneghel et al. (2017).

(v) FTIR micro-spectroscopy: biochemical characterization of cells before freezing and after freeze-thawing, in aqueous conditions

The biochemical characteristics of *C. maltaromaticum* samples in aqueous environment were measured using a FTIR microscope (Nicolet iN10, Thermo Fisher Scientific, Madison, WI, USA) associated with a demountable micro-chamber of CaF_2 windows (Hellma Analytics, Paris, France), according to the method recently published and described in more detail by Meneghel et al. (Meneghel et al. 2020)

Briefly: fresh and thawed cryoprotected cell suspensions were washed three times in saline water, then centrifuged at 16,100 × g for 5 min. A very small amount (less than one microliter, or the tip of a 200 µL pipette cone) of the resulting pellet was deposited on one side of the micro-chamber, separated from the diluent side (containing saline water) by a 2.5 µm thick strip of Mylar® film (Goodfellow; Lille, France).

Spectra acquisition was performed using the Omnic software (version 8.1; Thermo Fisher Scientific; Madison, WI, USA) with apertures set at 50 x 50 µm. A background spectrum was acquired in an air bubble on the diluent side of the micro-chamber and spectra on multiple areas of both the diluent and the cell sample were measured. Each spectrum was obtained from 128 co-added scans in the mid-IR region between 4000 and 900 cm^{-1} at a 4 cm^{-1} resolution. The spectra of the *L. bulgaricus* strains were acquired during the PhD project of Julie Meneghel and results obtained from fresh samples were previously published (Meneghel et al. 2020).

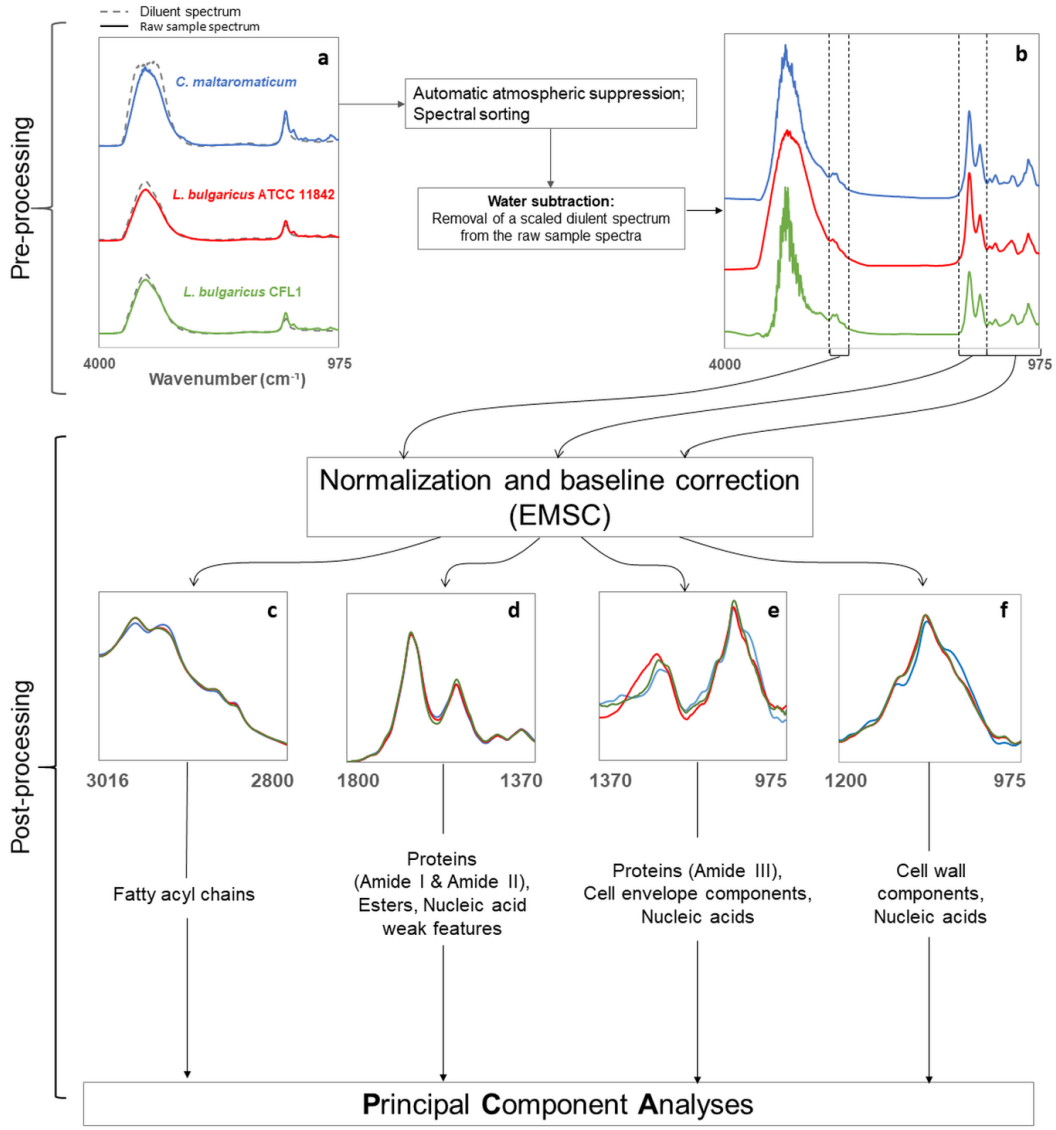

Figure III.3-2: *Illustration of the spectral data processing steps: pre-processing of (**a**) raw FTIR spectra of C. maltaromaticum CNCM I-3298 (blue), L. bulgaricus ATCC 11842 (red) and L. bulgaricus CFL1 (green), to obtain (**b**) sample spectra after atmospheric suppression and water subtraction; and post-processing of resulting spectra including normalization and baseline correction (EMSC: extended multiplicative scatter correction) of four spectral regions (**c, d, e, f**) and further principal component analysis (PCA).*

An illustration of the subsequent spectral processing steps is presented in **Figure III.3-2**. Spectral pre-processing (**Fig. III.3-2a** and **Fig. III.3-2b**) was carried out in part using the Omnic software, for automatic atmospheric correction and spectra sorting. A specifically developed program implemented in Matlab (TheMathWorks Inc., Natick, MA, version 2014a, 8.3.0.532) was used for water subtraction. This program involves removing an optimized scaled diluent spectrum to the sample spectra. The scaling factor is determined by an algorithm designed to obtain spectra presenting a similar Amide I/II area ratio to those of dried cells. The Amide I/II area ratios of strains in the dry state were 2.17 for *L. bulgaricus* CFL1, 2.34 for *L. bulgaricus* ATCC 11842 (Meneghel et al. (Meneghel et al. 2020)) and 2.33 for *Carnobacterium maltaromaticum* CNCM I-3298 (this work). A more detailed description of this water subtraction procedure is presented in Meneghel et al. (Meneghel et al. 2020).

Post-processing of the water subtracted spectra was done using the Unscrambler® X software package (version 10.2, Camo Software AS; Olso, Norway). In total, 188, 199 and 188 water-subtracted infra-red spectra of fresh and thawed cells from three biological replicates were analyzed for *C. maltaromaticum* CNCM I-3298, *L. bulgaricus* ATCC 11842 and *L. bulgaricus* CFL1 cells, respectively.

Analyses were carried out on three main distinct spectral regions: (i) the 3016 – 2800 cm^{-1} region containing information on fatty acyl chains of the bacterial membrane (**Fig. III.3-2c**); (ii) the 1800 – 1370 cm^{-1} region notably containing the Amide I and II bands, the most prominent vibrational bands of the cell proteins backbone (**Fig. III.3-2d**); (iii) the 1370 – 975 cm^{-1} region, containing information on protein, nucleic acids and cell wall components (phosphorylated molecules and polysaccharides) (**Fig. III.3-2e**). A sub-region of (iii), the 1200 – 1000 cm^{-1} region containing information on cell wall components and nucleic acids (PO_2^- groups and sugar rings) was also analysed (**Fig. III.3-2f**). Normalization and baseline corrections were performed in each region using an extended multiplicative scatter correction (EMSC).

Resulting spectra were then analyzed by Principal Component Analysis (PCA), to reveal data variance (score plots) and peak positions of interest (loading plots). The assignment of principal absorption bands was done using data from literature (see **Annex A-III.3, Table III.3-A1**).

To confirm spectral bands evidenced by the loading plots in the 1800 – 1370 cm^{-1} and 1200 – 1000 cm^{-1} regions, the normalized and averaged spectra of the three lactic acid bacteria before and after freeze-thawing were calculated, and the second-order derivatives were processed using a Savitzky-Golay algorithm (third-degree polynomial and a 9-point smoothing factor).

To visualize the components of the Amide I band (1700 – 1600 cm^{-1}) that provide information on the secondary structure of proteins: α-helix and β-sheet bands, respectively found at ~1654 and ~1637 cm^{-1}, normalization and baseline corrections were performed in the Amide I region (1700 – 1600 cm^{-1}) using an extended multiplicative scatter correction (EMSC).

Then, the second derivatives of the spectra were calculated using a Savitzky-Golay algorithm (third-degree polynomial and a 9-point smoothing factor). The height ratios between the α-helix band peak at approximately 1654 cm^{-1} (I_{1654}) and the β-sheet band peak at approximately 1637 cm^{-1} (I_{1637}) in the second derivative spectra ($I_{1654}/1_{1637}$) were calculated and used as a measure for secondary protein structure changes between fresh and thawed cells.

III.3.4.d. Statistical analysis

The nonparametric Kruskal-Wallis and the post-hoc Conover Iman tests were performed using XLSTAT 19.6 (Addinsoft, Paris, France), to compare data concerning biological activity, fatty acid composition, fluorescence anisotropy, dynamic FTIR spectroscopy, DSC measurements, and $I_{1654}/1_{1638}$ ratio. A significance level of 95 % ($p < 0.05$) was considered.

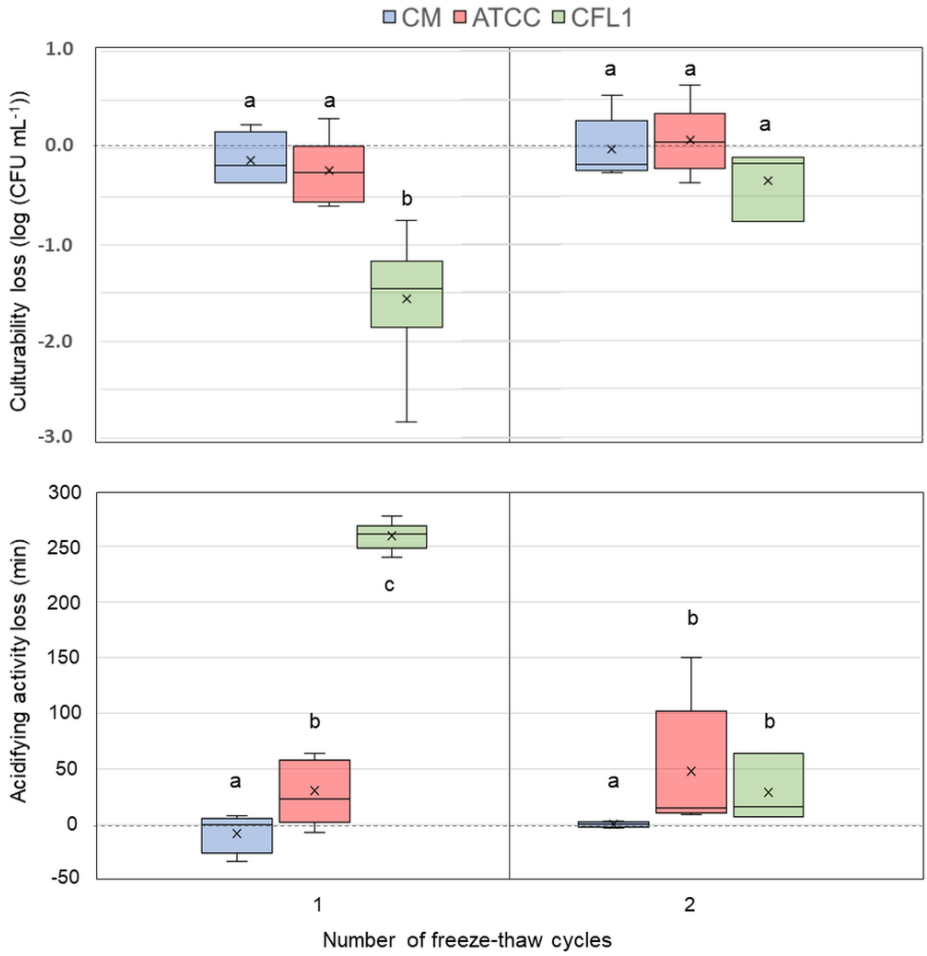

Figure III.3-3: *Biological activity loss (culturability loss determined by plate counts method and acidifying activity loss determined with the Cinac system, median values) of* C. maltaromaticum *CNCM I-3298 (CM),* L. bulgaricus *ATCC 11842 (ATCC) and* L. bulgaricus *CFL1 (CFL1) cells following two freeze-thaw cycles. Letters (a, b, c) represent statistical differences between samples at a 95 % confidence level.*

III.3.5. Results

Cultivability and acidifying activity losses in response to freezing

The loss in culturability and acidifying activity of all three strains after a first and a second freeze-thaw cycle is presented in **Figure III.3-3**. Results for up to seven freeze-thaw cycles are reported in supplementary material (see **Annex Table III.3-A2)**.
The highest losses in both culturability and acidifying activity after the first freeze-thaw cycle was measured in *L. bulgaricus* CFL1 (CFL1): -1.46 log units in culturability and +261 min (4.35 h) in acidifying time. *L. bulgaricus* ATCC 11842 (ATCC) showed no significant loss of culturability after the first or the second freeze-thaw cycles, similarly to *C. maltaromaticum* (CM). However, *L. bulgaricus* ATCC 11842 did show loss of acidifying activity after both the first (+23 min) and the second (+15 min) freeze-thaw cycles, while *C. maltaromaticum* did not. After 4 freezing cycles, the cumulative losses in culturability and in acidifying activity for the three strains were the following: 3 log units and 366 min for *L. bulgaricus* CFL1; 0.6 log units and 94 min for *L. bulgaricus* ATCC 11842; and 0 log unit and 14 min for *C. maltaromaticum*. *C. maltaromaticum* showed no significant loss of culturability or acidifying activity for up to 7 freeze-thaw cycles (see **Annex A-III.3, Table III.3-A2**), thus confirming *C. maltaromaticum* CNCM I-3298's exceptional cryoresistance.

Among the three studied strains, *C. maltaromaticum* therefore presented the highest cryoresistance, *L. bulgaricus* CFL1, the lowest cryoresistance and *L. bulgaricus* ATCC 11842 intermediate cryoresistance.
The cultivability and acidifying activity losses of *C. maltaromaticum* cells presented above were initially measured in cells frozen in a trehalose-based cryoprotective solution (20 % (wt/wt) in saline water) at a ratio of 1:2, while the *L. bulgaricus* cells were cryoprotected in a sucrose-based solution (20 % (wt/wt) in saline water) at a ratio of 1:1. The cryoresistance of *C. maltaromaticum* cells frozen in a sucrose-based (20 % (wt/wt) in saline water) and trehalose-based (20 % (wt/wt) in saline water) at a ratio of 1:1 were also tested.

Results showed no statistically significant loss of either culturability or acidifying activity, regardless the protective conditions (see **Annex A-III.3, Table III.3-A3**). The freeze-thaw behaviour of *C. maltaromaticum* seemed no to be influenced by the nature and the concentration of the disaccharides used as cryoprotective agent, within the tested range of conditions.

Cytoplasmic membrane properties

Fatty acid composition of the lipid membrane

The fatty acid compositions of the studied strains are presented in **Table III.3-2**. *C. maltaromaticum* CNCM I-3298 lipid membranes are mainly composed of oleic acid (C18:1), accounting for over 80 % of their total fatty acid content. Such a high percentage of C18:1 leads to *C. maltaromaticum* presenting the highest content of long chain fatty acids (87 %) and highest unsaturated to saturate fatty acid ratio (UFA/SFA = 5.60) among the three strains. *L. bulgaricus* ATCC 11842 and *L. bulgaricus* CFL1 lipid membranes are composed of four main types of fatty acids (C14:0, C16:0, C16:1 and C18:1), accounting for over 80 % of their total fatty acid composition.

Table III.3-2: *Membrane fatty acid composition (relative percentages) of* C. maltaromaticum *CNCM I-3298,* L. bulgaricus *ATCC 11842 and* L. bulgaricus *CFL1 and cells. Values for* L. bulgaricus *ATCC 11842 and* L. bulgaricus *CFL1 were recalculated from raw data available from Meneghel et al. (2017).*

Fatty acids (%)	*C. maltaromaticum* CNCM I-3298	*L. bulgaricus* ATCC 11842	*L. bulgaricus* CFL1
C12:0	0.3 ^{c}	3.3 ^{a}	1.9 ^{b}
C14:0	1.9 ^{c}	6.9 ^{b}	10.3 ^{a}
C15:0	0.2 ^{b}	0.8 ^{a}	0.7 ^{a}
C16:0	10.7 ^{c}	25.4 ^{b}	36.7 ^{a}
C16:1	0.2 ^{b}	23.8 ^{a}	22.2 ^{a}
C17:0	0.15 ^{b}	0.3 ^{a}	0.1 ^{b}
C18:0	1.6 ^{b}	6.2 ^{a}	7.0 ^{a}
C18:1	82.8 ^{a}	26.2 ^{b}	15.9 ^{c}
C18:2	0.0 ^{c}	2.0 ^{a}	1.5 ^{b}
C19cyc	0.0 ^{c}	4.6 ^{a}	3.1 ^{b}
C20:0	0.0 ^{b}	0.2 ^{a}	0.1 ^{a}
C18:2 conj	1.8 ^{a}	0.1 ^{b}	0 ^{c}
C22:0	0.3 ^{b}	0.3 ^{b}	0.5 ^{a}
Total SFA*	15.2 ^{c}	43.4 ^{b}	57.2 ^{a}
Total UFA**	84.9 ^{a}	50.2 ^{b}	38 ^{c}
UFA/SFA	5.6 ^{a}	1.2 ^{b}	0.7 ^{c}
Total long chain FA***	86.7 ^{a}	39.8 ^{b}	28.3 ^{c}

Data presented are means of at least three independent replicates
Superscript letters (a, b, c) represent statistical differences for each fatty acid between strains at the 95 % confidence level.
SFA: Saturated Fatty Acids; UFA: Unsaturated Fatty Acids
* Totals include fatty acids not shown in the table, representing less than 1 % of total FA
** Total UFA does not comprise C19:0cyc
*** Long chain FA comprise fatty acids made up of 18 carbon atoms or more

The higher percentage of C18:1 in *L. bulgaricus* ATCC 11842 (26 %) compared to *L. bulgaricus* CFL1 (16 %) also results in a higher UFA/SFA ratio in *L. bulgaricus* ATCC 11842 versus *L. bulgaricus* CFL1 (1.2 *vs* 0.7). *L. bulgaricus* CFL1, the most cryosensitive strain, showed the lowest relative content of UFA among the studied strains.

Membrane fluidity during cooling

The evolution of membrane fluidity for the three bacterial strains in a 25 % sucrose solution as a function of temperature is presented in **Figure III.3-4**. Fluorescence anisotropy is inversely proportional to membrane fluidity: the higher the anisotropy (r) is, the more rigid the membrane is. Regardless of the strain, decreasing temperature from 35 °C to 0 °C resulted in increasing fluorescence anisotropy and thus in membrane rigidification. From 25 °C downwards, *L. bulgaricus* CFL1 cells (CFL1, in green) exhibited higher anisotropy values (lower membrane fluidity) than *L. bulgaricus* ATCC 11842 (ATCC, in red) and *C. maltaromaticum* (CM, in blue) cells, while the latter two exhibited similar anisotropy values at all temperatures above 5 °C. At 0 °C, *C. maltaromaticum* cells presented the lowest anisotropy (and highest membrane fluidity) (0.209), followed by *L. bulgaricus* ATCC 11842 (0.239) and then *L. bulgaricus* CFL1 (0.273).

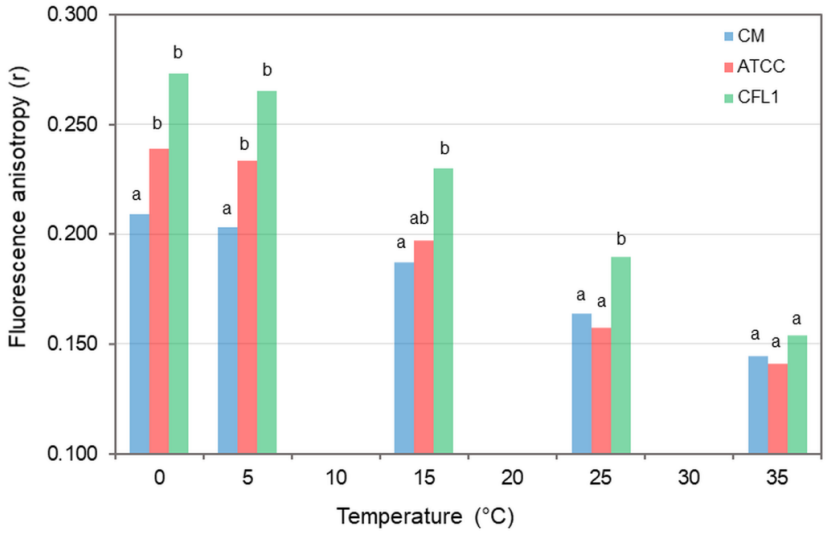

Figure III.3-4*: Membrane fluorescence anisotropy (median values) upon cooling of* C. maltaromaticum *CNCM I-3298 (CM, blue bars),* L. bulgaricus *ATCC 11842 (ATCC, red bars) and* L. bulgaricus *CFL1 (CFL1, green bars) cells suspended in a 25% sucrose solution. Letters (a, b) represent statistical differences between samples at a 95 % confidence level.*

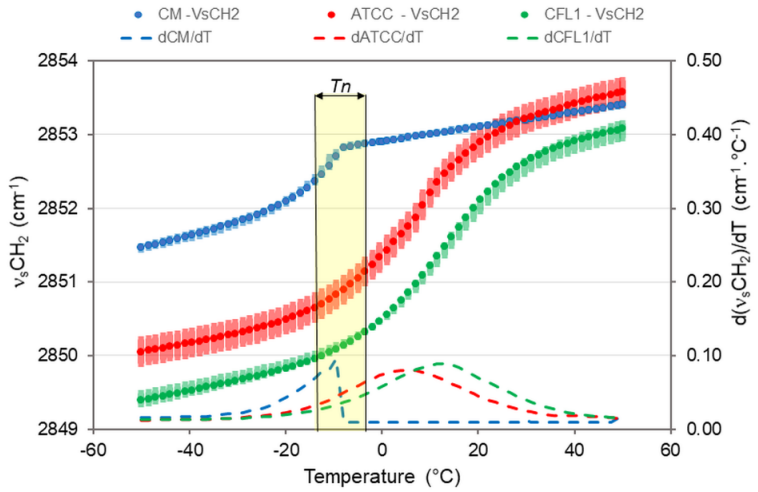

Figure III.3-5: *Peak positions of the symmetric CH_2 stretching vibration band (ν_sCH_2) arising from* C. maltaromaticum *CNCM I-3298 (CM, blue circles),* L. bulgaricus *ATCC 11842 (ATCC, red circles) and* L. bulgaricus *CFl1 (CFL1, green circles) upon cooling of fresh cells suspended in a 25 % sucrose solution. Data points correspond to the medians of three replicates for each strain and the error bars to the associated interquartile ranges. The temperature range of water nucleation (Tn) is highlighted. Dotted curves indicate the first derivatives of the symmetric CH_2 stretching vibration band (ν_sCH_2), and the maximum of each curve corresponds to the lipid transition temperature Ts reported in Table III.3-3 for each microorganism.*

Table III.3-3: *Main parameters characterizing membrane lipid phase transition of C. maltaromaticum CNCM I-3298, L. bulgaricus ATCC 11842 and L. bulgaricus CFL1 cells obtained by monitoring the peak position of ν_sCH_2 around 2850 cm^{-1} (Ts and ν_sCH_2) and the upshift of the vibration water band from approx. 2100 to 2220 cm^{-1} during cooling (Tn) (**Fig. III.3-5**)*

	C. maltaromaticum CNCM I-3298	*L. bulgaricus* ATCC 11842	*L. bulgaricus* CFL1
Ts (°C)	-8.1 [a]	5.6 [b]	13.6 [c]
Tn (°C)	-9.6 [a]	-13.6 [a]	-10.2 [a]
ν_sCH_2 at Tn (cm^{-1})	2852.8 [a]	2850.7 [b]	2850.1 [c]
ν_sCH_2 at -48°C (cm^{-1})	2851.5 [a]	2850.1 [b]	2849.4 [c]

Data presented are medians of three independent replicates for each strain
Superscript letters (a, b, c) represent statistical differences, for each parameter, between strains at the 95 % confidence level
Ts: lipid membrane phase transition temperature during cooling
Tn: water nucleation temperature

Membrane lipid phase transition during freezing, assessed by FTIR spectroscopy.

Figure III.3-5 displays the evolution of the $\nu_s CH_2$ peak positions following cooling from 50 °C to -50 °C for all three strains, in a 25 % sucrose solution. Decreasing temperatures resulted in a shift of $\nu_s CH_2$ peak positions to lower wavenumbers. This reflects the lipid membrane's phase transition from a disordered fluid state, referred to as the liquid crystalline phase, to an ordered rigid state, referred to as the gel phase (Wolkers and Oldenhof 2015). The first derivative of the $\nu_s CH_2$ curve as a function of temperature was plotted to determine the lipid membrane phase transition temperature during cooling (Ts). The νH_2O peak positions were simultaneously monitored during cooling to determine, for each sample, the temperature of ice nucleation (Tn) as the upshift of the combination water band from approx. 2100 to 2220 cm^{-1} (the data is not shown on Fig. 6, for sake of clarity). The main results derived from these measurements are presented in **Table III.3-3**. *C. maltaromaticum* cells exhibited the lowest Ts values (-8.1 °C), followed by *L. bulgaricus* ATCC 11842 (5.6 °C) and then *L. bulgaricus* CFL1 (13.6 °C). At Tn, the $\nu_s CH_2$ frequencies exhibited by *C. maltaromaticum*, *L. bulgaricus* ATCC 11842 and *L. bulgaricus* CFL1 were 2852.8 cm^{-1}, 2850.7 cm^{-1} and 2850.1 cm^{-1}, respectively. This suggests that when ice formation begins, the lipid membrane of *C. maltaromaticum* cells still exhibits a high degree of disorganization and fluidity, whereas the lipid membranes of the other two strains have already transitioned into the gel phase. Regardless of temperature, and especially in the frozen state (temperatures below Tn), *L. bulgaricus* CFL1 cells showed the lowest $\nu_s CH_2$ frequencies (i.e. highest degree of acyl chain organization) among the three strains. The differences in the lipid organization observed among strains at Tn were the same at the frozen state (-48°C)

<u>Intracellular glass transition temperature</u>

Intracellular glass transition temperature measurements of washed cells revealed no significant differences (p <0.05) between the *L. bulgaricus* strains: a median value of -19.3 °C for *L. bulgaricus* ATCC 11842 and of -17.9 °C for *L. bulgaricus* CFL1. The intracellular glass transition temperature of washed *C. maltaromaticum* cells was significantly higher than the other two strains, with a median value of -15.2 °C. However, adding the cryoprotective solution (20 % sucrose in saline water) led to a Tg'i decrease in all three strains, down to not significantly different median values (p < 0.05) for *C. maltaromaticum* (-26.6 °C), *L. bulgaricus* ATCC 11842 (-26.4 °C) and *L. bulgaricus* CFL1 (-27.0 °C).

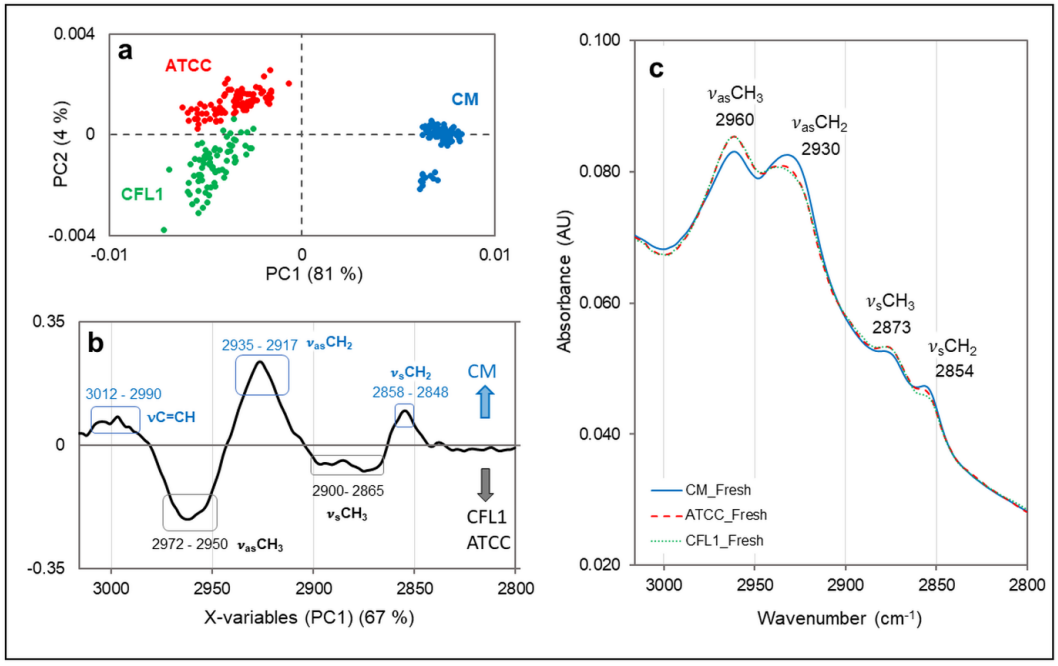

Figure III.3-6 : *Principal component analysis (PCA) of FTIR spectra of fresh* C. maltaromaticum *CNCM I-3298 (CM, blue circles),* L. bulgaricus *ATCC 11842 (ATCC, red circles)* and L. bulgaricus *CFL1 (CFL1, green circles) cells in an aqueous environment, in the 3016 cm^{-1} to 2800 cm^{-1} range:* ***a*** *PC1 versus PC2 score plots explaining 81 % and 4 % of the variance, respectively.* ***b*** *Loading plot of PC1, separating CM from ATCC and CFL1: positive peaks in PC1 characterized* C. maltaromaticum*, whereas negative peaks characterized L. bulgaricus ATCC and CFL1 cells* ***c*** *Mean FTIR spectra of fresh cells used for the PCA. The characteristic absorption bands arising from fatty acid chains are indicated.*

Differences in biochemical compositions on fresh and freeze-thawed cells, assessed by FTIR micro-spectroscopy

The 3016 – 2800 cm^{-1} spectral region.

PCA was performed on normalized water subtracted spectra of fresh cells in the 3016 – 2800 cm^{-1} range. The PC1 versus PC2 score plot, the corresponding PC1 loading plot and the averaged spectra of each strain are reported in **Figures III.3-6a, 6b** and **6c,** respectively.

PCA score plots separated the *C. maltaromaticum* CNCM I-3298 (CM) cluster from the *L. bulgaricus* ATCC 11842 and CFL1 clusters according to PC1 (81% of total variance) and the *L. bulgaricus* ATCC 11842 cluster from the *L. bulgaricus* CFL1 cluster according to PC2 (4 % of total variance). The loading plot of PC1 (**Fig. III.3-6b**) indicates that *C. maltaromaticum* (CM) cells are correlated to CH_2 vibration bands ($\nu_{as}CH_2$ (2935 – 2917cm^{-1}) and ν_sCH_2 (2858 – 2848 cm^{-1})) and C=CH vibration bands (3010 – 2990), while the *L. bulgaricus* cells (ATCC and CFL1) are correlated to CH_3 vibration bands ($\nu_{as}CH_3$ (2972 – 2950cm^{-1}) and ν_sCH_3 (2900 – 2865 cm^{-1})). This can also be seen in the averaged spectra (**Fig. III.3-6c**), where *C. maltaromaticum* cells present a higher absorbance in CH_2 vibration bands (2854 cm^{-1}, 2930 cm^{-1}) and lower absorbance in CH_3 vibration bands (2873 cm^{-1}, 2960 cm^{-1}) than the *L. bulgaricus* strains.

The averaged spectra, in accordance with the information presented by the loading plot of PC2 (see **Annex A-III.3, Fig. III.3-A1**), also show that *L. bulgaricus* ATCC 11842 cells exhibit a higher absorbance in the ν_sCH_2 (2860-2854 cm^{-1}) vibration band than *L. bulgaricus* CFL1 cells.

PCA was also performed by combining the spectra acquired on fresh and thawed samples of the three bacteria (see **Annex A-III.3, Fig. III.3-A2a** and **A2b**). The PC1 versus PC2 and PC1 versus PC3 score plots revealed a separation between the fresh and the thawed samples of L. bulgaricus strains, whereas no differentiation was observed for C. maltaromaticum. We observed a shift of the L. bulgaricus (ATCC and CFL1) thawed samples to positive direction of PC1 and PC2, and an increased dispersion within the bacterial spectra. Freezing and thawing processes would therefore induce a disorganization of the lipid membrane of L. bulgaricus strains.

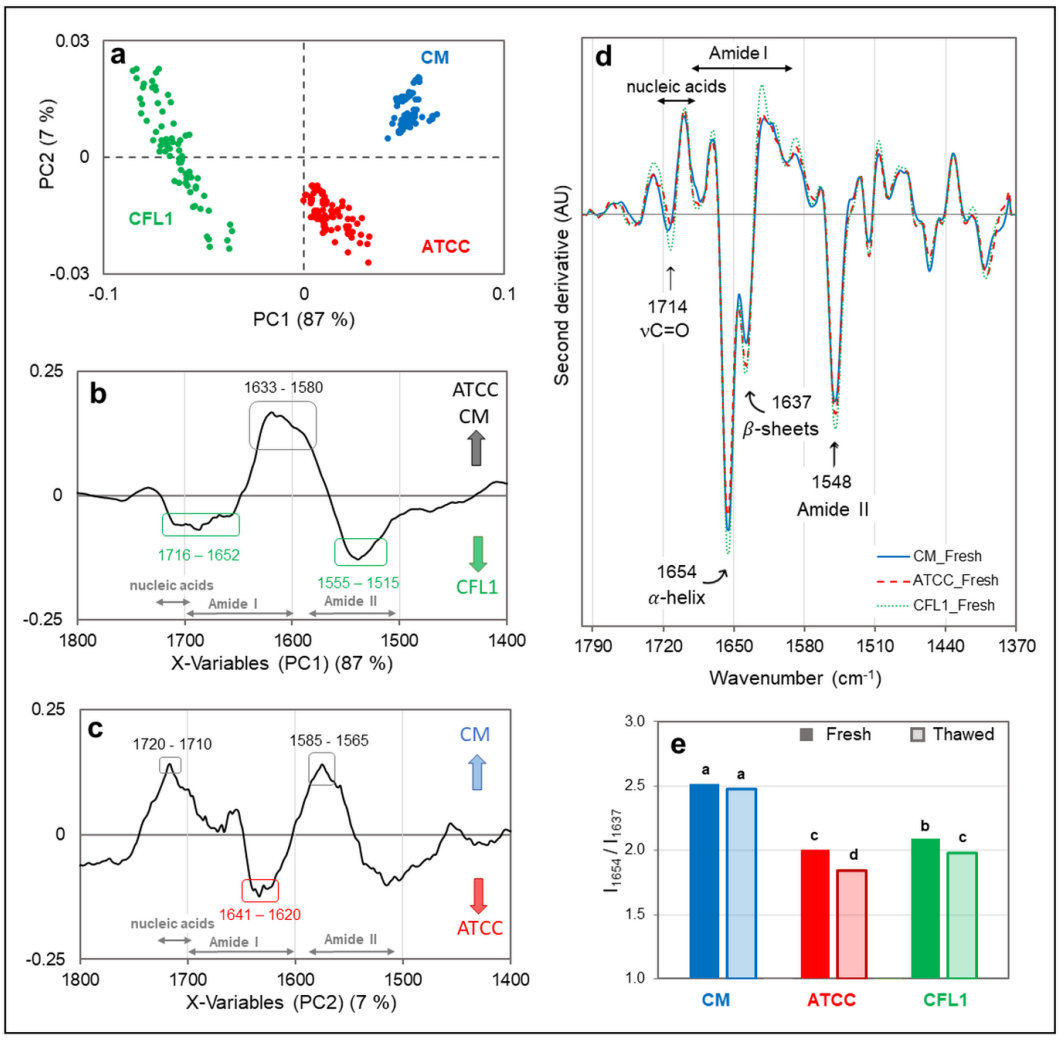

Figure III.3-7: *Principal component analysis (PCA) of FTIR spectra of fresh* C. maltaromaticum *(CM, blue circles),* L. bulgaricus *ATCC 11842 (ATCC, red circles) and* L. bulgaricus *CFL1 (CFL1, green circles) cells in an aqueous environment, in the 1800 cm^{-1} to 1370 cm^{-1} range:* ***a*** *PC1 versus PC2 score plots explaining 87 % and 7 % of the variance, respectively.* ***b, c*** *Loading plots of the PC1 and PC2 axis, respectively. Positive peaks in PC1 characterized C. maltaromaticum and L. bulgaricus ATCC 11842 cells, whereas negative peaks characterized L. bulgaricus CFL1 cells. Positive peaks in PC2 characterized C. maltaromaticum cells, whereas negative peaks characterized L. bulgaricus ATCC 11842.* ***d*** *Mean second derivatives of the FTIR spectra of fresh cells used for the PCA. The characteristic absorption bands arising from esters and nucleic acids, protein secondary structures (α-helix, β-sheets) and Amide II are indicated.* ***e*** *Mean ratios of the α-helix and β-sheets band intensities at respectively 1654 cm^{-1} and 1637 cm^{-1} of the derived spectra measured in fresh (dark bars) and thawed (light bars) cells. Letters (a, b, c, d) represent statistical differences between samples at a 95 % confidence level.*

The 1800 – 1370 cm^{-1} region.

PCA was performed on normalized, water subtracted spectra of fresh cells in the 1800 – 1370 cm^{-1} range. The PC1 versus PC2 score plot and corresponding PC1 and PC2 loading plots are presented in **Figures III.3-7a, 7b** and **7c** respectively.

PCA separated the *C. maltaromaticum* CNCM I-3298 (CM) cluster from the *L. bulgaricus* CFL1 (CFL1) cluster according to PC1 (87 % of total variance) and from the *L. bulgaricus* ATCC 11842 (ATCC) cluster according to PC2 (7 % of total variance). The loading plots of PC1 and PC2 (**Fig. III.3-7b** and **7c**) indicate that cluster discrimination was linked to nucleic acids, Amide I band components and the Amide II band. Furthermore, the fresh samples of *L. bulgaricus* CFL1 exhibited the highest sample's dispersion along PC2 axis. The potential damaging effect of freezing on protein was investigated by performing PCA using the spectra acquired on fresh and thawed samples of the three bacteria (see **Annex A-III.3, Fig III.3-A3**). The thawed samples of *L. bulgaricus* strains were slightly shifted from the fresh samples to negative direction of PC2 (see **Annex A-III.3, Fig III.3-A3a**, PC1 versus PC2 score plot). The shift appeared more pronounced for *L. bulgaricus* ATCC 11842 than *L. bulgaricus* CFL1. No separation between the fresh and the frozen samples was observed for *C. maltaromaticum*. The major contribution to spectral variation between fresh and frozen samples of *L. bulgaricus* strains arose from the following bands: 1637 cm^{-1}, corresponding to the β-sheet components of the Amide I bands, and 1753 cm^{-1} (C=O vibrations of esters) (see **Annex A-III.3, Fig. III.3-A3c** and **Fig. A3d**).

To further analyze the secondary structure of proteins, the second derivative of the averaged spectra were plotted (**Fig. III.3-7d**) and the ratios of α-helix band intensity at 1654 cm^{-1} over those of β-sheet band intensity at 1637 cm^{-1} (I_{1654}/I_{1637}) were calculated for fresh and thawed cells of each strain. Results are presented in **Figure III.3-7e**.

When comparing the averaged I_{1654}/I_{1637} ratios measured in fresh cells, *C. maltaromaticum* (CM) cells showed the highest ratio (2.52) among the strains (i.e. the highest content of proteins presenting α-helical structures over β-sheet structures), whereas *L. bulgaricus* ATCC 11842 (ATCC) cells showed the lowest ratio (2.01).
When comparing the average ratios measured between fresh and thawed cells of each strain, *L. bulgaricus* CFL1 cells (the least cryoresistant strain) (CFL1) presented the most significant difference in ratio, followed by *L. bulgaricus* ATCC 11842 cells. *C. maltaromaticum*, the most cryoresistant strain, did not present a significant difference in I_{1654}/I_{1637} ratio between fresh and thawed cells.

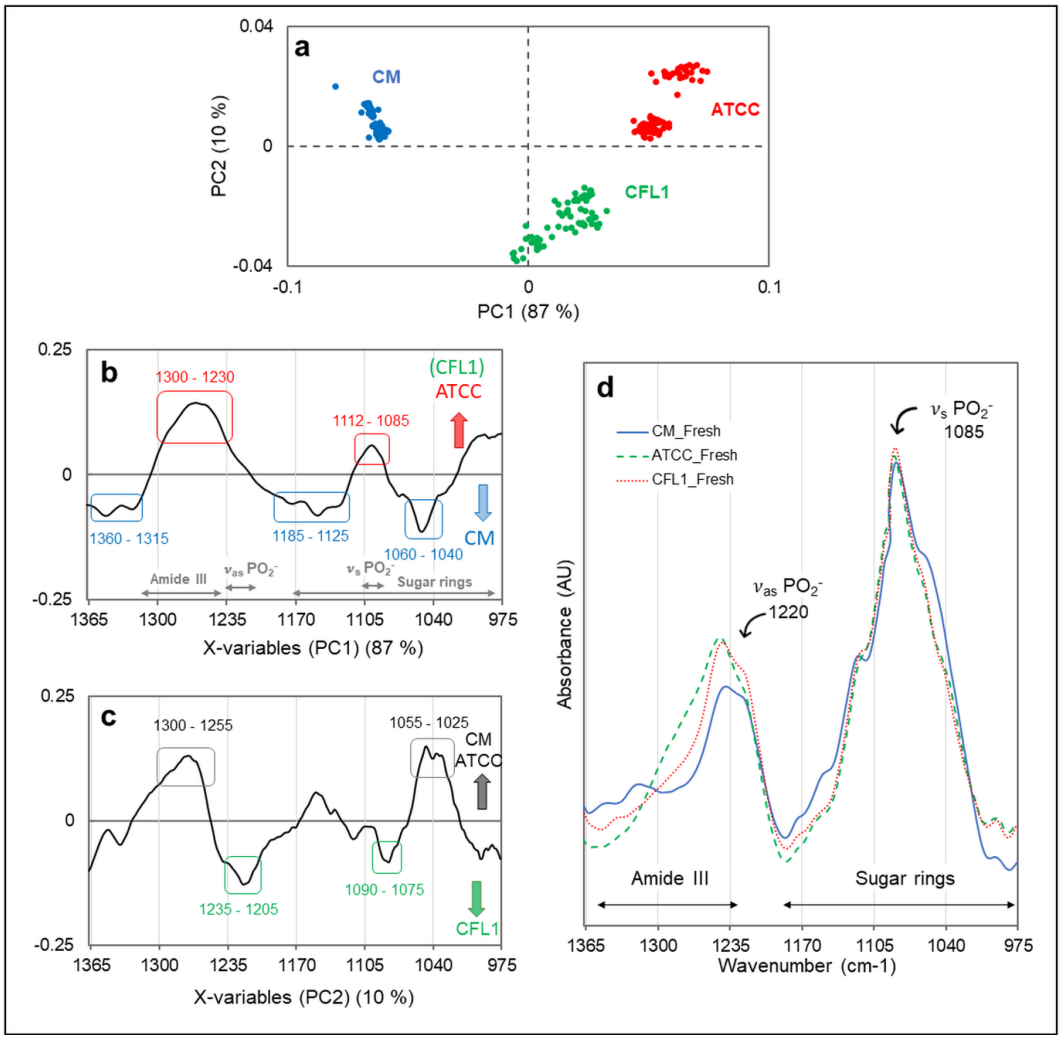

Figure III.3-8 : *Principal component analysis (PCA) of FTIR spectra of fresh* C. maltaromaticum *CNCM I-3298 (CM, blue circles),* L. bulgaricus *ATCC 11842 (ATCC, red circles) and* L. bulgaricus *CFL1 (CFL1, green circles) cells in an aqueous environment, in the 1367 cm^{-1} to 975 cm^{-1} range:* ***a*** *PC1 versus PC2 score plots explaining 87 % and 10 % of variance, respectively.* ***b, c*** *Loading plots of the PC1 and PC2 axis, respectively. Positive peaks in PC1 characterized L. bulgaricus ATCC 11842 and CFL1 cells, whereas negative peaks characterized C. maltaromaticum cells. Positive peaks in PC2 characterized C. maltaromaticum and L. bulgaricus ATCC 11842 and CFL1 cells, whereas negative peaks characterized L. bulgaricus CFL1 cells.* ***d*** *Mean FTIR spectra of fresh cells used for the PCA. The Amide III region and the characteristic absorption bands of PO_2^- , as well as the sugar rings region are indicated.*

The 1370 – 975 cm^{-1} region.

PCA was performed on normalized, water subtracted spectra of fresh cells in the 1370 – 975 cm^{-1} range. The PC1 versus PC2 score plot and the corresponding loading plots of PC1 and PC2 are reported in **Fig. III.3-8a, 8b** and **8c**, respectively. The averaged spectrum of each strain is plotted in **Fig. III.3-8d**.

The *C. maltaromaticum* CNCM I-3298 (CM) cluster is separated from the *L. bulgaricus* ATCC 11842 (ATCC) cluster along PC1 (87% of variance). The positive peaks in the loading plot of PC1 (**Fig. III.3-8b**) reveal that *L. bulgaricus* ATCC 11842 cells are characterized by spectral features in the 1300 – 1230 cm^{-1} range, encompassing notably the Amide III region of proteins, and the 1112 – 1085 cm^{-1} range, arising from sugar rings, as well as phosphodiester (PO_2^-) functional groups of phospholipids, teichoic acids (charged polymers present in the cell wall of Gram-positive bacteria) or nucleic acid structures (Quilès et al. 2010; Lasch and Naumann 2015; Kochan et al. 2018). The negative peaks in the loading plot of PC1 reveal that *C. maltaromaticum* cells were characterized by spectral features in the 1360 – 1315 and 1185 – 1125 cm^{-1} ranges, as well as a higher contribution of complex sugar ring modes in the 1060 – 1044 cm^{-1} range, arising from the peptidoglycan of the cell wall (Naumann et al. 1982; Kochan et al. 2018).

The most cryosensitive strain, *L. bulgaricus* CFL1, is separated from the other two strains along PC2 (10 % of total variance). The negative peaks in the loading plot of PC2 (**Fig. III.3-8c**) reveal that *L. bulgaricus* CFL1 cells were characterized by a higher contribution of PO_2^- groups (1235 – 1205 cm^{-1}; 1090 – 1075 cm^{-1}).

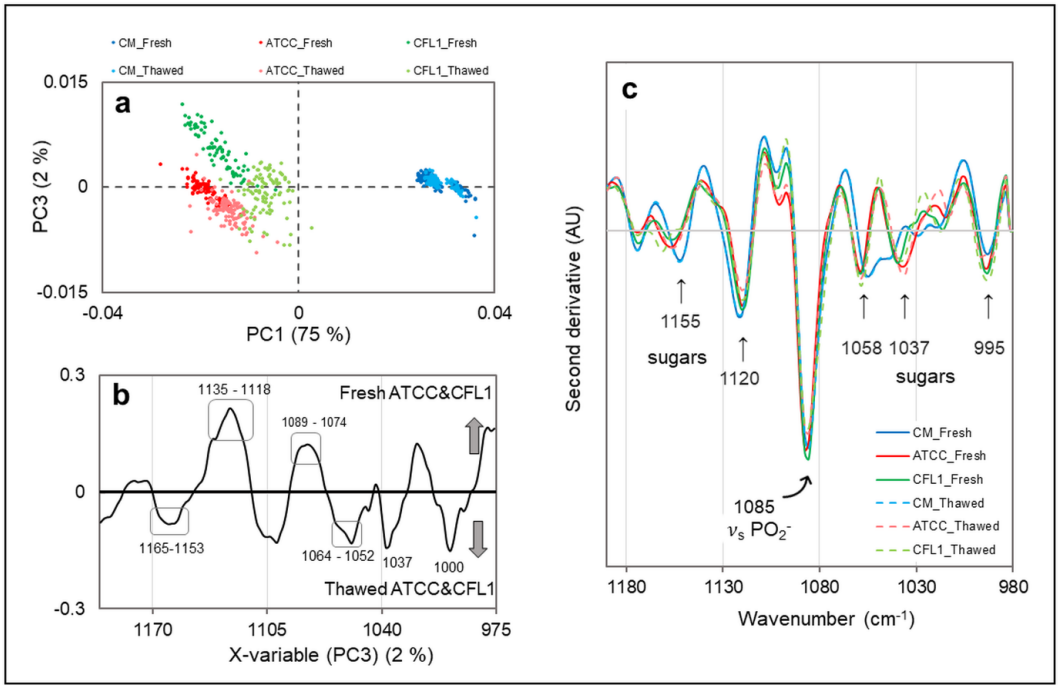

Figure III.3-9: *Principal component analysis (PCA) of FTIR spectra of fresh and thawed* C. maltaromaticum *CNCM I-3298 (CM, blue circles),* L. bulgaricus *ATCC 11842 (ATCC, red circles) and* L. bulgaricus *CFL1 (CFL1, green circles) cells in an aqueous environment, in the 1200 cm^{-1} to 975 cm^{-1} range:* ***a*** *PC1 versus PC3 score plot explaining 75 % and 2 % of variance, respectively.* ***b*** *loading plot of PC3, indicating separation of L. bulgaricus ATCC 11842 and L. bulgaricus CFL1 thawed cells from fresh cells, shifting to negative values of PC3 after freeze-thawing.* ***c*** *Mean second derivatives of the FTIR spectra of fresh and thawed cells used for the PCA. The characteristic symmetric absorption band of PO_2^- and sugar rings are indicated.*

The 1200 – 975 cm^{-1} region.

PCA was performed in the 1200 – 975 cm^{-1} region mainly containing information on cell wall components (PO_2^- groups and sugar rings) and nucleic acid (PO_2^- groups) using spectra of fresh and thawed samples (**Fig. III.3-9**). The contribution from membrane phospholipids to the PO_2^- groups' vibration band is expected to be small, given the Gram-positive bacteria membrane is composed of a single lipid bilayer with associated proteins (Kochan et al. 2018). The PC1 versus PC3 score plot revealed no cluster for *C. maltaromaticum* (CM) between fresh and thawed samples, whereas a separation was observed for *L. bulgaricus* strains (**Fig. III.3-9a**). The separation between fresh and thawed samples appeared more pronounced for the *L. bulgaricus* CFL1 cells than for the *L. bulgaricus* ATCC 11842 cells, with a shift of thawed samples to the negative direction of PC3. The loading plot of PC3 (**Fig. III.3-9b**) indicated that thawed samples of *L. bulgaricus* were characterized by a higher spectral contribution of some bands associated with sugar rings vibrations (1064 – 1052 cm^{-1} and 1037 cm^{-1}). **Figure III.3-9c** displayed the averaged second derivative of fresh and thawed samples for the three strains and enables better identification of the spectral changes induced by the freeze-thaw process. Freezing resulted in several modifications in this spectral region: (i) a decrease in the peak height of the vibration bands at 1120 cm^{-1} (sugars) and 1085 cm^{-1} (phosphodiester (PO_2^-) groups); (ii) a slight increase of the peak height at 1058 cm^{-1} (sugars); and (iii) for the vibration band at 1037 cm^{-1}, an increase of the peak height for *L. bulgaricus* ATCC 11842, but a shift to lower wavenumber for *L. bulgaricus* CFL1.

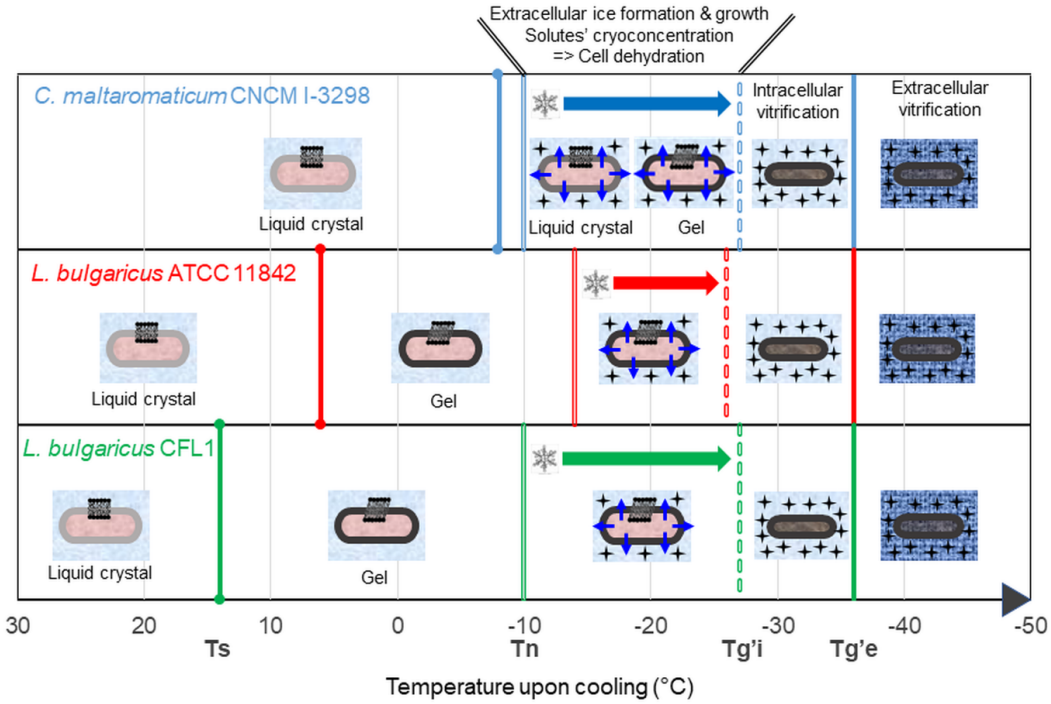

Figure III.3-10: *Schematic representation of the behavior of the three LAB cells following freezing from the culture temperature to -80°C, considering the major physical events taking place: membrane lipid phase transition at Ts, ice nucleation at Tn, intracellular glass transition of cryoprotected cells at Tg'i and glass transition of the extracellular medium (20 % sucrose in saline water) at Tg'e.*

III.3.6. Discussion

The interest for lactic acid bacteria (LAB) has been continuously growing, particularly because of their probiotic properties. However, some promising bacteria remain under-exploited due to their inability to overcome the environmental stresses induced by stabilization processes. Even if freezing is widely used for preserving LAB, some irreversible losses of functionality and viability are still observed. By comparing the properties of three LAB exhibiting various levels of freeze-sensitivity – *C. maltaromaticum* CNCM I-3298 (displaying the highest cryoresistance), *L. bulgaricus* ATCC 11842 (displaying intermediate cryoresistance) and *L. bulgaricus* CFL1 (displaying the lowest cryoresistant)) – our objective is to better understand the cellular damage induced by freezing as well as to identify markers of cryoresistance that could be used for screening LAB strains.

The major physical events that take place during the slow freezing of LAB have been well described by Fonseca et al. (Fonseca et al. 2016) and Meneghel et al. (Meneghel et al. 2017), according to four main physical properties: i) membrane lipid phase transition temperature following cooling (Ts); ii) ice nucleation temperature (Tn); iii) intracellular glass transition temperature (Tg'i); and iv) extracellular glass transition temperature (Tg'e). To discuss the relevance of these properties to explain the freeze-resistance, a dynamic representation of the behavior of the three bacterial cells following freezing from the growth temperature to -80°C is shown in **Fig. III.3-10**. Schematic drawings of the physical state of the cells are also included. After growth, LAB membranes are in a fluid crystalline phase and following cooling, they change to a gel state (at Ts). At approximately −10 °C (Tn), ice nucleation occurs and the formation of ice crystals in the extracellular medium begins. The cryoconcentration of the extracellular matrix results in water efflux from the cell and in cell volume reduction (cell dehydration). Cell dehydration ceases at Tg'i with the vitrification of the intracellular matrix. Cells thus become osmotically irresponsive to the extracellular medium (Fonseca et al. 2016). At Tg'e, the vitrification of the extracellular medium occurs, and the bacteria are immobilized in a high viscous matrix (glassy state) where diffusive damaging reactions are prevented, due to the low molecular mobility characterizing this state. When comparing the three LAB of this study, the main difference is the value of their membrane lipid phase transition temperature (Ts). The membrane of *L. bulgaricus* CFL1 and ATCC 11842 is in the gel phase during the event of cell dehydration induced by the cryoconcentration of the extracellular medium (osmotic stress), whereas the membrane of *C. maltaromaticum* remains more fluid in the liquid crystalline state. The higher membrane fluidity of *C. maltaromaticum* at subzero temperature is also confirmed by the highest wavenumber of $\nu_s CH_2$ at ice nucleation temperature and at -48 °C (**Table III.3-3**), as well as by the lowest value of fluorescence anisotropy (r) at 0 °C (highest membrane fluidity, **Fig. III.3-4**).

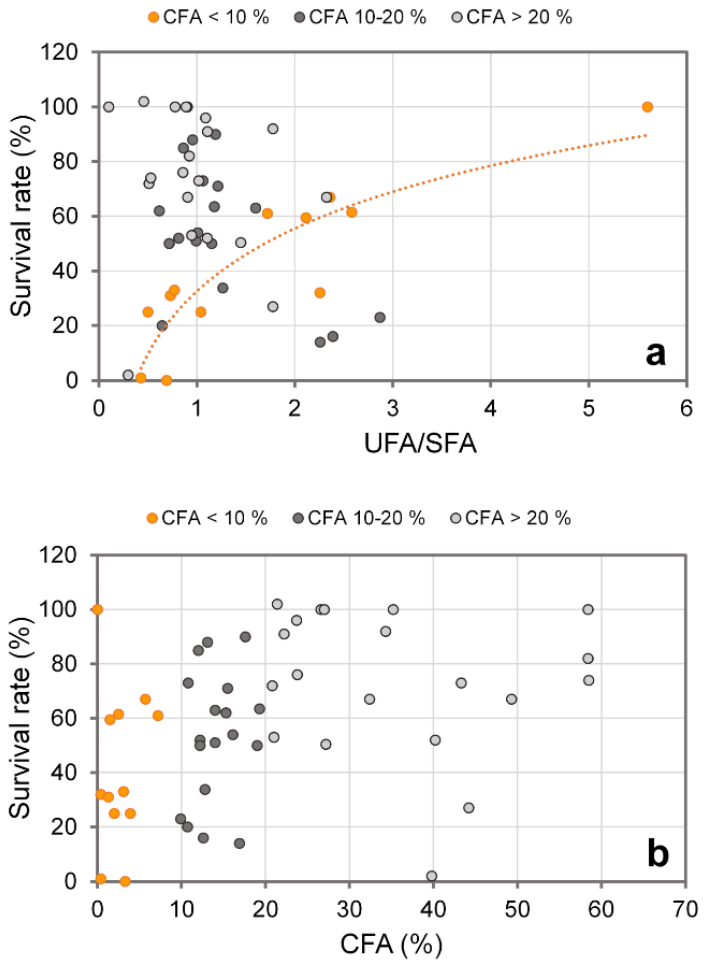

Figure III.3-11: Effect of the membrane fatty acid composition on the survival rate of LAB after freezing, according to the literature *(Gilliland and Speck 1974; Smittle et al. 1974; Goldberg and Eschar 1977; Broadbent and Lin 1999; Gómez-Zavaglia et al. 2000; Fernandez et al. 2000; Béal et al. 2001; Wang et al. 2011; Gautier et al. 2013; Meneghel et al. 2017)*. The survival rate is presented as a function of (**a**) the ratio (UFA/SFA) between the unsaturated fatty acids (UFA) and the saturated fatty acids (SFA) and (**b**) the cyclic fatty acid (CFA) content expressed as a percentage of total membrane fatty acids. The data is grouped according to the CFA content: CFA lower than 10 % (orange circles), CFA values between 10 and 20 % (dark grey circles), and CFA values higher than 20 % (light grey circles).

Freezing can be considered as a combination of different stresses applied to bacterial cells: exposure to cold temperatures, ice formation, and high solutes concentration. Osmotic stress has been reported as the main source of cellular damage for the most freeze-sensitive bacteria, *L. bulgaricus* CFL1 (Meneghel et al. 2017). The maintenance of a more fluid and flexible membrane around water nucleation temperature facilitates water efflux from the intracellular medium and cell volume reduction, thus limiting mechanical constraints on the cell membrane during freezing.

Several authors used the UFA/SFA ratio for assessing membrane fluidity and correlated the improvement of LAB freeze-resistance with change in membrane composition, in particular with higher UFA/SFA ratio and/or higher content of CFA (**Table III.3-1**) (Fonseca et al. 2019). The data from the studies reported in **Table III.3-1** have been used to calculate the UFA/SFA ratio (excluding CFA) and to plot the survival rate obtained after freezing as a function of the UFA/SFA ratio (**Fig. III.3-11a**). For CFA contents lower than 10%, the survival rate appears to be positively correlated with the UFA/SFA ratio, which is not the case when CFA contents are higher than 10 % of the FA composition. However, the increase of CFA content in membrane fatty acid composition seems to result in increasing the survival rate after freezing (**Fig. III.3-11b**). The contribution of CFA to LAB cryoresistance might thus be linked to the presence of other lipid types in the cell membrane. One study reported increased cryoresistance with increased CFA contents in strains natively low in UFA; and conversely, decreased cryoresistance with increased CFA contents in strains natively high in UFA (Gómez-Zavaglia et al. 2000). The effect of CFA, as well as the UFA/SFA ratio on both LAB cryoresistance and membrane properties, remains unclear and requires additional studies.

Lactococcus lactis subsp. *lactis* TOMSC161 has been reported as freeze-resistant while exhibiting a UFA/SFA ratio of 0.1, a CFA content of 35 % and a Ts value of 13 °C (Velly et al. 2015). Bacterial resistance to osmotic stress occurring during freezing is influenced not only by membrane properties and membrane fluidity but also by cell morphology (size and shape). Some studies have related bacterial freeze-sensitivity to the surface area-to-volume ratio of cells (Fonseca et al. 2000; Dumont et al. 2004). For instance, the freeze-sensitive lactobacilli strain *L. bulgaricus* CFL1, exhibited a surface area-to-volume ratio three to four times lower than strains of *Streptococcus thermophilus*, a freeze-resistant species of LAB (Fonseca et al. 2000).
Cryoconcentration of the extracellular medium (osmotic stress) being the most damaging stress for LAB during freezing (Meneghel et al. 2017), the bacterial membrane appears as the first target of injury due to its proximity to the extracellular medium. Most studies investigating the cryoinjury of bacterial cells reported a loss of membrane integrity, membrane permeabilization, and leakage of intracellular contents when slow cooling rates were applied (Fernandez et al. 2000; Rault et al. 2007; Moussa et al. 2008; Gautier et al. 2013; Simonin et al. 2015).

An alteration of cell wall components was also evidenced after exposure to osmotic stress (Piuri et al. 2005). Growth of *Lactobacillus casei* in high salt conditions (1 M NaCl) modified the structural properties of its peptidoglycan layer (decrease in the cross-linking degree) (Piuri et al. 2005). In this work, we have evidenced by probing bacterial populations with FTIR micro-spectroscopy, that the freeze-thaw process induced not only changes in membrane lipid components (spectral region 3016-2800 cm^{-1}), but also in proteins (1700 – 1600 cm^{-1}) and the peptidoglycan cell wall (1200 – 1000 cm^{-1}). Furthermore, the cellular damage induced by freezing seemed to increase heterogeneity within the freeze-thawed bacterial populations (**Fig. III.3-9a and Annex A-III.3**, **Fig. III.3-A2a, III.3-A3a and**).

FTIR spectroscopy techniques have already been used to investigate biochemical changes induced by freezing of LAB (analysis of LAB cells in the dried state)), or by exposure to environmental modifications of LAB (drying processes (Hlaing et al. 2017)) or other microorganisms (thermal stress (Al-Qadiri et al. 2008b); cold stress (Lu et al. 2011), silver ions stress (Saulou et al. 2013); air-drying of yeast (Pénicaud et al. 2014)). A loss of α-helical proteins structures and/or an increase in β-sheet (or β-turns) structures were systematically noticed in all studies, suggesting protein denaturation after applying the stressful treatment to the microbial population. Alteration of cell wall polysaccharides and nucleic acids were also observed (Al-Qadiri et al. 2008b; Lu et al. 2011; Pénicaud et al. 2014; Hlaing et al. 2017). Damage of nucleic acids was assessed by investigating the spectral region associated with the asymmetric and symmetric PO_2^- stretching vibration at approximately 1220 cm^{-1} and 1080 cm^{-1}, respectively. Even if the PO_2^- groups are present in the phosphodiester functional groups of DNA/RNA polysaccharide backbones, they are also involved in the polar head groups of phospholipids and phosphorus-containing carbohydrates such as teichoic acids and lipoteichoic acids (charged polymers present in the cell wall of Gram-positive bacteria). Kochan et al. (Kochan et al. 2018)investigated by atomic force microscopy-infrared (AFM-IR) spectroscopy the cell-wall signature of Gram-positive and Gram-negative bacteria, as well as the dynamical changes occurring in the cell wall during cell division of *Staphylococcus aureus* (Gram-positive bacteria). Their results indicated that when considering Gram-positive bacteria, the changes observed in the spectral range of PO_2^- group vibrations are mostly ascribed to cell wall components. Further studies are thus required to evidence potential damage of nucleic acids following freeze-thawing of LAB.

The FTIR microscopic approach developed by Meneghel et al. (Meneghel et al. 2020) for anlysing samples in an aqueous environment not only enables the identification of cellular damage induced by freezing but also the discrimination of bacterial populations before freezing. The three investigated LAB exhibited different biochemical compositions regardless of the spectral regions considered, and thus the cellular components (lipid membrane, protein, cell wall, **Fig. III.3-6, 7** and **8**). The largest spectral differences among the strains were measured in the 1370 – 975 cm^{-1}

region (**Fig. III.3-8**). This region harbors information arising from the Amide III band as well as cell wall components, such as phosphate-containing cellular compounds (i.e. teichoic acids) and complex sugar rings of the peptidoglycan (Quilès et al. 2010; Lasch and Naumann 2015; Kochan et al. 2018). The more cryoresistant strains (*C. maltaromaticum* and *L. bulgaricus* ATCC 11842) were characterized by higher absorbance bands arising from complex sugar ring modes of the peptidoglycan compared to the cryosensitive strain, suggesting that the peptidoglycan is likely involved in cryoresistance mechanisms. By acquiring infrared spectra and cryoresistance data on new LAB (or in LAB grown and or protected in different conditions), it could be possible to apply statistical approaches developed for identifying bacteria species based on infrared spectra (Udelhoven et al. 2000; Winder and Goodacre 2004; Naumann 2006; AlRabiah et al. 2013) and thus to classify the bacteria according to their degree of freeze-tolerance by considering their proximity to the cryoresistant LAB *C. maltaromaticum*, or the cryosensitive LAB, *L. bulgaricus* CFL1. The information directly gathered from the FTIR micro-spectroscopy spectra (i.e. protein conformation, cell wall composition) and through multivariate analysis could be used as a fast screening method for selecting adequate culture conditions, composition of protective solution, or freezing conditions that improve the freezing resistance of a given bacteria, before confirming with freeze-thaw biological activity measurements.

Table III.3-4: *Summary of the markers of LAB cryoresistance put forward in this study, according to the analytical method employed*

Methods	**Markers of cryoresistance**
Membrane fatty acid composition	UFA/SFA > 1.5 for CFA < 10 %* Or CFA > 20 % *
Lipid membrane phase transition Symmetric CH_2 stretching vibration band (νsCH_2)	Ts < 0 °C (CFA < 10 %) *vs*CH_2 frequency at -48 °C > 2850 cm^{-1}
Fluorescence anisotropy (r)	Ratio between the anisotropy values at 0°C and 35 °C (r_0/r_{35}) < 1.5
FTIR microscopy in aqueous conditions (before and after freeze-thawing process)	No reduction of the ratio I_{1654}/I_{1637} after freeze-thawing (or difference lower than 0.1 compared to the fresh cells) No reduction of the absorbance of the spectral bands at 1120 cm^{-1} and 1085 cm^{-1} after freeze-thawing

* survival rate higher than 50 % (Fig. III.3-11)
UFA: unsaturated fatty acids; SFA: saturated fatty acids; CFA: cyclic fatty acids; UFA/SFA does not include CFA; Ts: lipid membrane phase transition temperature following freezing

III.3.7. Conclusions

Our work focused on the in-depth characterization of three lactic acid bacteria exhibiting different levels of sensitivity to the freezing process using multiple analytical methods. Classical methods used for determining fatty acid composition or membrane fluidity, as well as a recently developed FTIR micro-spectroscopy approach allowing the study of the whole mid-infrared region of live bacteria, in their aqueous environment, were applied to understand the cellular damage induced by freezing and identify markers of cryoresistance.

We proposed in **Table III.3-4**, a list of markers. Some were already reported in the literature such as the UFA/SFA ratio, the lipid membrane phase transition temperature (Ts), while others are new, and coming from the multivariate analysis of infrared spectra performed in this work. For LAB exhibiting low membrane content of CFA (lower than 10 %), cryoresistant cells can be mainly characterized by a UFA/SFA ratio higher than 1.5, a Ts value lower than 0 °C, and an anisotropy ratio between 0 °C and 35 °C lower than 1.5. These properties favor the maintenance of a high degree of membrane fluidity at low temperatures when ice nucleation occurs.

The FTIR micro-spectroscopy results evidenced the cellular damage induced by freeze-thawing, especially an alteration of protein conformation and the peptidoglycan cell wall. A reduction in the α-helical over β-sheet band intensities (I_{1654}/I_{1637} ratio), as well as intensity reductions in bands corresponding to cell wall components (1120 cm^{-1} and 1085 cm^{-1}) were observed after freeze-thawing in the freeze-sensitive *L. bulgaricus* ATCC 11842 and CFL1 populations. The absorbance intensity changes of these specific spectral bands following freezing were proposed as new markers of cryoresistance. Although the membrane fatty acid composition is the most documented property in literature, systematic studies relating LAB cryoresistance to their membrane physical properties and FTIR spectra before and after freeze-thawing become essential for confirming and enriching the proposed cellular markers of cryoresistance.

III.3.8. Key takeaways

→ A high UFA/SFA ratio, a low lipid membrane phase transition temperature and a more fluid membrane at freezing temperatures were confirmed to be markers of cryo-resistance;

→ FTIR micro-spectroscopic measurements in aqueous conditions emerged as a relevant method to finely characterize biochemical differences between bacterial populations and search for markers of stress resistance/injury.

→ A higher FTIR absorbance of bands arising from complex sugar ring modes of the peptidoglycan, measured in the more cryoresistant strains: peptidoglycan is likely to be involved cryoresistance mechanisms

→ A decrease in the contribution of α-helical protein structures over β-sheet structures, a newly identified likely marker of cryo-injury.

→ An intensity reduction in infrared bands associated with cell wall components (1120 cm^{-1} and 1085 cm^{-1}), a newly identified likely marker of cryo-injury.

General conclusions

The most relevant tools and results obtained from this work are summarized in the following three sections.

1. **Development of a simple surface response model based on changing fermentation temperature, pH and harvest time, to produce *C. maltaromaticum* concentrates exhibiting different acidification activities**

The first part of this PhD was aimed at identifying strategies for the production of *C. maltaromaticum* concentrates exhibiting technological properties of interest for biological TTI. A particular focus was made on modulating the physiological state of *C. maltaromaticum* to obtain cells presenting a wide range of acidification activities.
The influence of three main fermentation parameters (temperature, pH and harvest time) on the technological properties (viability, acidification activity and freeze-thaw resistance) of *C. maltaromaticum* were assessed by cultivating cells at different temperatures (20 to 37 °C) and pH (6.0 to 9.5) according to a modified central composite design and harvesting at increasing times up to 10 hours of stationary phase. Although temperature did modulate acidification activity, pH and harvest time were identified as the main fermentation parameters impacting the acidification activity of the harvested concentrates. Growth under an acidic pH (pH 6) and a harvest at the beginning of stationary growth phase led to concentrates exhibiting fast acidification activities. Growth under an alkaline pH (pH 9.5) and a harvest four to six hours into stationary phase led to concentrates exhibiting slow acidification activities. Interestingly, growth under these extreme culture conditions did not impact the freeze-thaw resistance of the harvested cells, confirming the strain's exceptional cryoresistance.
This work led to the development of a surface response model able to predict the acidification activity of the harvested concentrates, according to culture temperature, pH and duration (**Chapter III.1**, Girardeau et al. 2019).

2. **Development of a dynamic model describing the growth and metabolite production of *C. maltaromaticum* in a pilot-scale bioreactor**

The study presented in **Chapter III.1** provided information on the impact of temperature and pH stress during fermentation on the subsequent acidification

activity of harvested concentrates. The focus in this following study was turned to the impact those stresses had on the growth and metabolic activity of the cells, during fermentation (i.e., before harvest). The aim here, was to develop a dynamic model able to define temperature and pH values that optimize industrial *C. maltaromaticum* cultures. The only dynamic model dealing with *C. maltaromaticum* had previously been published by Ellouze et al. (2008). However, that research was carried out on cells in a sausage-like growth medium, instead of a bioreactor and considered lactic acid as the only metabolite produced. Though *Carnobacteria* are regarded to be homofermentative, their production of acids has been shown to be strain dependent (De Bruyn et al. 1988; Borch and Molin 1989; Laursen et al. 2006). In fact, a recent study reported that *C. maltaromaticum* could produce lactic, formic and acetic acids in a meat juice medium (Zhang et al. 2019).
In our study, kinetic data on cell growth, total acid production, substrate consumption and metabolite production were gathered during 16 independent fermentations, covering a broad spectrum of culture conditions (temperatures between 20 and 37 °C; pH between 6.0 and 9.5).

This data enabled the development of a dynamic model, predicting with satisfactory accuracy, the growth of *C. maltaromaticum* as well as the conversion of trehalose into four primary metabolites (lactic acid, acetic acid, formic acid and ethanol), within a wide range of temperature and pH conditions (**Chapter III.2**, Puentes et al. 2021). The model was successfully used to determine fermentation conditions that maximize or minimize the final concentration and productivity of biomass and selected metabolites.

3. Identification of lactic acid bacteria markers of cryoinjury and cryoresistance

In **Chapters III.1** and **III.2**, growth under a wide range of stress conditions was shown to change many of *C. maltaromaticum*'s cellular characteristics (growth rate, metabolite production, acidification activity of the harvested concentrates). However, as mentioned, these changes did not impact the cells' ability to resist freezing, suggesting that the strain likely presented robust cryoresistance mechanisms, making it an interesting model for cryobiology research.
With the aim of identifying lactic acid bacteria markers of cryoinjury and cryoresistance, the biophysical and biochemical properties of fresh and thawed *C. maltaromaticum* cells were compared to those of two other lactic acid bacteria: *L. bulgaricus* ATCC 11842, exhibiting intermediate cryoresistance and *L. bulgaricus* CFL1, exhibiting the lowest cryoresistance among the three strains.

Cryoinjury markers

The search for cryoinjury markers was carried out by comparing the biochemical characterization of each strain, before and after freeze-thaw. This was done using a FTIR micro-spectroscopic approach recently developed by Meneghel *et al.* (2020), enabling the simultaneous investigation of all cellular components, in aqueous conditions.
No biochemical differences were observed between fresh and thawed *C. maltaromaticum* cells, the most cryoresistant bacterium. Spectral differences were however observed in the more cryosensitive *L. bulgaricus* strains, particularly in regions associated with proteins and cell wall components. Few studies on lactic acid bacteria had thus far investigated the effect of freezing on cellular components other than the membrane, and this was the first one carried out on cells in aqueous conditions.

- Changes in protein conformation

Significant reductions in the α-helix over β-sheet band intensity ratios were measured in the thawed *L. bulgaricus* cells, with *L. bulgaricus* ATCC 11842 exhibiting a smaller reduction than *L. bulgaricus* CFL1, the most cryosensitive strain. A decrease in the contribution of α-helical protein structures over β-sheet structures thus appeared to be linked with sensitivity to freezing and likely be a marker of cryoinjury.

- Intensity reductions of bands arising from cell wall components

A decrease in the spectral contributions of bands associated with phosphodiester groups (likely arising from teichoic acids) and complex sugar rings (arising from the peptidoglycan) were also measured in thawed *L. bulgaricus* cells. The intensity differences were noticeably more prominent in *L. bulgaricus* CFL1, suggesting that the cell wall might also be a target of freeze-injury and determine sensitivity to freezing.

Cryoresistance markers

The search for cryoresistance markers was carried out by investigating differences between cellular characteristics of the three strains. Their cytoplasmic membrane properties were compared: their lipid membrane phase transition temperature, assessed using dynamic FTIR spectroscopy, their membrane fluidity by measuring fluorescence anisotropy and their fatty acid composition, by GC-MS. In addition, differences in their overall biochemical characteristics were assessed using the same FTIR micro-spectroscopic approach mentioned above.

- Cytoplasmic membrane properties that favor a more fluid membrane around water nucleation temperature

C. maltaromaticum presented the lowest lipid membrane transition temperature among the three strains. Its lipid membrane transition from a fluid, liquid crystalline phase to a more rigid gel phase occurred at a temperature below water nucleation. In the case of the *L. bulgaricus* strains, their membrane was already in gel phase as ice formation began. This indicated that the lipid membrane of *C. maltaromaticum*, unlike the *L. bulgaricus* strains, was still in a fluid state during the event of cell dehydration caused by the cryoconcentration of the extracellular matrix, which likely facilitated water efflux and limited mechanical constraints on the cell membrane during freezing. The higher membrane fluidity of *C. maltaromaticum* at freezing temperatures compared to the other two strains was confirmed by the higher level of fatty acyl chain disorganization (higher $\nu_s CH_2$ wavenumber) measured at -48 °C, and the lower anisotropy values at 0°C. Furthermore, *C. maltaromaticum* presented the highest unsaturated over saturated fatty acid ratio (UFA:SFA) among the three strains, which is well known in literature to lead to high membrane fluidity (Fonseca et al. 2019).
This study thus confirmed that low lipid membrane transition temperatures, high $\nu_s CH_2$ wavenumbers at sub-zero temperatures, low anisotropy values at 0 °C and high UFA:SFA ratios are all markers of cryoresistance.

- Higher FTIR absorbance bands associated to the peptidoglycan of the cell wall

The more cryo-resistant strains (*C. maltaromaticum* and *L. bulgaricus* ATCC 11842) were characterized by higher absorbance bands arising from complex sugar ring modes of the peptidoglycan compared to the cryo-sensitive strain, suggesting that peptidoglycan is likely involved in cryo-resistance mechanisms.

Perspectives

1. Short-term perspectives

○ Related to TTI development

- Changing the fermentation medium composition of *C. maltaromaticum* to further modulate the physiological state of harvested concentrates

The approach carried out to modulate the physiological state of *C. maltaromaticum* in the first part of the PhD, only focused on temperature, pH and growth phase upon harvest (**Chapter III.1**). However, changing the fermentation medium composition could also be a relevant lever to accelerate or slow down the metabolic activity of the harvested concentrates.
Growth rate and acidification activity of *C. maltaromaticum* LM28 in milk was shown to increase when the milk was enriched with 1 g/L of yeast extract (Edima et al. 2008). A preliminary study on the effect of increasing the amount of proteose peptone (an ingredient rich in amino acids) might have on the growth and acidification activity of *C. maltaromaticum* CNCM I-3298 was thus started by Wenfan Cao, as part of her final engineering internship in the SayFood laboratory (INRAE, France). Results seemed to indicate that the acidification activity of *C. maltaromaticum* could indeed be improved by increasing the amount of proteose peptone in the fermentation medium. Additional experiments must however be performed to confirm this result. Research could also be carried out on the effect of changing the carbon source of fermentation. The production of acetic acid by *C. maltaromaticum* has been shown to increase relative to lactic acid if glucose is substituted by ribose (Leisner et al. 2007). Since acetic acid has a higher pKa than lactic acid, the resulting acidifying power would likely be reduced.

- Extend the developed dynamic model to predict growth and metabolite production of *C. maltaromaticum* in a TTI label-like environment

The dynamic model developed in **Chapter III.2** only simulates the growth and metabolite production of *C. maltaromaticum* in a bioreactor, at a controlled pH and temperature. This model could be extended to predict the growth and acidifying kinetics of *C. maltaromaticum* in an environment where temperature varies in an arbitrary but known way and pH is not controlled but depends on the produced acids and the buffer capacity of the medium. Such an environment would thus closer mimic the one encountered by *C. maltaromaticum* within a time-temperature integrator label.

- **Related to lactic acid bacteria cryoresistance**

- Investigate the role of specific fatty acids and lipid headgroups of the *C. maltaromaticum* membrane, in relation to cryoresistance

The assessment of the fatty acid composition of *C. maltaromaticum* (**Chapter III.3**) revealed that it had a very different composition from that of the other LAB strains, notably with regards to its extremely high oleic acid content (>70 %). This has raised the interest for further investigating this strain's lipid membrane by assessing the polar head composition and fatty acid composition of each lipid family. This work has been initiated in collaboration with Ha-Phuong Ta and Marie-Hélène Ropers, from the BIA laboratory (INRAE, Nantes).

- Further investigate differences between *C. maltaromaticum*, *L. bulgaricus* ATCC and L. *bulgaricus* CFL1 with regards to the interaction of their lipid membrane and cryoprotectants

The position of the $\nu_{as}PO_2^-$ band of *L. bulgaricus* ATCC 11842 and *L. bulgaricus* CFL1 under cold and osmotic stress was monitored by Meneghel et al. (2017) to evaluate the behavior of the polar headgroup of phospholipids in their membrane. Their results showed that osmotic stress extensively downshifted this peak position in the FTIR spectra of the cryosensitive, *L. bulgaricus* CFL1 but not in the case of *L. bulgaricus* ATCC 11842, suggesting the existence of different types of interactions between the concentrated sucrose matrix and the membrane phospholipid headgroups of both strains. Such investigation could be performed on *C. maltaromaticum* to evaluate a possible difference in sucrose interaction with its membrane. This could also be extended to evaluate the protective mechanisms of different cryoprotective molecules.

- Evaluate the resistance of *C. maltaromaticum* to other stabilization processes such as freeze-drying

The work carried out thus far on *C. maltaromaticum* has confirmed the strain's exceptional cryoresistance. However, preliminary work investigating the strain's ability to resist freeze-drying showed that it exhibits poor resistance. Ongoing work is being done to evaluate the effect of changing fermentation parameters on the strain's resistance to freeze-drying and subsequent storage at room temperature. Thus far, results seem to indicate that resistance to freeze-drying and storage may be improved by applying sub-lethal stress during fermentation.

An FTIR micro-spectroscopic study of fresh and rehydrated *C. maltaromaticum* cells is underway, to search for markers of resistance to freeze-drying, similarly to the approach taken to search for markers of cryoresistance in **Chapter III.3**.

2. Medium to long-term perspectives

- Acquire infrared spectra and cryoresistance data on new lactic acid bacteria to validate the identified potential markers of cryoresistance and cryoinjury

Applying a similar approach to what was carried out in **Chapter III.3**, to other lactic acid bacteria strains (or populations grown and/or protected in different conditions), could help confirm the proposed markers of cryoinjury and cryoresistance identified in infrared spectra. This would make it possible, at some point, to rapidly assess the cryoresistance of new lactic acid bacteria, based on their infrared spectral characteristics alone.

- Develop an FTIR method combining micro-spectroscopy in aqueous conditions and dynamic measurements

Two different FTIR spectroscopic setups were used in this PhD: (i) a dynamic setup, providing information on lipid membrane behavior during freezing, but without access to protein information due to the spectral interference of water; and (ii) a static, micro-spectroscopy setup associated to a water subtraction spectral processing method that has made it possible to access the entire mid infrared region of cells, but only at room temperature. Combining both setups by developing a special sample chamber that can be cooled and used with the FTIR micro-spectroscopic approach would allow the monitoring of the entire mid-infrared region of cells during freezing. This would provide valuable, real-time information on the impact of freezing on all cellular components, and thus offer a better understanding of bacterial cryoinjury.

Although the research carried out with Cryolog did not go as far as initially hoped, this PhD project produced useful building blocks for future development of labels with a broader shelf-life and contributed to the acquisition of fundamental knowledge on the mechanisms of adaptation to stress in lactic acid bacteria, within the PREMIUM project framework.

References

Afzal MI, Boulahya K-A, Paris C, Delaunay S, Cailliez-Grimal C (2013) Effect of oxygen on the biosynthesis of flavor compound 3-methylbutanal from leucine catabolism during batch culture in *Carnobacterium maltaromaticum* LMA 28. J Dairy Sci 96:352–359. https://doi.org/10.3168/jds.2012-6088

Afzal MI, Delaunay S, Paris C, Borges F, Revol-Junelles A-M, Cailliez-Grimal C (2012) Identification of metabolic pathways involved in the biosynthesis of flavor compound 3-methylbutanal from leucine catabolism by *Carnobacterium maltaromaticum* LMA 28. Int J Food Microbiol 157:332–339. https://doi.org/10.1016/j.ijfoodmicro.2012.05.010

Afzal MI, Jacquet T, Delaunay S, Borges F, Millière J-B, Revol-Junelles A-M, Cailliez-Grimal C (2010) *Carnobacterium maltaromaticum*: Identification, isolation tools, ecology and technological aspects in dairy products. Food Microbiol 27:573–579. https://doi.org/10.1016/j.fm.2010.03.019

Aiba S, Shoda M (1969) Reassessment of the product inhibition in alcohol fermentation. J Ferment Technol 47:790–794

Al-Qadiri HM, Al-Alami NI, Al-Holy MA, Rasco BA (2008a) Using Fourier transform infrared (FT-IR) absorbance spectroscopy and multivariate analysis to study the effect of chlorine-induced bacterial injury in water. J Agric Food Chem 56:8992–8997. https://doi.org/10.1021/jf801604p

Al-Qadiri HM, Lin M, Al-Holy MA, Cavinato AG, Rasco BA (2008b) Detection of sublethal thermal injury in *Salmonella enterica* serotype typhimurium and *Listeria monocytogenes* using Fourier transform infrared (FT-IR) spectroscopy (4000 to 600 cm^{-1}). J Food Sci 73:M54–M61. https://doi.org/10/bwkvkt

AlRabiah H, Correa E, Upton M, Goodacre R (2013) High-throughput phenotyping of uropathogenic *E. coli* isolates with Fourier transform infrared spectroscopy. The Analyst 138:1363. https://doi.org/10/gmf9d6

Andersson U, Rådström P (2002) Beta-glucose 1-phosphate-interconverting enzymes in maltose- and trehalose-fermenting lactic acid bacteria. Environ Microbiol 4:81–88. https://doi.org/10.1046/j.1462-2920.2002.00268.x

Antelo LT, Passot S, Fonseca F, Trelea IC, Alonso AA (2012) Towards optimal operation conditions of freeze-drying processes via a multi-level approach. Dry Technol 112:536–548. http://dx.doi.org/10.1080/07373937.2012.686079

Arena ME, Saguir FM, Manca de Nadra MC (1999) Arginine, citrulline and ornithine metabolism by lactic acid bacteria from wine. Int J Food Microbiol 52:155–161. https://doi.org/10.1016/S0168-1605(99)00133-6

Arrondo JLR, Goñi FM (1998) Infrared studies of protein-induced perturbation of lipids in lipoproteins and membranes. Chem Phys Lipids 96:53–68. https://doi.org/10.1016/S0009-3084(98)00080-2

Ates O (2015) Systems Biology of Microbial Exopolysaccharides Production. Front Bioeng Biotechnol 3. https://doi.org/10.3389/fbioe.2015.00200

Bailey JE (1998) Mathematical Modeling and Analysis in Biochemical Engineering: Past Accomplishments and Future Opportunities. Biotechnol Prog 14:8–20. https://doi.org/10.1021/bp9701269

Balsa-Canto E, Alonso AA, Arias-Méndez A, García MR, López-Núñez A, Mosquera-Fernández M, Vázquez C, Vilas C (2016) Modeling and Optimization Techniques with Applications in Food Processes, Bio-processes and Bio-systems. In: Higueras I, Roldán T, Torrens JJ (eds) Numerical Simulation in Physics and Engineering: Lecture Notes of the XVI "Jacques-Louis Lions" Spanish-French School. Springer International Publishing, Cham, pp 187–216

Barakat RK, Griffiths MW, Harris LJ (2000) Isolation and characterization of *Carnobacterium*, *Lactococcus*, and *Enterococcus* spp. from cooked, modified atmosphere packaged, refrigerated, poultry meat. Int J Food Microbiol 62:83–94. https://doi.org/10.1016/s0168-1605(00)00381-0

Baranyi null (1998) Comparison of Stochastic and Deterministic Concepts of Bacterial Lag. J Theor Biol 192:403–408. https://doi.org/10.1006/jtbi.1998.0673

Baranyi J, Roberts TA (1994) A dynamic approach to predicting bacterial growth in food. Int J Food Microbiol 23:277–294. https://doi.org/10.1016/0168-1605(94)90157-0

Barth A (2007) Infrared spectroscopy of proteins. Biochim Biophys Acta BBA - Bioenerg 1767:1073–1101. https://doi.org/10.1016/j.bbabio.2007.06.004

Bastin G, Dochain D (1990) Dynamic models of Bioreactors. In: Bastin G, Dochain D (eds) On-line Estimation and Adaptive Control of Bioreactors. Elsevier, Amsterdam, pp 1–82

Battley EH (1960) Growth-Reaction Equations for *Saccharomyces cerevisiae*. Physiol Plant 13:192–203. https://doi.org/10.1111/j.1399-3054.1960.tb08023.x

Baumann DP, Reinbold GW (1966) Freezing of Lactic Cultures. J Dairy Sci 49:259–264. https://doi.org/10.3168/jds.S0022-0302(66)87846-3

Béal C, Fonseca F (2015) Freezing of Probiotic Bacteria. In: Foerst P, Santivarangkna C (eds) Advances in Probiotic Technology. CRC Press, pp 179–212

Béal C, Fonseca F, Corrieu G (2001) Resistance to freezing and frozen storage of *Streptococcus thermophilus* is related to membrane fatty acid composition. J Dairy Sci 84:2347–2356. https://doi.org/10.3168/jds.S0022-0302(01)74683-8

Bellgardt K-H (2000) Bioprocess Models. In: Bioreaction Engineering: Modeling and Control. Springer-Verlag, Berlin Heidelberg, pp 44–105

Beney L, Gervais P (2001) Influence of the fluidity of the membrane on the response of microorganisms to environmental stresses. Appl Microbiol Biotechnol 57:34–42. https://doi.org/10.1007/s002530100754

Beney L, Mille Y, Gervais P (2004) Death of *Escherichia coli* during rapid and severe dehydration is related to lipid phase transition. Appl Microbiol Biotechnol 65:457–464. https://doi.org/10.1007/s00253-004-1574-x

Berner D, Viernstein H (2006) Effect of protective agents on the viability of *Lactococcus lactis* subjected to freeze-thawing and freeze-drying. Sci Pharm 74:137–149. https://doi.org/10.3797/scipharm.2006.74.137

Bhargava R (2012) Infrared Spectroscopic Imaging: The Next Generation. Appl Spectrosc 66:1091–1120. https://doi.org/10.1366/12-06801

Bittman R (2013) Glycerolipids: Chemistry. In: Roberts GCK (ed) Encyclopedia of Biophysics. Springer, Berlin, Heidelberg, pp 907–914

Borch E, Molin G (1989) The aerobic growth and product formation of *Lactobacillus*, *Leuconostoc*, *Brochothrix*, and *Carnobacterium* in batch cultures. Appl Microbiol Biotechnol 30:81–88. https://doi.org/10.1007/BF00256001

Bouville M (2007) Fermentation kinetics including product and substrate inhibitions plus biomass death: a mathematical analysis. Biotechnol Lett 29:737–741. https://doi.org/10.1007/s10529-006-9296-z

Brillet A, Pilet M-F, Prevost H, Bouttefroy A, Leroi F (2004) Biodiversity of *Listeria monocytogenes* sensitivity to bacteriocin-producing *Carnobacterium* strains and application in sterile cold-smoked salmon. J Appl Microbiol 97:1029–1037. https://doi.org/10.1111/j.1365-2672.2004.02383.x

Brillet-Viel A, Pilet M-F, Courcoux P, Prévost H, Leroi F (2016) Optimization of Growth and Bacteriocin Activity of the Food Bioprotective *Carnobacterium divergens* V41 in an Animal Origin Protein Free Medium. Front Mar Sci 3:168. https://doi.org/10.3389/fmars.2016.00128

Broadbent JR, Lin C (1999) Effect of heat shock or cold shock treatment on the resistance of *Lactococcus lactis* to freezing and lyophilization. Cryobiology 39:88–102. https://doi.org/10.1006/cryo.1999.2190

Buchanan RL, Bagi LK (1997) Microbial Competition: Effect of Culture Conditions on the Suppression of *Listeria monocytogenes* Scott A by *Carnobacterium piscicola* †. J Food Prot 60:254–261. https://doi.org/10.4315/0362-028X-60.3.254

Buchanan RL, Klawitter LA (1991) Effectiveness of *Carnobacterium piscicola* LK5 for controlling the growth of *Listeria monocytogenes* Scott A in refrigerated foods. J Food Saf 12:219–236. https://doi.org/10.1111/j.1745-4565.1991.tb00080.x

Budin-Verneuil A, Maguin E, Auffray Y, Ehrlich SD, Pichereau V (2003) An essential role for arginine catabolism in the acid tolerance of *Lactococcus lactis* MG1363. Le Lait 84:61–68. https://doi.org/10.1051/lait:2003033

Cai S, Singh BR (2004) A Distinct Utility of the Amide III Infrared Band for Secondary Structure Estimation of Aqueous Protein Solutions Using Partial Least Squares Methods †. Biochemistry 43:2541–2549. https://doi.org/10.1021/bi030149y

Cailliez-Grimal C, Edima HC, Revol-Junelles A-M, Millière J-B (2007) Short Communication: *Carnobacterium maltaromaticum*: The Only *Carnobacterium* Species in French Ripened Soft Cheeses as Revealed by Polymerase Chain Reaction Detection. J Dairy Sci 90:1133–1138. https://doi.org/10.3168/jds.S0022-0302(07)71599-0

Cao-Hoang L, Dumont F, Marechal PA, Gervais P (2010) Inactivation of *Escherichia coli* and *Lactobacillus plantarum* in relation to membrane permeabilization due to rapid chilling followed by cold storage. Arch Microbiol 192:299–305. https://doi.org/10.1007/s00203-010-0555-y

Cárcoba R, Rodríguez A (2000) Influence of cryoprotectants on the viability and acidifying activity of frozen and freeze-dried cells of the novel starter strain *Lactococcus lactis* subsp. *lactis* CECT 5180. Eur Food Res Technol 211:433–437. https://doi.org/10.1007/s002170000194

Cárcoba R, Rodriguez A (2000) Influence of cryoprotectants on the viability and acidifying activity of frozen and freeze-dried cells of the novel starter strain *Lactococcus lactis* subsp. *lactis* CECT 5180. Eur Food Res Technol 211:433–437

Carvalho AS, Silva J, Ho P, Teixeira P, Malcata FX, Gibbs P (2004) Relevant factors for the preparation of freeze-dried lactic acid bacteria. Int Dairy J 14:835–847. https://doi.org/10.1016/j.idairyj.2004.02.001

Cayley S, Lewis B, Guttman H, Record M (1991) Characterization of the Cytoplasm of *Escherichia Coli* K-12 as a Function of External Osmolarity - Implications for Protein Dna Interactions Invivo. J Mol Biol 222:281–300. https://doi.org/10.1016/0022-2836(91)90212-O

Chandler D (2005) Interfaces and the driving force of hydrophobic assembly. Nature 437:640–647. https://doi.org/10.1038/nature04162

Chmelař D, Matušek A, Korger J, Durnová E, Steffen M, Chmelařová E (2002) Isolation of *Carnobacterium piscicola* from human Pus—Case report. Folia Microbiol (Praha) 47:455–457. https://doi.org/10.1007/BF02818708

Claret C, Bories A, Soucaille P (1993) Inhibitory effect of dihydroxyacetone on Gluconobacter oxydans: Kinetic aspects and expression by mathematical equations. J Ind Microbiol 11:105–112. https://doi.org/10.1007/BF01583682

Clarke A, Morris GJ, Fonseca F, Murray BJ, Acton E, Price HC (2013a) A Low Temperature Limit for Life on Earth. PLoS ONE 8. https://doi.org/10.1371/journal.pone.0066207

Cohen DPA, Renes J, Bouwman FG, Zoetendal EG, Mariman E, Vos WM de, Vaughan EE (2006) Proteomic analysis of log to stationary growth phase *Lactobacillus plantarum* cells and a 2-DE database. Proteomics 6:6485–6493. https://doi.org/10.1002/pmic.200600361

Corrieu G, Spinnler HE, Picque D, Jomier Y (1988). Automated system to follow up and control the acidification activity of lactic acid starters. Fr. Pat. Appl. FR2629612.

Crowe JH, Crowe LM, Chapman D (1984) Infrared spectroscopic studies on interactions of water and carbohydrates with a biological membrane. Arch Biochem Biophys 232:400–407. https://doi.org/10.1016/0003-9861(84)90555-1

Dalgaard P (1995) Quality and Quality Changes in Fresh Fish. Food and Agriculture Organization, Rome

de Angelis M, Gobbetti M (2004) Environmental stress responses in *Lactobacillus*: A review. Proteomics 4:106–122. https://doi.org/10.1002/pmic.200300497

de Antoni GL, Pérez P, Abraham A, Añón MC (1989) Trehalose, a cryoprotectant for *Lactobacillus bulgaricus*. Cryobiology 26:149–153. https://doi.org/10.1016/0011-2240(89)90045-X

De Bruyn IN, Holzapfel WH, Visser L, Louw AI (1988) Glucose metabolism by *Lactobacillus divergens*. J Gen Microbiol 134:2103–2109. https://doi.org/10.1099/00221287-134-8-2103

De Bruyn IN, Louw AI, Visser L, Holzapfel WH (1987) *Lactobacillus divergens* is a homofermentative Organism. Syst Appl Microbiol 9:173–175. https://doi.org/10.1016/S0723-2020(87)80018-8

De Paoli P (2005) Bio-banking in microbiology: from sample collection to epidemiology, diagnosis and research. FEMS Microbiol Rev 29:897–910. https://doi.org/10.1016/j.femsre.2005.01.005

Denich TJ, Beaudette LA, Lee H, Trevors JT (2003) Effect of selected environmental and physico-chemical factors on bacterial cytoplasmic membranes. J Microbiol Methods 52:149–182. https://doi.org/10.1016/S0167-7012(02)00155-0

Dertli E, Mayer MJ, Narbad A (2015) Impact of the exopolysaccharide layer on biofilms, adhesion and resistance to stress in *Lactobacillus johnsonii* FI9785. BMC Microbiol 15:8. https://doi.org/10.1186/s12866-015-0347-2

Derzelle S, Hallet B, Ferain T, Delcour J, Hols P (2003) Improved Adaptation to Cold-Shock, Stationary-Phase, and Freezing Stresses in *Lactobacillus plantarum* Overproducing Cold-Shock Proteins. Appl Environ Microbiol 69:4285–4290. https://doi.org/10.1128/AEM.69.7.4285-4290.2003

Deutscher J, Francke C, Postma PW (2006) How phosphotransferase system-related protein phosphorylation regulates carbohydrate metabolism in bacteria. Microbiol Mol Biol Rev MMBR 70:939–1031. https://doi.org/10.1128/MMBR.00024-06

Dianawati D, Mishra V, Shah NP (2012) Role of Calcium Alginate and Mannitol in Protecting *Bifidobacterium*. Appl Environ Microbiol 78:6914–6921. https://doi.org/10.1128/AEM.01724-12

Dias CL, Ala-Nissila T, Wong-ekkabut J, Vattulainen I, Grant M, Karttunen M (2010) The hydrophobic effect and its role in cold denaturation. Cryobiology 60:91–99. https://doi.org/10.1016/j.cryobiol.2009.07.005

Dmitriev B, Toukach F, Ehlers S (2005) Towards a comprehensive view of the bacterial cell wall. Trends Microbiol 13:569–574. https://doi.org/10.1016/j.tim.2005.10.001

dos Reis FB, de Souza VM, Thomaz MRS, Fernandes LP, de Oliveira WP, De Martinis ECP (2011) Use of *Carnobacterium maltaromaticum* cultures and hydroalcoholic extract of Lippia sidoides Cham. against *Listeria monocytogenes* in fish model systems. Int J Food Microbiol 146:228–234. https://doi.org/10.1016/j.ijfoodmicro.2011.02.012

Drider D, Fimland G, Héchard Y, McMullen LM, Prévost H (2006) The continuing story of class IIa bacteriocins. Microbiol Mol Biol Rev MMBR 70:564–582. https://doi.org/10.1128/MMBR.00016-05

Drobnis EZ, Crowe LM, Berger T, Anchordoguy TJ, Overstreet JW, Crowe JH (1993) Cold shock damage is due to lipid phase transitions in cell membranes: a demonstration using sperm as a model. J Exp Zool 265:432–437. https://doi.org/10.1002/jez.1402650413

Dumas P, Miller L (2003) Biological and Biomedical Applications of Synchrotron Infrared Microspectroscopy. J Biol Phys 29:201–218. https://doi.org/10.1023/A:1024448910761

Dumont F, Marechal P-A, Gervais P (2004a) Cell Size and Water Permeability as Determining Factors for Cell Viability after Freezing at Different Cooling Rates. Appl Environ Microbiol 70:268–272. https://doi.org/10.1128/AEM.70.1.268-272.2004

Dumont F, Marechal P-A, Gervais P (2004b) Cell size and water permeability as determining factors for cell viability after freezing at different cooling rates. Appl Environ Microbiol 70:268–272. https://doi.org/10.1128/AEM.70.1.268-272.2004

Edima H, Cailliez-Grimal C, Revol-Junelles A-M, Tonti L, Linder M, Millière J-B (2006) A selective enumeration medium for *Carnobacterium maltaromaticum*. J Microbiol Methods 68:516–521. https://doi.org/10.1016/j.mimet.2006.10.006

Edima HC, Cailliez-Grimal C, Revol-Junelles A-M, Rondags E, Millière J-B (2007) Short communication: impact of pH and temperature on the acidifying activity of *Carnobacterium maltaromaticum*. J Dairy Sci 91:3806–3813. https://doi.org/10.3168/jds.2007-0878

Ellouze M, Augustin J-C (2010) Applicability of biological time temperature integrators as quality and safety indicators for meat products. Int J Food Microbiol 138:119–129. https://doi.org/10.1016/j.ijfoodmicro.2009.12.012

Ellouze M, Gauchi J-P, Augustin J-C (2011) Use of global sensitivity analysis in quantitative microbial risk assessment: Application to the evaluation of a biological time temperature integrator as a quality and safety indicator for cold smoked salmon. Food Microbiol 28:755–769. https://doi.org/10.1016/j.fm.2010.05.022

Ellouze M, Pichaud M, Bonaiti C, Coroller L, Couvert O, Thuault D, Vaillant R (2008) Modelling pH evolution and lactic acid production in the growth medium of a

lactic acid bacterium: Application to set a biological TTI. Int J Food Microbiol 128:101–107. https://doi.org/10.1016/j.ijfoodmicro.2008.06.035

Fernandez ML, Cabrera GM, de Valdez GF, Disalvo A, Seldes AM (2000) Influence of growth temperature on cryotolerance and lipid composition of *Lactobacillus acidophilus*. J Appl Microbiol 88:342–348. https://doi.org/10.1046/j.1365-2672.2000.00967.x

Filip Z, Herrmann S, Kubat J (2004) FT-IR spectroscopic characteristics of differently cultivated *Bacillus subtilis*. Microbiol Res 159:257–262. https://doi.org/10.1016/j.micres.2004.05.002

Finne G, Matches JR (1976) Spin-labeling studies on the lipids of psychrophilic, psychrotrophic, and mesophilic *Clostridia*. J Bacteriol 125:211–219. https://doi.org/10.1128/JB.125.1.211-219.1976

Fonseca F, BéAl C, Corrieu G (2000) Method of quantifying the loss of acidification activity of lactic acid starters during freezing and frozen storage. J Dairy Res 67:83–90. https://doi.org/10.1017/S002202999900401X

Fonseca F, Béal C, Corrieu G (2001) Operating Conditions That Affect the Resistance of Lactic Acid Bacteria to Freezing and Frozen Storage. Cryobiology 43:189–198. https://doi.org/10.1006/cryo.2001.2343

Fonseca F, Béal C, Mihoub F, Marin M, Corrieu G (2003) Improvement of cryopreservation of *Lactobacillus delbrueckii* subsp. *bulgaricus* CFL1 with additives displaying different protective effects. Int Dairy J 13:917–926. https://doi.org/10.1016/S0958-6946(03)00119-5

Fonseca F, Marin M, Morris GJ (2006b) Stabilization of frozen *Lactobacillus delbrueckii* subsp. *bulgaricus* in glycerol suspensions: freezing ksinetics and storage temperature effects. Appl Environ Microbiol 72:6474–6482. https://doi.org/10.1128/aem.00998-06

Fonseca F, Meneghel J, Cenard S, Passot S, Morris GJ (2016) Determination of Intracellular Vitrification Temperatures for Unicellular Micro Organisms under Conditions Relevant for Cryopreservation. PLOS ONE 11:e0152939. https://doi.org/10.1371/journal.pone.0152939

Fonseca F, Pénicaud C, Tymczyszyn EE, Gómez-Zavaglia A, Passot S (2019) Factors influencing the membrane fluidity and the impact on production of lactic acid bacteria starters. Appl Microbiol Biotechnol 103:6867–6883. https://doi.org/10.1007/s00253-019-10002-1

Fu F-N, Deoliveira DB, Trumble WR, Sarkar HK, Singh BR (1994) Secondary Structure Estimation of Proteins Using the Amide III Region of Fourier Transform

Infrared Spectroscopy: Application to Analyze Calcium-Binding-Induced Structural Changes in Calsequestrin. Appl Spectrosc 48:1432–1441. https://doi.org/10.1366/0003702944028065

Galagan Y, Su W-F (2008) Fadable ink for time–temperature control of food freshness: Novel new time–temperature indicator. Food Res Int 41:653–657. https://doi.org/10.1016/j.foodres.2008.04.012

Gänzle MG (2015) Lactic metabolism revisited: metabolism of lactic acid bacteria in food fermentations and food spoilage. Curr Opin Food Sci 2:106–117. https://doi.org/10.1016/j.cofs.2015.03.001

Garnier M, Matamoros S, Chevret D, Pilet M-F, Leroi F, Tresse O (2010) Adaptation to Cold and Proteomic Responses of the Psychrotrophic Biopreservative *Lactococcus piscium* Strain CNCM I-4031. Appl Environ Microbiol 76:8011–8018. https://doi.org/10.1128/AEM.01331-10

Gautier J, Passot S, Pénicaud C, Guillemin H, Cenard S, Lieben P, Fonseca F (2013a) A low membrane lipid phase transition temperature is associated with a high cryotolerance of *Lactobacillus delbrueckii* subspecies *bulgaricus* CFL1. J Dairy Sci 96:5591–5602. https://doi.org/10.3168/jds.2013-6802

Gautier J, Passot S, Pénicaud C, Guillemin H, Cenard S, Lieben P, Fonseca F (2013b) A low membrane lipid phase transition temperature is associated with a high cryotolerance of *Lactobacillus delbrueckii* subsp. *bulgaricus* CFL1. J Dairy Sci 96:5591–5602. https://doi.org/10.3168/jds.2013-6802

Gilliland SE, Speck ML (1974) Relationship of Cellular Components to the Stability of Concentrated *Lactic Streptococcus* Cultures at -17 C. Appl Microbiol 27:793–796. https://doi.org/10.1128/am.27.4.793-796.1974

Girardeau A, Puentes C, Keravec S, Peteuil P, Trelea IC, Fonseca F (2019) Influence of culture conditions on the technological properties of *Carnobacterium maltaromaticum* CNCM I-3298 starters. J Appl Microbiol jam.14223. https://doi.org/10.1111/jam.14223

Giulio BD, Orlando P, Barba G, Coppola R, Rosa MD, Sada A, Prisco PPD, Nazzaro F (2005) Use of alginate and cryo-protective sugars to improve the viability of lactic acid bacteria after freezing and freeze-drying. World J Microbiol Biotechnol 21:739–746. https://doi.org/10.1007/s11274-004-4735-2

Goldberg I, Eschar L (1977) Stability of Lactic Acid Bacteria to Freezing as Related to Their Fatty Acid Composition. Appl Environ Microbiol 33:489–496. https://doi.org/10.1128/AEM.33.3.489-496.1977

Gomez Zavaglia A, Disalvo EA, De Antoni GL (2000) Fatty acid composition and freeze-thaw resistance in lactobacilli. J Dairy Res 67:241–247. https://doi.org/10.1017/s0022029900004179

González-Cabaleiro R, Lema JM, Rodríguez J (2015) Metabolic Energy-Based Modelling Explains Product Yielding in Anaerobic Mixed Culture Fermentations. PLOS ONE 10:e0126739. https://doi.org/10.1371/journal.pone.0126739

Gou M, Guo G, Zhang J, Men K, Song J, Luo F, Zhao X, Qian Z, Wei Y (2010) Time–temperature chromatic sensor based on polydiacetylene (PDA) vesicle and amphiphilic copolymer. Sens Actuators B Chem 150:406–411. https://doi.org/10.1016/j.snb.2010.06.041

Graumann P, Wendrich TM, Weber MH, Schröder K, Marahiel MA (1997) A family of cold shock proteins in *Bacillus subtilis* is essential for cellular growth and for efficient protein synthesis at optimal and low temperatures. Mol Microbiol 25:741–756. https://doi.org/10.1046/j.1365-2958.1997.5121878.x

Hansen G, Johansen CL, Marten G, Wilmes J, Jespersen L, Arneborg N (2016) Influence of extracellular pH on growth, viability, cell size, acidification activity, and intracellular pH of *Lactococcus lactis* in batch fermentations. Appl Microbiol Biotechnol 100:5965–5976. https://doi.org/10.1007/s00253-016-7454-3

Hlaing MM, Wood BR, McNaughton D, Ying D, Dumsday G, Augustin MA (2017) Effect of drying methods on protein and DNA conformation changes in *Lactobacillus rhamnosus* GG cells by Fourier transform infrared spectroscopy. J Agric Food Chem 65:1724–1731. https://doi.org/10/f9rfwx

Hochman A (1997) Programmed Cell Death in Prokaryotes. Crit Rev Microbiol 23:207–214. https://doi.org/10.3109/10408419709115136

Hüfner E, Hertel C (2008) Improvement of Raw Sausage Fermentation by Stress-Conditioning of the Starter Organism *Lactobacillus sakei*. Curr Microbiol 57:490–496. https://doi.org/10.1007/s00284-008-9274-x

Hughes AH, Hancock IC, Baddiley J (1973) The function of teichoic acids in cation control in bacterial membranes. Biochem J 132:83–93. https://doi.org/10.1042/bj1320083

Jiang W, Saxena A, Song B, Ward BB, Beveridge TJ, Myneni SCB (2004) Elucidation of Functional Groups on Gram-Positive and Gram-Negative Bacterial Surfaces Using Infrared Spectroscopy. Langmuir 20:11433–11442. https://doi.org/10.1021/la049043+

Katla T, Møretrø T, Sveen I, Aasen IM, Axelsson L, Rørvik LM, Naterstad K (2002) Inhibition of *Listeria monocytogenes* in chicken cold cuts by addition of sakacin P and sakacin P-producing *Lactobacillus sakei*. J Appl Microbiol 93:191–196

Keto-Timonen R, Hietala N, Palonen E, Hakakorpi A, Lindström M, Korkeala H (2016) Cold Shock Proteins: A Minireview with Special Emphasis on Csp-family of Enteropathogenic Yersinia. Front Microbiol 7. https://doi.org/10/gmf7jn

Kim WS, Dunn NW (1997b) Identification of a Cold Shock Gene in Lactic Acid Bacteria and the Effect of Cold Shock on Cryotolerance. Curr Microbiol 35:59–63. https://doi.org/10.1007/s002849900212

Kim WS, Ren J, Dunn NW (1999) Differentiation of *Lactococcus lactis* subspecies *lactis* and subspecies *cremoris* strains by their adaptive response to stresses. FEMS Microbiol Lett 171:57–65. https://doi.org/10.1111/j.1574-6968.1999.tb13412.x

Kim Y-A, Jung S-W, Park H-R, Chung K-Y, Lee S-J (2012) Application of a Prototype of Microbial Time Temperature Indicator (TTI) to the Prediction of Ground Beef Qualities during Storage. Korean J Food Sci Anim Resour 32:448–457. https://doi.org/10.5851/kosfa.2012.32.4.448

Kiparissides A, Pistikopoulos EN, Mantalaris A (2015) On the model-based optimization of secreting mammalian cell (GS-NS0) cultures. Biotechnol Bioeng 112:536–548. https://doi.org/10.1002/bit.25457

Kochan K, Perez-Guaita D, Pissang J, Jiang J-H, Peleg AY, McNaughton D, Heraud P, Wood BR (2018) In vivo atomic force microscopy–infrared spectroscopy of bacteria. J R Soc Interface 15:20180115. https://doi.org/10.1098/rsif.2018.0115

Konings WN, Lolkema JS, Bolhuis H, van Veen HW, Poolman B, Driessen AJM (1997) The role of transport processes in survival of lactic acid bacteria, Energy transduction and multidrug resistance. Antonie Van Leeuwenhoek 71:117–128. https://doi.org/10.1023/A:1000143525601

Lairion F, Disalvo EA (2007) Effect of trehalose on the contributions to the dipole potential of lipid monolayers. Chem Phys Lipids 150:117–124. https://doi.org/10.1016/j.chemphyslip.2007.06.221

Lambruschini C, Relini A, Ridi A, Cordone L, Gliozzi A (2000) Trehalose Interacts with Phospholipid Polar Heads in Langmuir Monolayers. Langmuir 16:5467–5470. https://doi.org/10.1021/la991641e

Laroche C, Gervais P (2003) Achievement of rapid osmotic dehydration at specific temperatures could maintain high *Saccharomyces cerevisiae* viability. Appl Microbiol Biotechnol 60:743–747. https://doi.org/10.1007/s00253-002-1167-5

Lasch P, Naumann D (2015) Infrared Spectroscopy in Microbiology. In: Meyers RA (ed) Encyclopedia of Analytical Chemistry. John Wiley & Sons, Ltd, Chichester, UK, pp 1–32

Laursen BG, Leisner JJ, Dalgaard P (2006) *Carnobacterium* Species: Effect of Metabolic Activity and Interaction with *Brochothrix thermosphacta* on Sensory Characteristics of Modified Atmosphere Packed Shrimp. J Agric Food Chem 54:3604–3611. https://doi.org/10.1021/jf053017f

Le Gal JM, Manfait M, Theophanides T (1991) Applications of FTIR spectroscopy in structural studies of cells and bacteria. J Mol Struct 242:397–407. https://doi.org/10.1016/0022-2860(91)87150-G

Lee SJ, Jung SW (2016) Time-temperature indicator, method for manufacturing the time-temperature indicator, quality guarantee system using the time-temperature indicator, and quality guarantee method using the quality guarantee system

Leisner JJ (1992) Characterisation of lactic acid bacteria isolated from lightly preserved fish products and their ability to metabolise various carbohydrates and amino acids. In: Ph.D. Thesis manuscript

Leisner JJ, Laursen BG, Prévost H, Drider D, Dalgaard P (2007) *Carnobacterium*: positive and negative effects in the environment and in foods. FEMS Microbiol Rev 31:592–613. https://doi.org/10.1111/j.1574-6976.2007.00080.x

Leisner JJ, Tidemand J, Larsen LM (1994) Catabolism of arginine by *Carnobacterium* spp. isolated from vacuum-packed sugar-salted fish. Curr Microbiol 29:95–99. https://doi.org/10.1007/BF01575755

Leroi F, Arbey N, Joffraud J-J, Chevalier F (1996) Effect of inoculation with lactic acid bacteria on extending the shelf-life of vacuum-packed cold smoked salmon. Int J Food Sci Technol 31:497–504. https://doi.org/10.1046/j.1365-2621.1996.00366.x

Letellier L, Moudden H, Shechter E (1977) Lipid and protein segregation in Escherichia coli membrane: morphological and structural study of different cytoplasmic membrane fractions. Proc Natl Acad Sci U S A 74:452–456. https://doi.org/10.1073/pnas.74.2.452

Levenspiel O (1980) The monod equation: A revisit and a generalization to product inhibition situations. Biotechnol Bioeng 22:1671–1687. https://doi.org/10.1002/bit.260220810

Levisauskas D, Galvanauskas V, Henrich S, Wilhelm K, Volk N, Lübbert A (2003) Model-based optimization of viral capsid protein production in fed-batch

culture of recombinant Escherichia coli. Bioprocess Biosyst Eng 25:255–262. https://doi.org/10.1007/s00449-002-0305-x

Lewis RNAH, McElhaney RN (1998) The structure and organization of phospholipid bilayers as revealed by infrared spectroscopy. Chem Phys Lipids 96:9–21. https://doi.org/10.1016/S0009-3084(98)00077-2

Lewis RNAH, McElhaney RN (2013) Membrane lipid phase transitions and phase organization studied by Fourier transform infrared spectroscopy. Biochim Biophys Acta BBA - Biomembr 1828:2347–2358. https://doi.org/10.1016/j.bbamem.2012.10.018

Li C, Zhao J-L, Wang Y-T, Han X, Liu N (2009) Synthesis of cyclopropane fatty acid and its effect on freeze-drying survival of *Lactobacillus bulgaricus* L2 at different growth conditions. World J Microbiol Biotechnol 25:1659–1665. https://doi.org/10.1007/s11274-009-0060-0

Libnau FO, Kvalheim OM, Christy AA, Toft J (1994) Spectra of water in the near- and mid-infrared region. Vib Spectrosc 7:243–254. https://doi.org/10.1016/0924-2031(94)85014-3

Lim SH, Choe WY, Son BH, Hong K (2014) Development of a microbial time-temperature integrator system using lactic acid bacteria. Food Sci Biotechnol 23:483–487. https://doi.org/10.1007/s10068-014-0066-8

Lorca GL, de Valdez GF (2001) A Low-pH-Inducible, Stationary-Phase Acid Tolerance Response in *Lactobacillus acidophilus* CRL 639. Curr Microbiol 42:21–25. https://doi.org/10.1007/s002840010172

Lorca GL, de Valdez GF (1999) The Effect of Suboptimal Growth Temperature and Growth Phase on Resistance of *Lactobacillus acidophilus* to Environmental Stress. Cryobiology 39:144–149. https://doi.org/10.1006/cryo.1999.2193

Louvet O, Thuault D, Vaillant R (2005) Method and device for determining if a product is in condition for use or consuption.

Lu X, Liu Q, Wu D, Al-Qadiri HM, Al-Alami NI, Kang D-H, Shin J-H, Tang J, Jabal JMF, Aston ED, Rasco BA (2011) Using of infrared spectroscopy to study the survival and injury of *Escherichia coli* O157:H7, *Campylobacter jejuni* and *Pseudomonas aeruginosa* under cold stress in low nutrient media. Food Microbiol 28:537–546. https://doi.org/10.1016/j.fm.2010.11.002

Machado MC, López CS, Heras H, Rivas EA (2004) Osmotic response in *Lactobacillus casei* ATCC 393: biochemical and biophysical characteristics of membrane. Arch Biochem Biophys 422:61–70. https://doi.org/10.1016/j.abb.2003.11.001

Madigan MT, Martinko JM, Brock TD (2006) Biology of microorganisms. Pearson Prentice Hall, Upper Saddle River, NJ

Marceau A, Zagorec M, Chaillou S, Mera T, Champomier-Verges M-C (2004) Evidence for Involvement of at Least Six Proteins in Adaptation of *Lactobacillus sakei* to Cold Temperatures and Addition of NaCl. Appl Environ Microbiol 70:7260–7268. https://doi.org/10.1128/AEM.70.12.7260-7268.2004

Marcolli C, Peter T (2005) Water activity in polyol/water systems: new UNIFAC parameterization. Atmos Chem Phys 5:1545–1555. https://doi.org/10.5194/acp-5-1545-2005

Marquis RE, Bender GR, Murray DR, Wong A (1987) Arginine deiminase system and bacterial adaptation to acid environments. Appl Env Microbiol 53:198–200. https://doi.org/10.1128/aem.53.1.198-200.1987

Mathieu F, Michel M, Lebrihi A, Lefebvre G (1994) Effect of the bacteriocin carnocin CP5 and of the producing strain *Carnobacterium piscicola* CP5 on the viability of *Listeria monocytogenes* ATCC 15313 in salt solution, broth and skimmed milk, at various incubation temperatures. Int J Food Microbiol 22:155–172. https://doi.org/10.1016/0168-1605(94)90139-2

Mazmanian SK, Schneewind O (2002) Cell Wall-Anchored Surface Proteins and Lipoproteins of Gram-Positive Bacteria. Bacillus Subtilis Its Closest Relat 57–70. https://doi.org/10.1128/9781555817992.ch6

Mazur P (1970) Cryobiology: the freezing of Biological Systems. Science 168:939–949. https://doi.org/10.1126/science.168.3934.939

Mazur P (1977) The role of intracellular freezing in the death of cells cooled at supraoptimal rates. Cryobiology 14:251–272. https://doi.org/10.1016/0011-2240(77)90175-4

Mazur P, Leibo SP, Chu EHY (1972) A two-factor hypothesis of freezing injury: Evidence from Chinese hamster tissue-culture cells. Exp Cell Res 71:345–355. https://doi.org/10.1016/0014-4827(72)90303-5

McLeod A, Zagorec M, Champomier-Vergès M-C, Naterstad K, Axelsson L (2010) Primary metabolism in *Lactobacillus sakei* food isolates by proteomic analysis. BMC Microbiol 10:120. https://doi.org/10.1186/1471-2180-10-120

Meneghel J, Passot S, Dupont S, Fonseca F (2017) Biophysical characterization of the *Lactobacillus delbrueckii* subsp. *bulgaricus* membrane during cold and osmotic stress and its relevance for cryopreservation. Appl Microbiol Biotechnol 101:1427–1441. https://doi.org/10.1007/s00253-016-7935-4

Meneghel J, Passot S, Jamme F, Lefrançois S, Lieben P, Dumas P, Fonseca F (2020) FTIR micro-spectroscopy using synchrotron-based and thermal source-based radiation for probing live bacteria. Anal Bioanal Chem. https://doi.org/10.1007/s00216-020-02835-x

Meryman HT (1968) Modified Model for the Mechanism of Freezing Injury in Erythrocytes. Nature 218:333–336. https://doi.org/10.1038/218333a0

Mika JT, Poolman B (2011) Macromolecule diffusion and confinement in prokaryotic cells. Curr Opin Biotechnol 22:117–126. https://doi.org/10.1016/j.copbio.2010.09.009

Miller A, Morgan ME, Libbey LM (1974) *Lactobacillus maltaromicus*, a New Species Producing a Malty Aroma. Int J Syst Bacteriol 24:346–354. https://doi.org/10.1099/00207713-24-3-346

Miller LM, Dumas P (2006) Chemical imaging of biological tissue with synchrotron infrared light. Biochim Biophys Acta BBA - Biomembr 1758:846–857. https://doi.org/10.1016/j.bbamem.2006.04.010

Miller LM, Smith GD, Carr GL (2003) Synchrotron-based Biological Microspectroscopy: From the Mid-Infrared through the Far-Infrared Regimes. J Biol Phys 29:219–230. https://doi.org/10.1023/A:1024401027599

Misra G, Rojas ER, Gopinathan A, Huang KC (2013) Mechanical Consequences of Cell-Wall Turnover in the Elongation of a Gram-Positive Bacterium. Biophys J 104:2342–2352. https://doi.org/10.1016/j.bpj.2013.04.047

Monod J (1942) Recherches sur la croissance des cultures bactériennes. Hermann & cie, Paris

Monod J (1949) The growth of bacterial cultures. Annu Rev Microbiol 3:371–394. https://doi.org/10.1146/annurev.mi.03.100149.002103

Mora-Villalobos JA, Montero-Zamora J, Barboza N, Rojas-Garbanzo C, Usaga J, Redondo-Solano M, Schroedter L, Olszewska-Widdrat A, López-Gómez JP (2020) Multi-Product Lactic Acid Bacteria Fermentations: A Review. Fermentation 6:23. https://doi.org/10.3390/fermentation6010023

Morice M, Bracquart P, Linden G (1992) Colonial Variation and Freeze-Thaw Resistance of Streptococcus thermophilus. J Dairy Sci 75:1197–1203. https://doi.org/10.3168/jds.S0022-0302(92)77867-9

Moussa M, Dumont F, Perrier-Cornet J-M, Gervais P (2008) Cell inactivation and membrane damage after long-term treatments at sub-zero temperature in the supercooled and frozen states. Biotechnol Bioeng 101:1245–1255. https://doi.org/10.1002/bit.21981

Movasaghi Z, Rehman S, ur Rehman DrI (2008) Fourier Transform Infrared (FTIR) Spectroscopy of Biological Tissues. Appl Spectrosc Rev 43:134–179. https://doi.org/10.1080/05704920701829043

Murga MLF, Cabrera GM, de Valdez GF, Disalvo A, Seldes AM (2000) Influence of growth temperature on cryotolerance and lipid composition of *Lactobacillus acidophilus*. J Appl Microbiol 88:342–348. https://doi.org/10.1046/j.1365-2672.2000.00967.x

Murga MLF, de Valdez GF, Disalvo EA (2001) Effect of Lipid Composition on the Stability of Cellular Membranes during Freeze–Thawing of *Lactobacillus acidophilus* Grown at Different Temperatures. Arch Biochem Biophys 388:179–184. https://doi.org/10.1006/abbi.2001.2274

Naumann D (2006) Infrared Spectroscopy in Microbiology. In: Meyers RA (ed) Encyclopedia of Analytical Chemistry. John Wiley & Sons, Ltd, Chichester, UK, p a0117

Naumann D, Barnickel G, Bradaczek H, Labischinski H, Giesbrecht P (1982) Infrared Spectroscopy, a Tool for Probing Bacterial Peptidoglycan: Potentialities of Infrared Spectroscopy for Cell Wall Analytical Studies and Rejection of Models Based on Crystalline Chitin. Eur J Biochem 125:505–515. https://doi.org/10.1111/j.1432-1033.1982.tb06711.x

Navarre WW, Schneewind O (1999) Surface Proteins of Gram-Positive Bacteria and Mechanisms of Their Targeting to the Cell Wall Envelope. Microbiol Mol Biol Rev 63:174–229. https://doi.org/10.1128/MMBR.63.1.174-229.1999

Neuhaus FC, Baddiley J (2003) A continuum of anionic charge: structures and functions of D-alanyl-teichoic acids in gram-positive bacteria. Microbiol Mol Biol Rev MMBR 67:686–723. https://doi.org/10.1128/mmbr.67.4.686-723.2003

Nikaido H, Vaara M (1985) Molecular basis of bacterial outer membrane permeability. Microbiol Rev 49:1–32. https://doi.org/10.1128/MMBR.49.1.1-32.1985

Nilsson L, Ng YY, Christiansen JN, Jorgensen BL, Grotinum D, Gram L (2004) The contribution of bacteriocin to inhibition of *Listeria monocytogenes* by *Carnobacterium piscicola* strains in cold-smoked salmon systems. J Appl Microbiol 96:133–143. https://doi.org/10.1046/j.1365-2672.2003.02129.x

Oldenhof H, Wolkers WF, Fonseca F, Passot S, Marin M (2005) Effect of Sucrose and Maltodextrin on the Physical Properties and Survival of Air-Dried Lactobacillus bulgaricus: An in Situ Fourier Transform Infrared Spectroscopy Study. Biotechnol Prog 21:885–892. https://doi.org/10.1021/bp049559j

Ophir T, Gutnick DL (1994) A Role for Exopolysaccharides in the Protection of Microorganisms from Desiccation. Appl Environ Microbiol 60:740–745. https://doi.org/10.1128/aem.60.2.740-745.1994

Othman M, Ariff AB, Rios-Solis L, Halim M (2017) Extractive Fermentation of Lactic Acid in Lactic Acid Bacteria Cultivation: A Review. Front Microbiol 8. https://doi.org/10.3389/fmicb.2017.02285

Owens JD, Legan JD (1987) Determination of the Monod substrate saturation constant for microbial growth. FEMS Microbiol Rev 3:419–432. https://doi.org/10.1111/j.1574-6968.1987.tb02478.x

Panoff J-M, Legrand S, Thammavongs B, Boutibonnes P (1994) The cold shock response in *Lactococcus lactis* subsp. *lactis*. Curr Microbiol 29:213–216. https://doi.org/10.1007/BF01570156

Panoff J-M, Thammavongs B, Guéguen M (2000) Cryoprotectants Lead to Phenotypic Adaptation to Freeze–Thaw Stress in *Lactobacillus delbrueckii* subsp. *bulgaricus* CIP 101027T. Cryobiology 40:264–269. https://doi.org/10.1006/cryo.2000.2240

Passot S, Gautier J, Jamme F, Cenard S, Dumas P, Fonseca F (2015) Understanding the cryotolerance of lactic acid bacteria using combined synchrotron infrared and fluorescence microscopies. The Analyst 140:5920–5928. https://doi.org/10.1039/C5AN00654F

Passot S, Jamme F, Réfrégiers M, Gautier J, Cenard S, Fonseca F (2014) Synchrotron UV fluorescence microscopy for determining membrane fluidity modification of single bacteria with temperatures. Biomed Spectrosc Imaging 3:203–210. https://doi.org/10.3233/BSI-140062

Pénicaud C, Landaud S, Jamme F, Talbot P, Bouix M, Ghorbal S, Fonseca F (2014) Physiological and biochemical responses of *Yarrowia lipolytica* to dehydration induced by air-drying and freezing. PLoS ONE 9:e111138. https://doi.org/10.1371/journal.pone.0111138

Péter G, Reichart O (2001)The effect of growth phase, cryoprotectants and freezing rates on the survival of selected micro-organisms during freezing and thawing. Acta Aliment 30:89–97. https://doi.org/10.1556/AAlim.30.2001.1.10

Piard JC, Desmazeaud M (1991) Inhibiting factors produced by lactic acid bacteria. 1. Oxygen metabolites and catabolism end-products. Le Lait 71:525–541. https://doi.org/10.1051/lait:1991541

Pinhal S, Ropers D, Geiselmann J, Jong H de (2019) Acetate Metabolism and the Inhibition of Bacterial Growth by Acetate. J Bacteriol 201. https://doi.org/10.1128/JB.00147-19

Piuri M, Sanchez-Rivas C, Ruzal SM (2005) Cell wall modifications during osmotic stress in Lactobacillus casei. J Appl Microbiol 98:84–95. https://doi.org/10/bqr54z

Prakash O, Nimonkar Y, Shouche YS (2013) Practice and prospects of microbial preservation. FEMS Microbiol Lett 339:1–9. https://doi.org/10.1111/1574-6968.12034

Quilès F, Humbert F, Delille A (2010) Analysis of changes in attenuated total reflection FTIR fingerprints of *Pseudomonas fluorescens* from planktonic state to nascent biofilm state. Spectrochim Acta A Mol Biomol Spectrosc 75:610–616. https://doi.org/10.1016/j.saa.2009.11.026

Quinn PJ (1985) A Lipid-Phase Sepeation Model of Low-Temperature Damage to Biological Membranes. Cryobiology 22:128–146. https://doi.org/10.1016/0011-2240(85)90167-1

Ragoonanan V, Hubel A, Aksan A (2010) Response of the cell membrane-cytoskeleton complex to osmotic and freeze/thaw stresses. Cryobiology 61:335–344. https://doi.org/10.1016/j.cryobiol.2010.10.160

Rahman A, El Kheir SM, Back A, Mangavel C, Revol-Junelles A-M, Borges F (2016) Repeat-based Sequence Typing of *Carnobacterium maltaromaticum*. Int J Food Microbiol 226:1–4. https://doi.org/10.1016/j.ijfoodmicro.2016.03.003

Rahman A, Gleinser M, Lanhers M-C, Riedel CU, Foligné B, Hanse M, Yen FT, Klouj A, Afzal MI, Back A, Mangavel C, Cailliez-Grimal C, Revol-Junelles A-M, Borges F (2014) Adaptation of the lactic acid bacterium *Carnobacterium maltaromaticum* LMA 28 to the mammalian gastrointestinal tract: From survival in mice to interaction with human cells. Int Dairy J 34:93–99. https://doi.org/10.1016/j.idairyj.2013.07.003

Rault A, Béal C, Ghorbal S, Ogier J-C, Bouix M (2007b) Multiparametric flow cytometry allows rapid assessment and comparison of lactic acid bacteria viability after freezing and during frozen storage. Cryobiology 55:35–43. https://doi.org/10.1016/j.cryobiol.2007.04.005

Rault A, Bouix M, Beal C (2009) Fermentation pH Influences the Physiological-State Dynamics of *Lactobacillus bulgaricus* CFL1 during pH-Controlled Culture. Appl Environ Microbiol 75:4374–4381. https://doi.org/10.1128/AEM.02725-08

Rault A, Bouix M, Béal C (2008) Dynamic analysis of *Lactobacillus delbrueckii* subsp. *bulgaricus* CFL1 physiological characteristics during fermentation. Appl Microbiol Biotechnol 81:559–570. https://doi.org/10.1007/s00253-008-1699-4

Rault A, Bouix M, Béal C (2010) Cryotolerance of *Lactobacillus delbrueckii* subsp. *bulgaricus* CFL1 is influenced by the physiological state during fermentation. Int Dairy J 20:792–799. https://doi.org/10.1016/j.idairyj.2010.05.002

Ricciardi A, Parente E, Zotta T (2009) Modelling the growth of *Weissella cibaria* as a function of fermentation conditions. J Appl Microbiol 107:1528–1535. https://doi.org/10.1111/j.1365-2672.2009.04335.x

Rodríguez J, Lema JM, Kleerebezem R (2008) Energy-based models for environmental biotechnology. Trends Biotechnol 26:366–374. https://doi.org/10.1016/j.tibtech.2008.04.003

Rolfe MD, Rice CJ, Lucchini S, Pin C, Thompson A, Cameron ADS, Alston M, Stringer MF, Betts RP, Baranyi J, Peck MW, Hinton JCD (2012) Lag Phase Is a Distinct Growth Phase That Prepares Bacteria for Exponential Growth and Involves Transient Metal Accumulation. J Bacteriol 194:686–701. https://doi.org/10.1128/JB.06112-11

Ruiz-Barba JL, Jiménez-Díaz R (1994) Vitamin and amino acid requirements of *Lactobacillus plantarum* strains isolated from green olive fermentations. J Appl Bacteriol 76:350–355. https://doi.org/10.1111/j.1365-2672.1994.tb01639.x

Saad N, Delattre C, Urdaci M, Schmitter JM, Bressollier P (2013) An overview of the last advances in probiotic and prebiotic field. Lwt-Food Sci Technol 50:1–16. https://doi.org/10.1016/j.lwt.2012.05.014

Salman H, Tenetov E, Feiler L, Raimann T (2009) Time-temperature indicator based on oligomeric spiroaromatics

Sánchez-Castañeda AK, Athès V, Moussa M, López-Miranda J, Páez-Lerma JB, Soto-Cruz NÓ, Trelea IC (2018) Modeling of isoamyl acetate production by fermentation with *Pichia fermentans* in an aerated system coupled to in situ extraction. Process Biochem 65:11–20. https://doi.org/10.1016/j.procbio.2017.10.010

Santivarangkna C, Wenning M, Foerst P, Kulozik U (2007) Damage of cell envelope of *Lactobacillus helveticus* during vacuum drying. J Appl Microbiol 102:748–756. https://doi.org/10.1111/j.1365-2672.2006.03123.x

Sasaki Y, Horiuchi H, Kawashima H, Mukai T, Yamamoto Y (2014) NADH Oxidase of *Streptococcus thermophilus* 1131 is Required for the Effective Yogurt Fermentation with *Lactobacillus delbrueckii* subsp. *bulgaricus* 2038. Biosci Microbiota Food Health 33:31–40. https://doi.org/10.12938/bmfh.33.31

Saulou C, Jamme F, Girbal L, Maranges C, Fourquaux I, Cocaign-Bousquet M, Dumas P, Mercier-Bonin M (2013) Synchrotron FTIR microspectroscopy of *Escherichia coli* at single-cell scale under silver-induced stress conditions. Anal Bioanal Chem 405:2685–2697. https://doi.org/10.1007/s00216-013-6725-4

Schillinger U, Holzapfel WH (1995) The genus Carnobacterium. In: Wood BJB, Holzapfel WH (eds) The Genera of Lactic Acid Bacteria. Springer US, Boston, MA, pp 307–326

Schneewind O, Fowler A, Faull KF (1995) Structure of the cell wall anchor of surface proteins in *Staphylococcus aureus*. Science 268:103–106. https://doi.org/10.1126/science.7701329

Schoug Å, Fischer J, Heipieper HJ, Schnürer J, Håkansson S (2008) Impact of fermentation pH and temperature on freeze-drying survival and membrane lipid composition of Lactobacillus coryniformis Si3. J Ind Microbiol Biotechnol 35:175–181. https://doi.org/10.1007/s10295-007-0281-x

Seber GAF, Wild CJ (2003) Nonlinear Regression. In: Nonlinear Regression, 2nd edn. John Wiley & Sons, Inc., Hoboken, NJ, USA

She RC, Petti CA (2015) Procedures for the Storage of Microorganisms. In: Manual of Clinical Microbiology. John Wiley & Sons, Ltd, pp 161–168

Sieuwerts S (2016) Microbial Interactions in the Yoghurt Consortium: Current Status and Product Implications. SOJ Microbiol Infect Dis 4:01–05. https://doi.org/10.15226/sojmid/4/2/00150

Simonin H, Bergaoui IM, Perrier-Cornet JM, Gervais P (2015a) Cryopreservation of *Escherichia coli* K12TG1: Protection from the damaging effects of supercooling by freezing. Cryobiology 70:115–121. https://doi.org/10.1016/j.cryobiol.2014.12.006

Simonin H, Bergaoui IM, Perrier-Cornet JM, Gervais P (2015b) Cryopreservation of *Escherichia coli* K12TG1: Protection from the damaging effects of supercooling by freezing. Cryobiology 70:115–121. https://doi.org/10/f67n8m

Sinner P, Kager J, Daume S, Herwig C (2019) Model-based Analysis and Optimisation of a Continuous Corynebacterium glutamicum Bioprocess Utilizing Lignocellulosic Waste. IFAC-Pap 52:181–186. https://doi.org/10.1016/j.ifacol.2019.12.255

Sleator RD, Hill C (2002) Bacterial osmoadaptation: the role of osmolytes in bacterial stress and virulence. FEMS Microbiol Rev 26:49–71. https://doi.org/10.1111/j.1574-6976.2002.tb00598.x

Smith D, Ryan MJ, Stackebrandt E (2008) The ex situ conservation of microorganisms: aiming at a certified quality management. In: Biotechnology. Eolss Publishers, Oxford ,UK, p 31

Smittle RB, Gilliland SE, Speck ML (1972) Death of *Lactobacillus bulgaricus* Resulting from Liquid Nitrogen Freezing. Appl Microbiol 24:551–554. https://doi.org/10.1128/am.24.4.551-554.1972

Smittle RB, Gilliland SE, Speck ML, Walter WM (1974) Relationship of Cellular Fatty Acid Composition to Survival of *Lactobacillus bulgaricus* in Liquid Nitrogen1. Appl Microbiol 27:738–743. https://doi.org/10.1128/AEM.27.4.738-743.1974

Song S, Bae D-W, Lim K, Griffiths MW, Oh S (2014) Cold stress improves the ability of *Lactobacillus plantarum* L67 to survive freezing. Int J Food Microbiol 191:135–143. https://doi.org/10.1016/j.ijfoodmicro.2014.09.017

Strasser S, Neureiter M, Geppl M, Braun R, Danner H (2009) Influence of lyophilization, fluidized bed drying, addition of protectants, and storage on the viability of lactic acid bacteria. J Appl Microbiol 107:167–177. https://doi.org/10.1111/j.1365-2672.2009.04192.x

Streit F, Delettre J, Corrieu G, Béal C (2008) Acid adaptation of *Lactobacillus delbrueckii* subsp. *bulgaricus* induces physiological responses at membrane and cytosolic levels that improves cryotolerance. J Appl Microbiol 105:1071–1080. https://doi.org/10.1111/j.1365-2672.2008.03848.x

Stuart MR, Chou LS, Weimer BC (1999) Influence of Carbohydrate Starvation and Arginine on Culturability and Amino Acid Utilization of *Lactococcus lactis* subsp. *lactis*. Appl Environ Microbiol 65:665–73. https://doi.org/10.1128/AEM.65.2.665-673.1999

Stubbs CD (1983) Membrane fluidity: structure and dynamics of membrane lipids. Essays Biochem 19:1–39

Suzuki M, Yamamoto T, Kawai Y, Inoue N, Yamazaki K (2005) Mode of action of piscicocin CS526 produced by *Carnobacterium piscicola* CS526. J Appl Microbiol 98:1146–1151. https://doi.org/10.1111/j.1365-2672.2005.02546.x

Tablin F, Wolkers WF, Walker NJ, Oliver AE, Tsvetkova NM, Gousset K, Crowe LM, Crowe JH (2001) Membrane Reorganization during Chilling: Implications for Long-Term Stabilization of Platelets. Cryobiology 43:114–123. https://doi.org/10.1006/cryo.2001.2355

Taoukis PS, Labuza TP (1989a) Applicability of time-temperature indicators as shelf life monitors of food products. J Food Sci 54:783–788. https://doi.org/10.1111/j.1365-2621.1989.tb07882.x

Thammavongs B, Corroler D, Panoff J-M, Auffray Y, Boutibonnes P (1996) Physiological response of *Enterococcus faecalis* JH2-2 to cold shock: growth at low temperatures and freezing/thawing challenge. Lett Appl Microbiol 23:398–402. https://doi.org/10.1111/j.1472-765X.1996.tb01345.x

Thomas CM, Summers D (2008) Bacterial Plasmids. In: John Wiley & Sons, Ltd (ed) Encyclopedia of Life Sciences. John Wiley & Sons, Ltd, Chichester, UK, p a0000468.pub2

Troller JA, Stinson JV (1981) Moisture Requirements for Growth and Metabolite Production by Lactic Acid Bacteria. Appl Environ Microbiol 42:682–687. https://doi.org/10.1128/aem.42.4.682-687.1981

Tsvetkov T, Shishkova I (1982) Studies on the effects of low temperatures on lactic acid bacteria. Cryobiology 19:211–214. https://doi.org/10.1016/0011-2240(82)90143-2

Udelhoven T, Naumann D, Schmitt J (2000) Development of a hierarchical classification system with artificial neural networks and FT-IR spectra for the identification of bacteria. Appl Spectrosc 54:1471–1479. https://doi.org/10/bz9v6b

Uribe S, Sampedro JG (2003) Measuring Solution Viscosity and its Effect on Enzyme Activity. Biol Proced Online 5:108–115. https://doi.org/10.1251/bpo52

Vaikousi H, Biliaderis CG, Koutsoumanis KP (2009) Applicability of a microbial Time Temperature Indicator (TTI) for monitoring spoilage of modified atmosphere packed minced meat. Int J Food Microbiol 133:272–278. https://doi.org/10.1016/j.ijfoodmicro.2009.05.030

Vaikousi H, Biliaderis CG, Koutsoumanis KP (2008) Development of a Microbial Time/Temperature Indicator Prototype for Monitoring the Microbiological Quality of Chilled Foods. Appl Env Microbiol 74:3242–3250. https://doi.org/10.1128/AEM.02717-07

van de Guchte M, Serror P, Chervaux C, Smokvina T, Ehrlich SD, Maguin E (2002) Stress responses in lactic acid bacteria. In: Siezen RJ, Kok J, Abee T, Schasfsma G (eds) Lactic Acid Bacteria: Genetics, Metabolism and Applications. Springer Netherlands, Dordrecht, pp 187–216

van Dijk E, Hoogeveen A, Abeln S (2015) The Hydrophobic Temperature Dependence of Amino Acids Directly Calculated from Protein Structures. PLoS Comput Biol 11. https://doi.org/10.1371/journal.pcbi.1004277

Varlet-Grancher X (2006) Time temperature indicator (tti) system

Varmanen P, Savijoki K (2011) Responses of Lactic Acid Bacteria to Heat Stress. In: Tsakalidou E, Papadimitriou K (eds) Stress Responses of Lactic Acid Bacteria. Springer US, Boston, MA, pp 55–66

Velly H, Bouix M, Passot S, Penicaud C, Beinsteiner H, Ghorbal S, Lieben P, Fonseca F (2015) Cyclopropanation of unsaturated fatty acids and membrane rigidification improve the freeze-drying resistance of *Lactococcus lactis* subsp. *lactis* TOMSC161. Appl Microbiol Biotechnol 99:907–918. https://doi.org/10.1007/s00253-014-6152-2

Velly H, Fonseca F, Passot S, Delacroix-Buchet A, Bouix M (2014) Cell growth and resistance of *Lactococcus lactis* subsp. *lactis* TOMSC161 following freezing, drying and freeze-dried storage are differentially affected by fermentation conditions. J Appl Microbiol 117:729–740. https://doi.org/10.1111/jam.12577

Verma PK, Kundu A, Puretz MS, Dhoonmoon C, Chegwidden OS, Londergan CH, Cho M (2018) The Bend+Libration Combination Band Is an Intrinsic, Collective, and Strongly Solute-Dependent Reporter on the Hydrogen Bonding Network of Liquid Water. J Phys Chem B 122:2587–2599. https://doi.org/10.1021/acs.jpcb.7b09641

VitaFoods (2020) Probiotics dietary supplements market to reach $7.10 billion by 2026. In: Vitafoods Insights. https://www.vitafoodsinsights.com/digestive-and-probiotics/probiotics-dietary-supplements-market-reach-710-billion-2026. Accessed 15 Sep 2021

Volkert M, Ananta E, Luscher C, Knorr D (2008) Effect of air freezing, spray freezing, and pressure shift freezing on membrane integrity and viability of *Lactobacillus rhamnosus* GG. J Food Eng 87:532–540. https://doi.org/10.1016/j.jfoodeng.2008.01.008

Vollmer W, Seligman SJ (2010) Architecture of peptidoglycan: more data and more models. Trends Microbiol 18:59–66. https://doi.org/10.1016/j.tim.2009.12.004

Walker VK, Palmer GR, Voordouw G (2006) Freeze-thaw tolerance and clues to the winter survival of a soil community. Appl Environ Microbiol 72:1784–1792. https://doi.org/10.1128/AEM.72.3.1784-1792.2006

Wan J, Harmark K, Davidson BE, Hillier AJ, Gordon JB, Wilcock A, Hickey MW, Coventry MJ (1997) Inhibition of *Listeria monocytogenes* by piscicolin 126 in milk and Camembert cheese manufactured with a thermophilic starter. J Appl Microbiol 82:273–280. https://doi.org/10.1046/j.1365-2672.1997.00349.x

Wang G, Yu X, Lu Z, Yang Y, Xia Y, Lai PF-H, Ai L (2019a) Optimal combination of multiple cryoprotectants and freezing-thawing conditions for high lactobacilli survival rate during freezing and frozen storage. LWT 99:217–223. https://doi.org/10.1016/j.lwt.2018.09.065

Wang S, Liu X, Yang M, Zhang Y, Xiang K, Tang R (2015) Review of Time Temperature Indicators as Quality Monitors in Food Packaging: Review of Time Temperature Indicators. Packag Technol Sci 28:839–867. https://doi.org/10.1002/pts.2148

Wang Y, Corrieu G, Béal C (2005a) Fermentation pH and temperature influence the cryotolerance of *Lactobacillus acidophilus* RD758. J Dairy Sci 88:21–29. https://doi.org/10/d3qbpr

Wang Y, Delettre J, Corrieu G, Béal C (2011) Starvation induces physiological changes that act on the cryotolerance of *Lactobacillus acidophilus* RD758. Biotechnol Prog 27:342–350. https://doi.org/10.1002/btpr.566

Wang Y, Delettre J, Guillot A, Corrieu G, Béal C (2005b) Influence of cooling temperature and duration on cold adaptation of *Lactobacillus acidophilus* RD758. Cryobiology 50:294–307. https://doi.org/10.1016/j.cryobiol.2005.03.001

Ward B (2015) Bacterial Energy Metabolism. In: Molecular Medical Microbiology. Elsevier, pp 201–233

Winder CL, Goodacre R (2004) Comparison of diffuse-reflectance absorbance and attenuated total reflectance FT-IR for the discrimination of bacteria. The Analyst 129:1118. https://doi.org/10/c85bk9

Wolkers WF, Oldenhof H (2015) Use of in situ Fourier transform infrared spectroscopy to study freezing and drying of cells. In: Wolkers WF, Oldenhof H (eds) Cryopreservation and Freeze-Drying Protocols. Springer New York, New York, NY, pp 147–161

Wouters JA, Jeynov B, Rombouts FM, de Vos WM, Kuipers OP, Abee T (1999a) Analysis of the role of 7 kDa cold-shock proteins of *Lactococcus lactis* MG1363 in cryoprotection. Microbiol Read Engl 145 (Pt 11):3185–3194. https://doi.org/10.1099/00221287-145-11-3185

Wouters JA, Kamphuis HH, Hugenholtz J, Kuipers OP, de Vos WM, Abee T (2000) Changes in Glycolytic Activity of *Lactococcus lactis* Induced by Low Temperature. Appl Environ Microbiol 66:3686–3691. https://doi.org/10.1128/AEM.66.9.3686-3691.2000

Wouters JA, Rombouts FM, Vos WM de, Kuipers OP, Abee T (1999b) Cold Shock Proteins and Low-Temperature Response of *Streptococcus thermophilus* CNRZ302. Appl Env Microbiol 65:4436–4442. https://doi.org/10.1128/AEM.65.10.4436-4442.1999

Zeng J, Roberts S, Xia Y (2010) Nanocrystal-Based Time–Temperature Indicators. Chem – Eur J 16:12559–12563. https://doi.org/10.1002/chem.201002665

Zhang P, Badoni M, Gänzle M, Yang X (2018) Growth of *Carnobacterium* spp. isolated from chilled vacuum-packaged meat under relevant acidic conditions. Int J Food Microbiol 286:120–127. https://doi.org/10.1016/j.ijfoodmicro.2018.07.032

Zhang P, Gänzle M, Yang X (2019) Complementary Antibacterial Effects of Bacteriocins and Organic Acids as Revealed by Comparative Analysis of *Carnobacterium* spp. from Meat. Appl Environ Microbiol 85:e01227-19, /aem/85/20/AEM.01227-19.atom. https://doi.org/10.1128/AEM.01227-19

Zhang Y-M, Rock CO (2008) Membrane lipid homeostasis in bacteria. Nat Rev Microbiol 6:222–233. https://doi.org/10.1038/nrmicro1839

Zweig SE (2005) Electronic time-temperature indicator

Annexes

Annex A-II.5: *An introduction to Fourier Transform Infrared Spectroscopy for the analyses of biological samples*

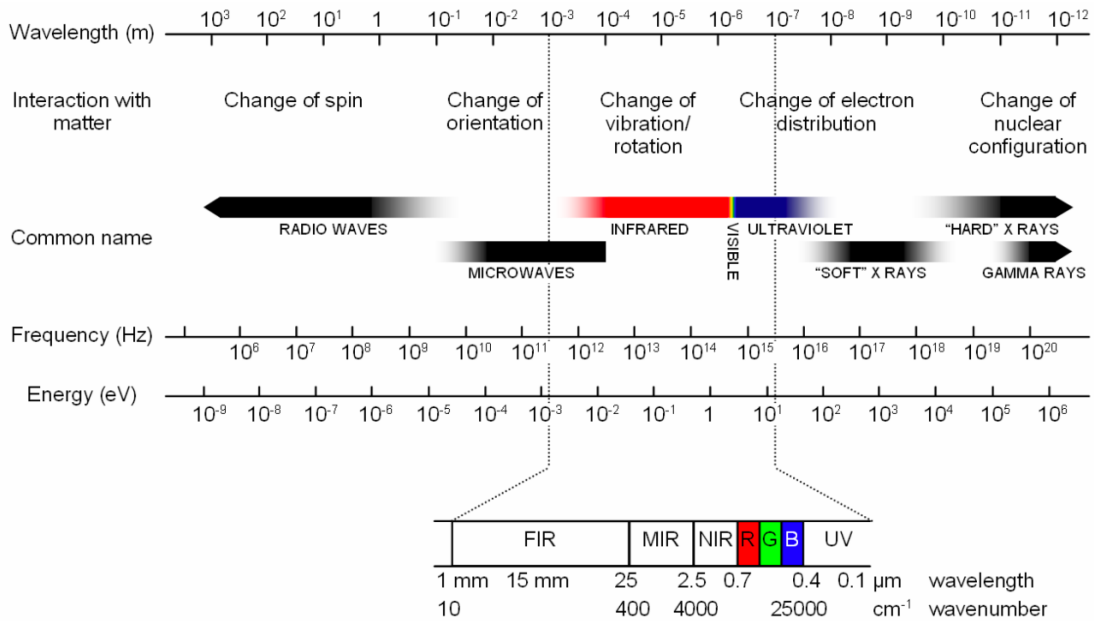

Figure II.5-A1: *Representation of the electromagnetic spectrum as a function of wavelength (m), frequency (Hz) and energy (eV), with an emphasis on the infrared region, and specifically on the mid-infrared region between 4000 and 400 cm^{-1}. Adapted from Hielscher, 2009.*

Fourier Transform Infra-Red (FTIR) spectroscopy will be presented in the following, as a tool to gain insight into bacterial markers of cryoresistance and cryoinjury. First, the physical principles of Fourier Transform Infra-Red (FTIR) spectroscopy will be briefly introduced, followed by the presentation of main equipment used and finally, the spectral features of the main biological building blocks of bacterial cells.

A-II.5.1. A powerful tool to assess cellular biochemical characteristics

Infrared spectroscopy is a powerful tool for the characterization of biological samples. It provides information on molecules present in a sample, in the form of more or less complex spectra. The interpretation of these spectra reveals the chemical components that constitute the analyzed sample. The study of lactic acid bacteria (LAB) by infrared spectroscopy can therefore help to understand the damages that freezing can cause to different cellular biomolecules (lipids, proteins, polysaccharides and nucleic acids). In addition, it does not require the introduction of exogenous dyes or probes and does not produce radiation damage to the sample, thus potentially allowing analyses of live bacterial samples.

A-II.5.1.a. The basics of FTIR spectroscopy

Spectroscopy is an analytical method based on the interaction between electromagnetic radiation and matter. Electromagnetic radiation refers to the waves of the electromagnetic field propagating through space, carrying a quantity of energy related to a frequency (ν, in s^{-1}) or a wavelength (λ, in m). Frequency and wavelength are related according to the following relationship:

$$\nu = c/\lambda \qquad \text{(II.5-A1)}$$

Where ***c*** is the speed of light (3.10^8 $m.s^{-1}$).

Depending on their frequency, electromagnetic radiations carry different names: radio waves, microwaves, infrared radiation, visible light, ultraviolet radiation, X-rays, and gamma rays (**Figure II.5-A1**). The effect of electromagnetic radiation on a chemical compound depends on its radiation energy (E, in J), which in turn, depends on its frequency. According to the quantic model, radiation energy can be calculated as follows:

$$E = h.\nu = h.c/\lambda \qquad \text{(II.5-A2)}$$

Where ***h*** is the Planck constant (6.626. 10^{-34} J.s).

The effect of gamma rays, for example, with low wavelength and consequently high energy, will be a change of nuclear configuration, whereas the effect of radio waves will only be a change of spin. The radiation from intermediate frequency waves (*i.e.* visible light, infrared, microwaves and radio waves) does not carry enough energy to ionize atoms or molecules and cannot break chemical bonds. The effect of these radiations on chemical systems can primarily be reduced to heating effects induced by the release of energy.

Infrared spectroscopy is based on the absorption of infrared energy by a molecule resulting in changes in vibrational or rotational modes of its atomic bonds. Upon absorption of infrared energy, the cloud of electrons surrounding a chemical bond moves to a higher vibrational energy state, thus causing the molecular bond to contract or expand as the electric dipole moment changes. This can thus only happen with heteronuclear diatomic molecules (*i.e.,* molecules of two atoms belonging to two different chemical elements). Homonuclear diatomic molecules (*e.g.* H_2, O_2), are termed "infrared inactive".

The vibration of a molecule composed of two atoms A and B can be represented by a harmonic oscillator and the chemical bond connecting the atoms would be a spring obeying Hooke's law:

$$F = k.d \qquad \text{(II.5-A3)}$$

The force **F** (in N) needed to extend or compress a spring by some distance (***d***, in m) depends on the force constant ***k*** (in $N.m^{-1}$) – the stiffness of the spring – and scales linearly with respect to that distance. Diatomic molecules carrying a single bond will therefore have a lower ***k*** value than those carrying a double or triple bond. The bond strength ***k*** can also be modified by interactions with neighboring molecules and is thus dependent on the environment of the molecule.

The wavelength, or wavenumber ($\tilde{\nu}$ = 1/λ, in m^{-1}) of a vibration depends on the force constant ***k***, the speed of light ***c*** (3.10^8 $m.s^{-1}$) and the reduced mass of the atoms **μ** (in kg), according to the following equation:

$$\tilde{\nu} = \frac{1}{2\,\pi\,c}\sqrt{\frac{k}{\mu}} \qquad with \quad \mu = \frac{m_A \cdot m_B}{m_A + m_B} \qquad \text{(II.5-A4)}$$

Where $\mathbf{m_A}$ and $\mathbf{m_B}$ (in kg) are the masses of the atoms A and B, respectively.

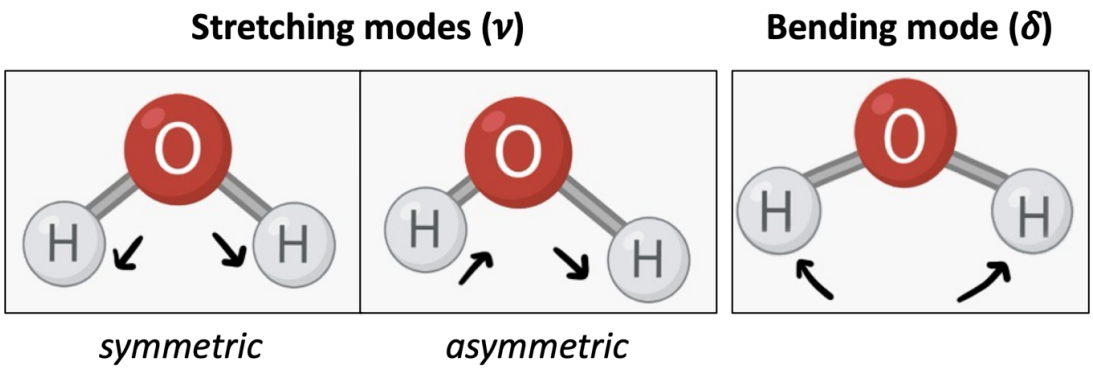

Figure II.5-A2. *Illustration of the three vibrational modes of a water molecule: symmetric stretching (ν_s), asymmetric stretching (ν_{as}) and bending (δ).*

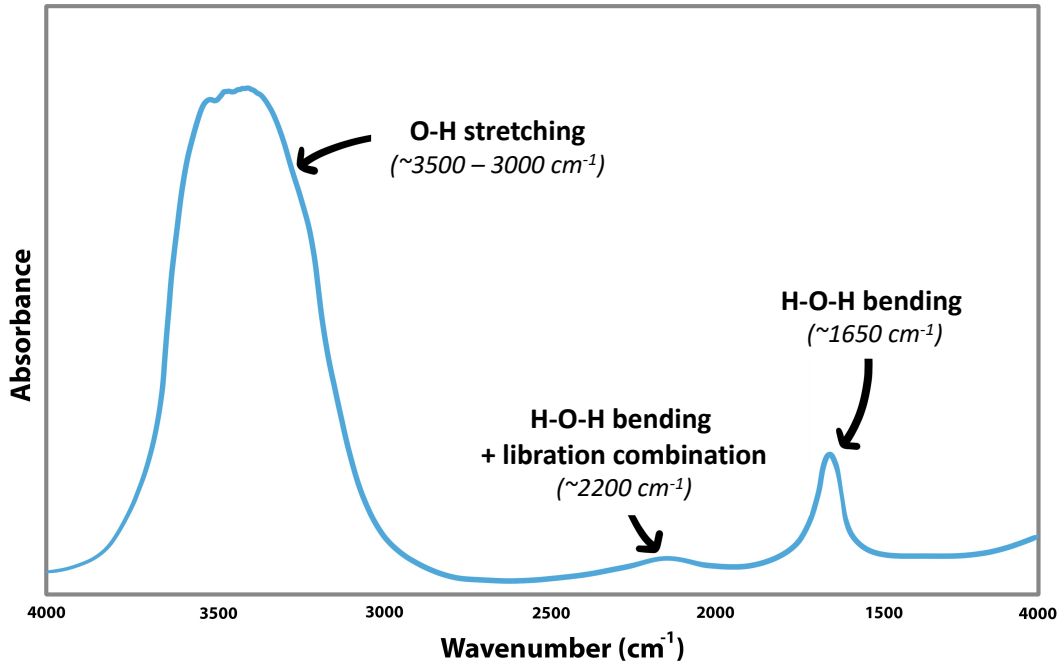

Figure II.5-A3: *FTIR spectrum of pure water. The stretching modes of water giving rise to an absorption band between 3500 and 3000 cm^{-1}, the libration and bending combination band around 2200 cm^{-1} and the bending mode around 1650 cm^{-1}(Verma et al. 2018).*

From this equation, we can deduce that the wavenumber of a vibration is proportional to the force constant ***k*** and inversely proportional to the reduced mass of the atoms, ***μ***. Single bond diatomic molecules will therefore absorb at lower wavenumbers than double bond molecules and molecules composed of lighter atoms will absorb at higher wavenumbers than those composed of heavy atoms.

The absorption of infrared radiation by polyatomic molecules (*i.e.,* molecules containing more than two atoms, such as CO_2 or H_2O) results in changes of the vibrational modes of their atomic bonds. These vibrational modes include stretching (ν) or bending (δ) of their bonds. An illustration of the vibrational modes of water is given as an example in **Figure II.5-A2**. The symmetrical and asymmetrical stretching vibration modes refer to the symmetrical and asymmetrical modifications of O-H bond lengths, while the bending mode refers to the H-O-H bond angle modifications. These vibration modes give rise to different infrared absorptions bands, at different wavenumbers (**Fig. II.5-A3**). The symmetric and asymmetric stretching modes of water give rise to an absorption band between 3500 and 3000 cm^{-1}, the bending mode around 1650 cm^{-1} and a relatively weak band around 2200 cm^{-1} assigned to a combination of the bending and the "librational" motion of water molecules (Libnau et al. 1994; Verma et al. 2018). The librational motion is associated to the hindered rotation of mutually H-bonded water molecules (Verma et al. 2018).

Since two different molecules result in two distinct infrared spectra, the infrared spectrum of a sample containing many different molecules is a composite molecular fingerprint of that sample. Therefore, by considering biological samples as complex assemblies of molecules, infrared spectroscopy can be used for their chemical characterization.

Fourier-transform infrared (FTIR) spectroscopy is the preferred method used in infrared spectroscopy to characterize or differentiate biological samples such as bacterial cells, according to their biochemical characteristics (Lasch and Naumann 2015). The term "Fourier-transform" refers to the mathematical process required to convert simultaneously collected data over a wide spectral range into one spectrum. The workings of an FTIR spectrometer will be presented in more detail in the following section.

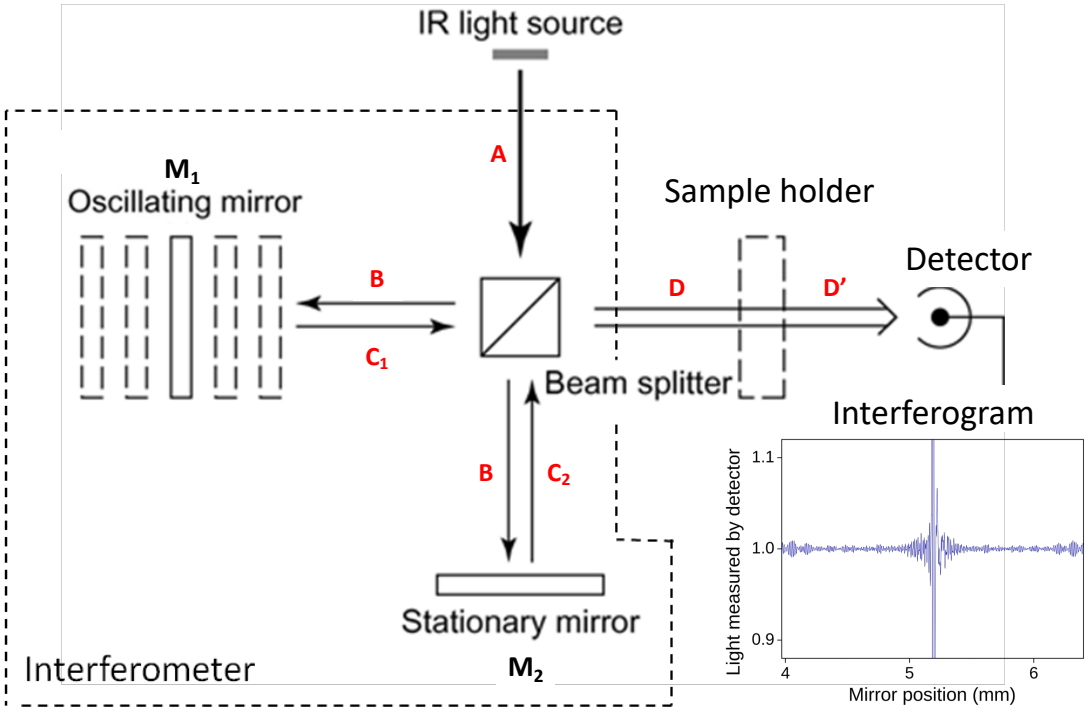

Figure II.5-A4: *Block diagram of a FTIR spectrometer. Adapted from Meneghel 2017.*

A-II.5.2. Equipment and technology used for FTIR analyses of biological samples

(i) The FTIR spectrometer

An FTIR spectrometer consists of four main components: an IR light source, a detector, an interferometer and a sample holder (**Figure II.5-A4**):

The IR light source of a typical FTIR spectrometer operating in the mid-infrared region is an internal thermal source usually made of a silicon carbide rod heated up to a temperature between 1000 and 1650 °C.
The detector commonly used when analyzing biological samples in an extended frequency domain is the broad band MCT (Mercury Cadmium Telluride) detector, cooled to -196 °C with liquid nitrogen.
The interferometer generally used is a Michelson interferometer. This interferometer consists of two perpendicularly oriented mirrors (**M_1** and **M_2**) and a beam splitter. **M_1** is an oscillating mirror and **M_2** is a fixed mirror. When the IR beam from the light source (Fig 4, **A**) hits the beam splitter, half of its intensity (Fig 4, **B**) is reflected to the oscillating mirror and the other half, to the fixed mirror. Both beams (Fig 4, **C_1** and **C_2**) are reflected back onto the beam splitter. Depending on the position of the oscillating mirror, the beams will be under constructive or destructive interferences as they recombine at the beam splitter (Fig. 4, **D**). The recombined signal passes through the sample holder and into the detector (Fig 4, **D'**), producing an interferogram plot.

Generally, the process of recording the IR spectrum of a sample first involves recording a reference interferogram without any sample in the sample holder. Subsequently, a sample interferogram is recorded and then is subtracted from the reference interferogram. The result is an interferogram reflecting the energy absorbed by the sample. The interferogram plot is then mathematically *Fourier transformed* into the more familiar IR spectrum representing spectral information in the frequency domain.

(ii) The FTIR micro-spectrometer

Fourier transform infrared micro-spectroscopy is a valuable tool that combines a microscope to a FTIR spectrometer to obtain spatially resolved biochemical characterization of complex and heterogeneous biological samples (Bhargava 2012; Lasch and Naumann 2015). The setup for FTIR micro-spectroscopy analyses is similar to that of a FTIR spectrometer, to which is coupled a microscope that can accommodate both visible light (like a conventional optical microscope) and infrared light. Light microscopy is used to magnify sample structural detail, while infrared spectroscopy provides information on molecular chemistry. Together, chemical analysis can be performed with microscopic detail (Miller and Dumas 2006).

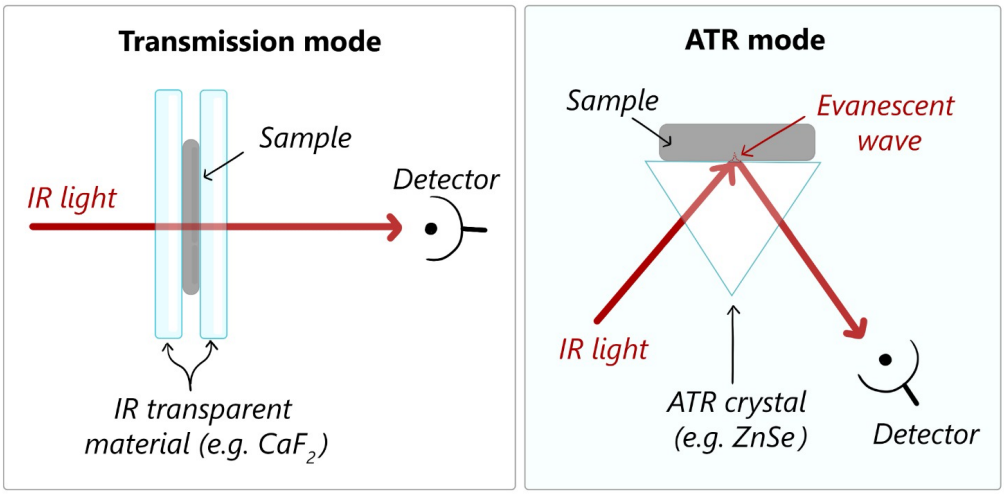

Figure II.5-A5: *Schematic illustration of the two main acquisition modes suitable for biological applications. Inspired by Barker et al. 2014*

While standard FTIR measurements probe between 10^7 and 10^8 individual microbial cells, IR micro-spectroscopy can allow spectral measurements of 10^2 to 10^3 cells or of single cells, when using a thermal or a synchrotron-based IR source, respectively (Dumas and Miller 2003; Lasch and Naumann 2015), thus providing information on population heterogeneity.

(iii) The two main acquisition modes used for FTIR spectroscopy analyses of biological sample

The two main acquisition modes used for the analysis of biological samples are the transmission and the attenuated total reflection (ATR) mode (**Fig. II.5-A5**)

Transmission mode

In transmission mode, the sample is deposited on – or sandwiched in-between – IR transparent material such as calcium fluoride (CaF_2), zinc selenide (ZnSe) or germanium (Ge). The material will be chosen depending on its resistance to the sample characteristics (e.g., hydration level or pH) and measurement protocol (e.g., temperature variations), as well as its IR transparency. The IR beam passes perpendicularly through the IR transparent material and through the sample, into the detector.

ATR mode

In ATR mode, the sample is placed on a IR transparent, high refractive index crystal, such as ZnSe, Ge or diamond. The IR beam is directed towards the surface of the crystal in contact with the sample, passes through the crystal and is reflected internally. A small part of the beam, called the evanescent wave, penetrates the crystal-sample interface and interacts with the sample. The IR beam that is reflected internally through the crystal is attenuated, as some of its energy was absorbed by the sample. This beam therefore carries the absorption information of the sample, which is collected by the detector.

A-II.5.3. Spectral features of the main biological building blocks of bacterial cells

Lactic acid bacteria are composed of complex biomolecules such as lipids, nucleic acids, proteins and carbohydrates; a complexity that is reflected in their IR spectra (Miller and Dumas 2006; Lasch and Naumann 2015). The typical mid-IR spectrum of these main biological building blocks are shown in **Figure II.5-A6**. The most prominent absorption bands of each biomolecule are highlighted in the figure and described in the following.

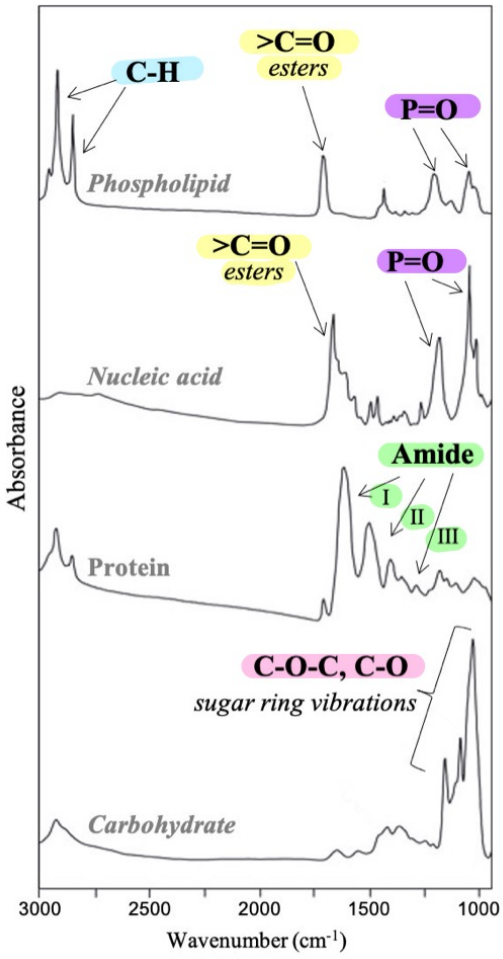

Figure II.5-A6: *Infrared spectra of a phospholipid (dimyristoylphosphatidylcholin), nucleic acid (calf thymus desoxyribonucleic acid), protein (collagen type I) and carbohydrate (glycogen), illustrating the most prominent IR absorption features of cells. Adapted from Lasch and Naumann (2015).*

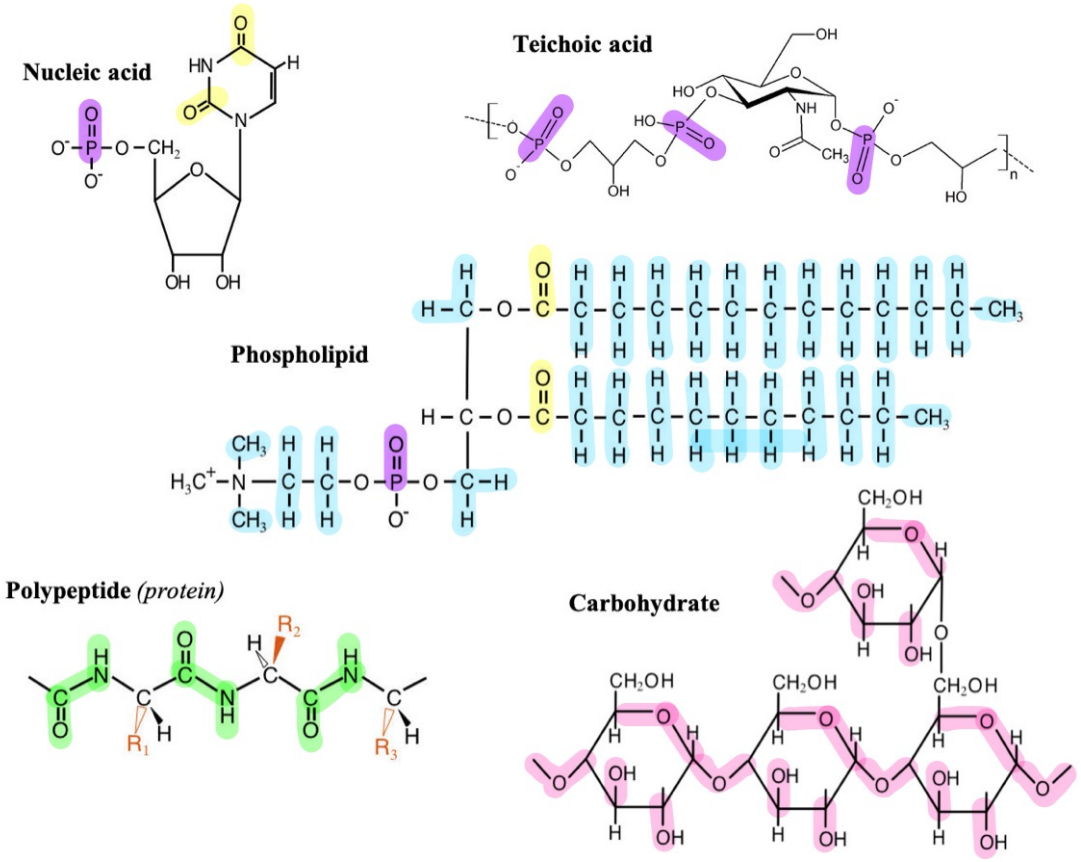

Figure II.5-A7: *Chemical structures of a nucleic acid (ribonucleotide), a teichoic acid repeat unit, a phospholipid, a polypeptide and a carbohydrate (glycogen). In green highlights are bonds mainly contributing to the Amide vibration bands. In blue highlights are bonds contributing to the CH_2 stretching bands of lipids. In yellow highlights are the bonds contributing to C=O stretching band of esters in nucleic acids and phospholipids, respectively. In purple highlights the bonds contributing to the PO_2 stretching band of phosphate groups (found in phospholipids, nucleic acids and teichoic acids). In pink highlights are the bonds contributing to the C-O stretching bands of carbohydrates.*

The C-H stretching bands typically found between 3000 cm^{-1} and 2800 cm^{-1} correspond to the absorption bands of the symmetric and asymmetric stretching vibration bands of CH_2 and CH_3 bonds, mainly arising from the hydrocarbon chains of lipids (**Fig. II.5-A7**, blue highlights on the phospholipid) (Lewis and McElhaney 2013).

The C=O stretching bands located around ~1740-1730 cm^{-1} and ~1715-1680 cm^{-1} mainly arise from ester bonds of phospholipids and nucleic acids, respectively (**Fig. II.5-A7**, yellow highlights on the nucleic acid and the phospholipid) (Lasch and Naumann 2015).

The Amide I, II and III bands, respectively located around ~1650 cm^{-1}, ~1550 cm^{-1}, ~1300 cm^{-1} mainly result from C=O, C-N and N-H bond vibrations of the protein backbones (**Fig. II.5-A7**, green highlights on the polypeptide). The Amide bands are thus characteristic signals found in the IR spectra of proteins and polypeptides. The Amide bands are hardly affected by the nature of the protein side chains but are sensitive to protein secondary structures (Miller et al. 2003; Barth 2007). This is especially the case for the Amide I band, which carries information on α-helical and β-sheet protein structures.

The P=O stretching bands found around ~1220 cm^{-1} and ~1085 cm^{-1} correspond respectively to the asymmetric and symmetric vibration bands of a phosphate group. In biological samples, these can be attributed to phospholipid headgroups, nucleic acids and phosphorus-containing carbohydrates such as cell wall teichoic acids (**Fig. II.5-A7**, blue highlights on the nucleic acid, phospholipid and teichoic acid repeat unit) (Lasch and Naumann 2015).

The C-O-C, C-O stretching bands are found between 1200 cm^{-1} and 900 cm^{-1} and arise mainly from sugar ring vibrations of carbohydrates (**Fig. II.5-A7**, pink highlights on carbohydrate) (Lasch and Naumann 2015).

A-II.5.4. References

Barth A (2007) Infrared spectroscopy of proteins. Biochim Biophys Acta BBA - Bioenerg 1767:1073–1101. https://doi.org/10.1016/j.bbabio.2007.06.004

Bhargava R (2012) Infrared Spectroscopic Imaging: The Next Generation. Appl Spectrosc 66:1091–1120. https://doi.org/10.1366/12-06801

Dumas P, Miller L (2003) Biological and Biomedical Applications of Synchrotron Infrared Microspectroscopy. J Biol Phys 29:201–218. https://doi.org/10.1023/A:1024448910761

Lasch P, Naumann D (2015) Infrared Spectroscopy in Microbiology. In: Encyclopedia of Analytical Chemistry. American Cancer Society, pp 1–32

Lewis RNAH, McElhaney RN (2013) Membrane lipid phase transitions and phase organization studied by Fourier transform infrared spectroscopy. Biochim Biophys Acta BBA - Biomembr 1828:2347–2358. https://doi.org/10.1016/j.bbamem.2012.10.018

Libnau FO, Kvalheim OM, Christy AA, Toft J (1994) Spectra of water in the near- and mid-infrared region. Vib Spectrosc 7:243–254. https://doi.org/10.1016/0924-2031(94)85014-3

Miller LM, Dumas P (2006) Chemical imaging of biological tissue with synchrotron infrared light. Biochim Biophys Acta BBA - Biomembr 1758:846–857. https://doi.org/10.1016/j.bbamem.2006.04.010

Miller LM, Smith GD, Carr GL (2003) Synchrotron-based Biological Microspectroscopy: From the Mid-Infrared through the Far-Infrared Regimes. J Biol Phys 29:219–230. https://doi.org/10.1023/A:1024401027599

Verma PK, Kundu A, Puretz MS, Dhoonmoon C, Chegwidden OS, Londergan CH, Cho M (2018) The Bend+Libration Combination Band Is an Intrinsic, Collective, and Strongly Solute-Dependent Reporter on the Hydrogen Bonding Network of Liquid Water. J Phys Chem B 122:2587–2599. https://doi.org/10.1021/acs.jpcb.7b09641

Annex A-III.1: Supplementary data of Chapter III.1

Table III.1-A1: *dtpH1.5 (in min) and viability (in CFU mL-1) measurements of freeze thawed Carnobacterium maltaromaticum CNCM I-3298 concentrates produced according to the culture conditions of the experimental design presented in Figure III.1-1 (B and C).*

Fermentation	*Culture conditions*			*Biological properties*	
	pH	T (°C)	Harvest time (h)	dtpH1.5 (min)	viability (CFU mL^{-1})
1	7	30	0.22	443	2.35E+11
	7	30	2.22	454	1.57E+11
	7	30	4.22	475	1.16E+11
2	7	30	0.24	431	1.78E+11
	7	30	2.24	454	1.19E+11
	7	30	4.24	451	1.32E+11
	7	30	6.24	464	1.41E+11
	7	30	8.24	464	2.90E+11
3	6	30	0.38	392	4.03E+11
	6	30	2.38	416	2.71E+11
	6	30	4.38	403	3.03E+11
	6	30	6.38	415	-
	6	30	8.38	409	-
4	9.5	30	-1.51	482	8.56E+10
	9.5	30	0.49	511	7.15E+10
	9.5	30	2.49	548	4.09E+10
	9.5	30	4.49	571	3.11E+10
5	7	20	2.00	427	3.19E+11
	7	20	4.00	437	3.49E+11
	7	20	6.00	433	3.89E+11
	7	20	8.00	431	3.99E+11
6	7	35	-3.07	434	2.67E+11
	7	35	0.55	430	4.37E+11
7	7	37	-2.28	454	2.29E+11
	7	37	-0.28	442	2.95E+11
	7	37	1.72	461	2.91E+11
8	9.5	20	-2.20	451	6.94E+10
	9.5	20	-0.20	478	3.48E+10
	9.5	20	1.80	502	4.41E+10
	9.5	20	2.80	524	4.90E+10
9	5.7	20	5.26	409	4.01E+10
10	6	37	5.53	505	2.56E+11
11	9	30	0.33	470	-

	9	30	2.37	508	-
	9	30	4.35	543	-
	9	30	6.45	584	-
	9	30	9.50	625	-
12	9	20	-6.03	400	-
	9	20	-4.58	405	-
	9	20	-0.363	427	-
	9	20	1.054	446	-
13	8	30	-1.68	475	9.08E+10
	8	30	0.237	495	5.77E+10
	8	30	3.437	515	8.67E+10
	8	30	5.304	520	1.18E+11
	8	30	8.704	519	1.16E+11
14	6	35	-2.83	397	2.40E+11
	6	35	0.87	387	2.38E+11
	6	35	3.887	389	2.84E+11
	6	35	6.854	399	2.43E+11
	6	35	23.437	441	2.42E+11

Annex A-III.2: Supplementary data of Chapter III.2

Model parameter identification

Table III.2-A1: *Residual modelling error with model parameters determined for each experiment and summarized in Table III.2-2.*

	RMSE (mol L^{-1})							RME (%)						
	X	S	F	A	L	E	Atotal	X	S	F	A	L	E	Atotal
F01	0.008	0.006	0.010	0.007	0.022	0.007	0.033	4	4	7	13	6	10	7
F02	0.005	0.007	0.006	0.003	0.004	0.003	0.005	4	16	8	8	8	7	3
F03	0.005	0.006	0.003	0.001	0.003	0.001	0.006	4	9	3	2	3	2	1
F04	0.006	0.006	0.003	0.001	0.005	0.002	0.005	7	13	5	5	6	6	3
F05	0.008	0.005	0.014	0.007	0.027	0.007	0.034	4	4	9	11	10	9	8
F06	0.006	0.004	0.012	0.005	0.024	0.006	0.012	5	2	7	7	8	8	3
F07	0.006	0.007	0.011	0.006	0.009	0.006	0.007	4	5	14	33	4	11	2
F08	0.006	0.007	0.011	0.005	0.030	0.004	0.003	4	5	17	23	8	7	1
F09	0.004	0.005	0.002	0.001	0.002	0.002	0.003	7	17	6	7	5	6	2
F10	0.005	0.009	0.006	0.004	0.028	0.004	0.026	3	7	4	7	9	5	6
F11	0.003	0.018	0.009	0.005	0.011	0.006	0.032	3	27	9	10	9	11	6
F12	0.005	0.013	0.002	0.001	0.003	0.001	0.004	13	61	3	4	8	2	2
F13	0.002	0.006	0.012	0.005	0.024	0.005	0.007	2	4	7	6	6	5	2
F14	0.003	0.003	0.009	0.005	0.012	0.006	0.015	4	3	16	20	5	12	4
F15	0.009	0.005	0.009	0.006	0.023	0.005	0.011	5	4	7	13	8	8	2
F16	0.003	0.001	0.001	0.001	0.008	0.001	0.014	2	1	2	4	6	2	3
Mean	0.005	0.007	0.008	0.004	0.015	0.004	0.014	5	11	8	11	7	7	4

Response surface model for parameter dependence on fermentation conditions

Table III.2-A2: *Response surface coefficients fitted to experimental data by multiple regression.*

Variable	Coefficient	μ_{maxX} (h^{-1})	π_{maxF} (h^{-1})	π_{maxA} (h^{-1})	π_{maxL} (h^{-1})	π_{maxE} (h^{-1})	KI_X (mol.L^{-1})	KI_m (mol.L^{-1})
Constant	Value (β_0)	$-1.38\cdot10^{1}$	$-1.64\cdot10^{1}$	$-1.74\cdot10^{1}$	$-1.21\cdot10^{1}$	$-1.12\cdot10^{1}$	$-8.61\cdot10^{-1}$	$1.19\cdot10^{1}$
	Standard error	$0.05\cdot10^{1}$	$0.07\cdot10^{1}$	$0.09\cdot10^{1}$	$0.09\cdot10^{1}$	$0.07\cdot10^{1}$	$0.05\cdot10^{-1}$	$0.03\cdot10^{1}$
T	Value (β_1)	$2.63\cdot10^{-1}$	$2.66\cdot10^{-1}$	$2.71\cdot10^{-1}$	$1.82\cdot10^{-1}$	$1.27\cdot10^{-1}$	$-1.87\cdot10^{-1}$	$-5.80\cdot10^{-1}$
	Standard error	$0.13\cdot10^{-1}$	$0.26\cdot10^{-1}$	$0.28\cdot10^{-1}$	$0.23\cdot10^{-1}$	$0.14\cdot10^{-1}$	$0.05\cdot10^{-1}$	$0.17\cdot10^{-1}$
pH	Value (β_2)	$2.42\cdot10^{0}$	$2.89\cdot10^{0}$	$3.01\cdot10^{0}$	$2.27\cdot10^{0}$	$2.02\cdot10^{0}$	$6.65\cdot10^{-1}$	$-1.27\cdot10^{0}$
	Standard error	$0.11\cdot10^{0}$	$0.14\cdot10^{0}$	$0.19\cdot10^{0}$	$0.16\cdot10^{0}$	$0.13\cdot10^{0}$	$0.45\cdot10^{-1}$	$0.16\cdot10^{0}$
T^2	Value (β_3)	$-4.26\cdot10^{-3}$	$-3.45\cdot10^{-3}$	$-3.26\cdot10^{-3}$	$-2.05\cdot10^{-3}$	$-1.92\cdot10^{-3}$	$3.97\cdot10^{-3}$	$7.95\cdot10^{-3}$
	Standard error	$0.13\cdot10^{-3}$	$0.32\cdot10^{-3}$	$0.33\cdot10^{-3}$	$0.81\cdot10^{-3}$	$0.22\cdot10^{-3}$	$0.09\cdot10^{-3}$	$0.32\cdot10^{-3}$
pH^2	Value (β_4)	$-1.46\cdot10^{-1}$	$-1.63\cdot10^{-1}$	$-1.66\cdot10^{-1}$	$-1.34\cdot10^{-1}$	$-1.22\cdot10^{-1}$	$-4.03\cdot10^{-2}$	$4.35\cdot10^{-2}$
	Standard error	$0.06\cdot10^{-1}$	$0.10\cdot10^{-1}$	$0.12\cdot10^{-1}$	$0.10\cdot10^{-1}$	$0.09\cdot10^{-1}$	$0.31\cdot10^{-2}$	$0.55\cdot10^{-2}$
T·pH	Value (β_5)	$-3.53\cdot10^{-3}$	$-7.58\cdot10^{-3}$	$-9.17\cdot10^{-3}$	$-7.22\cdot10^{-3}$	$-4.68\cdot10^{-3}$	$-3.54\cdot10^{-3}$	$1.86\cdot10^{-2}$
	Standard error	$0.11\cdot10^{-3}$	$0.97\cdot10^{-3}$	$1.17\cdot10^{-3}$	$0.91\cdot10^{-3}$	$0.05\cdot10^{-3}$	$0.06\cdot10^{-3}$	$0.01\cdot10^{-2}$

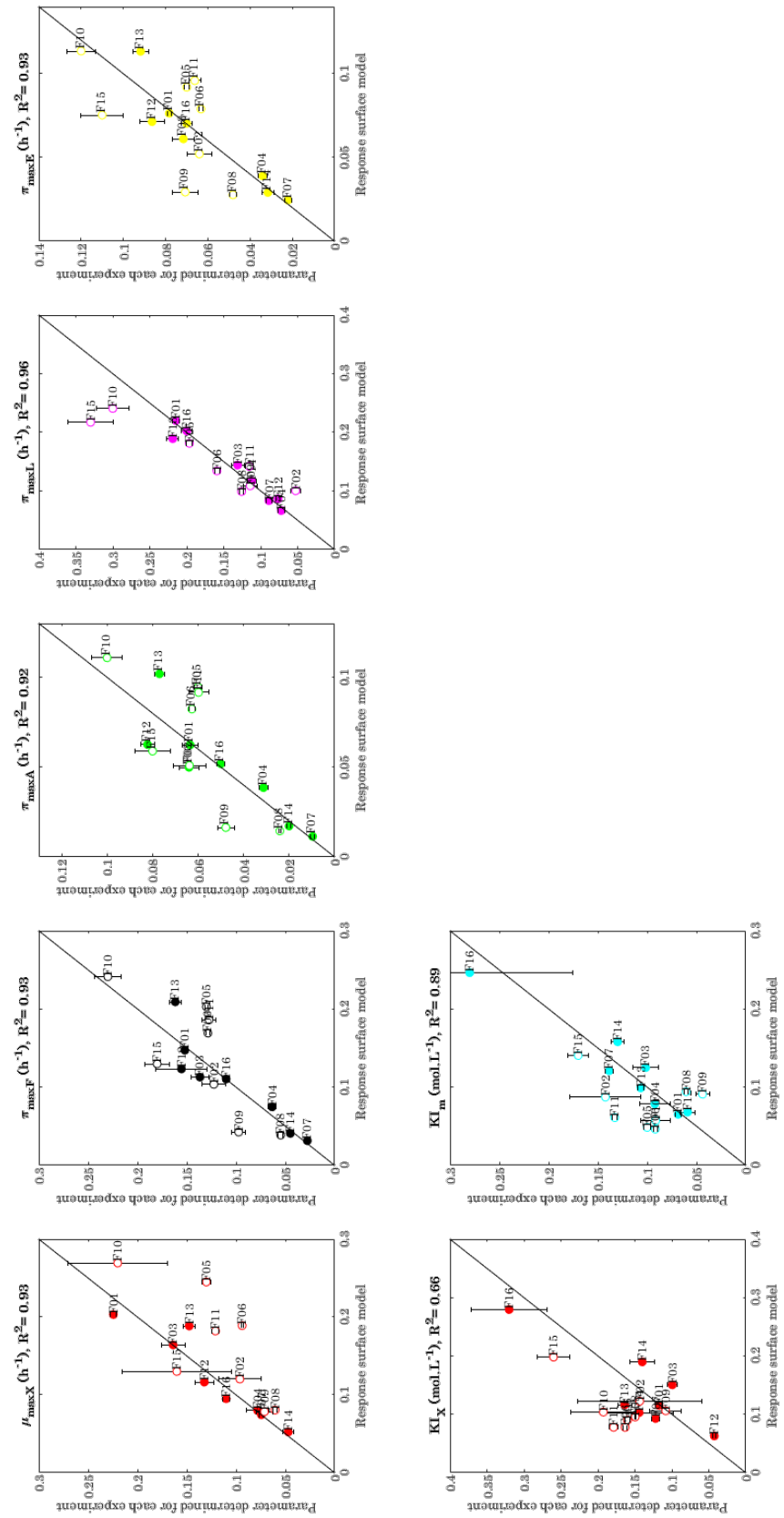

Figure III.2-A1 : *Comparison between model parameters determined for each experiment (Table III.2-2) and parameters computed with the response surface models (equation III.2-17 using coefficients in Table III.2-A1).*

Model validation

Error indicators RMSE and RME for calibration and validation sets are summarized in Annex **Table III.2-A3**. The RME values vary from 1 % to 53 % with an average of 15% for calibration set and 13 % for validation set. Likewise, the average RME is lower than 15 % for most of experiments, except for runs F12 (17 %), F15 (18 %), F09 (20 %) and F16 (34 %). Considering both calibration and validation sets, the average RME is 10 % for biomass and 14 % for substrate and metabolites.

Table III.2-A3: *Quality of fit of the model with parameters computed with the response surface models.*

Fermentation		RMSE (mol.L^{-1})							RME (%)						
		X	S	F	A	L	E	At	X	S	F	A	L	E	At
Calibration	F01	0.010	0.010	0.021	0.010	0.041	0.014	0.033	5	6	14	20	10	18	7
	F03	0.021	0.009	0.008	0.005	0.008	0.003	0.012	15	14	7	9	7	5	4
	F04	0.005	0.010	0.009	0.006	0.007	0.005	0.015	5	26	18	23	9	17	9
	F07	0.012	0.009	0.010	0.006	0.015	0.006	0.009	9	8	13	31	5	10	3
	F12	0.003	0.011	0.008	0.005	0.003	0.004	0.009	8	53	13	16	8	11	6
	F13	0.010	0.007	0.006	0.003	0.036	0.003	0.011	7	5	4	4	8	4	2
	F14	0.015	0.002	0.013	0.007	0.004	0.009	0.012	20	2	23	28	2	16	3
	F16	0.011	0.023	0.033	0.014	0.064	0.018	0.085	9	33	50	45	48	38	18
	Mean	0.011	0.010	0.014	0.007	0.022	0.008	0.023	10	18	18	22	12	15	7
Validation	F02	0.005	0.003	0.017	0.009	0.008	0.009	0.007	5	8	20	22	15	21	4
	F05	0.011	0.008	0.007	0.006	0.045	0.005	0.016	7	7	4	8	13	8	4
	F06	0.008	0.009	0.013	0.005	0.044	0.007	0.032	6	5	7	6	11	9	6
	F08	0.009	0.010	0.012	0.006	0.026	0.008	0.003	7	8	19	25	8	14	1
	F09	0.011	0.006	0.005	0.004	0.018	0.004	0.009	19	22	15	24	35	15	7
	F10	0.021	0.014	0.025	0.011	0.063	0.014	0.044	11	10	17	18	20	20	10
	F11	0.018	0.013	0.007	0.003	0.017	0.004	0.050	16	20	7	6	12	8	9
	F15	0.028	0.023	0.026	0.010	0.047	0.014	0.036	15	20	22	21	17	21	7
	Mean	0.014	0.011	0.014	0.007	0.033	0.008	0.025	11	13	14	16	16	15	6

Model-based optimization of fermentation conditions

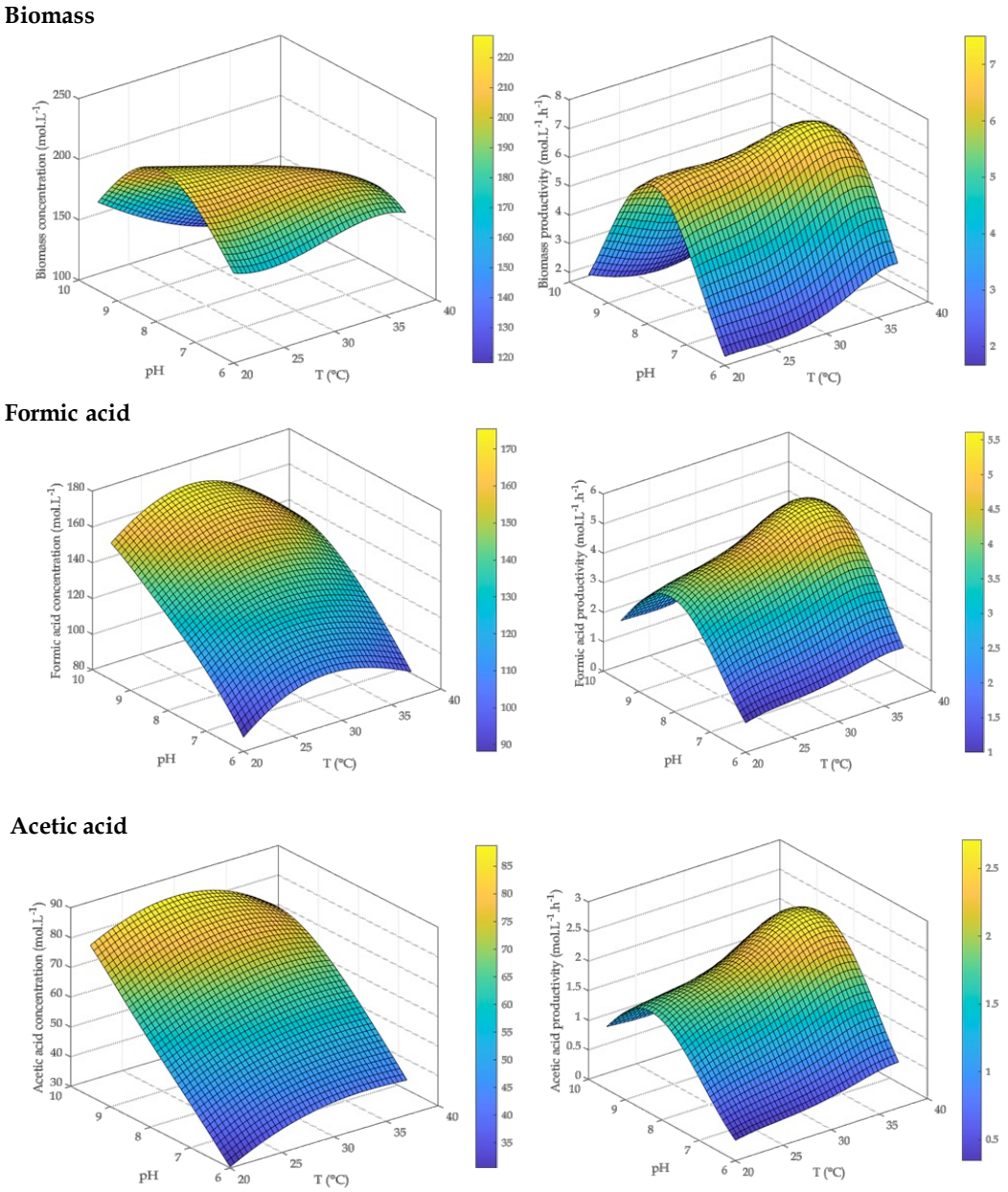

Figure III.2-A2: *Evolution of final concentrations (left) and batch-average productivities (right) with temperature and pH for biomass, formic acid and acetic acid.*

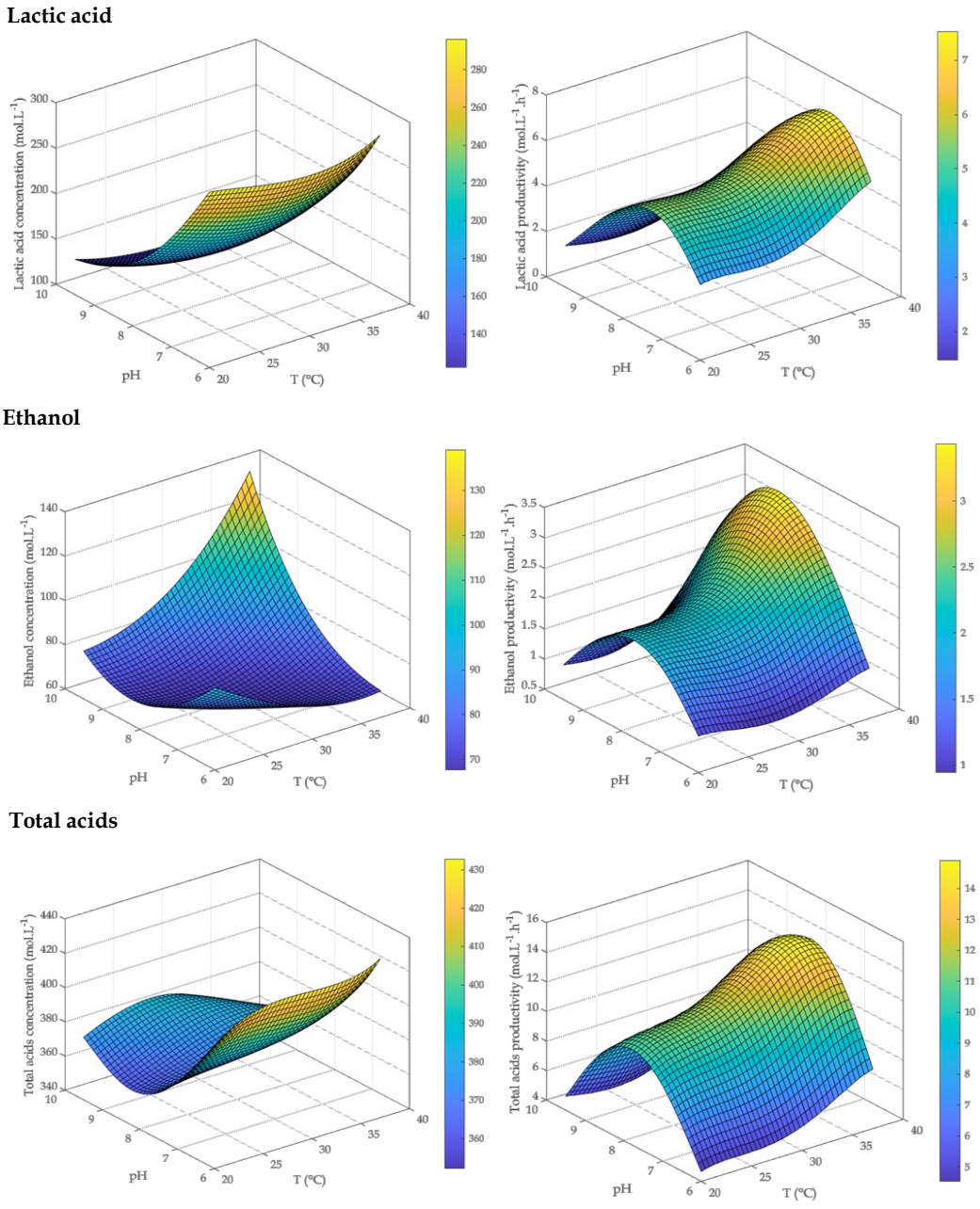

Figure III.2-A2 (continued): *Evolution of final concentrations (left) and batch-average productivities (right) with temperature and pH for lactic acid, ethanol and total acids.*

Annex A-III.3: Supplementary data of Chapter III.3

Table III.3-A1: *Assignments of main vibrational bands of the 3016—975 cm-1 region of the infrared spectra of the studied LAB, according to literature.*

Wavenumber range and~ peak position (cm^{-1})		Assignment	Main cellular compounds and compartments associated	References
this work*	**literature**			
3012-2290/~2998	~3010/3006/2997	νC=C-H	Fatty acyl chain (membrane lipids and peptidoglycan=> 2930 [9])	[1–10]
~2960	~2961/2959/2956	ν_{as}–CH_3		
~2930	~2921/2925/2918/2930	ν_{as} > CH_2		
~2873	~2875/2874/2872/2867	ν_{s}–CH_3		
~2854	~2854/2852/2850	ν_{s} > CH_2		
1754-1747/~1753	~1740/1736/1730	νC=O	Esters from lipids / membranes/peptidoglycan	[1,2,9,11,12]
1716-1652/~1714	~1715/1713	νC=O	Esters, carboxylic acids	
	1715-1680	νC=O, νC=N, νC=C, δNH	ADN/ARN bases /nucleic acids (weak features of nucleic acids often overlapped by amide I)	
	~1715/1713			
	1695-1662	Amide I (νC=O), antiparallel pleated β sheets and β-turns structures	Proteins (membranes, cytoplasm)	[1,13]
	~1695/1685/1675			
~1654	1657-1648	Amide I (νC=O), α-helical structures	Proteins (membranes, cytoplasm)	[1,10,12,13]
	~1655/1654/1656			[3]
	~1645	random coiled structures		
1641-1620 / 1632-1580	1641-1623, 1631-1627	Amide I (νC=O), antiparallel pleated β-sheet structures	Proteins (membranes, cytoplasm)	[1,3,10,10,12, 13]
~1637,	~1637, 1633, 1624			
1585-1565	~1585, 1570	νCOO- asym	Aspartate, glutamate	
1555-1525	1550-1520	Amide II (δN-H combined with νC-N)	Proteins (membranes, cytoplasm)	[1,12–14]
~1548	~1542/1540/1550			
	~1468/1470	C-H deformation /scissoring CH_2,	Proteins or fatty acyl chain (membrane lipids)	[1–3]
	~1455	C-H deformation /scissoring CH_3		
	~1400	νC=O sym of COO-	Amino acids, fatty acyl chains (peptidoglycan)	[2,3]
	~1415	νC-O sym of COO-	In phospholipids only	[3]
1300-1230	1400-1200	Amide III (νC-N combined with δN-H)	Proteins (membranes, cytoplasm)	[1,3,13–16]
	~1250, 1235			

Wavenumber range and~ peak position (cm^{-1})		Assignment	Main cellular compounds and compartments associated	References
this work*	**literature**			
1225-1212 ~1220	1250-1220, 1240-1210, 1253-1238 ~1243/1238/1218	νPO_{2-} asym	Phosphodiesters, phospholipids (membrane), teichoic acids, lipoteichoic acids (cell wall), nucleic acids (nucleoid)	[1,2,9,4,12,10]
~1085	1095-1075, 1085-1074 ~1085 ~1096	νPO2_ sym	Phosphodiesters, phospholipids (membrane), nucleic acids (nucleoid), teichoic acids (peptidoglycan)	[1,4,12,17,18]
	1200 – 900	νC-O, νC-C, C-O-C deformation, νP-O-C, νP-O-P	Polysaccharides, sugar rings (cell wall, peptidoglycan)	
~1155	1155-1130			[1,2,9,4,18,19, 12]
~1120/1135-1118	1100-1112/~1117			
~1058	1067-1060/1057, 1076-1052			
~1037	1046-1035, 1045-1010			
~995	994-996, ~993	νC-O ribose, νC-C	Ribose skeleton (ARN) ribosomes, sugars	[2,4]

(ν: stretching, δ: bending, sym.: symmetric, asym.: antisymmetric);
* ~peak positions and wavenumber ranges obtained from Figures III.3-6 to 9 and III.3-A1 to A3.
Fourteen [1–3, 5–7,9–12,14,17–19] over nineteen reported works in table III.3-A1 were carried out on micro-organisms.

References cited in Table A1

1. Naumann D. Infrared Spectroscopy in Microbiology. In: Meyers RA, editor. Encyclopedia of Analytical Chemistry [Internet]. Chichester, UK: John Wiley & Sons, Ltd; 2006 [cited 2020 Mar 29]. p. a0117. Available from: http://doi.wiley.com/10.1002/9780470027318.a0117

2. Quilès F, Humbert F, Delille A. Analysis of changes in attenuated total reflection FTIR fingerprints of Pseudomonas fluorescens from planktonic state to nascent biofilm state. Spectrochim Acta A [Internet]. 2010 [cited 2020 Mar 16];75:610–6. Available from: https://linkinghub.elsevier.com/retrieve/pii/S1386142509006027

3. Le Gal J-. M, Manfait M, Theophanides T. Applications of FTIR spectroscopy in structural studies of cells and bacteria. J Mol Struct. 1991;242:397–407.

4. Movasaghi Z, Rehman S, Rehman I. Fourier Transform Infrared (FTIR) Spectroscopy of Biological Tissues. Appl Spectrosc Rev [Internet]. 2008 [cited 2015 Feb 4];43:134–79. Available from: http://www.tandfonline.com/doi/abs/10.1080/05704920701829043

5. Saulou C, Jamme F, Girbal L, Maranges C, Fourquaux I, Cocaign-Bousquet M, et al. Synchrotron FTIR microspectroscopy of Escherichia coli at single-cell scale under silver-induced stress conditions. Anal Bioanal Chem [Internet]. 2013 [cited 2015 Feb 4];405:2685–97. Available from: http://link.springer.com/10.1007/s00216-013-6725-4

6. Lasch P, Naumann D. Infrared Spectroscopy in Microbiology. In: Meyers RA, editor. Encyclopedia of Analytical Chemistry [Internet]. Chichester, UK: John Wiley & Sons, Ltd; 2015 [cited 2020 Mar 29]. p. 1–32. Available from: http://doi.wiley.com/10.1002/9780470027318.a0117.pub2

7. Dianawati D, Mishra V, Shah NP. Role of Calcium Alginate and Mannitol in Protecting Bifidobacterium . Appl Environ Microbiol [Internet]. 2012 [cited 2015 Feb 4];78:6914–21. Available from: http://aem.asm.org/cgi/doi/10.1128/AEM.01724-12

8. Arrondo JLR, Goni FM. Infrared studies of protein-induced perturbation of lipids in lipoproteins and membranes. Chemistry and Physics of Lipids. 1998;96:53–68.

9. Naumann D, Barnickel G, Bradaczek H, Labischinski H, Giesbrecht P. Infrared spectroscopy, a tool for probing bacterial peptidoglycan: Potentialities of infrared spectroscopy for cell wall analytical studies and rejection of models based on crystalline chitin. Eur J Biochem [Internet]. 1982 [cited

2020 Mar 16];125:505–15. Available from: http://doi.wiley.com/10.1111/j.1432-1033.1982.tb06711.x

10. Passot S, Gautier J, Jamme F, Cenard S, Dumas P, Fonseca F. Understanding the cryotolerance of lactic acid bacteria using combined synchrotron infrared and fluorescence microscopies. Analyst [Internet]. 2015 [cited 2018 Nov 2];140:5920–8. Available from: http://xlink.rsc.org/?DOI=C5AN00654F

11. Santivarangkna C, Wenning M, Foerst P, Kulozik U. Damage of cell envelope of <i>Lactobacillus helveticus<i> during vacuum drying. J Appl Microbiol [Internet]. 2007 [cited 2015 Feb 4];102:748–56. Available from: http://doi.wiley.com/10.1111/j.1365-2672.2006.03123.x

12. Meneghel J, Passot S, Jamme F, Lefrançois S, Lieben P, Dumas P, et al. FTIR micro-spectroscopy using synchrotron-based and thermal source-based radiation for probing live bacteria. Anal Bioanal Chem [Internet]. 2020 [cited 2020 Nov 19];412:7049–61. Available from: http://link.springer.com/10.1007/s00216-020-02835-x

13. Barth A. Infrared spectroscopy of proteins. Biochim Biophys Acta Bioenergetics [Internet]. 2007 [cited 2015 Feb 4];1767:1073–101. Available from: http://linkinghub.elsevier.com/retrieve/pii/S0005272807001375

14. Filip Z, Herrmann S, Kubat J. FT-IR spectroscopic characteristics of differently cultivated Bacillus subtilis. Microbiol Res [Internet]. 2004 [cited 2020 Mar 16];159:257–62. Available from: https://linkinghub.elsevier.com/retrieve/pii/S0944501304000473

15. Cai S, Singh BR. A Distinct Utility of the Amide III Infrared Band for Secondary Structure Estimation of Aqueous Protein Solutions Using Partial Least Squares Methods †. Biochemistry [Internet]. 2004 [cited 2021 Aug 16];43:2541–9. Available from: https://pubs.acs.org/doi/10.1021/bi030149y

16. Fu F-N, Deoliveira DB, Trumble WR, Sarkar HK, Singh BR. Secondary Structure Estimation of Proteins Using the Amide III Region of Fourier Transform Infrared Spectroscopy: Application to Analyze Calcium-Binding-Induced Structural Changes in Calsequestrin. Appl Spectrosc [Internet]. 1994 [cited 2021 Aug 16];48:1432–41. Available from: http://journals.sagepub.com/doi/10.1366/0003702944028065

17. Kochan K, Perez-Guaita D, Pissang J, Jiang J-H, Peleg AY, McNaughton D, et al. In vivo atomic force microscopy–infrared spectroscopy of bacteria. J R Soc Interface [Internet]. 2018 [cited 2021 Aug 10];15:20180115. Available from: https://royalsocietypublishing.org/doi/10.1098/rsif.2018.0115

18. Hlaing MM, Wood BR, McNaughton D, Ying D, Dumsday G, Augustin MA. Effect of drying methods on protein and DNA conformation changes in Lactobacillus rhamnosus GG cells by Fourier transform infrared spectroscopy. J Agric Food Chem [Internet]. 2017 [cited 2021 Aug 10];65:1724–31. Available from: https://pubs.acs.org/doi/10.1021/acs.jafc.6b05508

19. Jiang W, Saxena A, Song B, Ward BB, Beveridge TJ, Myneni SCB. Elucidation of Functional Groups on Gram-Positive and Gram-Negative Bacterial Surfaces Using Infrared Spectroscopy. Langmuir. 2004;20:11433–42.

Table III.3-A2: *Biological activity losses (culturability loss determined by plate counts method and acidification activity loss determined with the Cinac system (Corrieu et al. 1988)) following multiple freeze-thaw cycles of C. maltaromaticum CNCM I-3298, L. bulgaricus ATCC 11842 and L. bulgaricus CFL1 and cells. For every freeze-thaw cycle, the loss was calculated versus the previous freeze-thaw cycle, as described in the Materials and Methods section of the manuscript. L. bulgaricus strains were protected with 20 % sucrose in saline water (weight ratio protective solution: cells = 1:1) and C. maltaromaticum with 20 % trehalose in saline water (weight ratio protective solution:cells = 1:2).*

Culturability loss (log(CFU.mL^{-1}))

Freeze-thaw cycle	*C. maltaromaticum* CNCM I-3298	*L. bulgaricus* ATCC 11842	*L. bulgaricus* CFL1
1	-0.18 ^{a}	-0.26 ^{a}	-1.46 ^{b}
2	-0.18 ^{a}	0.06 ^{a}	-0.16 ^{ab}
3	0.01 ^{a}	-0.02 ^{a}	-1.09* ^{ab}
4	0.55 ^{a}	-0.63 ^{ab}	-0.39* ^{ab}
5	-0.21 ^{a}	NA	NA
6	0.19 ^{a}	NA	NA
7	-0.10 ^{a}	NA	NA

Acidifying activity loss (min)

Freeze-thaw cycle	*C. maltaromaticum* CNCM I-3298	*L. bulgaricus* ATCC 11842	*L. bulgaricus* CFL1
1	0 ^{a}	23 ^{ab}	261 ^{c}
2	1 ^{ab}	15 ^{abc}	16 ^{abc}
3	10 ^{ab}	11 ^{ab}	7* ^{ab}
4	3 ^{ab}	45 ^{ab}	82* ^{bc}
5	9 ^{ab}	NA	NA
6	4 ^{ab}	NA	NA
7	8 ^{ab}	NA	NA

Most data presented are medians of three or more biological replicates (medians of two replicates are indicated by (*))
Superscript letters (a, b, c) represent, for each variable, statistical differences between all samples in the table at the 95 % confidence level; NA: data not available

Table III.3-A3: *Comparison of biological activity losses following one freeze-thaw cycle of C. maltaromaticum CNCM I-3298 cells protected with sucrose in similar conditions as L. bulgaricus ATCC 11842 and L. bulgaricus CFL1 strains (ratio cells:protective solution 1:1) and with trehalose at two different ratios (1:1 and 1:2)*

Culturability loss (log(CFU.mL^{-1}))

Protective solution / ratio	*C. maltaromaticum* CNCM I-3298	*L. bulgaricus* ATCC 11842	*L. bulgaricus* CFL1
Sucrose / 1:1	0.31 ^{a}	-0.26 ^{a}	-1.46 ^{b}
Trehalose / 1:2	-0.18 ^{a}	NA	NA
Trehalose / 1:1	0.10 ^{a}	NA	NA

Acidifying activity loss (min)

Protective solution / ratio	*C. maltaromaticum* CNCM I-3298	*L. bulgaricus* ATCC 11842	*L. bulgaricus* CFL1
Sucrose / 1:1	0 ^{ab}	23 ^{b}	261 ^{c}
Trehalose / 1:2	0 ^{a}	NA	NA
Trehalose / 1:1	4 ^{ab}	NA	NA

Data presented are medians of three or more biological replicates
Superscript letters (a, b, c) represent, for each variable, statistical differences between all samples in the table, at the 95 % confidence level; NA: data not available

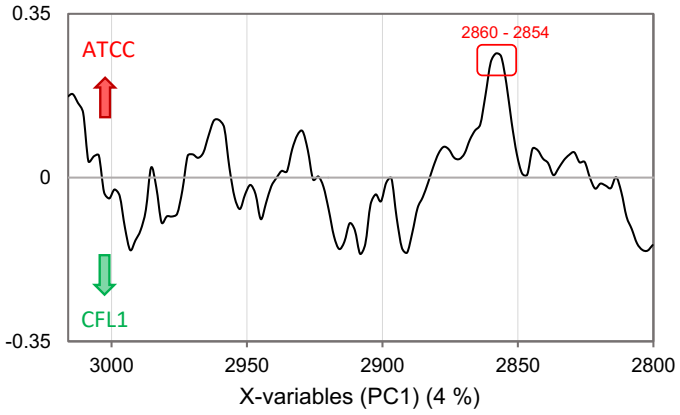

Figure III.3-A1: *PC2 loading plot of the principal component analysis (PCA) of FTIR spectra in the 3016 – 2800 cm^{-1} region presented in Figure 6 of the results section (ATCC: L. bulgaricus ATCC 11842; CFL1: L. bulgaricus CFL1).*

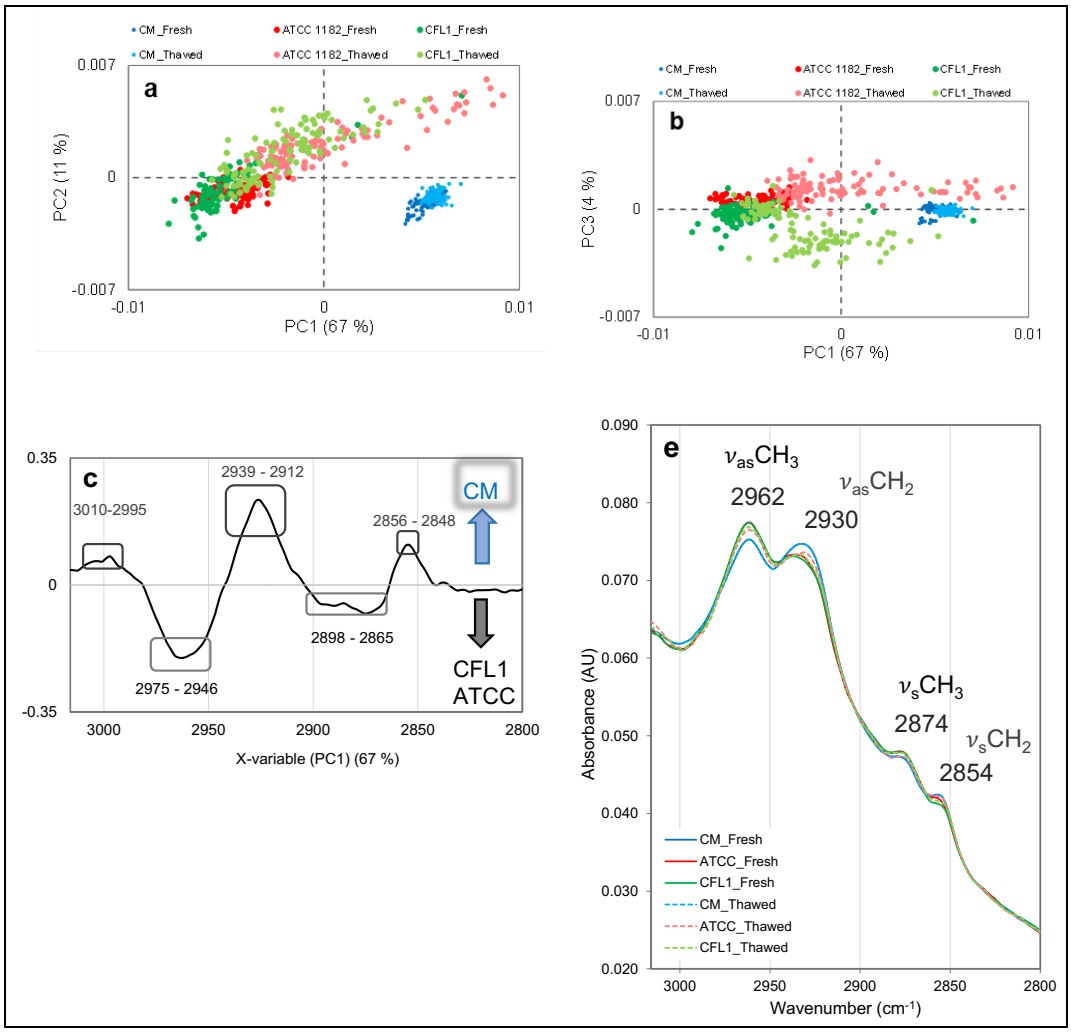

Figure III.3-A2: *Principal component analysis (PCA) of FTIR spectra of fresh and thawed C. maltaromaticum CNCM I-3298 (CM), L. bulgaricus ATCC 11842 (ATCC) and L. bulgaricus CFL1 (CFL1) cells, acquired in an aqueous environment in the 3016 cm^{-1} to 2800 cm^{-1} region:* ***a*** *PC1 versus PC2 score plots explaining 67 % and 11 % of variance, respectively;* ***b*** *PC1 versus PC3 score plots explaining 67 % and 4 % of variance, respectively;* ***c*** *loading plot of PC1, separating mainly CM from ATCC and CFL1 and indicating the heterogeneity provoked by freeze-thawing on L. bulgaricus cells and homogeneity of CM;* ***d*** *Mean spectra of the fresh and thawed cells used for the PCA. The characteristic absorption bands arising from fatty acid chains are indicated.*

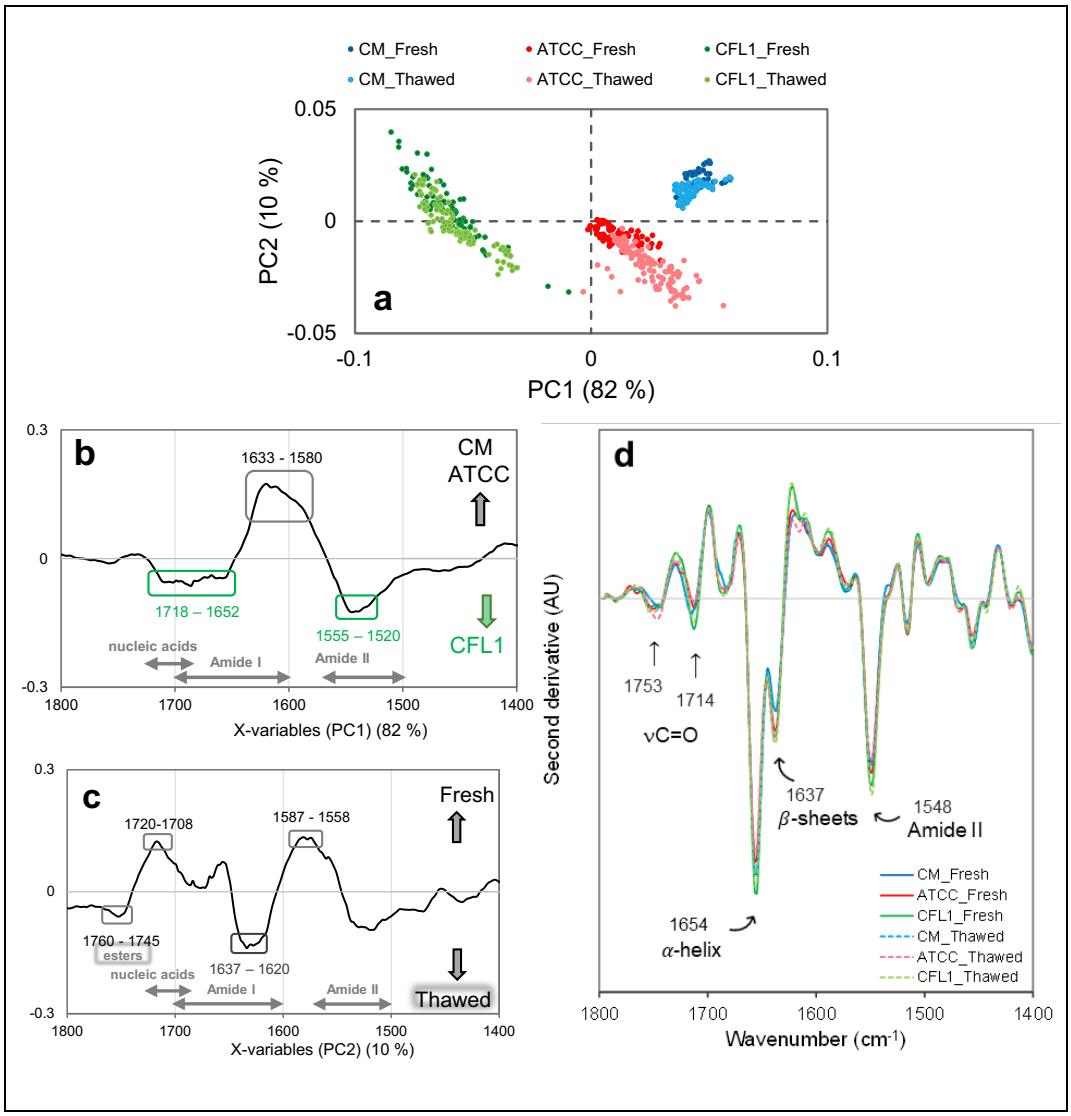

Figure III.3-A3: *Principal component analysis (PCA) of FTIR spectra of fresh and thawed C. maltaromaticum CNCM I-3298 (CM), L. bulgaricus ATCC 11842 (ATCC) and L. bulgaricus CFL1 (CFL1) cells, acquired in an aqueous environment in the 1800 cm^{-1} to 1370 cm^{-1} range:* ***a*** *PC1 versus PC2 score plots explaining 82 % and 10 % of variance, respectively;* ***b*** *loading plot of PC1, separating mainly CM and ATCC from CFL1;* ***c*** *loading plot of PC2, indicates the changes in absorption bands from fresh to thawed cells;* ***d*** *Mean second derivatives of the spectra of fresh and thawed cells used for the PCA. The characteristic absorption bands arising from the protein backbone vibrations (Amide I and Amide II) and carboxyl groups of esters and nucleic acids are indicated.*

RESUMÉ SUBTANTIEL EN FRANCAIS

La fermentation est une méthode de conservation des aliments utilisée depuis des siècles. Elle exploite la capacité des bactéries lactiques (entre autres microorganismes) à coloniser et à acidifier leur environnement en produisant de l'acide lactique, inhibant ainsi la croissance d'agents pathogènes et autres microorganismes d'altération. Cette propriété technologique des bactéries lactiques est encore largement utilisée aujourd'hui pour produire toute une gamme d'aliments fermentés, tels que le yaourt, le fromage, les charcuteries, la choucroute ou le kimchi. Le marché des concentrés de ferments lactiques (*starters*) est en plein essor, en raison du développement croissant de produits ou suppléments alimentaires fonctionnels tels que les yaourts végétaux ou encore les probiotiques. Cette famille de microorganismes est aussi d'une grande importance dans les biotechnologies, un domaine en forte expansion. Les bactéries lactiques sont en effet capables d'utiliser divers substrats provenant de ressources renouvelables pour produire des produits chimiques d'intérêt industriel. Ces dernières années, la propriété acidifiante des bactéries lactiques est utilisée dans les intégrateurs temps-température biologiques, pour suivre la durée de vie des aliments périssables.

Les intégrateurs temps-température (ITT) fonctionnent comme des "étiquettes intelligentes" qui transmettent, par un signe facilement interprétable et irréversible, l'historique temps-température et la qualité de l'aliment auquel elles sont attachées. Les ITT biologiques sont généralement basés sur la baisse du pH du milieu contenu dans l'étiquette, engendrée par la croissance et à l'acidification des bactéries lactiques. En cas d'accident thermique (rupture plus ou moins importante de la chaîne du froid), les bactéries contenues dans l'étiquette se développent et acidifient leur milieu. Cela provoque un changement de couleur et/ou une réaction d'opacification indiquant une altération significative de l'aliment suivit, et donc l'aboutissement de sa date limite de consommation (DLC). La vitesse à laquelle l'ITT atteint son point final dépend donc de la cinétique de croissance et d'acidification de la souche bactérienne, en réponse à un profil temps-température donné.

À ce jour, Cryolog Clock-°T (Nantes, France) est la seule société ayant mis sur le marché un ITT biologique. Leurs étiquettes reposent sur la croissance et l'acidification de *Carnobacterium maltaromaticum* CNCM I-3298, une bactérie lactique que l'on peut couramment trouver dans les fromages à pâte molle et

autres aliments à haute teneur protéique tels que les poissons et les viandes fumés. Dans leur dernière gamme d'étiquettes (TopCryo®), la croissance de *C. maltaromaticum* induit une acidification du milieu de l'étiquette, entraînant son changement de couleur du vert au rouge (brevet européen n° EP 1 664 334). Les concentrés de *Carnobacterium maltaromaticum* utilisés pour inoculer les étiquettes TopCryo® sont produits comme d'autres ferments lactiques, par une succession d'étapes : fermentation, concentration, protection, stabilisation (par congélation ou lyophilisation) et stockage. Pour produire les étiquettes ITT, des concentrés bactériens congelés sont d'abord décongelés puis un volume précis de la suspension cellulaire est mélangé au milieu de l'étiquette, en fonction de la DLC souhaitée (ex : faibles concentrations pour DLC longues). Les étiquettes sont ensuite stabilisée par congélation et stockées à -80°C jusqu'à leur utilisation. Ces étiquettes sont activées par une décongélation rapide à température ambiante. La DLC exprimée par ces ITT dépend donc à la fois de la concentration des cellules et de leur activité acidifiante. Les DLC couvertes par les étiquettes TopCryo® varient de 30 h à 192 h (8 jours) à 4 °C. La DLC de 30 heures est atteinte en inoculant l'étiquette avec la plus forte concentration cellulaire possible, au-delà de laquelle la couleur initiale de l'ITT ne serait plus verte. La DLC de 8 jours est obtenue par analogie en inoculant l'étiquette avec la plus faible concentration cellulaire permettant des cinétiques d'acidification reproductibles. Les temps de réponse au changement de couleur de 30 heures et 8 jours à 4 °C correspondent donc respectivement à la DLC la plus courte et à la plus longue obtenue par les étiquettes TopCryo®. Cependant, de nombreux aliments périssables ont des DLC au-delà de la gamme proposée par Cryolog. Les dates de péremption des produits carnés, par exemple, varient entre 3 et 21 jours, et celles des crustacés entre 0,5 et 3 jours. Souhaitant augmenter la durée de conservation de ses étiquettes ITT, Cryolog a contacté le groupe de recherche ProBioSSep - dans lequel j'ai effectué la majeure partie de mon travail de doctorat - pour explorer les moyens de moduler la croissance et l'activité acidifiante de *C. maltaromaticum* CNCM I-3298 dans ses ITT.

ProBioSSep, est une équipe de recherche spécialisée dans l'étude de la production et de la stabilisation de bactéries lactiques. Une grande partie de leurs travaux visent à caractériser l'impact de conditions de culture sur l'état physiologique et les propriétés technologiques de ferments lactiques, tels que leur activité acidifiante, mais aussi leur résistance à des procédés de stabilisation industriels tels que la congélation et la lyophilisation. Bien que la congélation soit l'une des techniques les plus couramment utilisées pour la préservation de micro-organismes (maintien de leurs fonctionnalités sur de longues périodes), elle expose néanmoins les cellules à des stress importants. Selon la population bactérienne, ces stress peuvent conduire à une perte plus ou moins significative de leur activité biologique (perte de viabilité et/ou d'activité acidifiante). Cependant, dans le cas de *C. maltaromaticum*, une étude a montré que 11 cycles de congélation-décongélation

n'ont pas eu d'effet significatif sur la viabilité des cellules, indiquant ainsi que la souche est extrêmement cryorésistante (Walker et al. 2006).

Un programme européen d'échange de personnel RISE intitulé PREMIUM a été initié en 2017 entre cinq partenaires académiques européens et trois partenaires industriels européens : ce projet, coordonné par Fernanda Fonseca de ProBioSSep, est consacré à l'étude et au développement de stratégies innovantes pour la préservation à long terme des bactéries lactiques, tout en considérant la qualité du produit, les conditions des procédés et leurs impacts environnementaux (www.inrae.fr/premium). Les activités des membres de PREMIUM sont principalement axées sur la compréhension des mécanismes de résistance des bactéries lactiques à divers procédés de stabilisation, sur la compréhension des mécanismes de protection présentés par les cryoprotecteurs à base d'oligosaccharides pendant la stabilisation des cellules, ainsi que sur le développement d'outils analytiques rapides pour la caractérisation et le criblage des cellules et des cryoprotecteurs. Cryolog Clock-°T fût l'un des premiers partenaires industriels de PREMIUM, proposant *C. maltaromaticum* CNCM I-3298 comme souche modèle de cryorésistance dans le cadre du projet.

Un an et demi après le début de mon doctorat, Cryolog Clock-T° a déposé le bilan. À ce moment-là, j'avais quantifié l'impact de trois paramètres de fermentation (température, pH et temps de récolte) sur l'activité d'acidifiante des concentrés de *C. maltaromaticum*, ce qui a conduit à un modèle prédictif pour la production d'inoculas pour étiquette ITT pouvant étendre la gamme de durée de conservation offerte par Cryolog. La perte du financement de Cryolog a toutefois entraîné une réorientation de mes recherches vers l'étude des caractéristiques cellulaire de *C. maltaromaticum* dans le cadre du projet PREMIUM.

Dans ce contexte, mon travail de doctorat visait initialement à améliorer les performances des concentrés de *C. maltaromaticum* en vue de leur utilisation dans des intégrateurs temps-température biologiques. Une attention particulière a été portée sur la modulation de l'état physiologique de *C. maltaromaticum* pour l'obtention de cellules présentant une large gamme d'activités d'acidifiante.
J'ai ensuite focalisé mon travail sur l'exploration des mécanismes cellulaires exprimés par *C. maltaromaticum* lui conférant sa cryorésistance exceptionnelle. À cet égard, le premier objectif de ma thèse était d'étudier la modulation de l'état physiologique des concentrés de *C. maltaromaticum* en réponse à des changements des conditions de production. L'objectif suivant était de caractériser la remarquable cryorésistance de *C. maltaromaticum* par rapport à d'autres souches de bactéries lactiques.

Principaux résultats

1. Développement d'un modèle utilisant la méthode des surfaces de réponses, basé sur la modification de la température de fermentation, du pH et du temps de récolte, pour produire des concentrés de *C. maltaromaticum* présentant différentes activités acidifiantes.

L'influence de trois principaux paramètres de fermentation (température, pH et temps de récolte) sur les propriétés technologiques (viabilité, activité d'acidifiante et résistance à la congélation) de *C. maltaromaticum* a été évaluée en cultivant les cellules à différentes températures (20 à 37 °C) et pH (6,0 à 9,5) selon un plan composite centré et en les récoltant à des temps croissants jusqu'à 10 heures de phase stationnaire. Bien que la température de fermentation ait aussi modulé l'activité acidifiante, le pH et le temps de récolte ont été identifiés comme les principaux paramètres de fermentation ayant un impact sur l'activité d'acidifiante des concentrés récoltés. La croissance sous pH acide (pH 6) et une récolte en début de phase de croissance stationnaire ont permis la production de concentrés présentant des activités acidifiantes rapides. La croissance sous pH alcalin (pH 9,5) et une récolte quatre à six heures après le début de la phase stationnaire ont conduit à des concentrés présentant des activités acidifiantes lentes. La croissance dans ces conditions de culture extrêmes n'a pas eu d'incidence sur la résistance à la congélation et à la décongélation des cellules récoltées, confirmant ainsi l'exceptionnelle cryorésistance de la souche.

Ces travaux ont permis le développement d'un modèle capable de prédire l'activité acidifiante des concentrés de *C. maltaromaticum* récoltés, en fonction de la température, du pH et de la durée de leur fermentation (Girardeau et al. 2019).

2. Développement d'un modèle dynamique décrivant la croissance de *C. maltaromaticum* et sa production de métabolites dans un bioréacteur à l'échelle pilote

L'étude présentée ci-dessus a fourni des informations sur l'impact des stress de température et de pH pendant la fermentation sur l'activité acidifiante ultérieure des concentrés récoltés. Dans cette étude, l'accent a été mis sur l'impact de ces contraintes sur la croissance et l'activité métabolique des cellules pendant la fermentation (c'est-à-dire avant la récolte). L'objectif ensuite, était de développer un modèle dynamique capable de définir les valeurs de température et de pH permettant d'optimiser les cultures industrielles de *C. maltaromaticum*. Le seul modèle dynamique traitant de *C. maltaromaticum* avait été publié par Ellouze et al. (2008). Cependant, cette recherche a été effectuée sur des cellules dans un milieu de croissance mimant de la chair à saucisse, au lieu d'un bioréacteur et considérant l'acide lactique comme seul métabolite produit. Bien que les

carnobactéries soient considérées comme homofermentaires, il a été démontré que leur production d'acides est souche-dépendante. Une étude récente a d'ailleurs montré que *C. maltaromaticum* peut produire de l'acide formique et acétique en plus de l'acide lactique, dans un milieu de jus de viande (Zhang et al. 2019).
Dans notre étude, des données cinétiques sur la croissance cellulaire, la production d'acide total, la consommation de substrat et la production de métabolites ont été recueillies au cours de 16 fermentations indépendantes, couvrant une large gamme de conditions de culture (températures entre 20 et 37 °C ; pH entre 6,0 et 9,5).

Ces données ont permis le développement d'un modèle dynamique prédisant avec une précision satisfaisante, la croissance de *C. maltaromaticum* ainsi que la conversion de tréhalose en quatre métabolites primaires (acide lactique, acide acétique, acide formique et éthanol), dans une large gamme de conditions de température et de pH (Puentes, Girardeau et al. 2021). Le modèle a été utilisé avec succès pour déterminer les conditions de fermentation permettant de maximiser ou minimiser concentrations finales et productivités de la biomasse et des métabolites sélectionnés.

3. Identification de marqueurs de dommages cellulaire et de résistance à la congélation chez les bactéries lactiques

A ce stade, il a ainsi été démontré que la croissance dans une large gamme de conditions de stress modifiait de nombreuses caractéristiques cellulaires de *C. maltaromaticum* (taux de croissance, production de métabolites, activité acidifiante des concentrés récoltés). Cependant, ces changements n'ont pas eu d'impact sur la capacité des cellules à résister à la congélation, suggérant que la souche présentait probablement des mécanismes de cryorésistance robustes, la faisant un modèle intéressant pour la recherche en cryobiologie.
Dans le but d'identifier les marqueurs de dommage cellulaire à la congélation et de cryorésistance des bactéries lactiques, les propriétés biophysiques et biochimiques des cellules fraîches et décongelées de *C. maltaromaticum* ont été comparées à celles de deux autres bactéries lactiques : *L. bulgaricus* ATCC 11842, présentant une cryorésistance intermédiaire et *L. bulgaricus* CFL1, présentant la cryorésistance la plus faible parmi les trois souches.

Marqueurs de dommages à la congélation

La recherche de marqueurs de dommage à la congélation a été effectuée en comparant la caractérisation biochimique de chaque souche, avant et après congélation-décongélation. Ceci a été fait en utilisant une approche micro-spectroscopique infrarouge à transformée de Fourier (IRTF) récemment

développée par Meneghel et al. (2020), permettant l'investigation simultanée de tous les composants cellulaires, en conditions aqueuses.
Aucune différence biochimique n'a été observée entre les cellules fraîches et décongelées de *C. maltaromaticum*. Des différences spectrales ont toutefois été observées chez les souches de *L. bulgaricus*, plus cryosensibles, en particulier dans les régions associées aux protéines et aux composants de la paroi cellulaire. Peu d'études sur les bactéries lactiques avaient jusqu'à présent examiné l'effet de la congélation sur les composants cellulaires autres que la membrane, et il s'agit de la première étude réalisée sur des cellules en milieu aqueux.

- Changements dans la conformation des protéines

Des réductions significatives des rapports d'intensité des bandes α-hélice sur β-feuillets ont été mesurées dans les cellules décongelées de *L. bulgaricus*, avec la souche ATCC 11842 présentant une réduction plus faible que la souche CFL1, la plus cryosensible. Une diminution de la contribution des structures protéiques α-hélicoïdales par rapport aux structures en β-feuillets semble donc être liée à la sensibilité à la congélation et pourrait être un marqueur de dommage cellulaire suite à la congélation-décongélation.

- Réduction de l'intensité des bandes provenant des composants de la paroi cellulaire

Une diminution des contributions spectrales des bandes associées aux groupes phosphodiester (provenant probablement des acides teichoïques) et des anneaux de sucre complexes (provenant du peptidoglycane) a également été mesurée dans les cellules décongelées de *L. bulgaricus*. Les différences d'intensité étaient nettement plus marquées chez *L. bulgaricus* CFL1, suggérant que la paroi cellulaire pourrait également être une cible de dommage à la congélation. Ce marqueur pourrait déterminer la sensibilité d'une population bactérienne à la congélation.

Marqueurs de cryorésistance

La recherche de marqueurs de cryorésistance a été effectuée en étudiant les différences entre les caractéristiques cellulaires des trois souches. Leurs propriétés membranaires cytoplasmiques ont été comparées : leur température de transition de la membrane lipidique, évaluée par spectroscopie IRTF dynamique, leur fluidité membranaire par mesure d'anisotropie de fluorescence et leur composition en acides gras, par GC-MS. En outre, les différences dans leurs caractéristiques biochimiques globales ont été évaluées à l'aide de la même approche micro-spectroscopique IRTF mentionnée ci-dessus.

- Propriétés de la membrane cytoplasmique favorisant une membrane plus fluide autour de la température de nucléation de l'eau

C. maltaromaticum a présenté la température de transition lipidique membranaire la plus basse parmi les trois souches étudiées. La transition de sa membrane lipidique d'une phase fluide (liquide cristalline) à une phase gel plus rigide s'est produite à une température inférieure à celle de la nucléation de l'eau. Dans le cas des souches de *L. bulgaricus*, leur membrane était déjà en phase de gel lorsque la formation de cristaux de glace a commencé. Cela indique que la membrane lipidique de *C. maltaromaticum*, contrairement aux souches de *L. bulgaricus*, était encore dans un état fluide pendant la déshydratation des cellules causée par la cryoconcentration de la matrice extracellulaire, facilitant probablement ainsi l'efflux d'eau et limitant les contraintes mécaniques sur la membrane cellulaire pendant la congélation. La plus grande fluidité membranaire de *C. maltaromaticum* par rapport aux deux autres souches à des températures de congélation, a été confirmée par le niveau plus élevé de désorganisation de ses chaînes grasses (fréquences plus élevées des bandes $\nu_s CH_2$) mesuré à -48 °C, et ses valeurs d'anisotropie plus faibles à 0°C. En outre, *C. maltaromaticum* a présenté le rapport d'acides gras insaturés sur saturés (UFA:SFA) le plus élevé parmi les trois souches, ce qui est bien connu dans la littérature pour conduire à une fluidité membranaire élevée (Fonseca et al. 2019).

Cette étude a donc confirmé que de faibles températures de transition membranaire, des fréquences élevées de la bande $\nu_s CH_2$ à des températures inférieures à zéro, de faibles valeurs d'anisotropie à 0 °C et des rapports UFA:SFA élevés sont tous des marqueurs de cryorésistance.

- Intensités plus élevées des bandes d'absorbance IRTF associées au peptidoglycane de la paroi cellulaire

Les souches les plus cryorésistantes (*C. maltaromaticum* et *L. bulgaricus* ATCC 11842) étaient caractérisées par des bandes d'absorbance plus élevées provenant des modes d'anneaux de sucre complexes du peptidoglycane par rapport à la souche cryosensible, suggérant ainsi que le peptidoglycane est probablement impliqué dans des mécanismes de cryorésistance.

Perspectives

3. Perspectives à court terme

o En rapport avec le développement des ITT

- Modification de la composition du milieu de fermentation de *C. maltaromaticum* pour moduler davantage l'état physiologique des concentrés récoltés

L'approche réalisée pour moduler l'état physiologique de *C. maltaromaticum* dans la première partie de la thèse, s'est uniquement concentrée sur la température, le pH et la phase de croissance lors de la récolte. Cependant, la modification de la composition du milieu de fermentation pourrait également être un levier pertinent pour accélérer ou ralentir l'activité métabolique des concentrés récoltés.
Il a été démontré que la vitesse de croissance et l'activité acidifiante de *C. maltaromaticum* LM28 dans le lait augmentaient lorsque le lait était enrichi avec 1 g/L d'extrait de levure (Edima et al. 2008). Une étude préliminaire sur l'effet que pourrait avoir l'augmentation de la quantité de protéose peptone (un ingrédient riche en acides aminés) sur la croissance et l'activité acidifiante de *C. maltaromaticum* CNCM I-3298 a donc été entamée par Wenfan Cao, dans le cadre de son stage de fin d'études d'ingénieur au laboratoire SayFood (INRAE, France). Les résultats semblent indiquer que l'activité acidifiante de *C. maltaromaticum* pourrait effectivement être améliorée en augmentant la quantité de protéose peptone dans le milieu de fermentation. Des expériences supplémentaires doivent cependant être réalisées pour confirmer ce résultat. Des recherches pourraient également être menées sur l'effet de la modification de la source carbonée de la fermentation. Il a été démontré que la production d'acide acétique par *C. maltaromaticum* augmente par rapport à l'acide lactique si le glucose est remplacé par du ribose (Leisner et al. 2007). L'acide acétique ayant un pKa plus élevé que l'acide lactique, le pouvoir acidifiant résultant en serait probablement réduit.

- Étendre le modèle dynamique développé pour prédire la croissance et la production de métabolites de *C. maltaromaticum* dans un environnement plus similaire à celui rencontré dans une étiquette ITT

Le modèle dynamique développé lors de mon doctorat simule uniquement la croissance et la production de métabolites de *C. maltaromaticum* dans un bioréacteur, à température et pH contrôlés. Ce modèle pourrait être étendu pour prédire la cinétique de croissance et d'acidification de *C. maltaromaticum* dans un environnement où la température varie de manière arbitraire mais connue et où le pH n'est pas contrôlé mais dépend des acides produits et du pouvoir tampon du

milieu. Un tel environnement imiterait donc plus fidèlement celui rencontré par *C. maltaromaticum* dans une étiquette ITT.

- **En relation avec la cryorésistance des bactéries lactiques**

- Étudier le rôle des acides gras spécifiques et des groupements polaires des têtes lipidiques de la membrane de *C. maltaromaticum*, en relation avec la cryorésistance.

L'évaluation de la composition en acides gras de *C. maltaromaticum* a révélé que sa composition était très différente de celle des autres souches de bactéries lactiques, notamment en ce qui concerne sa teneur extrêmement élevée en acide oléique (>70 %). Ceci a suscité l'intérêt d'une étude plus approfondie de la membrane lipidique de cette souche en évaluant la composition des têtes polaires et des acides gras de chaque famille de lipides. Ce travail a été initié en collaboration avec Ha-Phuong Ta et Marie-Hélène Ropers, du laboratoire BIA (INRAE, Nantes).

- Approfondir l'étude des différences entre *C. maltaromaticum, L. bulgaricus* ATCC et *L. bulgaricus* CFL1 en ce qui concerne l'interaction de leur membrane lipidique avec des cryoprotecteurs.

La position de la bande $\nu_{as}PO_2^-$ de *L. bulgaricus* ATCC 11842 et de *L. bulgaricus* CFL1 sous stress froid et osmotique a été suivie par Meneghel et al. (2017) pour évaluer le comportement du groupement polaire des phospholipides dans leur membrane. Leurs résultats ont montré que le stress osmotique a largement déplacé la position de ce pic dans les spectres IRTF de *L. bulgaricus* CFL1, la souche cryosensible, mais pas dans le cas de *L. bulgaricus* ATCC 11842, suggèrant l'existence de différents types d'interactions entre la matrice de saccharose concentrée et les groupes de tête des phospholipides membranaires des deux souches. Une telle investigation pourrait être réalisée sur *C. maltaromaticum* pour évaluer une éventuelle différence dans l'interaction du saccharose avec sa membrane. Ceci pourrait également être étendu pour évaluer les mécanismes de protection de différentes molécules cryoprotectrices.

- Évaluer la résistance de C. maltaromaticum à d'autres processus de stabilisation tels que la lyophilisation.

Les travaux réalisés jusqu'à présent sur *C. maltaromaticum* ont confirmé la cryorésistance exceptionnelle de la souche. Cependant, des travaux préliminaires sur la capacité de la souche à résister à la lyophilisation ont montré qu'elle présentait une faible résistance à ce procédé de stabilisation. Des travaux sont en cours pour évaluer l'effet de la modification des paramètres de fermentation sur la

résistance de la souche à la lyophilisation et au stockage ultérieur à température ambiante. Jusqu'à présent, les résultats semblent indiquer que la résistance à la lyophilisation et au stockage peut être améliorée en appliquant un stress sublétal pendant la fermentation.
Une étude micro-spectroscopique IRTF des cellules fraîches et réhydratées de *C. maltaromaticum* est en cours, afin de rechercher des marqueurs de résistance à la lyophilisation, similaire à l'approche adoptée ici pour la rechercher des marqueurs de cryorésistance.

4. Perspectives à moyen et long terme

- Acquérir des spectres infrarouges et des données de cryorésistance sur de nouvelles bactéries lactiques afin de valider les marqueurs potentiels de cryorésistance et de dommages identifiés.

L'application d'une approche similaire à celle réalisée lors de mon projet de thèse, à d'autres souches de bactéries lactiques (ou populations cultivées et/ou protégées dans des conditions différentes), pourrait aider à confirmer les marqueurs proposés de dommage et de cryorésistance identifiés dans les spectres infrarouges. Il serait ainsi possible, à terme, d'évaluer rapidement la cryorésistance de nouvelles bactéries lactiques, sur la base de leurs seules caractéristiques spectrales.

- Développer une méthode IRTF combinant la micro-spectroscopie en conditions aqueuses et les mesures dynamiques

Deux configurations différentes de spectroscopie IRTF ont été utilisées dans lors de ma thèse : (i) une configuration dynamique, fournissant des informations sur le comportement des membranes lipidiques pendant la congélation, mais sans accès aux informations sur les protéines en raison de l'interférence spectrale de l'eau ; et (ii) une configuration de micro-spectroscopie statique associée à une méthode de traitement spectral par soustraction d'eau, permettant d'accéder à toute la région infrarouge moyenne des cellules, mais uniquement à température ambiante. En combinant les deux montages par le développement d’une chambre à échantillon spéciale pouvant être refroidie et utilisée avec l'approche micro-spectroscopique IRTF, il serait possible de suivre toute la région infrarouge moyenne des cellules pendant la congélation et la décongélation. Cela fournirait des informations précieuses, en temps réel, sur l'impact de la congélation et de la décongélation sur tous les composants cellulaires, et permettrait ainsi de mieux comprendre les dommages cellulaires bactériens liés à cette méthode de stabilisation.

Bien que les recherches menées avec Cryolog ne soient pas allées aussi loin que prévu, ce projet de doctorat a produit des éléments de base utiles pour le développement futur d'étiquettes ayant une durée de conservation plus longue et a contribué à l'acquisition de connaissances fondamentales sur les mécanismes d'adaptation au stress chez les bactéries lactiques, dans le cadre du projet européen PREMIUM.

université PARIS-SACLAY

ÉCOLE DOCTORALE
Agriculture, alimentation, biologie, environnement, santé (ABIES)

Titre : Étude de *C. maltaromaticum* CNCM I-3298 afin d'améliorer les performances d'intégrateurs temps-température biologiques et de mieux comprendre la cryorésistance des bactéries lactiques.

Mots clés : Bactéries lactiques – Fermentation – Modélisation – Spectroscopie infrarouge – Cryobiologie

Résumé : *C. maltaromaticum* a été sélectionnée pour le développement d'intégrateurs temps-température (ITT) biologiques, en raison de sa capacité à se développer dans une gamme de température de stockage des aliments réfrigérés et de son exceptionnelle cryorésistance. Chez d'autres bactéries lactiques, celle-ci peut entrainer des dégradations de leurs fonctionnalités technologiques (viabilité et activité acidifiante), rendant difficile leur utilisation à l'échelle industrielle. Cela est particulièrement le cas chez *Lactobacillus delbrueckii* ssp. *bulgaricus,* un ferment de l'industrie laitière. Ce travail a été structuré autour de deux objectifs : (i) concevoir des stratégies pour la production de concentrés de *C. maltaromaticum* présentant des réponses physiologiques d'intérêt pour les ITT et (ii) utiliser *C. maltaromaticum* comme souche modèle de cryorésistance, dans l'optique d'identifier des marqueurs de cryorésistance chez les bactéries lactiques.

Pour répondre au premier objectif, la cinétique de croissance et de production de métabolites, ainsi que l'état physiologique de *C. maltaromaticum* ont été évalués pour différentes conditions de culture. Deux modèles ont été développés pour optimiser la culture de *C. maltaromaticum* et produire des concentrés pour une utilisation dans un ITT suivant une durée de conservation spécifique. Pour répondre au deuxième objectif, la spectroscopie infrarouge à transformée de Fourier (IRTF) et d'autres approches analytiques ont été utilisées pour caractériser des échantillons frais et décongelés de *C. maltaromaticum* et deux souches de *L. bulgaricus* présentant des cryorésistance variables. Les résultats obtenus par IRTF ont notamment révélé qu'une altération de la conformation des protéines et du peptidoglycane de la paroi cellulaire pourrait être un marqueur cellulaire d'évaluation de la cryorésistance des bactéries lactiques.

Title : Study of *C. maltaromaticum* CNCM I-3298 to improve performance of biological time-temperature integrators and gain more insight into lactic acid bacteria cryoresistance.

Keywords : Lactic acid bacteria – Fermentation – Modelling – Infrared spectroscopy – Cryobiology

Abstract: *C. maltaromaticum* was selected in the development of biological time-temperature integrators (TTI), mainly because it is a lactic acid bacterium able to grow within the storage temperature range of perishable foods and it exhibits exceptional cryoresistance. In other lactic acid bacteria, freezing can lead to degradation of their technological functions (viability and acidifying activity), making their use at industrial scale difficult. This is particularly the case for *Lactobacillus delbrueckii* subsp. *bulgaricus*, an industrially relevant dairy starter. This work was structured around two objectives: (i) design strategies for the production of *C. maltaromaticum* concentrates with physiological responses of interest for TTIs and (ii) use *C. maltaromaticum* as a model strain of lactic acid bacteria cryoresistance, to help identify markers of cryoresistance.

To address the first objective, concentrates were produced under different culture conditions, and their growth, metabolite production and final physiological state were evaluated. This allowed the development of two models; one to optimize the culture of *C. maltaromaticum* and the other to produce concentrates for use in a TTI following a specific shelf life. To address the second objective, Fourier transform infrared (FTIR) spectroscopy and other analytical approaches were used to characterize fresh and thawed samples of *C. maltaromaticum* and two *L. bulgaricus* strains with varying cryoresistances. The maintenance upon freezing of a highly fluid membrane, of protein conformation and of the infrared band intensities associated to cell wall components were identified as cellular markers of LAB cryoresistance.

Maison du doctorat de l'Université Paris-Saclay
2ème étage aile ouest, Ecole normale supérieure Paris-Saclay
4 avenue des Sciences,
91190 Gif sur Yvette, France